Process Mineralogical Characterisation of the Kansanshi Copper Ore, NW Zambia

by

Tamzon Talisa Jacobs

A thesis submitted at the University of Cape Town in fulfilment of the requirements for the degree of

Master of Science

Department of Chemical Engineering

University of Cape Town

May 2016

SYNOPSIS

Kansanshi mine is the largest copper producer in Africa. The deposit is mineralogically and texturally complex due to supergene enrichment resulting in the presence of a variety of primary and secondary copper minerals. This necessitates the processing of ore through three separate circuits: sulphide flotation, mixed flotation and oxide leach, followed by solvent extraction and electro-winning. This study revisits the process mineralogy of the ore using modern mineralogy tools, which for such a large and complex deposit cannot but deliver significant value. Specific focus is given to copper mineralisation and the flotation of the sulphide ores in compliment to another MSc study from the Centre for Minerals Research focusing on mixed ore flotation (Kalichini, 2015).

A series of hand samples and grab samples representing the variation in mineralogy and texture of the Kansanshi ore, as well as two run of mine sulphide ore flotation feed samples were used for this investigation. Process mineralogical characterisation entailed optical microscopy, XRF, QXRD, QEMSCAN and EPMA investigations, alongside a series of laboratory scale batch flotation tests of two sulphide ores at two grinds (80% passing 150 µm, 80% passing 212 µm).

Copper mineralisation at Kansanshi occurs as both vein-hosted mineralisation, and to a lesser extent sediment-hosted mineralisation. Later breccia-hosted and supergene mineralisation have overprinted all previous mineralisation styles. Chalcopyrite is the main ore mineral for both vein-hosted and sediment-hosted mineralisation styles. Vein-hosted mineralisation is characterized by an overall coarse-grained texture (>0.5 mm), compared to sediment-hosted mineralisation that is characterised by fine-grained disseminated textures that occur parallel to the bedding and foliation planes. Breccia-hosted and supergene related mineralisation have led to the formation of an array of secondary copper minerals, such as chalcocite, covellite, malachite and chrysocolla. These minerals show a variety of complex intergrowth textures between one another. Secondary copper oxide mineralisation is commonly associated with distinctive stockwork and boxwork textures, with replacement being partial or complete depending on the extent of oxidation. The variety of textures related to the replacement reactions result in grain size variations that cause a decrease in the chalcopyrite grain size and produce secondary copper sulphides that are of equivalent to or of a finer grain size (< 0.2 mm) than that of the primary copper sulphide.

Mineralogical investigations of two run of mine sulphide flotation feed samples showed that the dominant ore mineral is chalcopyrite with an overall coarse-grained (> 0.5 mm) texture

with minimal fine composite particles, which results in good chalcopyrite liberation. Results of this laboratory study show good copper recoveries (~89%) during rougher flotation, because chalcopyrite liberation was over 90% at a grind of 80% passing 150 µm. The effect of coarsening the grind caused an insignificant loss of copper recovery. This good performance during flotation can be attributed to a number of mineralogical characteristics, including minimal fine composite particles, the natural hydrophobicity of chalcopyrite and the high degree of liberation of chalcopyrite associated with the overall coarse texture of the sulphide ore. Mineralogical investigations suggest that the relatively low copper grades from batch flotation cannot be attributed to the presence of composite particles, and can potentially be improved using a series of cleaner floats.

The effects of supergene enrichment on mineralogy and texture, and its influence on processing, have been used to develop a simplified process mineralogy matrix for Kansanshi. The matrix demonstrates the continuum of mineralogy and textures due to supergene enrichment and their potential influences on mineral processing. Some ideas for regular on-site use of mineralogical analyses at Kansanshi have also been proposed. Ultimately, this information can be incorporated into the existing geometallurgical framework at Kansanshi, adding to the understanding and predictability of the ore being fed into each circuit.

DECLARATION

I declare that this thesis is my own work. It is being submitted for the degree of Master of Science (MSc) in the University of Cape Town. This thesis has not been submitted before for any degree or examination in any other university.

Signed by candidate

Signature Removed

Tamzon Jacobs

22 Day of May 2016

ACKNOWLEDGEMENTS

I recognize that the successful completion of this project would not have been possible without the following:

I would like to express my sincerest gratitude to my supervisors, Dr Megan Becker and Dr Lynnette Greyling, for their on-going support, understanding and patience throughout my Master's experience. To Dr Megan Becker, thank you for the initial opportunity and assistance in obtaining funding for this project. I am appreciative of her sharing her vast knowledge of process mineralogy, analytical techniques, presentation and writing skills and helping me bridge the gap between geology and engineering. To Dr Lynnette Greyling, thank you for your invaluable geological and technical input, for assisting me in understanding the Copperbelt geology and for teaching me how to carry out concise and methodical petrographic and EMPA investigations. Thank you both for helping me grow in character and maturity.

Professor David Reid is an inspiration to me and I cannot express my gratitude more to him for his motivation and encouragement throughout my undergraduate and postgraduate career, for seeing potential in me and so many others and helping us to realize our dreams of becoming young scientists. Thank you for introducing me to both my supervisors and by doing so, making this project possible. For assisting me in analysing and understanding both my XRD and XRF data, for broadening my understanding of geology and mineralogy.

My sincere appreciation goes to First Quantum Minerals and Kansanshi Mine for their financial and logistical support in enabling this project to go ahead. Special thanks are also due to Christopher Beaumont, Monica Kalichini, Reoccardo Mumba, Chanda Ngulube, Craig van der Merwe, Louis van Heerden and Crosby Chongo who have all played a significant role in the project and in hosting my visit to Kansanshi.

Thank you also to the Department of Chemical Engineering and the entire CMR team for their financial, technical and logistical support throughout my thesis and for welcoming me into the team. I would also like to thank Lorraine Nkemba for sample preparations, Gaynor Yorath for her assistance throughout all the aspects of using the QEMSCAN.

I recognize that this research would not have been possible without the assistance of Christel Tinguely, David Wilson and Jonathan van Rooyen from the Department of Geological Sciences and Kirsten Corin, Monde Bekaphi, Moegsien Southgate and Rubin van Schalkwyk of the Department of Chemical Engineering, my thanks for their assistance with various aspects of the research.

I would like to thank the National Research Foundation (NRF) for bursaries support of my MSc studies.

To my family, friends and to boyfriend Ronen Agranat, thank you for being my armour-bearers, I would not have been capable of finishing this thesis without you. To my Lord and saviour Jesus Christ – in all things I give you all the praise and glory.

LIST OF PUBLICATIONS AND PRESENTATIONS

Jacobs, T., Becker, M., Greyling, L., Reid, D.L., Kalichini, M., 2014. Process mineralogical characterisation of the Kansanshi copper ore, NW Zambia. SAIMM Mineral-processing Conference, 7-8 August 2014, Cape Town.

Jacobs, T., Becker, M., Greyling, L., Reid, D.L., Kalichini, M., 2014. Process mineralogical characterisation of the Kansanshi copper ore, NW Zambia. International Mineralogical Association Conference, 1-5 September 2014, Johannesburg.

TABLE OF CONTENTS

LIST OF FIGURES

LIST OF TABLES

NOMENCLATURE

List of abbreviations and acronyms

ASCu	Acid soluble copper
AICu	Acid insoluble copper
AAS	Atomic absorption spectroscopy
BMS	Base metal sulphides
BMA	Bulk modal analysis
BSE	Back-scattered electron
C	Fraction of the total feed weight that reports to the concentrate
c	Concentrate assay
LOI	Lose of Ignition
MLA	Mineral Liberation Analyser
NaHS	Sodium Hydrogen Sulphide
PMA	Particle Mineralogical Analyses
PSD	Particle Size Distribution
QEMSCAN	Quantitative Evaluation of Minerals by Scanning Electron Microscopy
Rg	% recovery of gangue into concentrate
Rm	% recovery of valuable mineral
SE	Separation Efficiency
SIP	Species identification protocol
TCu	Total copper
XRD	X-ray Diffraction
XRF	X-ray Fluorescence Spectrometry

EPMA	Electron Probe Micro-analyser
Wt. %	Weight percentage
WDXRF	Wavelength dispersive X-ray Fluorescence Spectrometry

Mineral abbreviations

ab	Albite
am	Amphibole
az	Azurite
bn	Bornite
bt	Biotite
cal	Calcite
cc	Chalcocite
ccl	Chrysocolla
ccp	Chalcopyrite
chl	Chlorite
cv	Covellite
di	Digenite
dj	Djurleite
dol	Dolomite
ge	Geerite
grt	Garnet
gt	Goethite

gr	Graphite
kln	Kaolinite
lim	Limonite
mal	Malachite
ms	Muscovite
py	Pyrite
qtz	Quartz
tn	Tenorite

Mineral names and formulas

Native copper	Cu
Cuprite	Cu_2O
Tenorite	CuO
Chalcocite	Cu_2S
Covellite	CuS
Digenite	Cu_9S_5
Djurleite	$Cu_{31}S_{16}$
Geerite	Cu_8S_5
Bornite	Cu_5FeS_4
Chalcopyrite	$CuFeS_2$
Malachite	$Cu_2CO_3(OH)_2$

Azurite	$Cu_3(CO_3)_2(OH)_2$
Chrysocolla	$(Cu,Al)_2H_2Si_2O_5(OH)_4.n(H_2O)$
Muscovite	$KAl_2\ (AlSi_3O_{10})\ (OH)_2$
Chlorite	$(Mg,Fe)_3(Si,Al)_4O_{10}(OH)_2.(Mg,Fe)_3(OH)_6$
Biotite	$K\ (Mg,\ Fe_3^{2+})\ (Al,\ Fe^{3+})\ Si_3O_{10}\ (OH,\ F)_2$
Calcite	$CaCO_3$
Dolomite	$CaMg(CO_3)_2$
Pyrite	FeS_2
Pyrrhotite	$Fe_{1-x}S$
Rutile/Ilmenite	TiO_2 - $FeTiO_3$
Quartz	SiO_2

Glossary

Anhedral: Textural term to describe a mineral grain that does not show a well-developed crystal form.

Area %: Particles are exposed at the surface of a polished section as two-dimensional cross-sections. Any quantification of mineral/particle characteristics are based on measurements, in pixels, of the exposed areas.

Association Mineral %: The number of pixels of a mineral type adjacent to the mineral of interest expressed as a percentage of all the pixels associated with the mineral of interest.

Average Grain Size: The average size of a specific mineral type, measured as the average intercept length in x-direction.

Average Particle Size: The average size of a particle, measured as the average intercept length in x-direction across the particle (regardless of the mineral type).

Copper oxides: Those copper minerals containing oxidized anions, especially copper oxides, sulphates, phosphates, carbonates, and arsenates**.**

Disseminated: Textural description of an ore consisting of fine grains of valuable minerals dispersed throughout the bulk of the rock.

Epigenetic: A mineral deposit that formed later than the enclosing rocks. The mineral composition and chemical composition of epigenetic deposits differ markedly from the composition of the enclosing rocks

Euhedral: Textural term to describe a mineral grain that shows well-developed crystal form.

Exsolution: Un-mixing of two phases from a solid solution.

Grain: A mineral grain that consists of a single mineral type. Several grains can make a particle. In the case of a liberated grain, the terms 'grain' and 'particle' are equivalent.

Hypogene: Refers to processes that occur deep within the earth's crusts at temperatures and pressures, ranging on average from 650-250 ˚C and 0.5 to 1.5 kbar, respectively.

Hypothermal deposits: Form from sediments and/or opening in rocks that have been exposed to high temperature aqueous solutions rising in most cases from the action of deeply circulating water heated by magma. Other sources of heating that may be involved include energy released by radioactive decay or by faulting of the Earth's crust.

Liberation: The degree of liberation is typically based on the area % of the mineral grain(s) of interest in a particle.

Liberated: In the context of this report, when > 90 % of the area of a particle consists of the mineral of interest

Limonite: Grouping of amorphous yellowish-brown to black hydrated iron oxide minerals, with a mineral formula $FeO(OH)\cdot nH_2O$.

Locked: In the context of this report, when < 30 % of the area of the particle consists of the mineral grain of interest.

Middlings: In the context of this report, when the mineral grain of interest occupies between 30 to 90 % of the area of a particle.

Mineral associations: Association refers to one or more minerals are that occur next to each other, such that the mineral boundary of one mineral is in contact with the mineral boundary of other mineral. iExplorer scans the measured particles horizontally, from left to right, counting the associations that occur in the images.

Orogeny: The formation of mountain ranges by intense upward displacement of the earth's crust usually associated with folding, thrust faulting and other compressional processes.

Oxide zone: The rock volume representing a redox environment transitional between the highly oxidized conditions present in the leached capping and the reduced conditions characterizing the supergene sulphide zone.

Particle: Several grains make up a particle. A particle usually refers to a fragment of a rock or ore, the size of which is dependent on crushing and milling conditions as well as the size class it deports to.

Petrogenesis: Origin, formation and history of rocks.

Petrography: Description of rock textures and mineral assemblages.

Proterozoic Eon: The period of Earth's history that began 2.5 billion years ago and ended 542.0 million years ago is known as the Proterozoic, which is subdivided into three eras: the Paleoproterozoic (2.5 to 1.6 billion years ago), Mesoproterozoic (1.6 to 1 billion years ago), and Neoproterozoic (1 billion to 542.0 million years ago).

Subhedral: Textural term to describe a mineral grain that shows partially developed of crystal form.

Supergene: Refers to mineralisation caused by descending solutions – generally, the enrichment processes accompanying the weathering and oxidation of sulphide and oxide ores at or near the surface.

Syngenetic: Refers to ore deposits that form at the same time as their host rocks. In this study this includes deposits that form during the early stages of sediment diagenesis.

Enriched/transitional zone: A narrow zone below the water table. It is the richest part of the deposit but is not often present. The most common minerals stable in this reducing environment are chalcocite, covellite, and native copper among other secondary sulphides.

.

CHAPTER 1: INTRODUCTION

1.1 BACKGROUND

1.1.1 Global demand for copper

A review of the current copper metal price as illustrated in Figure 1.1 shows a strong decline since early 2011 attributed to the decreasing demand from China (consuming ~ 40% of the world's copper), falling oil prices and an oversupply of the metal (www.businessinsider.com). In such challenging circumstances, mining and processing of copper need to be done with maximum efficiency and minimum operational costs. The majority of the existing copper mines, as well as new discoveries are increasingly operating under stricter operational, financial and environmental regulations, in more remote areas, on deeper, harder and more mineralogically complex ores (Baum et al., 2004; Williams, 2013). A potential solution enabling improved efficiency is through the more efficient use of the inherent mineralogical data of the ore body, which ultimately governs minerals beneficiation performance (Baum et al., 2004; Tungpalan et al., 2015). The importance of designing and operating plants using mineralogy data is becoming increasingly more widely recognised through the discipline of process mineralogy (Evans et al., 2011; Powell, 2013; Baum, 2014).

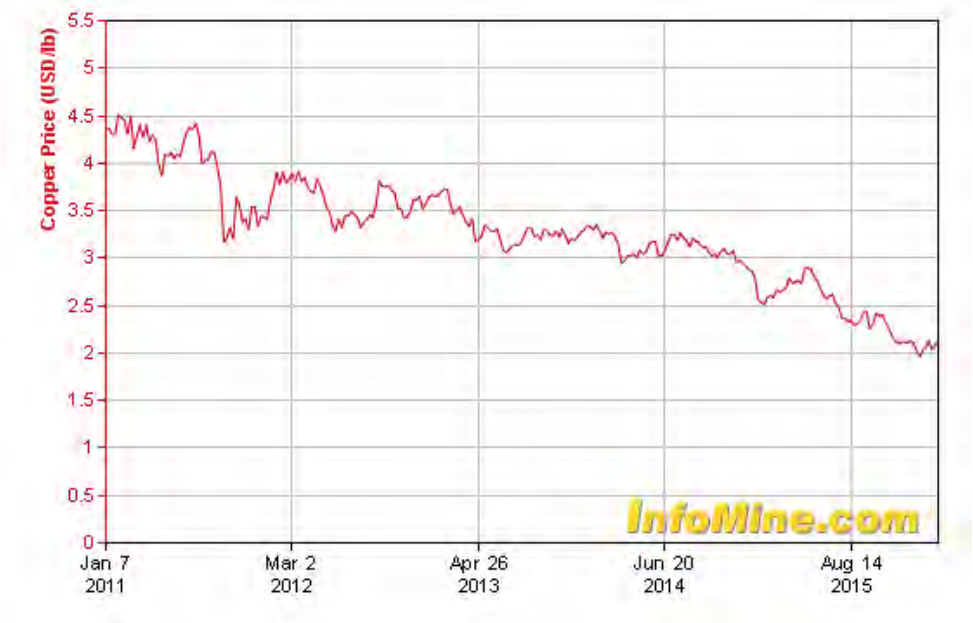

Figure 1.1: Global trends in copper prices since Jan-2011 to Aug-2015 (from **www.Infomine.com**).

1.1.2 Application of process mineralogy in the mining industry

Process mineralogy can be utilized to identify, diagnose and predict the behaviour of an ore during mineral processing and as such can be used to predict and optimize mining and mineral separation processes (Baum et al., 2004). The ore mineralogy and, more importantly, the texture of an ore control how the ore can be mined and processed. Process mineralogy is utilized in all stages of the mining cycle, and bridges the gap between mineralogy and mineral processing and therefore forms an integral part of any geometallurgy as it is the primary source of mineralogical data necessary for the successful application of a predictive geometallurgical block model (Evans et al., 2011; Powell, 2013; Baum, 2014). Process mineralogy can be considered part of the larger field of geometallurgy – which aims to directly address the issue of ore variability during processing, by developing geometallurgical models that allocate different characteristics of the ore-body into the block model. This information can be used in forecasting the main performance outputs (Bulled & Mcinnes, 2006; Williams, 2013).

Both process mineralogy and geometallurgy however, rely on the availability of mineralogical information characterising the composition of the valuable and gangue minerals and the textural interrelationships between them (Baum et al., 2004; 2014; Lotter et al., 2011; Hoal, 2013; Williams, 2013). The application of tools such as: a) automated scanning electron microscopes (MLA, TIMA and QEMSCAN); b) electron microprobe analyses (EPMA); c) micro-beam tomography (neutron and X-ray tomography) and (d) laser ablation inductively coupled plasma mass, amongst others, are instrumental in obtaining this information (Gottlieb et al., 2000; Goodall et al. 2005a; Goodall, 2008; Kyle et al., 2008;; Godel, 2013). In turn, this information can be used in understanding and predicting ore throughput, grade and recovery to forecast potential downstream problems linked to ore variability ultimately leading to a reduction of the associated processing risks (Baum, 2014).

1.1.3 Supergene enrichment and mineralogy

Historically, the most profitable copper mines have been the giant porphyry deposits that supply up to 60% of the world's copper (Cropp et al., 2013). Porphyry ore bodies are typically large in size (for example, the Chuquicamata mine in Chile is 4.3 km long, 3 km wide and 900 metres deep) and contain grades ranging from 0.2 to 2% copper (www.mining-technology.com). These copper sulphide deposits may be overprinted by later supergene enrichment (Lowell & Gilbert, 1968; Lodder et al., 2010).

Supergene enrichment is a process that occurs through the subsequent weathering, oxidation and surface leaching of the sulphide deposit, leading to the redistribution of valuable metals at depth through the downward percolation of acid-bearing solutions from the leached surface to produce higher concentrations (Evans, 1993; Chávez, 2000; Petruk, 2000). This process results in the formation of an intensely oxidized and leached upper portion of the orebody known as a "leached cap" or "gossan". Below the leached surface a "supergene blanket" may be present, where metals from the upper oxidized cap have been dissolved, transported down and precipitated below the water table. If a supergene blanket occurs, it may account for a large proportion of the ore (Gilbert & Park, 1986; Evans, 1993). The formation of a supergene blanket may produce an exotic array of secondary copper minerals, such as malachite, chrysocolla and various secondary copper sulphides for example chalcocite and covellite. These minerals also show a variety of complex intergrowth textures between one another as a result of the supergene enrichment.

One example where supergene enrichment has made a significant contribution to the mineralisation is at Kansanshi Cu-Au mine (Zambia). It is an epigenetic-vein-hosted type deposit. The Kansanshi deposit is located in the Domes Region in the western arm of the world-class Central African Copperbelt mining district. Kansanshi differs from the classic Copperbelt stratiform mineralisation style in being a vein-type deposit, hosted by the meta-sedimentary Kundelungu Group of the Katanga Supergroup (Broughton et al., 2002; Torrealday et al., 2000).

The host rocks at Kansanshi Cu-Au Mine have undergone multiple deformation events during the Pan-African orogeny, resulting in complex local structures (Torrealday et al., 2000; Broughton et al., 2002). Later supergene processes overprinted the primary mineralisation with secondary copper minerals (chalcocite, covellite, tenorite, malachite, azurite and chrysocolla) and associated changes in mineral textures.

1.1.4 Kansanshi Mine

The Kansanshi Cu-Au mine in Zambia is the largest copper producer in Africa, with estimated reserves at 725.5 Mt @ 0.82 % TCu and 0.15 g/t Au as of January, 2015 (www.first-quantum.com). The property is located 10 km north of Solwezi, and approximately 294 km north-west of Ndola. Ancient artisanal mining at the Kansanshi deposit, dating back to the early 19th and 20th century has been documented by Gunning (1961). Commercial exploitation of the deposit began in 1988, in the form of numerous small-scale underground operations and open pits, but ceased due to a drop in copper prices (First Quantum Minerals Ltd, 2003).

Currently, First Quantum Minerals Ltd (FQML) has 80% ownership and operational management of the Kansanshi deposit, with the remaining 20% retained by Zambia Consolidated Copper Mines (ZCCM).

Opencast operations are currently carried out at Kansanshi, with the orebodies being accessed from two open pits, Main and Northwest (NW). FQML began operations in April 2005, with processing of the ore occurring through three separate circuits: sulphide flotation, mixed flotation and oxide leach, followed by solvent extraction and electro-winning. According to FQML financial statements for total 2015, they produced 226,647 tonnes of copper and 136,257 ounces of gold in 2015 (www.first-quantum.com). The current life of the mine is 17 years.

1.2 PROBLEM STATEMENT

Kansanshi mine is the largest copper producer in Africa. The deposit is mineralogically and texturally complex due to supergene enrichment resulting in the presence of a variety of primary and secondary copper minerals (chalcopyrite, bornite, chalcocite, covellite, tenorite, malachite and chrysocolla). This necessitates the processing of ore through three separate circuits: sulphide flotation, mixed flotation and oxide leach, followed by solvent extraction and electro-winning. This study revisits the process mineralogy of the ore using modern mineralogy tools, which for such a large and complex deposit cannot but deliver significant value to the mine when incorporated into the existing geometallurgical framework. No systematic study of this type has previously been done.

1.3 OBJECTIVES OF THIS STUDY

The primary objective of this research is the detailed process mineralogical characterisation of the Kansanshi ore, with a focus on the flotation performance of the sulphide ore. The main objectives of this study are to:

1. Characterize the different ore types, focusing on their mineralogical composition, mode of occurrence, grain size distribution, Cu-deportment and liberation of Cu-sulphides, oxides, iron-sulphides; gangue minerals present within the sulphide, oxide and mixed ores.

2. Determine what affect the mineralogy has on the flotation performance of two slightly different sulphide ore samples.

The ultimate goal of this research is to provide process mineralogical information that can be fed into the geometallurgical framework currently being developed by Kansanshi mining.

1.4 KEY QUESTIONS

Within the context outlined in the introduction and the scope given, the following questions are fundamental in attaining the objective of this research:

1. What is the mineralogy and texture of each of the four lithologies common to the Kansanshi Stratigraphy?
2. What effect does the mineralogy have on the flotation behaviour of the sulphide ore?

   a) Can the primary grind be made coarser (i.e. p80 of 212 µm instead of the current primary grind, p80 of 150 µm), without a significant loss in copper recovery?

   b) What is the nature of the gangue minerals recovered during sulphide flotation?

1.5 SCOPE OF RESEARCH

The scope and boundaries of this study are illustrated in Figure 1.3. The mineralogical components of economic geology which are of importance for this study are supergene processes, secondary enrichment and ore texture. The ore textures were determined by using microscopy and QEMSCAN. This was done to determine their grain size distribution, liberation and mineral associations, all of which have a direct effect on the fineness of grind. The focus of this study was on copper process mineralogy and therefore excludes all other valuable metals (i.e. Au-Mo-U) associated with the Kansanshi ores.

The geometallurgy and mineral processing aspect of this study focuses on the method development and ore characterisation, looking at the bulk mineralogy, mineral chemistry, valuable mineral liberation and association. This information will be gathered using the following tools: optical microscopy, QXRD, XRF, EMPA and QEMSCAN. The results from this study will provide a process mineralogical method tailored for the correct characterisation of the Kansanshi copper ores. Areas of research beyond the scope of this component include:

process modelling, plant design, block model development and mineral kinetics. For the minerals beneficiation component of this study the only area of interest is flotation. In this study the focus is on the influence of mineralogy on the flotation performance of Cu-sulphide ore in terms of the copper grade and recoveries.

Furthermore, this study also focuses on coarse particle flotation, exploring what effect an increase in grind from 150 µm to 212 µm will have on the copper grades and recoveries. Laboratory scale batch flotation cells will be used for all flotation test-work. Assay data will be obtained using a Leco sulphur analyser and atomic adsorption spectroscopy for iron and total copper content, necessary for Cu-grade-recovery calculations. A complementary MSc by Kalichini, 2015 focuses on the flotation characteristics of complex copper ores (mixed ores) at Kansanshi Cu-Au mine.

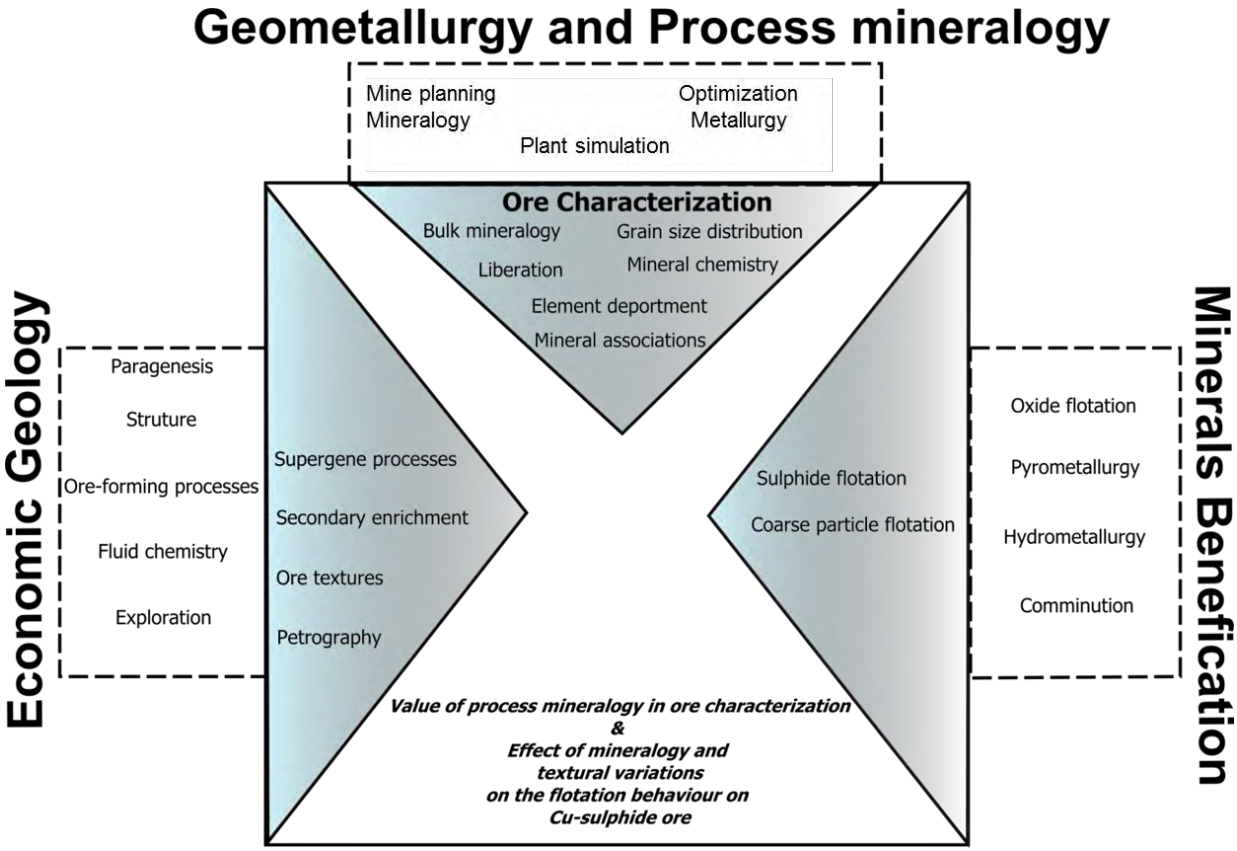

Figure 1.2: Schematic of the research scope and limitations with key areas of interest in the solid triangles.

1.6 ORGANISATION OF THE THESIS

The skeleton of this thesis is divided into six chapters beginning with the introduction where the background, aim of the study, research scope of the thesis, and key questions are covered in Chapter 1.

This is followed by a critical review of the literature in Chapter 2, focusing on the geological setting; mineralogy and supergene enrichment, process mineralogy and geometallurgy, and minerals beneficiation. Chapter 3 provides a detailed description of the techniques and experimental methods used for ore characterisation and batch flotation experiments. The results of this study are covered in Chapter 4 and have been divided into two sections. Section 1 covers the method development and characterisation of the four lithological units that are representative of the different mineralisation styles common to Kansanshi (Table 2.3) and Section 2 details the batch flotation experiments of sulphide ore. A detailed discussion of the results is presented in Chapter 5. The concluding remarks and a summary of the findings as well as recommendations for further research are given in Chapter 6. All results from the various analyses and experiments, and calculations are listed in the Appendices.

CHAPTER 2: LITERATURE REVIEW

2.1 MINERALOGY AND SUPERGENE ENRICHMENT

2.1.1 Mineralogy

Chemistry of Copper

Copper readily combines with other compounds as it has a tendency to form strong complexes in water or soil with inorganic ligands such as sulphur (S), hydrogen sulphide (HS^-), (S) phosphate (PO_4^{3-}), chloride (Cl^-) and ammonia (NH_3) (Conry, 2006). As a result the economic copper minerals are numerous. There are currently 17 copper minerals that are in use within the mining industry (Table 2.1) with 50 % of copper production being sourced from chalcopyrite (www.copper.co.za).

Table 2.1: Common copper minerals of economic significance arranged in order of decreasing copper content (from Evans, 1993; Ayres et al., 2002).

Minerals	Formula	Cu (wt. %)	Mineral Group
Native copper	Cu	100	Primary sulphides
Cuprite	Cu_2O	88.8	Cu-oxide
Tenorite	CuO	79.5	Cu-oxide
Chalcocite	Cu_2S	79.8	Secondary Cu-sulphide
Covellite	CuS	66.5	Secondary Cu-sulphide
Bornite	Cu_5FeS_4	63.3	Primary sulphides
Atacamite	$Cu_2Cl(OH)_3$	59.5	Cu-chlorite
Malachite	$Cu_2CO_3(OH)_2$	57.5	Cu-carbonate
Azurite	$Cu_3(CO_3)_2(OH)_2$	55.3	Cu-carbonate
Brochantite	$Cu_4SO_4(OH)_6$	56.2	Cu-carbonate
Antlerite	$Cu_3SO_4(OH)_4$	53.7	Cu-carbonate
Enargite	Cu_3AsS_4	48.4	Primary sulphides
Tennantite	$Cu_{12}As_4S_{13}$	47.5	Cu-As-sulphide
Chalcopyrite	$CuFeS_2$	34.6	Primary sulphides
Chrysocolla	$Cu(Fe,Mn)Ox\text{-}SiO_2\text{-}H_2O$	33.9	Cu-silicate
Tetrahedrite	$Cu_{12}Sb_4S_{13}$	34.8	Cu-Sb-sulfosalt
Chalcanthite	$CuSO_4 \cdot 5H_2O$	25.4	Cu-Sulphate

Copper ores are complex and in addition to the Cu-bearing minerals they commonly contain other sulphides, pyrite, pyrrhotite and sphalerite, additional accessory metals, such as, gold, nickel, cobalt, lead, and zinc, amongst others and trace elements Cd, Te and Re, which are hosted with various minerals, may also occur in minor abundance. Nonmetallic unwanted gangue minerals that are often present are quartz, feldspar and sericite (Kelly & Spottiswood, 1982; Ayres et al., 2002).

Hypogene Ore

Ore-forming processes associated with hydrothermal hypogene mineralisation involve the upward migration of aqueous solutions of varying source, temperature, pressure and composition from a depth below the deposit (Pirajno, 2010). Magmatic hydrothermal copper mineralisation can occur as disseminations within intrusions and/or wall-rock, or distributed in vein stockworks (for example, porphyry systems). Other hydrothermal systems include volcanogenic types (for example, VMS systems) and those associated with sedimentary basins (for example, SEDEX systems). An important variant of the latter is the classic stratiform sedimentary copper typical of the Zambian-Congo Copperbelt. Metamorphic and tectonic reworking of any of the above systems can result in redistribution as vein stockworks which can penetrate almost any overlying country rock.

The principle hypogene copper-sulphide mineral within porphyry and sediment-hosted deposits is chalcopyrite, with significant amounts of copper may occur as bornite, enargite and chalcocite (Cox et al., 2003; Berger et al., 2008). Common by-product minerals include molybdenite and native gold (Cox et al., 2003; Berger et al., 2008).

A summary of the chief hypogene minerals and associated host rocks for the four main deposit types are given in Table 2.2. Associated accessory phases include gold, silver (native or compounds) and cobalt minerals (McGoldrick & Large, 1998; Sillitoe, 2007).The gangue mineralogy is dependent upon the deposit type and its associated wall-rock alteration (Misra, 1999; Sillitoe, 2007).

Supergene Ore

The primary sulphide minerals formed during primary mineralization can be altered near the surface by supergene processes to produce copper oxides and/or secondary sulphides, that are contained primarily within the oxide and mixed ores, respectively (Robb, 2005; Sillitoe, 2007; Chávez, 2000).

Table 2.2: Four common copper-producing deposit types, including their principal ore minerals and host-rocks.

Deposit type	Major sulphide mi	Texture	Host rocks
Porphyry copper deposits **Example:** Chuquicamata, Atacama, Chile	ccp-bn-py	Ore minerals occur disseminated through the altered rock matrix and in discrete veins filling fractures	Intrusions range from coarse-grained phaneritic to porphyritic stocks, batholiths and dikes swarms, and rarely pegmatite (Hunt, 1977; Cooke et al., 2005)
Sediment-hosted-stratiform copper depoits **Example:** Konkola Cu-Co deposit, Zambia	cc-ccp-bn-gal-sph	Minerals are finely disseminted, stratabound, locally stratiform.	Calcareous or dolomitic siltstones, shales and carbonate rocks, sandstones, arkoses and conglomerates (Cailteux et al., 2005; Cox et al., 2003; Sweeney et al., 1989; 1991)
Volcanogenic Massive Sulphide deposits **Example:** Kidd Creek, Canada	ccp-sph-gal	Massive to coarse-grained sulphide	Felsic and mafic volcanic rocks (Bimodal volcanism) (Gibson et al., 2007; Zengqian et al., 2003)
Polymetallic or Replacement deposits **Example:** Kitumba, Zambia	sph-gal-eg-dg	Ranges from fine to medium grained	Sedimentary rocks, chiefly limestones, dolomite, shale. That are commonly overlain by volcanic rocks (Robertson et al., 2013)

Copper Oxides Ore

The oxide zone is located above the water table where the conditions are oxidizing (Chávez, 2000). The copper oxide minerals precipitated within this zone are compositionally and mineralogically complex, and can include a variety of copper carbonate, silicate, phosphate, sulphate, arsenate, as well as oxyhydroxide phases (Chávez, 2000).

Copper minerals that are precipitated in host rocks with high neutralizing capabilities are characterized by abundance of malachite, chrysocolla, and atacamite, and the notable absence of Cu-hydrosulphates such as brochantite and antlerite (Sillitoe, 2005). Deposition of these minerals occurs within open spaces such as fractures and cavities (Sillitoe, 2005). Chrysocolla and malachite normally form colloform textures, whilst the other copper minerals (i.e. copper-hydroxysulphates, hydroxychlorides and hydroxycarbonates) tend to form crystalline masses.

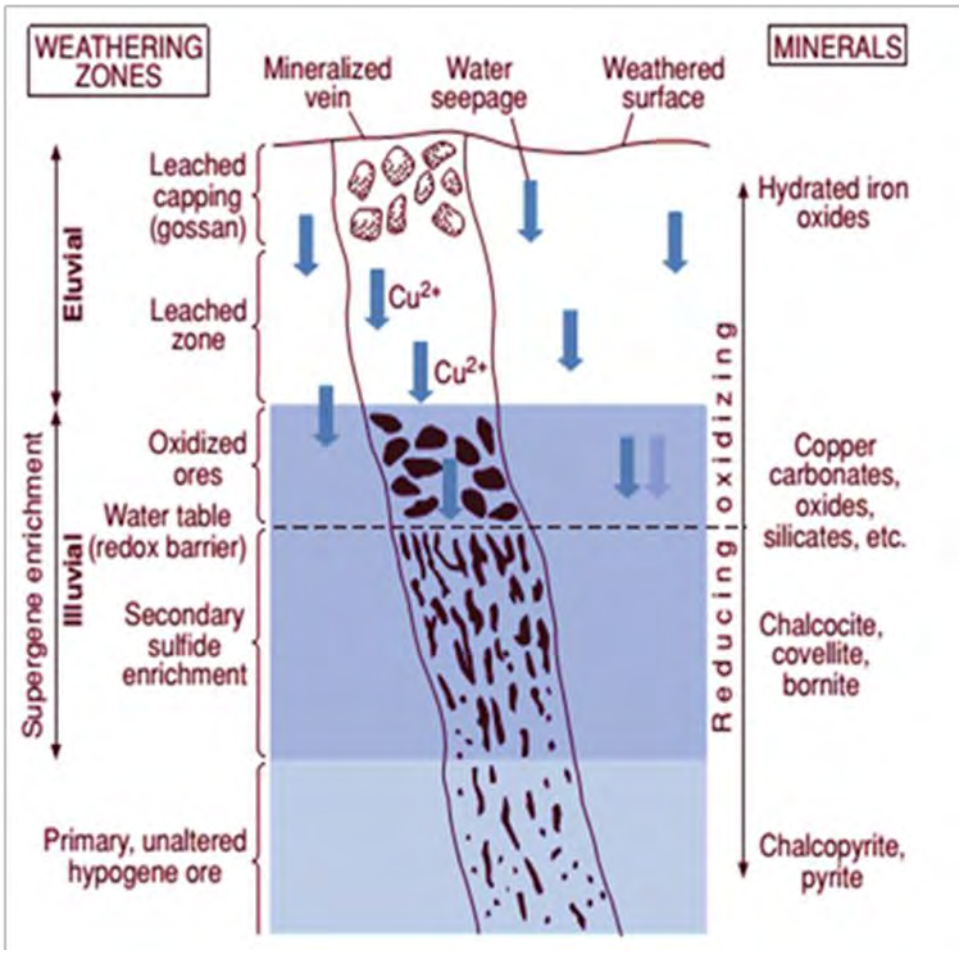

Figure 2.1: Weathering profile of a supergene enriched deposit (from Robb, 2005).

The paragenetic sequence is difficult to report precisely as the relationships between minerals are highly complex, including metastable mineral assemblages that are also present within the oxide zone. In general, malachite, azurite and chrysocolla occur late in the paragenetic sequence and form by replacing earlier sulphide minerals. Malachite and azurite form under near-surface conditions whilst chrysocolla forms deeper within the Oxide Zone at the expense of other oxide minerals, as a result malachite tends to form before chrysocolla (Chavez, 2000;Sillitoe, 2005).

Secondary copper sulphides

Beneath the water table conditions are usually reducing and primary minerals such as pyrite and chalcopyrite are still stable.

The dissolved Cu in such conditions tends to replace Fe in primary iron-sulphide minerals through cation-exchange reactions, which will be explained in detail in section 2.1.2. The copper sulphide minerals that typically form by this mechanism include chalcocite and covellite (Muthur et al., 2005).

2.1.2 Supergene Enrichment

The enrichment of various copper ore deposits (for example, Chuquicamata, Chile; Bingham Canyon; Utah; Central African Copperbelt) is due to supergene processes (Robb, 2005). These processes result in the reconcentration of metals at shallower levels after leaching, often resulting in the formation of an economically viable deposit from one which was previously too low-grade for exploitation (Robb, 2005; Reich et al., 2009). The process itself is based upon the oxidation of base metal sulphides, predominantly pyrite, when they come into contact with atmospheric oxygen and meteoric ground waters as follows (Eq. 1; 2):

$FeS_2 + 7O_2 + 2H_2O = 2FeSO_{4\ (aq)} + 2H_2SO_{4\ (aq)}$ [Eq. 1]
(Pyrite)

$FeS_2 + 8H_2O + 14Fe^{3+} = 15Fe^{2+} + 2SO_{4}^{2-} + 16H^+$ [Eq. 2]
(Pyrite)

In addition to the oxidation of pyrite, it can be further oxidized by ferric iron which is a considerably stronger oxidizing agent than O_2 alone (Sillitoe, 2005). The presence of various siderophile and chalcophile microorganisms further serves to stimulate the overall oxidation process by the conversion of ferrous iron to ferric iron (Bosecker, 1997) via the following reactions shown in (Eq. 3-5):

$FeS_2 + 1/2\ O_2 + H_2O \rightarrow Fe^{2+} + 2SO_4^{2-} + 2H^+$ [Eq. 3]
(Pyrite)

$2Fe^{2+} + 1/2\ O_2 + 2H^+ \xrightarrow{\textbf{Thiobacilli}} 2Fe^{3+} + 2SO_4^{2-} + H_2O$ [Eq. 4]

$14Fe^{3+} + FeS_2 + 8H_2O \rightarrow 15Fe^{2+} + + 16H^+$ [Eq. 5]

The combination of these various ionic species (Fe^{2+}, Fe^{3+}, SO_4^{2-}, H^+) results in a set of low pH, strongly oxidising ground waters, which then interact with other minerals in the primary ore, such as chalcopyrite (Eq. 6-7):

$CuFeS_2 + O_2 + H_2O + CO_2 = Fe(OH)_3 + CuSO_4 + H_2SO_4 + H_2CO_3$ [Eq. 6]
(Chalcopyrite)

$CuFeS_2 + Fe^{3+} + 8H_2O = Cu^{2+} + 17Fe^{2+} + 2SO4^{2-} + 16H^+$ [Eq. 7]
(Chalcopyrite)

Depending on the sulphide mineral assemblage, the oxidation reaction can be further catalysed by galvanic interactions between pyrite (cathode) and other less noble, more anodic sulphides (for example, chalcopyrite, sphalerite, galena and pyrrhotite).

These weakly acidic, metal-carrying, sulphate-rich solutions in turn percolate through the ore above the water table, forming a leached cap zone, often characterized by the presence of abundant goethite, limonite and hematite, constituting a gossan. A schematic of the supergene enrichment process, illustrated in Figure 2.1, shows that the weathering profile can be broadly subdivided into three zones: an upper zone of leaching underlain by an oxide zone, which is in turn underlain by the sulphide metastable zone which represents the of the original pre-oxidized ore. The transition from the zone of leaching to zone of oxidation is commonly accepted to be the level above the ground water table.

The oxide zone comprises a complex zone transitioning from the oxidising conditions of cap rock, to the more reducing conditions. The nature of the enrichment in the oxide zone is determined by a variety of conditions including mineralogy of the source (especially the ratio of Cu to Fe-sulphides and neutralising capacity), Eh-pH (Figure 2.2), porosity and permeability.

Within the oxide zone, copper oxide minerals form either through the direct oxidation and replacement of primary sulphides, silicates and oxides for example [Eq. 8]; or through the precipitation of metal ions in solution (for example, Cu^{2+}) when conditions become more reducing for example [Eq.9]. The precipitation reaction follows that of Shurmann's series (Gilbert and Park, 1986) whereby Cu is substituted for metals that have slightly lower affinities for sulphur (for example, Fe, Pb, Zn).

$4FeS_2 + 7CuSO_4 + 4H_2O = 7CuS + 4FeSO_4 + 4H_2SO_4$ [Eq. 8]
(Pyrite)

$CuFeS_2 + CuSO_4 = 2CuS + FeSO_4$ [Eq. 9]
(Chalcopyrite)

In a well-developed enrichment profile, the base of the enriched zone contains copper sulphides such as chalcocite and covellite, overlain by copper oxides cuprite, tenorite and even native copper with or without the presence of more exotic copper sulphates (brochantite, antlerite). If the host rock is carbonate-bearing (marble), the formation of copper carbonates (malachite, azurite) is likely. The formation of chrysocolla, a hydrous and amorphous copper silicate mineral in host rocks with abundant silica, is considered to be more characteristic of a mature copper oxide system.

The presence of other exotic copper minerals, such as the copper chlorides is dependent on the local climate and geology, for example, the very arid Atacama Desert, Chile.

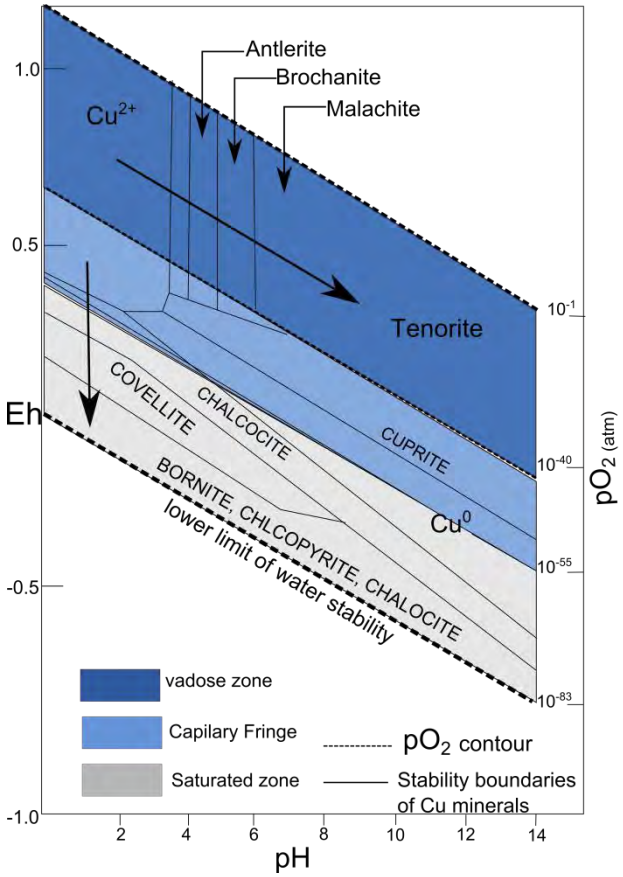

Figure 2.2: Eh-pH diagram for the system Cu-S-H_2O, showing the stability field for various copper minerals that occur within the weathering profile (adapted from Anderson, 1982; Sillitoe, 2005).

2.2 REGIONAL GEOLOGY

The sediment-hosted stratiform copper deposits within the Central African Copperbelt are hosted within Neoproterozoic meta-sedimentary rocks of the Katanga Supergroup. This is located in the ~800 km long Lufilian Arc that spans the border of Zambia and the Democratic Republic of Congo (DRC) (Figure 2.3) (Kampunzu and Cailteux, 1999).

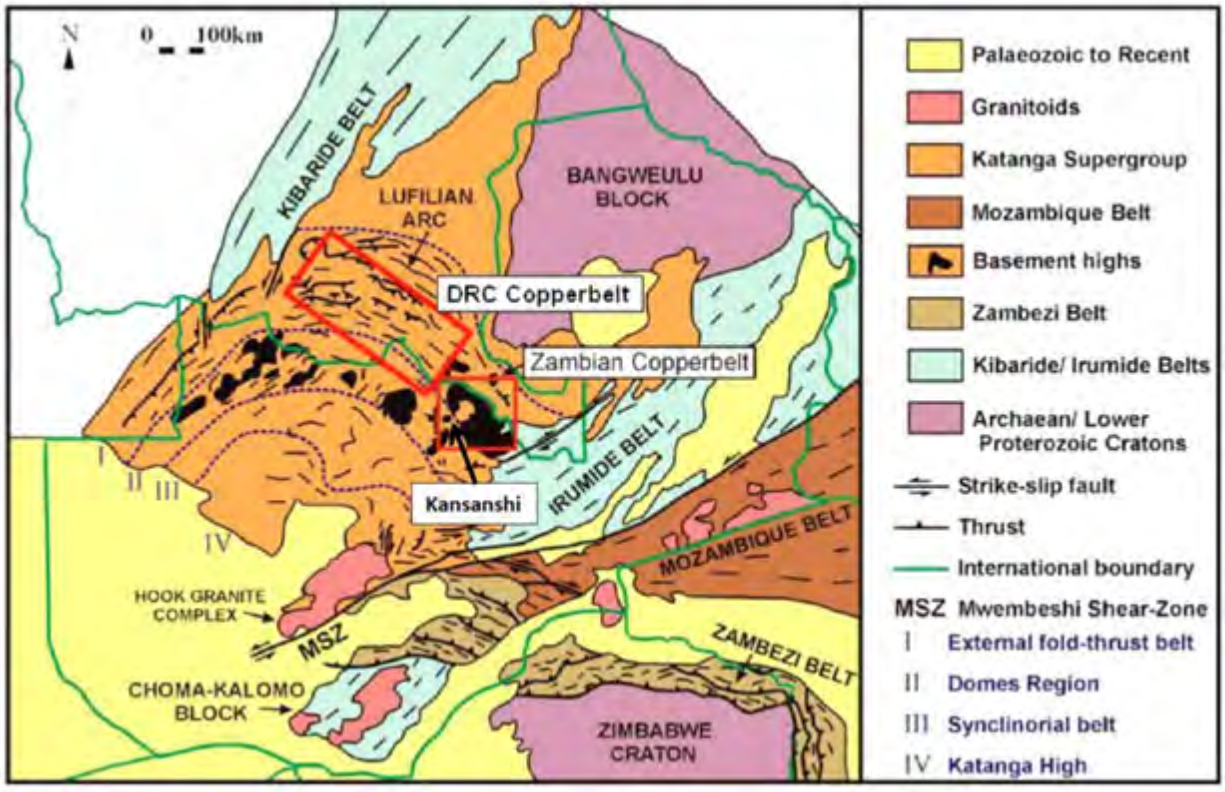

Figure 2.3: Regional geological map of the Central African Copperbelt, divided by international boundaries into Zambian Copperbelt and the DRC Copperbelt, including prominent structural geological features (modified from Porada & Berhorst, 2000). Red rectangles outline the DRC and Zambian Copperbelt.

The Katanga Supergroup is generally subdivided into three lithological groups (Figure 2.4): basal Roan, the middle Nguba (formerly Lower Kundelungu), and the Kundelungu (formerly Upper Kundelungu) at the top of the sedimentary package (Cailteux et al., 2007).

The Lufilian Arc is an arcuate-shaped fold belt of Neoproterozoic age Katangan sediments, located between the Kalahari and Congo cratons of Central and Southern Africa (Porada & Berhorst, 2000). It differs from other Pan-African orogenic belts concerning its convex shape, decreased thickness and its high metal endowment (Kampunzu & Cailteux, 1997; Porada & Berhost, 2000; Key et al., 2001; Selley et al., 2005).

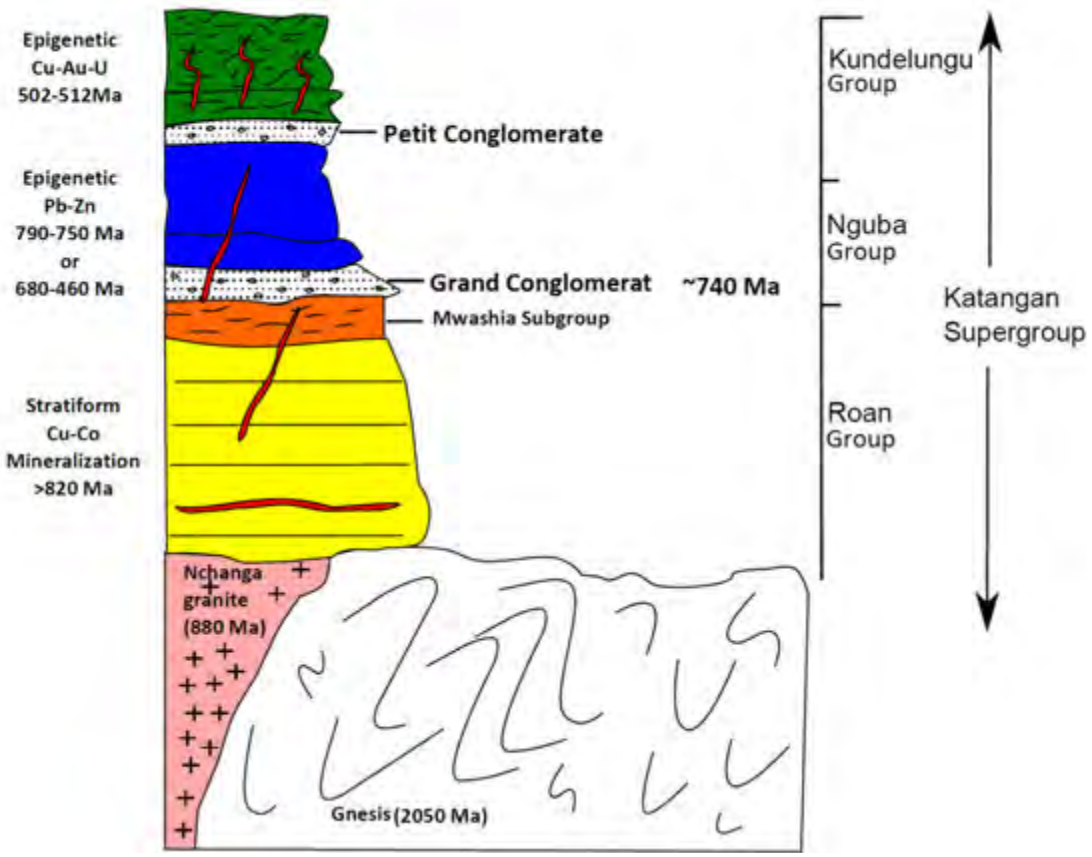

Figure 2.4: Simplified stratigraphic column of the Katangan Supergroup in the Zambian Copperbelt and the associated mineralisation styles and ages; see text for details (adapted from Robb et al., 2003; Rainaud et al., 2005).

The Neoproterozoic Katangan metasediments occur with the Lufilian arc, a fold belt, located between the Kalahari and Congo cratons of Central and Southern Africa (Porada & Berhorst, 2000). It differs from other Pan-African orogenic belts with regards to its convex shape, decreased thickness and its high metal endowment (Kampunzu & Cailteux, 1997; Porada & Berhost, 2000; Key et al., 2001; Selley et al., 2005). The Lufilian arc is one of several Pan-African orogenic fold belts that formed during the assembly of central Gondwana (Kampunzu & Cailteux, 1999; Cailteux et al., 2005; Selley et al., 2005).

The formation of the Lufilian arc is related to the ca. 560-550 Ma collision of the Kalahari and Congo cratons (Porada & Berhorst, 2000). This collision resulted in northeast- directed thrusting involving deep crustal detachments and forward propagating thrust faults (Porada & Berhorst, 2000). The Lufilian arc consists of four distinct tectonic zones from north to south as follows: 1) External Fold and Thrust Belt; 2) Domes Region; 3) Synclinorial Belt; 4) Katanga High; with these zones representing new techno-stratigraphic domains (Cailteux et al., 2007; Key et al., 2001; Porada & Berhost, 2000; Selley et al., 2005).

Located within the western forearm of the Lufilian arc is the Domes region, which is characterised by poly-deformed granitic basement inliers or domes that are unconformably overlain by deformed and metamorphosed Katangan sediments (Key et al., 2001, Barron, 2003).

Basement inliers in the Domes region are thought to represent antiformal stacks above mid-to-lower crustal ramps, indicating thicker-skinned deformation has occurred within the External Fold and Thrust Belt (Selley et al., 2005). According to Barron (2003), metamorphic grades vary within the different tectonic domains. Metamorphic grades within the Katangan metasediments are generally greenschist facies towards the External Fold and Thrust Belt (Barron, 2003). At the boundaries between the External Fold and Thrust Belt and the Domes Region metamorphic grades are usually higher, ranging from upper greenschist to amphibolite facies with the Domes region reaching the upper amphibolite facies and External Fold and Thrust Belt reaching the greenschist facies (Key et al., 2001; Barron, 2003).

2.3 KANSANSHI GEOLOGY

Mineralisation at Kansanshi occurs predominantly in undeformed, steep vein sets that crosscut Neoproterozoic rocks from the Katanga Supergroup (Torrealday et al., 2002; Broughton et al., 2002). Mineralisation was dated at 538.0 - 497.1 Ma and 1084 - 1059 Ma with the younger of the two events coincides with the Lufilian orogeny and the older event coinciding with the Irumide orogeny (Sillitoe et al., 2015) .Torrealday et al. (2000) determined the age of mineralisation at Kansanshi at 512.4 ± 1.2 Ma and 502.4 ± 1.2 Ma (Torrealday et al., 2000; Haest and Muchez, 2011). These dates suggest mineralisation took place during the waning stages of the Lufilian Orogeny during two discrete phases (Torrealday et al., 2000; Haest and Muchez, 2011). The mineralizing fluids are composed of H_2O-NaCl-$CaCl_2$-CO_2-CH_4 with temperatures between 230-310°C and pressures ranging between 1.2 and 2.5 kbar (Speiser et al., 1995; Torrealday et al., 2000).

2.3.1 Kansanshi Stratigraphy

The Kansanshi Mine Formation is hosted within the Kundelungu Group of the Katanga Supergroup (Figure 2.5) (Broughton et al., 2002). Regional stratigraphic correlations of the lithological units within the Kansanshi deposit are not clear due to metamorphic overprinting

and structural complexities, however, lithological units within the Kansanshi deposit are readily correlated into a local metamorphic stratigraphy (Broughton et al., 2002).

Contacts between lithological units are usually gradational and are commonly overprinted by hydrothermal alteration (Speiser et al., 1995; Broughton et al., 2002). Mineralisation occurs predominantly within the Kansanshi Mine Formation, which consists of five members, as follows, from the base: Lower Marble (LM), Lower Calcareous Sequence (LCS), Middle Mixed Clastics (MMC), Upper Marble (UM) and Upper Mixed Clastics (UMC) (Figure 2.5) (Broughton et al., 2000; Torrealday et al., 2000; Haest & Muchez, 2011).

These members consist of a sequence of marble, calcareous biotite schists, graphitic phyllites and knotted schists (Figure 2.5). The phyllites and calcareous phyllites are dark grey to black in colour, depending on the graphite content. The mica-garnet knotted schist and biotite schist also contain graphite with the amount of graphite present correlating to the degree of schistosity in the rock. Garnet produces a retrogression assemblage of quartz, chlorite, mica and calcite (Broughton et al., 2000).

Compositional banding is commonly displayed within the knotted schist but absent within the biotite schist. Marbles are grey with variable grain size and consist of calcite and dolomite alterations, plagioclase, scapolite, mica, graphite and pyrrhotite in varying amounts (Broughton et al., 2000). According to Kribek et al. (2005), the average organic carbon contains for unaltered and altered phyllites are 0.52 % and 0.08 %, respectively.

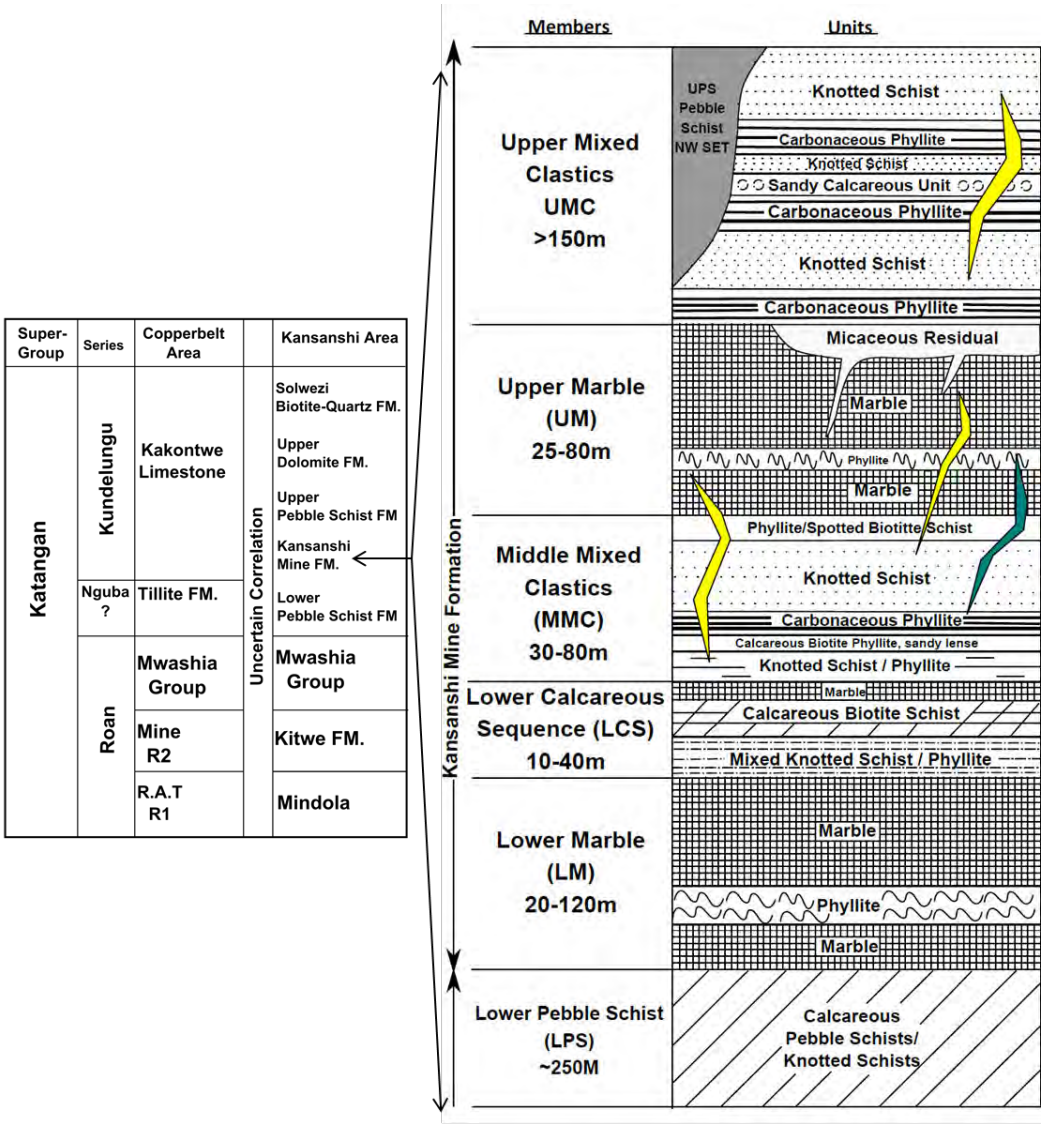

Figure 2.5: The position of Kansanshi Mine Formation within the Katangan Supergroup, including the stratigraphy of the Kansanshi Mine Formation (modified from Broughton et al., 2002). For this study, the blue structures with the stratigraphy represent breccia "4800" zone and the yellow structures represent the quartz-carbonate veins that cross-cut the Kansanshi stratigraphy.

2.3.2 Kansanshi Structural Geology

The deposit is located along a broad NW-SE trending anticline, known as the Kansanshi Anticline (Figure 2.6) (Torrealday et al.,2000). The NW-trending Kansanshi Antiform flanks the Solwezi Syncline to the north and is host to the Kansanshi deposit. The average trend of the antiform is about 310°. On the flanks of the antiform the rocks dip away to the NE and SW, generally at 10° to 30° (Chinyuku, 2013, Cyprus Amax, 2000). Refolding of the Kansanshi Anticline has created doubly-plunging, domed structures along the crest of the antiform.

Parasitic domal structures associated with the Kansanshi Antiform are host to the two orebodies: the Main Pit and NW pit. Three deformational events have been identified at Kansanshi beginning with deformational event (D1), which is a result of NNW-directed shorting, leading to the development of E-W- trending recumbent folds and later the NW-trending Kansanshi Antiform. D2 reflects NW -directed shorting and is responsible for the doming of the Kansanshi Antiform, which has been cut by numerous shear zones. D3 is associated with N-striking kind bands (Torrealday et al., 2000; Broughton et al., 2002).

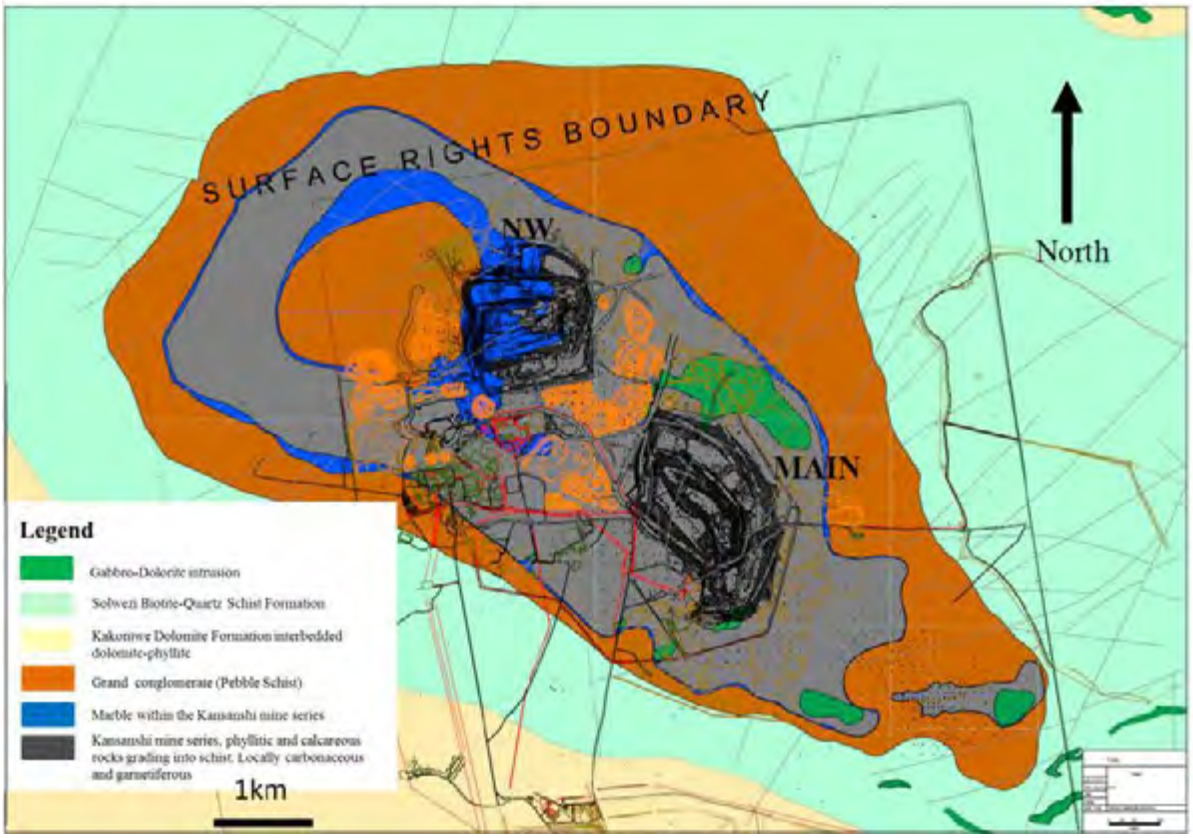

Figure 2.6: Simplified outline of the Kansanshi orebodies (Main and NW Pits), which are located along the crest of the Kansanshi Antiform, including associated domes (from Chinyuku, 2013).

2.3.3 Copper Mineralisation

Mineralisation within the Kansanshi deposit is characterized by four styles, namely, vein-hosted, sediment-hosted, breccia and supergene mineralisation (Table 2.3) (Speiser et al., 1995; Broughton et al., 2002; Kribek et al., 2005). Mineralisation is most prevalent within the clastic sedimentary rock, with the bulk mineralisation being hosted within the carbonaceous phyllite, schists and marbles of the Middle Mixed Clastics within the Kansanshi Mines formation (Figure 2.5) (Broughton et al., 2002; Gregory et al., 2005).

Table 2.3: Summary of the different styles of mineralisation present at Kansanshi, including the associated mineral assemblage and textural description**.**

Mineralisation style	Mineral assemblages	Description	Reference
Sediment-hosted	ccp-bn-py	Fine grained disseminations and stringers parallel to the bedding	Broughton et al., 2002; Kribek et al., 2005
Vein-hosted	ccp-py-po	Massive and coarse grained veins	Broughton et al., 2002; Torrealday et al., 2000
Breccia	ccp-cc-mal-ccl	Vein fragments in a matrix of dominated by carbonates	Broughton et al., 2002
Supergene enrichment	mal-ten-ccl-az	Occurs in veins, alteration haloes and dispersed throughout surrounding lithologues	Broughton et al., 2002; Koski, 2012

Sediment-hosted mineralisation

Sediment-hosted mineralisation is associated with alteration, mainly albite alteration, which is most prevalent within the clastic units (i.e. phyllites) in the UMC and MMC due to the high degree of albitization in these units. This mineralisation style also occurs within the calcareous units (LCS and LM) which are associated with alteration, but to a much lower extent in the knotted schists (Broughton et al., 2002; Chinyuku, 2013). Sediment-hosted mineralisation occurs in finely disseminated grains, thin bands and veinlets parallel to bedding/foliation. The primary sulphide mineral assemblage consists of chalcopyrite, pyrite, pyrrhotite and minor chalcocite and bonite.

Vein-hosted mineralisation

Mineralisation occurs predominantly within steeply dipping undeformed quartz-dolomite-calcite-chalcopyrite- (pyrrhotite-pyrite-molybdenite-uraninite-gold) veins, which are commonly associated with albite and carbonate (ferroan calcite and dolomite) alteration (Torrealday et al., 2000). Veins range in thickness from centimeters to meters in scale with vein density increasing towards the apex of the domal structures. The depth to primary sulphide mineralisation is fault- and fracture- controlled and highly variable, ranging from between 200 and 300m, to less than tens of meters (Hitzman et al., 2012).

The mineralogy of the mineralized veins consists of chalcopyrite-pyrrhotite-pyrite, with minor amounts of brannerite, uraninite, molybdenite and rare bornite. The gangue mineralogy is characterized by quartz, ferroan dolomite, ferroan calcite, rutile and biotite. Principle Cu-sulphide mineralisation occurs within three undeformed, high-angle vein sets and their associated alteration haloes. These vein sets crosscut all earlier mineralisation stages and occur in three overlapping stages (Speiser et al., 1995; Broughton et al., 2002; Haest and Muchez, 2011).

Within the Main pit the stage one vein set is characterized by quartz-carbonate-sulphide veins with N-S orientation, stage two by uranium-rich carbonate-sulphide veins with a NNE-SSW orientation and stage three by radial sulphide vein swarms surrounded by alteration haloes that appear to be confined to the Middle Mixed Clastics (Broughton et al., 2002; Haest & Muchez, 2011). Stage one and two vein sets have similar mineralogy with high chalcopyrite abundances and minor amounts of molybdenite, whereas stage three vein sets have minor amounts of chalcopyrite, higher amounts molybdenite and significant proportions of monzanite and brannerite (Torrealday et al., 2000; Broughton et al., 2002).

Within the Northwest pit, veining is denser, the veins are wider and the nature of mineralisation consists of coarse-grained chalcopyrite within quartz-carbonate veins. There are three main vein sets with the following orientation in the Northwest Pit: most common a vein set with a north-south orientation, a second set with an E-W orientation and a third set with WNW orientation. This style of mineralisation is commonly associated with alteration haloes. The most common type of alteration is albitization and bleaching of the host rocks. The veins are surrounded by albite, ferroan dolomite, ferroan calcite, quartz, and green mica (vanadium-rich muscovite) (Torrealday et al., 2000; Broughton et al., 2002).

Breccia-hosted and supergene mineralisation

The breccia-hosted and supergene mineralisation have been placed under one heading because the genesis these two mineralisation styles is poorly understood and beyond the scope of this thesis. All previous mineralisation styles have been overprinted by later supergene processes. This process results in the formation of a variety of copper oxides, secondary copper sulphide and iron oxyhydroxide mineral assemblages, resulting in the overall enrichment of the Kansanshi ore-body.

Primary sulphide mineralisation at Kansanshi is closely associated with veining and faulting, resulting in the movement of meteoric water through these openings and allowing for local oxidation to depths greater than 200m (Broughton et al., 2002). The weathering profiles along these structures have varying widths, depths and complex ore mineralogy.

The weathering profile is divided into the following zones: Upper Leached Zone, Oxide Zone, Transition/Mixed Zone and Primary Sulphide Zone. The Upper Leached Zone consists of a limonitic matrix of smectite clays, iron oxides and hydroxides. It contains little to no copper besides refractory cupriferous goethite and minor soluble copper (Broughton et al., 2000).

The Oxide Zone contains the most important acid soluble copper oxides; malachite and tenorite, and to a lesser extent azurite, cuprite and chrysocolla. Oxide mineralisation occurs in veins, alteration haloes and dispersed throughout the surrounding lithologies, with larger diffuse margins than the primary sulphide zoning due to the lateral and vertical mobilization of the copper minerals during weathering (Broughton et al., 2000). Gangue minerals are predominantly smectite clays, calcite, quartz, carbonates, iron oxides and hydroxides. In general the oxide zone tends to follow the morphology of the primary sulphide vein sets (Broughton et al., 2000).

The Transition/Mixed Zone is a zone of mixed mineralisation, occurring between the base of complete oxidation and the top of the fresh sulphide zone, comprising a mixed mineralogy containing primary copper sulphides, secondary enrichment copper sulphides and copper oxides (Broughton et al., 2000). The copper ore mineralogy within this zone is complex and includes primary sulphides, secondary copper sulphides and copper oxides. Primary sulphides include partially weathered chalcopyrite and rare bornite; secondary copper sulphides such as chalcocite, digenite, covellite, and copper oxides such as malachite and tenorite (Broughton et al., 2002; Köttgen & Bastin, 2009).

Brecciation is structurally controlled and corresponds to zones of greater intensity of veining and fracturing, which provide pathways for the movement of meteoric fluids. The breccias usually consist of angular to moderately rounded fragments, altered wall rock and mineralized vein fragments in a matrix dominated by ferroan dolomite or calcite, and to a lesser extent albite, quartz, minor rutile and rare chalcopyrite. This style of mineralisation occurs mainly within the Main Pit, where mineralisation is present throughout the stratigraphic units, reaching to the Lower Pebble Schist. This led to the development of wide zones of altered and oxide mineralized wall rock in addition to the pre-existing primary sulphide veins (Broughton et al., 2002).

Mineralized breccias occur in oxidized and supergene-enriched horizons which display a complex array of secondary copper-oxide minerals including malachite, azurite and chrysocolla. One of the main developments of breccia mineralisation occurs in the Main pit and is known as the 4800 zone; a linear N-S trending structure interpreted to represent a strike-slip fault.

2.3.4 Gold mineralisation

Kansanshi has a significant gold tenor compared to other deposits within the Copperbelt. Gold mineralisation occurs mainly within the sulphide-quartz veins, that cross-cut the deposit. Gold associated with sediment-hosted mineralisation is less common and is hosted within the carbonaceous phyllites (Chinyuku, 2013). Later supergene processes have led to the redistribution of gold into the mixed and oxide zones of the weathering profile. Consequently, the oxide and mixed ores make the largest contribution to the amount of gold produced (Chinyuku, 2013). Mineralogical investigations by GoodShip (2010) revealed that gold occurs as free grains in association with melonite ($NiTe_2$) and microfractured pyrite intergrown with chalcopyrite (GoodShip, 2010).

2.4 GEOMETALLURGY AND PROCESS MINERALOGY

2.4.1 Geometallurgy

Geometallurgy is considered a relatively 'new' science in the area of economic mineral extraction; however, geometallurgy practice in its various forms has been around since the late 1980s, with the general use and understanding of the term being known since 2003 (Baum et al., 2004; Williams, 2013). The key driving force for the emergence of geometallurgy was the realization that ore variability has a significant effect on metallurgical performance (Williams, 2013). The impact of ore variability on processing is well documented in the literature by authors such as Petruk et al. (1991) and Wright (1993) illustrating how ore variability could adversely impact processing performance if not adequately managed (Petruk et al., 1991; Wright, 1993; Dobby et al., 2002). Geometallurgical methodologies directly address the issue of ore variability during processing by developing geometallurgical models which allocate different characteristics of the ore-body into the block model, aiding in forecasting the main performance outputs (Bulled and Mcinnes, 2006; Williams, 2013). These models can also be adapted to address specific issues and evolve to accommodate shifts in plant operations.

The value of a geometallurgical approach is its ability to identity and quantify sources of error to evaluate the accuracy of the plant design and product forecast (Bulled and Mcinnes, 2006).

The success of a geometallurgical approach relies on availability of representative and comprehensive mineralogical data, as mineralogy is the primary controlling factor affecting metallurgical performance (Hoal, 2008; Ehrig, 2011; Williams et al., 2013). Hoal (2013) reviewed the importance of mineralogical inputs in geometallurgical programmes, commenting on the relationship between ore formation and ore extraction. This relationship is demonstrated in a paper by Oyarzún and Arevalo (2011) which showed that there is a link between grain boundary texture, surface energy and the Bond Work Index. Higher surficial energies result in a higher Bond Work Index, which impacts the amount of energy required for breakage during comminution (Oyarzún & Arevalo, 2011; Hoal, 2013).

The overall aim of geometallurgy is to reduce operation risks by understanding and managing ore variability within the deposit. To accomplish this, clearly an understanding of the geology, mineralogy and metallurgical implications of the ore is required (Dominy, 2011). The reliance of geometallurgy on comprehensive mineralogical data and an understanding of the distribution and behaviour of the ore have made process mineralogy a key tool in its successful application (Figure 2.7) (Baum et al., 2004; 2014; Lotter et al., 2011; Hoal, 2013; Williams, 2013).

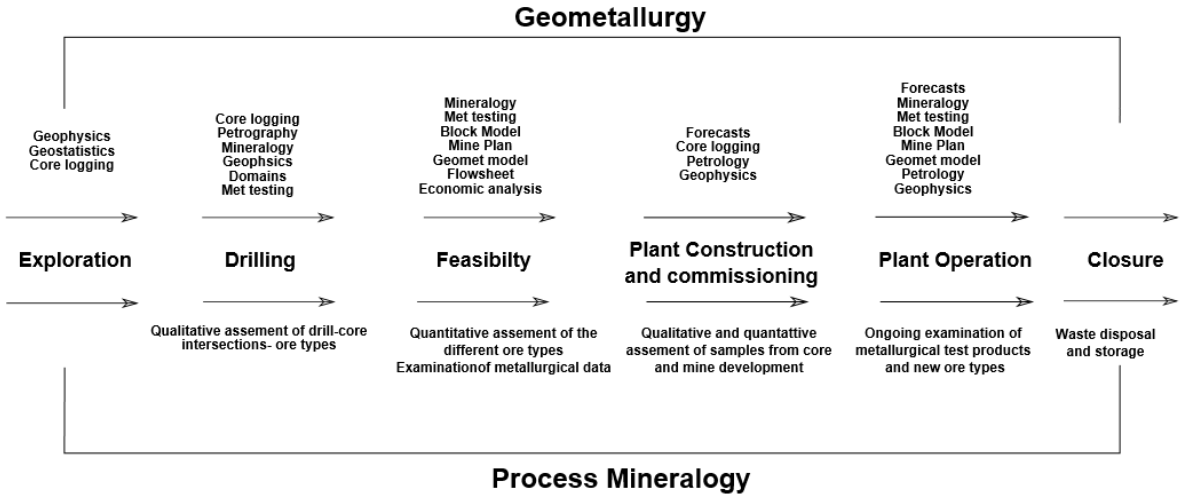

Figure 2.7: The geometallurgical and process mineralogical contribution into the mining value chain (adapted from Brough, 2008; Williams, 2013).

2.4.2 Process Mineralogy

The first application of process mineralogy in the literature was presented by Irving (1906) and Gaudin (1939). The field of process mineralogy has evolved over time and now combines different fields of study. Henley (1983) describes process mineralogy as the

application of mineralogical information to predict metallurgical performance, adding that if process mineralogy is to be effective, the mineralogist must have comprehensive mineralogical data and a good understanding of what this information means to the metallurgist (Henley, 1983; Baum et al., 2004; Schouwstra and Smit, 2011). Henley's work was aimed at developing a flowsheet that spanned the length of the project from exploration and drilling, preliminary metallurgical testing, pilot plant testing, plant design and engineering, plant construction and commissioning through to plant operation (Figure 2.7). The objective of this flowsheet was to produce a predictive process mineralogy model for the orebody by understanding the variation of the mineralogy through the flowsheet.

This was accomplished by merging two disciplines, mineral processing and mineralogy, whereby mineralogical information such as bulk mineralogy, liberation and gangue mineralogy would be given to the metallurgist to use in conjunction with pilot plant testing chemical data (i.e. assays) to characterize, diagnose and predict the potential performance limitations during operations (Henley, 1983; Baum et al., 2004). Henley's (1983) work, however, did not address the problems associated with lack of representative samples.

Later work by Lotter et al. (2002; 2003) and Baum (2004) has built on Henley's (1983) work by adding two additional parameters/factors to ensure the validity of the technique. Lotter et al. (2003) suggest that in order to obtain meaningful mineralogical data the different geometallurgical units – "ore type or group of ore types that encompasses a distinctive set of textural and compositional properties, which can be used to determine the processing behaviour of similar units"– must be defined (Lotter et al., 2003; Fragomeni et al., 2005; Lotter, 2011). These units are based on review of geological data including host rock, alteration, grain size, texture, structural geology, grade, sulphide mineralogy and metal ratios with focus on characteristics which are known to affect metallurgical performance (Lotter et al., 2003; 2011).

In the context of flotation the next step is to ensure representative sampling of these different geometallurgical units such that accurate diagnoses of untreated samples and/or extracted samples from the different production routes are attained (Baum, 2002; 2014; Lotter et al., 2003; 2011; Williams, 2013). According to Lotter (2011), un-oxidized drill core samples are the best representative of the geometallurgical unit they were extracted from.

This is a critical step in ensuring accuracies of data obtained from automated mineralogical techniques. Representativity is accomplished by thoroughly mixing the sample and subsequently splitting the sample into replicate subsamples using a rotatory splitter (Lotter et al., 2003; Fragomeni et al., 2005; Hoal et al., 2013).

Once the geometallurgical units are defined and representative samples have been collected, a strategic process mineralogical approach is followed to ensure accurate and meaningful mineralogical measurements are taken.

Modern Processing Techniques

The growing application of geometallurgy in the mining industry is a result of the increasing demand for sustainable and efficient mining practices. Process mineralogy is a key tool in the geometallurgical methodology used to achieve this goal; its application, in conjunction with automated mineralogy, has the potential to improve ore control and processing, leading to reduced operational costs and risks, higher recoveries and increased orebody knowledge.

Modern process mineralogy makes use of qualitative and quantitative analytical techniques including but not exclusive to: (i) X-ray diffraction; (ii) X-ray fluorescence spectrometry; (iii) electron microprobe (EPMA); (iv) automated scanning electron microscopes (MLA, TIMA and QEMSCAN) (Table 2.4). These Auto-SEM techniques can provide statistically reliable and quantitative data in a timeous manner compared to the traditional optical microscope, which is time consuming and heavily subject to human error (Gottlieb et al., 2000; Goodall et al. 2005). For the purpose of this chapter only the techniques used in the study will be covered.

X-Ray Fluorescence Spectrometry (XRF)

X-ray fluorescence spectrometry is an accurate and reliable technique used routinely for the bulk chemical analyses of major and trace elements. X-ray fluorescence spectrometry is capable of analysing elements from Beryllium (Be) to Uranium (U) in the concentration range from 100 % down to the sub-ppm-level. X-ray fluorescence spectrometry can be divided into energy-dispersive X-ray fluorescence (EDXRF) and wavelength-dispersive X-ray fluorescence spectrometry (WDXRF) (Enzweiler & Webb, 1996; Engelbrecht, 2011). The principal difference between EDXRF and WDXRF techniques is the energy (spectral) resolution. WDXRF techniques achieve resolutions between 5 eV and 20 eV, thus enabling a larger number of elements to be analysed, ranging from Beryllium to Uranium. EDXRF techniques provide resolutions ranging from 150 eV to 300 eV, permitting the analyses of elements from Sodium to Uranium.

Both technologies have similar strength in eliminating background radiation, a parameter that affects the both the detection limit and repeatability, therefore, detection limits for both technologies are similar (Enzweiler & Webb, 1996; Engelbrecht, 2011; www.skyrayxrf.com).

X-Ray Diffraction

X-ray diffraction is a versatile and inexpensive technique used for the quantification of crystalline phases and amorphous content (Macchiarola et al., 2007). This technique is commonly used in the analysis of complex ore, where twenty or more mineral phases may be present, as it is capable of quantifying and identifying minerals that other analytical tools have difficulty detecting.

In the case of copper ores, data collection is done using an X-ray diffractometer employing Co-radiation as most copper ores contain iron, chromium, manganese and cobalt. These elements cause X-ray fluorescence, which results in a high background scatter if Cu-radiation is used (Coetzee et al., 2011). Modern quantitative phase analyses are performed using the Rietveld refinement method, which utilizes the least squares approach to refine the structure of the crystal, increasing efficiency in identifying multiple phases and better dealing with other difficulties such as overlapping reflections and high background (Connolly, 2010; Lotter, 2011).

Electron Probe Microanalyser (EPMA)

The electron probe microanalyser (EPMA) is a tool that combines the capabilities of a scanning electron microscope (SEM) with that of an X-ray fluorescence (XRF) spectrometer with the added features of fine spot focusing (~ 1µm), optical microscope imaging and precision-automated sample positioning (Pownceby, 2006). The EPMA is capable of achieving such high analytical precision with lower detection limits (ppm) and higher peak resolutions as it is equipped with high-resolution wavelength dispersive spectrography (WD) and low resolution ED spectrometers to detect X-rays. In ore characterisation and processing EPMA provides quantitative data that can be used in a host of applications including the location of valuable elements within host mineral phases, trace elements abundances, individual mineral phase/s identification, textures and compositional variability with mineral phases (Pownceby et al., 2007; Lotter, 2011). The introduction of mapping facilities with new EPMAs allows for the mapping of element distributions which can provide absolute elemental concentration and also the spatial distribution of elemental concentrations (Pownceby et al., 2007).

Automated SEM (QEMSCAN)

The QEMSCAN (Quantitative Evaluation of Minerals By Scanning Electron Microscopy) is an automatic image analysis system that enables quantitative chemical analysis of coarse and feed samples and the generation of high-resolution false coloured mineral images and maps (Gottlieb et al., 2000). QEMSCAN makes use of a scanning electron microscopy platform (SEM) with an electron beam source in combination with energy-dispersive X-ray

spectrometers (EDS) (Ayling et al., 2012). In doing so, mineral identities can be assigned to each measurement point by comparing the EDS spectrum (i.e. chemical composition) and BSE signal against a mineral Species Identification Program (SIP) that is defined by the user (Gottlieb et al., 2000; Ayling et al., 2012).

Measurement types can be divided into three groups based on those using linear intercept or particle mapping. Bulk Mineral Analysis (BMA) is performed using the linear intercept method and provides statistically representative data on the modal mineralogy. Particle mapping modes, including Particle Mineral Analysis (PMA), Specific Mineral Search (SMS) analysis and Trace Mineral Search (TMS) analysis, provide detailed mineralogical information on mineral liberation, associations and textures. The particle mapping modes of measurement can also be used to derive theoretical grade versus recovery graphs. The Field Scan (FS) mode provides detailed mapping of larger samples such as drill cores that are mounted into a polished thin section. It collects a chemical spectrum at a set interval within the field of view (Gottlieb et al., 2000; Ayling et al., 2012).

Other SEM-based automated mineralogy based instrumentation on the market that can have similar applications are Carl Zeiss Mineralogic, FEI mineral liberation analyser (MLA) and the TESCAN Integrated Mineral Analyser (TIMA).

Table 2.4: Techniques used for ore characterisation.

Tools	Analysis	Outcome
Optical microscopy	Qualitative	• Mineralogy and texture
XRD	Semi-quantitative	• Bulk mineralogy
EPMA	Quantitative	• Mineral chemical compositions • Trace element abundance
QEMSCAN	Quantitative	• Modal mineralogy • Element deportment • Grain size distribution • Liberation characteristics
Batch flotation	Grade and Recovery	• Grade vs. Recovery curves • Solids vs. Water curves
Chemistry	Element percentages	• XRF: Oxide wt. % • Leco: Sulphur wt. %

Application of Process Mineralogy on Copper Ores

Process mineralogy has been used to solve and understand problems that occur throughout the mining cycle (Gaudin, 1939; Frew & Davey, 1993; Schouwstra et al., 2010; Hunt et al., 2011). Cropp et al. (2013) discuss examples of porphyry copper deposits where process

mineralogy has been used to evaluate the effect textural variations and gangue mineralogy have on copper recovery by flotation. Emphasis was put on how grain size, liberation, association and elemental distribution affect copper recovery and in addition the implications of these parameters on overall plant planning and operations.

Other aspects of processing have been covered elsewhere in the literature, such as comminution (Wills, 1990; King, 1994) and hydrometallurgy (Baum, 1999; Allen et al., 2007). Two case studies are reviewed here to illustrate its application: the first relates to the use of process mineralogy on a porphyry copper ore and the second relates to its application on a Copperbelt ore.

Case Study: Low Chalcopyrite Recoveries at KUCC

An investigation by Bradshaw et al. (2011) showed how process mineralogy was used to identify the cause of low chalcopyrite recoveries at the Kennecott Utah Copper Concentrator (KUCC). Two ores were compared: monzonite, a common porphyry ore with typical Cu and Mo recoveries, and limestone skarn ore (LSN) with poor Cu-Mo recoveries.

The mineralogical investigation looked at the nature and composition of the textures and gangue minerals, and the grain size distribution of the milled product. The tools used for this investigation include optical microscopy, EPMA, QEMSCAN and MLA.

The results showed that blending the monzonite with the LSN resulted in a higher proportion of Mg- and Ca-bearing minerals present with the feed ore. The primary Mg-bearing minerals within the monzonite ore are chlorite, biotite and phlogopite, which are evenly distributed across all size fractions. Talc, amphibole and pyroxene are the primary Mg-bearing minerals present with the LSN with the -20 μm fraction containing a higher proportion amphibole. The higher percentage of Mg-bearing minerals within the -20 μm fraction is thought to be the cause of the surface coating on the copper minerals, resulting in the overall decrease in chalcopyrite recovery to the flotation concentrate across all size fractions (Figure 2.8).

Prior to batch flotation, test assaying of the ores showed that both ore types had comparable amounts of total copper; however, LSN displayed lower theoretical copper grades and recoveries compared to the monzonite ore (Figure 2.8).

The particle size distribution curve for LSN ore showed an uneven particle size distribution with higher amounts of material reporting to the coarser and finer size fractions. QEMSCAN data showed that LSN had a higher percentage of the copper minerals reporting to the fines and a lower degree of liberation in the coarser fractions compared to the monzonite ore, suggesting that a larger amount of the Cu-bearing minerals remained locked within the

coarser grains. These results were supported by the lower recoveries in the flotation concentrate (Figure 2.9).

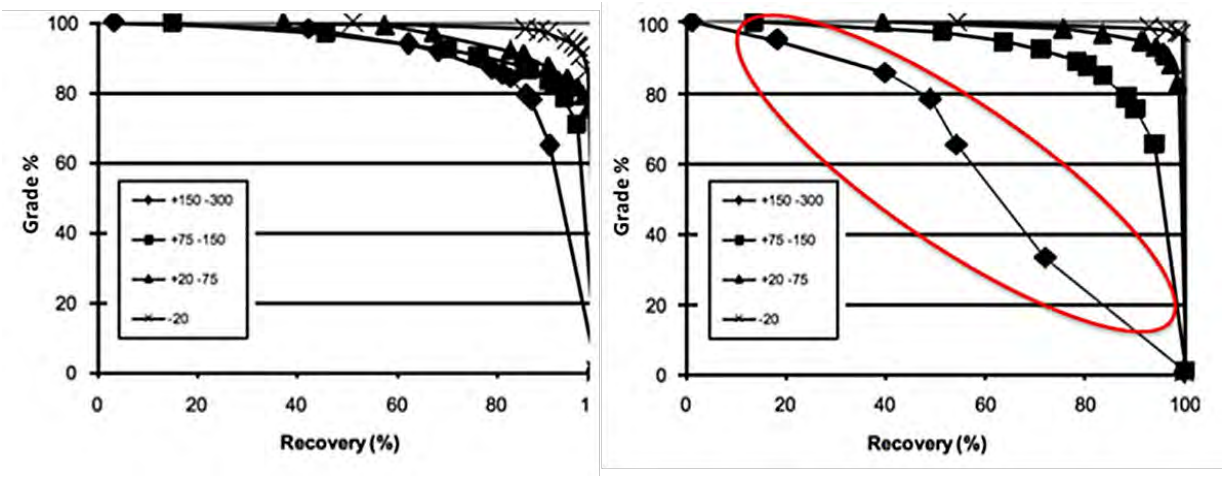

Figure 2.8: Theoretical grade-recovery curves of monzonite porphyry ore (left) and a limestone skarn (LSN – right). The coarse size fraction in the LSN displays a lower grade-recovery curve (circled in red) than the equivalent fraction in the monzonite ore due to the finer Cu-minerals remaining locked (after Bradshaw, Triffett and Kashuba, 2011; Cropp et al., 2013).

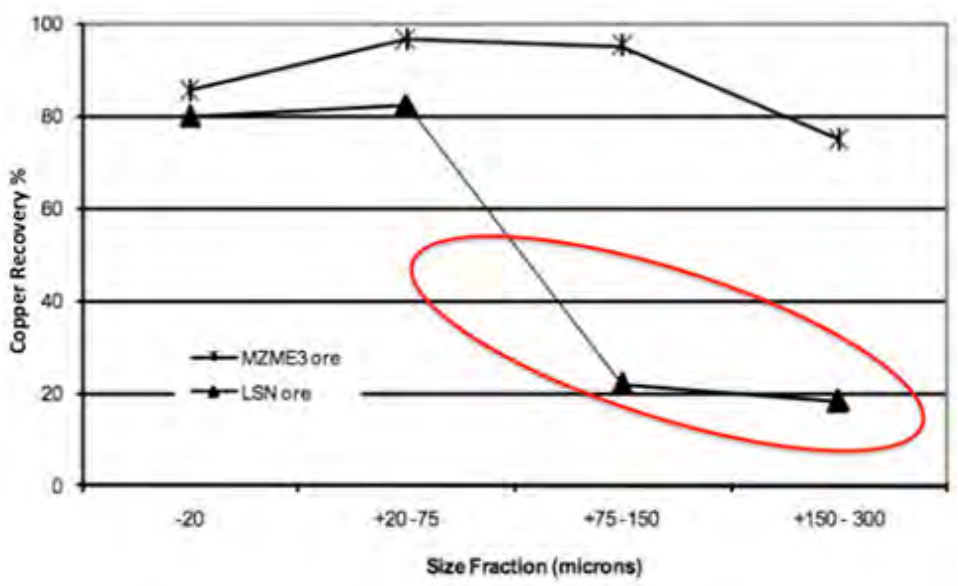

Figure 2.9: Actual recovery to flotation concentrates by size fraction of the monzonite porphyry ore (MZME3) and the limestone skarn ore (LSN) (from Bradshaw et al., 2011; Cropp et al., 2013).

Case study: Refractory Ore at Nchanga Mine

The Nchanga Cu-Co mine is located in the Northern Zambian Copperbelt, north of the town of Chingola (McGowan et al., 2003). The refractory over at Nchanga has been stockpiled over several decades as it was not economically viable to process these ores as they require an additional processing step and, as consequence, higher production costs. There was an estimated 150 Mt of ore in the stockpiles with average Cu grade at 0.87 wt.% valued at approximately US$11.5 billion as of 2008. Sikazwe et al. (2008) investigate the mineralogy of the refractory ore at Nchanga using process mineralogical techniques on a total of eleven samples; eight from the stockpile and three from drill core samples. Optical microscopy showed that fine grained chalcopyrite, bornite and malachite were not the causes of the refractory nature of the ores studied.

EPMA revealed that most of the copper occurred in solid solution within micas. Application of automated SEM techniques has provided a detailed understanding of the distribution of copper in these refractory ores. The investigation revealed that biotite and/or phlogopite is the main source of refractory copper in the stockpiles (Figure 2.10). Malachite and pseudomalachite were an additional source of copper in some of the stockpile samples; however, malachite and pseudomalachite are associated with bands of kaolinite and goethite rims, which can hinder usually easily recoverable copper. The presence of copper in mica is the principal reason for the refractory nature of the ores and they would require additional processing to recover. Cu-bearing goethite is present in most of these samples, but typically it contains <0.1 per cent Cu.

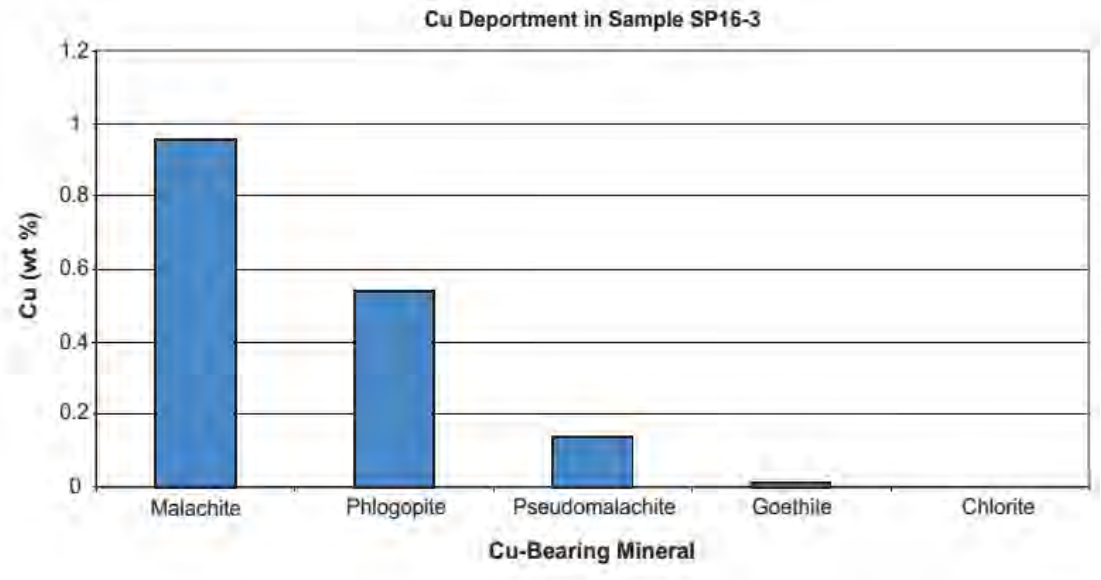

Figure 2.10: Copper deportment in SP16-3 utilizing microprobe data for phlogopite and goethite, showing phlogopite as the main refractory Cu-bearing phase (from Sikazwe et al., 2008).

2.5 MINERALS BENEFICATION

2.5.1 Mining of Copper Ores

Copper ores are primarily extracted through open-pit and underground mining. The method of extraction applied is dependent upon the characteristics of the ore body and its geographical location. Open-pit mining is the most common method used for copper extraction. Open-pit mining is associated with low-grade high tonnage, massive or steeply dipping ore-bodies, such as porphyry, skarn, sediment-hosted and epithermal deposits. Underground mining is associated with high grade, small or deep deposits with a shallow dip. Underground mining is less common due to the higher associated costs and safety issues. Some of the world's largest open-pit mining operations are associated with copper deposits such as the Escondida copper mine in Chile; the world's largest copper producing mine as of June 2013. It generates an output of 1.1 million tons (Mt), accounting for 5% of the global copper production (www.mining.com; www.mining-technology.com).

2.5.2 Comminution

In order to separate the minerals from unwanted gangue minerals it is necessary to break down the rock using crushing and grinding to liberate the valuable minerals from the composite particle so that they are partially or fully exposed (Wills, 1997; 2006). This process of size reduction is called comminution. The crushing and grinding of the ore will produce particles of varying grain sizes and degrees of liberation. Liberation is defined as the degree to which a valuable mineral is exposed from the gangue, based on the volume percent of the mineral grain in a particle (King, 1994). With the use of classifiers, any particles that do not fall into the required target particle size for physical separation or chemical extraction are returned to the crushing or the grinding circuit (Wills, 1997; 2006). Comminution is necessary as most minerals typically occur as fine grained dissemination that is intimately associated with the gangue minerals, so before any further concentrating can be done the valuable mineral must be liberated from the composite particle (Wills, 1997; 2006).

Comminution in the mineral processing plant is carried out in a sequential manner using crushers and screens followed by grinding mills and classifiers. The first stage in comminution is blasting, where explosives are used to separate the ore from the host rock.

The excavated ore is transported via scrapers, conveyers and ore carriers to the processing plant. Crushing is a dry process in which run-of-mine material is reduced to a size fraction, ranging between 10 to 30mm in diameter, for the easy transportation of the material along the conveyers to the secondary circuits. This is accomplished by compression of ore against rigid surfaces (Davenport et al., 2002; Wills, 1997; 2006). Grinding is usually a wet process and provides the slurry feed for flotation. It is accomplished by a combination of impact and abrasion of the ore in rotating cylindrical steel vessels (Wills, 2006).

The vessels contain free-moving stainless steel media, such as rods, balls or pebbles that break down the ore to a particle size suitable for effective flotation (Wills, 1997; 2006). The feed from the grinding circuit is directed to the hydrocyclone classifier that is used to return coarse material back to the ball or rod mill for further grinding (Wills, 2006). The overflow product, usually particles of size less than 150 μm, is sent to the flotation circuits. The underflow product, with particle size greater than 150 μm, is redirected to the milling circuit where the ore is reground (Lestage at al., 2002; Wills, 2006). The concentrating of the valuable mineral can take place after the ore is crushed, ground and classified into the required particle size distribution. There are a number of different techniques that can be implemented in concentrating the valuable minerals such as gravity and dense medium separation, magnetic separation and froth flotation. These techniques make use of the differences in physical or chemical properties of the valuable and gangue minerals. For the purpose of this study only froth flotation will be discussed as it is the most widely used technique in extractive metallurgy and is the most effective method for the extraction of sulphide minerals from low-grade and complex orebodies with a cut-off grade of 0.2 % Cu (Parekh & Miller, 1999; Wills, 2006).

2.5.3 Froth Flotation

Froth flotation is a complex physico-chemical process that utilizes the differences in surface properties by using air bubbles in a flotation cell to separate valuable minerals from unwanted gangue minerals (Wills, 2006; Rahman et al., 2012). This is accomplished through the chemical alteration of mineral surfaces with the use of reagents to enhance the hydrophobicity of certain valuable minerals (Klassen & Mokrousov, 1963). The flotation process contains two distinct zones — the pulp and the froth zone. The pulp zone is where mineral recovery occurs through particle-bubble collision and attachment. The froth zone lies above the pulp phase and allows for the concentration and separation of the valuable mineral from the slurry.

In the froth flotation cell, air bubbles are passed through the slurry from the bottom of the cell (Figure 2.11). The passing air bubbles collide and selectively attach to the hydrophobic particles in aqueous slurry. The bubble-particle aggregate rises to the surface from the pulp phase into the froth layer, which is concentrated in valuable minerals that are removed from the cell by a scraping mechanism (Wills & Napier-Munn, 2006). Particles which have reported to the froth phase by mechanisms other than true flotation may report back to the pulp zone.

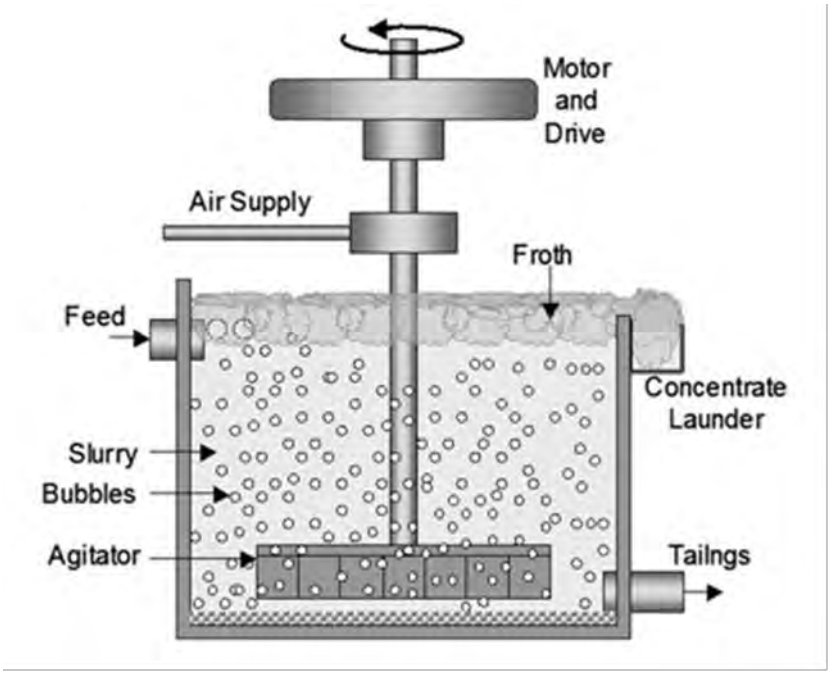

Figure 2.11: Simplified representation of flotation mechanism (Grewal, n.d).

The hydrophilic particles (i.e. gangue minerals) that do not get attached to the air bubble remain in the liquid phase and are removed as tailings (Lynch et al., 1974; Fuerstenau et al., 1985; Harris et al., 2002 Wills, 1997; Shean & Cilliers 2011). Mineral recovery can occur by true flotation or through entrainment. True flotation is the most common mechanism for mineral recovery, whereby reagents are added to the system to enhance the differences in mineral surface properties. It is directly affected by chemical changes to the system, such as the addition of collectors and depressants. Entrainment is the recovery of particles in the water moving from the pulp phase into froth phase. Entrainment is non-selective and this mechanism, together with entrapment, results in the recovery of both valuable and gangue minerals to the concentrate.

The flotation system is affected by approximately 25 parameters. Klimpel (1984) divided the major variables in flotation into three main groups, as follows: chemistry, equipment and operations; illustrated in (Figure 2.12). In this study of copper sulphide flotation, the focus is on copper sulphide mineralogy and how it affects flotation performance.

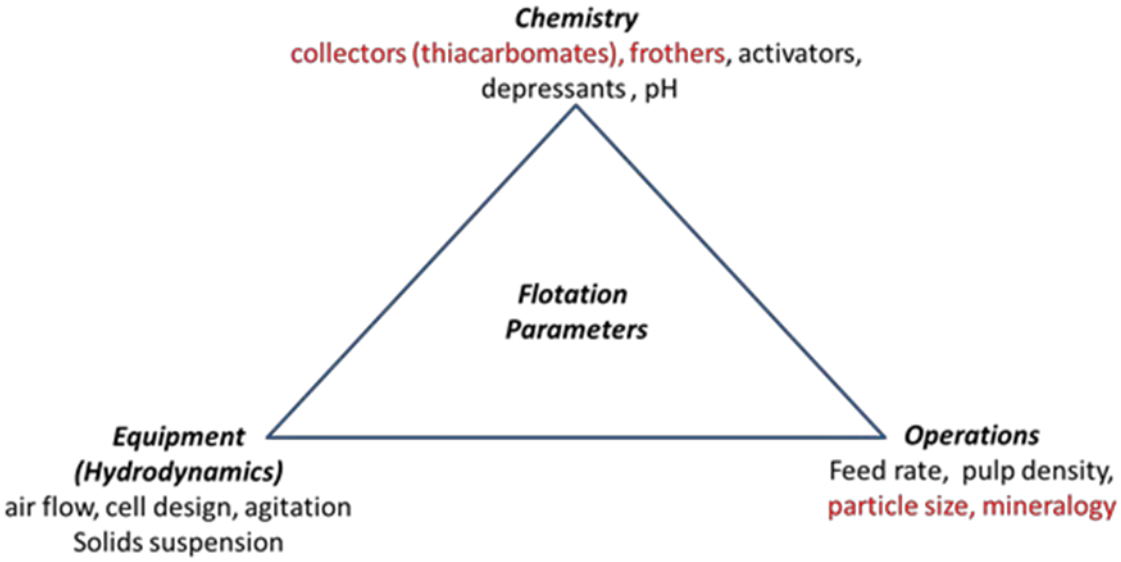

Figure 2.12: Summary of the variable active during flotation (adapted from Klimpel, 1984; 1995). Variables shown in red are the focus of this investigation.

Under the heading “operational parameters”, Klimpel (1984) included factors such as pulp density, feed rate, and ore mineralogy and particle size. The effect of particle size on flotation performance was first investigated by Gaudin (1931). Over the years the subject had been covered extensively by authors such as Tragar (1981), Feng and Aldrich (1999), and Jameson (2010). It was established that the flotation rate constant was dependent upon the particle size and that there is a size range in which mineral recovery is optimum and beyond this size range recovery drops dramatically; this behaviour is represented graphically in Figure 2.13.

The particle size fractions have been classified into three groups: fine, intermediate and coarse particles, with each group behaving differently during flotation (Gaudin et al., 1931; Gontijo et al., 2007; Jameson, 2012). The flotation of fine particles is determined by the efficiency of particle-bubble collision, which is poor due to the low inertia of fine particles (Pease et al., 2006; Miettinen et al., 2010). Compared to the flotation of coarse particles that have a high inertia where flotation is governed by ability of the bubble-particle aggregate to remain attached (Schulze, 1977; Jameson, 2010).

In high turbulence environments the effect of bubble-particle detachment of coarse particles during flotation is increased (Rahman et al., 2012). In addition, the poor liberation of the minerals also contributes the low recovery of coarse particles (Rao et al., 2011).

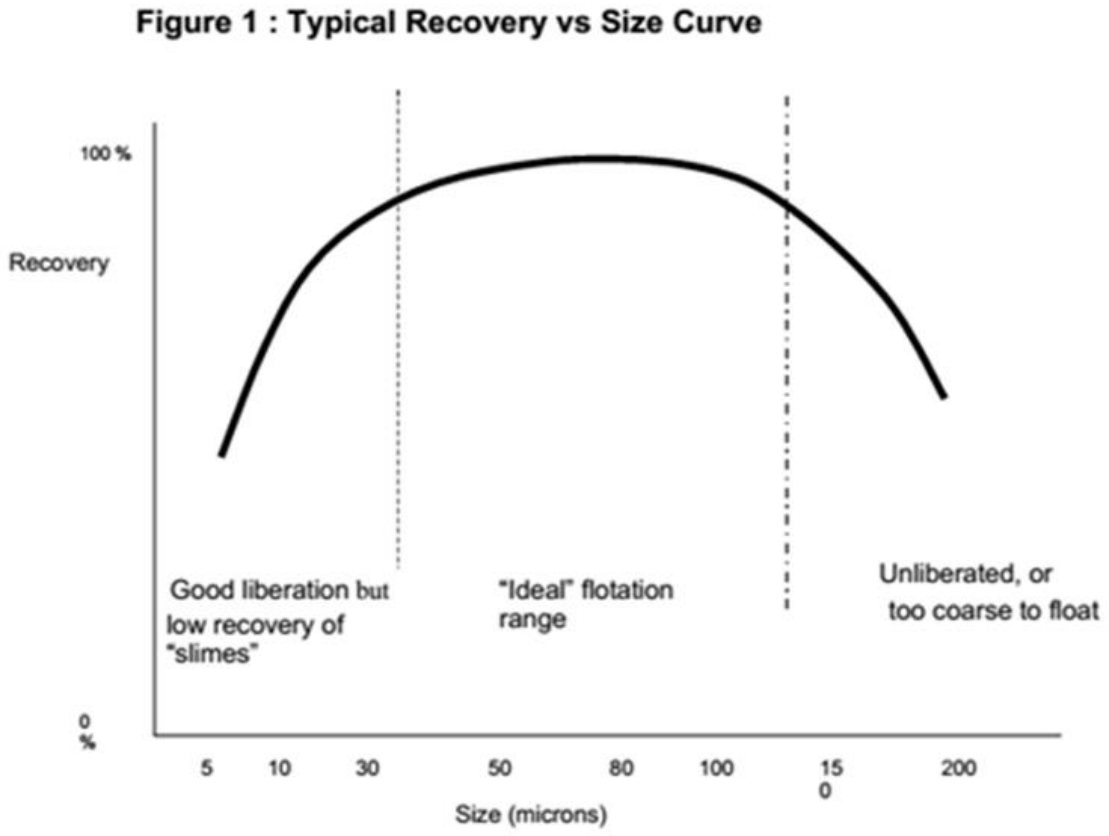

Figure 2.13: The relationship between particle size and recovery (from Pease et al., 2004).

In order to selectively recover the valuable minerals from gangue minerals, the ore needs to be sufficiently liberated. However, in practice 100% liberation is not achieved, producing particles containing locked gangue and valuable minerals, known as composites (Sutherland, 1989). The efficiency of composite particle flotation is dependent mainly on the degree of liberation and the type of locking texture as in simple or complex locking texture (Wen, 1992; Wang, 2010). Simple locking texture is defined as only having one interface between mineral phases in a locked particle and complex locking texture referring to particles that have more than one interface between phases (Wang, 2010; Fosu et al., 2015).

Coarse particle flotation

Communition is the most energy-intensive process in mining, accounting for an average of 36 % of energy consumption on gold and copper mines, and between 35 to 50 % of total operational costs (Benzer, 2005; Olubami et al., 2007; Ballantyne & Powell, 2014). Therefore, it is imperative to reduce energy consumption to ensure the profitability of a mine. This can be achieved by increasing the upper particle size limit required for flotation, which will reduce the grinding energy consumption and save costs. Sutherland (1989) also showed that valuable minerals locked within coarse composite particles make the largest contribution to the overall losses in recovery within many flotation plants. Work by Farrokhpay et al. (2011) demonstrated that increasing the upper size limit of flotation to 250 µm from 150 µm is possible without significant copper loses occurring provided the ore is well liberated. The studies reference above show that if the upper size limit required for flotation can be increased, this would result in higher throughput, decrease in copper losses to the tails and overall a more eco-efficient flowsheet.

According to Jameson (2010), sulphide minerals with particle sizes that range between 20 and 200µm float most efficiently during flotation; outside of this range recovery drops significantly (Figure 2.13). It has been repeatedly cited that mineral particle sizes outside this range are rarely recovered in a conventional flotation cell and as a result lost to the tailings (Awatey et al., 2013; Gontijo et al., 2007; Jameson, 2010). Mechanical flotation cells utilize a rotatory impeller to generate air bubbles and to keep the particles in suspension. Agitation caused by this mechanism results in a highly turbulent environment, which decreases coarse particle recovery (Xu et al., 2012; Govender et al., 2012) as optimal recovery of coarse particles occurs at a low froth depth and when turbulence at the pulp-froth phase is minimal (Jameson, 2010).

Rahman et al. (2012) investigate the effect of different flotation variables on the recovery of different silica particle fractions in the froth and pulp. It was shown that coarse particles are more prone to detachment and their flotation behaviour is highly sensitive to changes in operating conditions; increased concentration of fines enhances coarse particle flotation and high collector dosages have an adverse effect on coarse particle recovery as the froth is destabilized. The froth zone therefore acts as a major obstacle in the recovery of coarse particles (Rahman et al., 2012).The key issue limiting coarse particle recovery in a conventional float cell is the inability for the particles to remain attached to the bubble (Awatey et al., 2013; Jameson, 2010; Xu et al., 2012). Coarser particles are strongly affected by inertia and in a turbulent environment the shear flow field is increased and so is the energy of dissipation (Jameson, 2010).

An increase in energy dissipation results in a decrease in coarse particle recovery due to the increase in shear field stress acting on the particle attached to the bubble, thereby decreasing the stability of the bubble-particle aggregate (Xu et al., 2012; Govender et al., 2012). A recent study by Farrokhpay et al. (2011) showed that the flotation of coarse particles is possible without causing significant losses in grade and recovery in a high viscosity medium.

Gangue mineral recovery

There are three main mechanisms that contribute to the recovery of gangue minerals during froth flotation, these include entrainment, entrapment and slime coatings (Cilek and Umucu, 2001; Melo, 2001). Additional factors that can contribute to the recovery of liberated gangue minerals are through conventional flotation of naturally hydrophobic gangue minerals and metal ion activation of sulphide minerals. Graphite can be easily recovered through flotation because of its naturally hydrophobicity (Wakamatsu & Numata, 1991; Kaya & Canbazoglu, 2007). As a result minerals surfaces that are coated by graphite or associated with graphite will also become temporary hydrophobic and enter the froth phase via true flotation. Graphite is also known to have froth stabilizing properties, which increase the amount of solids and water recovered but hinders selectively due to higher mechanical entrainment of gangue particles (Li et al., 2013; Veras et al., 2014)

Metal ion activation also promotes gangue mineral recovery due to temporary hydrophobicity gained from collector adsorption, aggregation, surface oxidation dissolution of minerals and copper ions in water, among others (Lynch et al., 1974; Johnson, 2007; Deng et al., 2014). Copper activation of pyrite is typical example metal ion activation, in which galvanic interactions between chalcopyrite and pyrite during comminution, results in the oxidation of chalcopyrite and the copper activation of pyrite. This increases collector absorption onto pyrite surfaces, promoting its flotation and resulting in lower chalcopyrite grades (Owusu et al., 2011).

The most important mechanism for the recovery of liberated gangue minerals is entrainment of fine particles in recovered water (Smith & Warren, 1989; Cilek & Umucu, 2001). The consequence of gangue mineral recovery is a decrease in the overall concentrate grade. This effect is especially important to take note of in the flotation of fine particles (Neethling and Cilliers, 2009); however entrainment is unlikely to be a significant contributor to loss of grade during coarse particle flotation.

Reagents

Flotation reagents are added to the pulp to alter the mineral surface chemistry and in doing so enhance differences in mineral hydrophobicity, facilitating separation of valuable minerals from gangue minerals (Wiese et al., 2009). There are many different reagents involved in the froth flotation process; a typical reagents suite consists of collectors, frothers, depressants and activators, with the selection of reagents depending on the ore being treated. The reagents can be added to the flotation cell and dispersed throughout the cell with the aid of the impeller. The reagents are allowed to condition for predetermined periods of time to ensure complete mixing of reagents with the slurry and time for the adsorption onto the mineral surface; thereafter air is released into the cell.

Collector

Collectors attach to the valuable mineral's surface and render the mineral hydrophobic, aiding in the attachment of mineral particles to the passing air bubbles. Collectors are heteropolar molecules. Having the non-polar end of hydrocarbon chains extending outwards renders the overall mineral hydrophobic and as a result floatable. The most common collectors used in copper sulphide flotation are thio-compunds, where the sulphur group preferentially attaches to the Cu-sulphide mineral. Other collectors used are di-thio-phosphate and di-thio-carbamate (Herrera-Urbina et al., 1990; Klimpel, 1999).

Frothers

Frothers aid in bubble formation and froth stabilization. They also reduce coalescence and the speed at which the bubbles ascend (King, 1982).

These factors increase the residence time of the bubble within the pulp, consequentially increasing the probability of bubble-particle collision and attachment. Froth stability has a significant effect on the grade and recovery as a froth that is too stable will decrease recoveries and a froth that is unstable will decrease the grade of the concentrate due to the entrainment of gangue material (Sweet et al., 1997; Bulatovic, 2007). Ideal frothers have little or no collecting capability and have no influence on the mineral surface (Wills, 1997). Frothers are heteropolar molecules that absorb on the air-water interface with the non-polar hydrocarbon group within the bubble thus reducing the surface tension and in turn stabilising the bubble (Wills, 1997). The most common frothers are branch chain alcohols (Bulatovic, 2007). In the past natural compounds such as pine oil or terpinol were used but recently more synthetic compounds, such as methyl isobutyl carbinol, polyglycols and proprietary alcohol blends are utilized (Phillips, 2002).

Depressants

Depressants are used to inhibit the flotation of hydrophobic gangue minerals and to improve the selectivity of a flotation process. It is often used to increase selectivity by preventing one mineral from floating, while have no effect on the floatability of another mineral, such as the case with pyrite and chalcopyrite, common sulphide minerals typically associated with each other in copper sulphide ores (Burdukova, 2007).

2.5.4 Flotation of chalcopyrite

Chalcopyrite is naturally hydrophobic and floats without the addition of collectors. This natural hydrophobicity can be attributed to the surface oxidation reactions which either lead to the formation of elemental sulphur on the mineral's surface or cause iron atoms to migrate from the lattice, thus leaving a hydrophobic metal-deficient layer on the surface (Woodcock et al., 2007). In industrial flotation plants, however, a moderate amount of collector is usually required to achieve economic recovery of the mineral and this is attributed to the presence of surface precipitates and oxidation products which negate the mineral's natural floatability. The proposed mechanism of flotation has been ascribed to the formation of cuprous xanthate as well as dixanthogen (Woodcock et al., 2007). This was confirmed by Allison et al. (1972), who determined the products of the reaction between chalcopyrite and aqueous methyl, ethyl, propyl and butyl xanthates to be dixanthogen in each case.

Ackerman et al. 1987a demonstrates copper sulphides have a better flotation response with isopropyl xanthogen ethyl formate than pyrite. Yoon and Basilio (1993) reported that xanthate formed dixanthogen on chalcopyrite at potentials near the reversible potential for the xanthate/dixanthogen couple. At higher potentials, however, chalcopyrite oxidized and copper ions were released. These reacted to form the metal xanthate and this in turn co-existed with the dixanthogen. Xanthate adsorption may therefore be ascribed to the catalytic oxidation mechanism.

With regard to flotation with DTP, Finkelstein and Goold (1972) reported the presence of cuprous diethyl DTP, $Cu(DTP)_2$, on chalcopyrite after reaction with potassium diethyl DTP in alkaline conditions and proposed $CuDTP^+(DTP)_2$ formation in acid and neutral conditions.

2.5.5 Extraction methods

The metal is extracted from the concentrate by either pyrometallurgy or hydrometallurgy or both. The beneficiation method is chosen based on the specific mineralogical characteristic of the ore body. The key factors include the composition and texture of the ore, and the host rock mineralogy (i.e. gangue mineralogy) (Norgate & Jahanshahi, 2007; 2010). Pyrometallurgy involves the smelting, converting and electrolytic refining of the concentrate at high temperatures. Hydrometallurgy involves leaching, solvent extraction and electro-winning of ores/concentrates under relatively low temperatures. These two processing techniques, including their different routes, are illustrated in Figure 2.14 (Norgate & Jahanshahi, 2007; 2010).

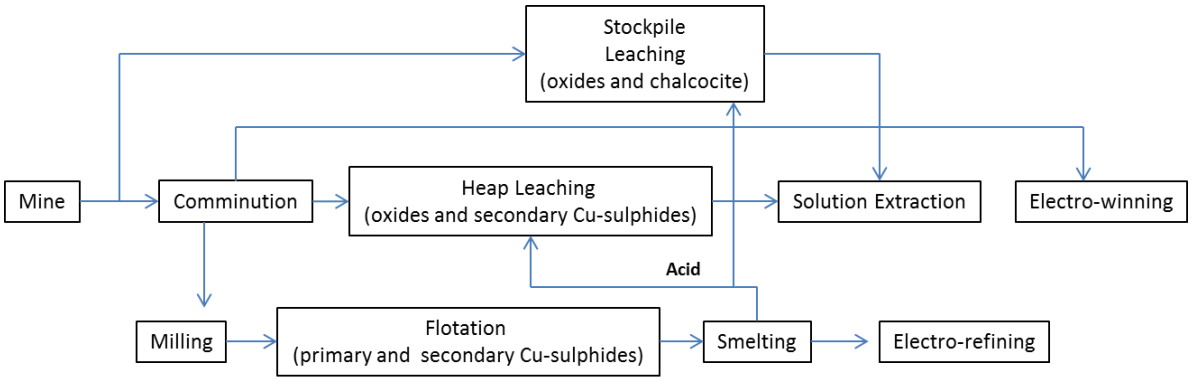

Figure 2.14: Processing routes for different copper minerals.

Approximately 80% of total copper produced is extracted form copper-iron sulphides with the most common host of copper being chalcopyrite ($CuFeS_2$) (Robertson et al., 2005; Norgate & Jahanshahi, 2010). Copper sulphides are notoriously difficult to dissolve by acidic solutions' hence copper is extracted from these minerals by pyrometallurgical processes. Hydrometallurgical processing of oxide ores (i.e. malachite and azurite) and secondary sulphide minerals (for example, chalcocite and covellite) account for the remaining 20% of total copper produced globally (Habashi, 1999; 2005).

2.5.6 Summary

The Kansanshi deposit was one of the earliest known significant copper occurrences in Zambia. It has experienced a protracted geological history, including later supergene enrichment which resulted in the development of zones of varying mineralogy and texture, adding further complexity to the deposit. Uncertainty around the intensity of oxidation and

alteration at each zone has made it difficult to get correct and consistent feed to the appropriate circuit. This poses challenges; each ore type has specific processing requirements as the mineralogy and texture of the ore define the theoretical grade-recovery curve for the feed ore. If the actual concentrate obtains grades and recoveries below the theoretical grade-recovery curve it can be attributed to the operational parameters and defines the opportunity for improvement.

Understanding the mineralogy and textural variations within the deposit can help in predicting the behaviour of the ore during processing, and in that lies the value of process mineralogy (Cropp et al., 2013). Process mineralogy has made significant advancements with the development of new technologies such as the QEMSCAN, MLA and developments in the EPMA (Evans et al., 2011). These tools have made ore characterisation simpler and faster, allowing for the quantification and understanding of parameters. This inadvertently leads to improvements in the copper grades and recoveries as improvement in grade-recovery can only be made by changing the particle properties of the feed to the circuit (Cropp et al., 2013).

From a metallurgical perspective the design and satisfactory operation of multiple circuits depends heavily on mineralogical information such as: (a) Composition, grain size and degree of locking of value minerals present. (b) Composition and mode of occurrence of oxide minerals present. (c) The type gangue minerals and host rocks present. (d) The type and amount of iron sulphide minerals present (O'Meara, 1961). The composition, grain size and degree of locking of value minerals present controls the grinding targets for the liberation of these minerals and the type of concentration method.

This influences the choice of metallurgical treatment and flow sheet design (for example, recovery of copper sulphides by flotation, recovery through leaching of copper oxides or non-recoverable copper hosted in silicate minerals such as Cu in mica (Sikazwe, 2008). The composition and mode of occurrence of oxide minerals will determine the total amount of acid soluble copper present, which significantly adds to the overall resource; however, when making these calculations knowledge of which oxide minerals contribute to acid soluble copper content is imperative. Certain oxide minerals, such as chrysocolla, can be considered refractory as they cannot be concentrated via conventional techniques and without this information incorrect resource estimations could be made (O'Meara, 1961). Gangue mineralogy and host rock lithologies, such as soluble gangue minerals (for example, calcite), provide an indication of the required acid strength and leach time. A problem currently faced by Kansanshi is that 11% of their cost lost is associated with acid consumption, due to the abundance of acid consuming gangue (ACG) minerals, such as carbonates. The mine is

now investigating alternative solutions for lowering their reagent costs and reduces overall processing costs, which is essential in this challenging economy (Swaby, 2013).

The key questions generated from the literature review and presented in the introduction (section 1.4) are repeated here:

1. What are the mineralogy and texture of each ore type?
2. What affect does the mineralogy have on the flotation behaviour of the sulphide ore?
   a) What effect does coarsening the grind to P_{80}= 212 µm have on the copper grade and recovery?

   b) What other gangue minerals (i.e. pyrite, pyrrhotite, and graphite) are floating with sulphide ore and in what quantity?

CHAPTER 3: EXPERIMENTAL METHODS AND EQUIPMENT

3.1 INTRODUCTION

The aim of this project, as stated in section 1.3, is the following: firstly to mineralogically characterise the different Kansanshi ore types, which are associated with different mineralisation styles (Table 2.1) hosted within various host rocks, using various process mineralogical techniques. Secondly, to determine the effect mineralogy has on the flotation performance of two sulphide ores. This chapter provides a description of the materials and methods used to characterize the samples and to investigate the sulphide flotation performance.

3.1.1 Samples and sample preparation

Two different sets of samples were characterized within this study: a series of hand specimens and grab samples collected from various locations within the Main and NW open pits (Figure 3.1). These samples were selected based on their representativeness of the four mineralisation styles present at Kansanshi deposit (Table 2.3 & Figure 3.2). The hand samples were cleaned and photographed prior to any further processing. Representative samples of each ore type were made into thin sections, polished thin sections and ore mounts for ore characterisation.

Two samples of Kansanshi sulphide ore representing the feed for the sulphide circuit of slightly differing lithologies and weighing approximately 100 kg each, were collected by Kansanshi personnel and sent to the Centre for Minerals Research (CMR) in the Department of Chemical Engineering at the University of Cape Town for flotation test work. These samples are henceforth referred to in this study as Ore 1 (quartz-carbonate vein) and Ore 2 (blend of several lithologies). The sulphide ore samples were prepared for batch flotation tests by screening the 100 kg samples through a 3.25 mm aperture stainless steel screen to remove the fines and then fed through a cone crusher to ensure that there were no rock chippings left in the sample larger than 3.25 mm.

The filtered fines and the sample produced from the cone crusher were then blended, riffled and split into representative 1 kg portions using a rotary sample splitter. The 1 kg samples were then bagged and labelled in preparation for the batch flotation tests.

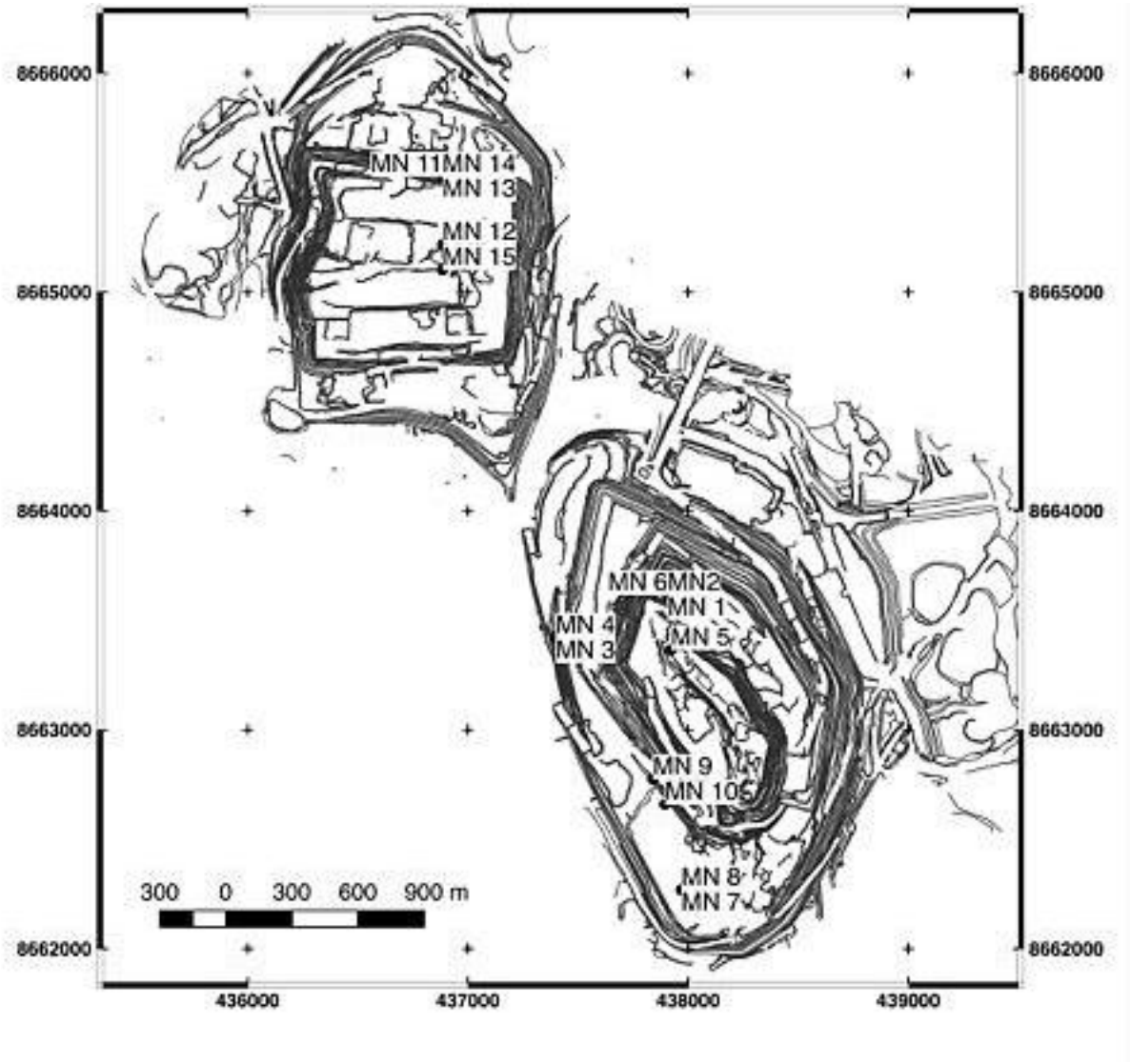

Figure 3.1: Outline of locations of the hand samples collected from the Main and NW pit. These sample locations can be related to their location within the Kansanshi stratigraphy (Appendix A).

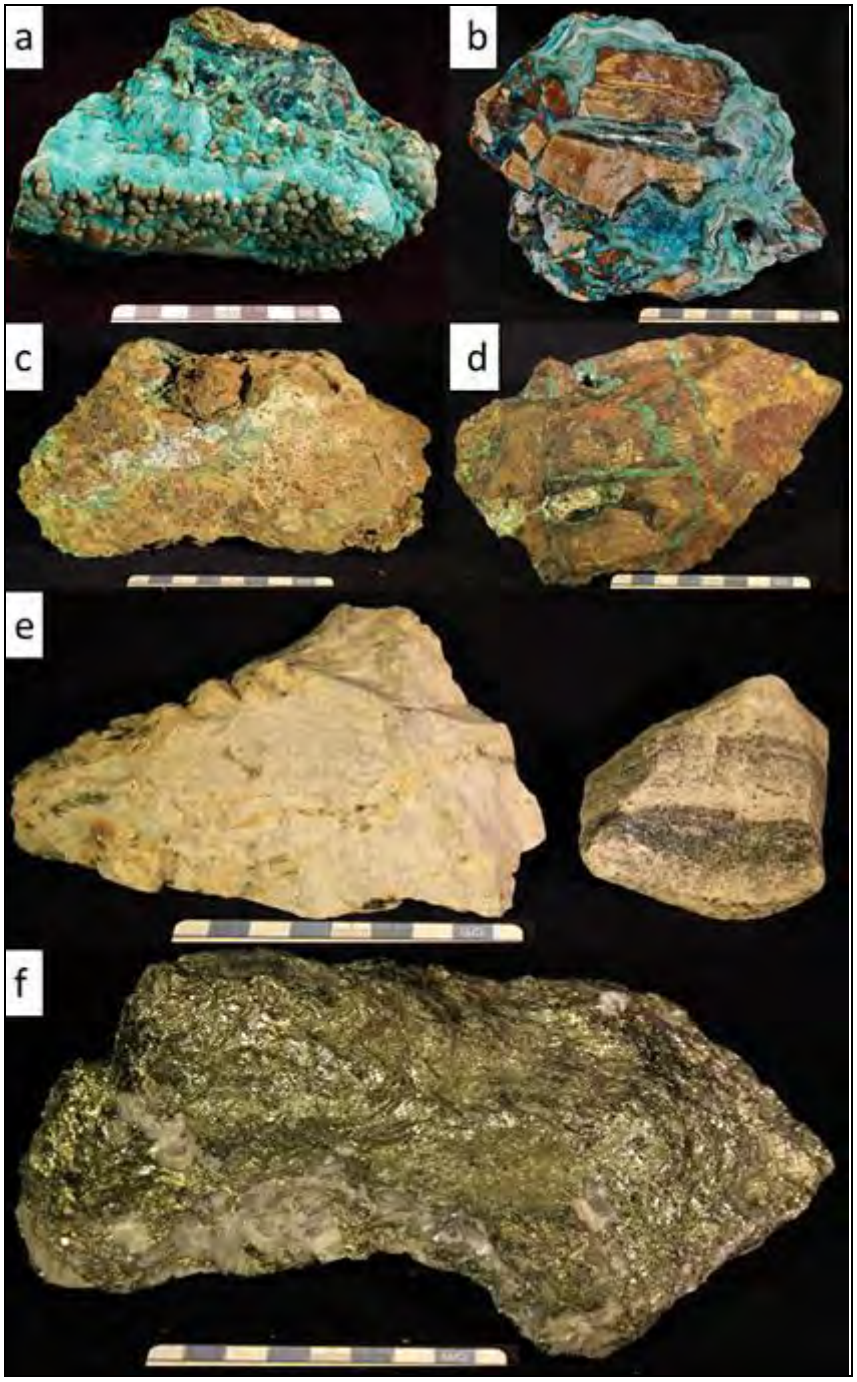

Figure 3.2: Photographs of seven out of the thirty-eight samples, representing the sulphide, mixed and oxide ores. (a) Sample MN 004, (oxide ore), with turquoise chrysocolla and boitrodial green malachite. (b) Sample MN 005, (oxide ore), breccia with collform chrysocolla and malachite. (c) Sample MN-014 A, (mixed ore), pyrite and iron-hydroxides in box-work texture with malachite veins. (d) Sample MN-014 B, (mixed ore), malachite and chrysocolla filling veins and cravities in a matrix of goethite and clays. (e) Sample MN-008, (sulphide ore), disseminated mineralisation associated with albite-carbonate alteration. (f) Sample MN-016, (sulphide ore), coarse-grained chalcopyrite and pyrite.

3.2 ORE CHARACTERISATION

3.2.1 Petrographic Analysis

Petrographic descriptions of the grab samples were performed on thin sections and polished epoxy ore mounts for transmitted and co-axial reflected light microscopy respectively. Photographs collected during the petrographic study were obtained using various techniques depending on the required scale of observation. Whole thin sections and ore mounts were photographed with a macro-lens camera. Centimetre-scale coverage was achieved with a Leica DST binocular microscope with a built-in digital camera connected to a PC running LASEC imaging software. Millimetre-scale photomicrographs were taken with a Nikon Optiphot microscope fitted with an Olympus SC20 digital camera with a Nikon 0.45x c-mount video adaptor, connected to a PC running Olympus Analysis Getit software.

3.2.2 X-ray Fluorescence (XRF) spectroscopy

The cleaned samples were split into hand-sized fragments with a hydraulic splitter, crushed by a Sturtevant jaw crusher with C-steel plates and milled in a Seibtechnik swingmill to less than 75 µm in a C-steel head. The powdered samples were split into six fractions with a RS-212 Retsch rotary sample divider. Due to the nature of the ore-bearing samples and potential difficulties they would pose in preparation and analysis, it was decided to subdivide the collection into three batches based initially on visual examination. Sulphide-rich samples (> 5%) were separated from those containing oxide copper, with the third batch representing host rock gangue assemblages.

The three subgroups were analysed using two specialized XRF analytical applications set up to (1) measure routine major oxides and gangue minerals and (2) base metal sulphides in the pellets. The pressed powder pellet was prepared by combining 6 g of finely milled powder with a liquid binder (Mowiol). The briquette was backed with crystalline boric acid and moulded with a pressure of 10 tons. This approach provided the best data for the sulphide-rich samples and provided a check for the visual examination. The remaining sulphide-poor samples were subject to further preparation involving borate fusion, prior to XRF analysis. Samples for borate fusion were prepared by drying 2 g of powdered sample in the oven for at least 4 hours.

The samples were then transferred to a furnace and reheated overnight at 950 °C to determine the loss on ignition (LOI), which is a composite of chemically bound water (H_2O^+), carbonates (CO_2) and the oxidation of ferrous iron. Fusion of accurately weighed 0.700 ± 0.001 g of roasted sample mixed with 6.000 ± 0.001 g of LiT / LiM (57: 43) flux was achieved in a Pt-95%: Au-5% crucible with a Claisse gas burner to create a fusion disk (Willis, 1999). In the case of the oxide copper rich samples, 50% dilution was achieved with silica prior to fusion. This latter step was required to ensure complete fusion and to comply with standard calibration ranges.

A Panalytical Axios Wavelength dispersive XRF spectrometer with a 4 kW Rh tube was used for analysis. Calibration standards include natural standards of SARM (South Africa Reference Materials) and USGS (United States Geological Survey) ranges, as well as artificial standards doped with Cu. Matrix corrections make use of the Fundamental Parameter method as described in Willis and Duncan (2008) and the references therein.

3.2.3 Quantitative X-ray diffraction (QXRD)

QXRD was used to quantify the relative proportions of each mineral phase present within the samples using the Rietveld method. The samples were prepared for QXRD by subjecting the samples to an additional milling stage using a McCrone micronizing mill to ensure a particle size of <10 µm, which is required for quantitative X-ray diffraction (Rietveld refinements), and left to dry overnight in the oven. Powder QXRD spectra were obtained with a Bruker D8 Advance powder diffractometer with Vantec detector and fixed divergence and receiving slits with Co-Ka radiation. Instrument conditions were set at a step size of 0.01 degree 2Θ, the a total measurement run time of 1 hour and 34 seconds and the detection limits depend on the sample type and preparation, the more crystalline, the better the data and the better the detection limits. In most cases, 5% is the cut off but this is dependent upon the quality of the refinement. The Bruker Topas 4.1 software was used to quantify the mineral phases (Coelho, 2007).

In order to ascertain whether the refinements were successful, two parameters were used; the weighted-profile R-value (Rwp) and goodness of fit (GOF) test (McCusker et al., 1999). Rwp defines how well the identified phases correlate and complete the scanned profile. Topas will calculate an ideal Rwp depending on the quality of the data given. Thereafter a GOF is used to check how well current Rwp correlates with the calculated value.

The Rietveld method has its limitations, including its inability to detect amorphous mineral phases, such as chrysocolla and other clay minerals that are non-diffracting.

The amorphous phase will produce a large bump distributed in a wide range (2 Theta) instead of high-intensity narrower peaks in the diffractogram (Cullity, 1978). The amount of amorphous material in a sample may be determined by the addition of a known weight of (crystalline) internal standard prior to the phase analysis. For the samples analysed in this study the amorphous content was determined by the addition of known amount (10 wt. %) of magnesium oxide (MgO) into each sample prior to phase analysis. These results were used for QEMSCAN data validation.

3.2.4 Electron micro-probe analysis (EMPA)

The electron microprobe was used for mineral chemical analysis, elemental mapping and imaging of compositional variations and textures. A Jeol JXA 8100 Superprobe located in the Department of Geological Sciences, University of Cape Town, equipped with four wavelength dispersive spectrometers, was utilized to obtain these measurements. Prior to analysis, the polished thin sections and ore mounts were coated with a thin layer of carbon. Elemental maps were run at a pixel size of 100 μm, counting times for all minerals and elements were 10 seconds on the peak and 5 seconds on each background.

Sulphides were analysed at 25 kv, 20 nA, feldspars and micas at 15 kv, 20 nA, peak and background peak times were 10 and 5 seconds. Spot sizes were between 1-3 μm. The standards used for external calibration were natural and synthetic. See Table 3.1 for, detection limits and standard deviation. Number of spots measured of major Cu-bearing and gangue minerals are shown in Table 3.2. Individual totals for feldspars, and sulphides were 99.00 to 100.99 wt. %, chlorite 90.00 to 94.00 wt. % and biotite 96.00 to 98.00 wt. %. The totals of chlorite and biotite are lower because of the water in these hydrous minerals cannot be analysed by the EMPA.

Table 3.1: Lower limit of detection (LLD) for chalcopyrite, chalcocite, digenite, biotite, chlorite and albite measurements using EMPA operating conditions as described in section 3.2.4.

	Lower limits of detection (wt. %)		
Elements	**Feldspar**	**Mica**	**Sulphides**
Al	0.01	0.01	
Si	0.02	0.02	
Ti	0.02		
K	0.01	0.01	
Mg	0.01	0.01	
Mn	0.02	0.02	
Cr	0.02	0.02	
Ca	0.01	0.01	
Na	0.02	0.02	
Fe	0.02	0.03	0.01
S			0.05
Mo			0.02
Ni			0.01
Ag			0.01
Co			0.01
Pb			
Zn			0.01
As			0.02
Au			0.04
Cu		0.9	0.01

Table 3.2: Summary of the number of spots analysed per mineral for the EMPA.

Mineral	**Number of spot analyses**
Chalcopyrite	102
Secondary copper sulphides	28
Pyrite	69
Feldspar	10
Chlorite	7
Biotite	19

3.2.5 QEMSCAN

Mineralogical characterisation was performed using two different QEMSCANs at the University of Cape Town. A LEO SEM with tungsten filament equipped with two Bruker 4010 SDD detectors was used at the start of the study for all Ore 1 at P_{80}=150 µm analyses. The QEMSCAN 650 F with 6th generation Bruker 6030 Si-drift EDS X-ray detectors and field emission gun was used for all Ore 2 P_{80}=150 µm analyses.

Samples were wet screened then dry screened into the following size fractions, -25; +25/-53; +53/-75; +75/-106; +106/-150; +150/-212 and +212/-1180 µm. Polished blocks were then made for each of the size fraction.

A total of three blocks were made per size fraction by splitting each size fraction into 1g aliquots using a micro rotary splitter. Two grams of milled graphite was added to each 1g of sample in order to minimize the effect of touching particles and improve electron conductivity during analysis. The mixture was placed in labelled and lubricated moulds and resin was added. The moulds were placed in a vacuum for 15 minutes so as to remove any air bubbles and then placed in a pressure pot to cure overnight. These moulds were further cured at 30 °C until dry. The mounts were then polished to a 1 µm diamond finish, washed in an ultrasonic bath and dried at 30 °C for an hour. The ore mounts/blocks were then carbon coated in preparation for analysis. Four analytical methods were used to quantify the data generated by the QEMSCAN (Table 3.3).

Data processing was done using QEMSCAN iExplorer software by performing the following functions on the particulates, touching particles and boundary phase processor for BMA and SMS analyses. Field images of coarse particles acquired using QEMSCAN were stitched together using field stitch and boundary phases processor in order to obtain a complete image.

The SIP file needed to be tailored specifically for the Kansanshi ores. This was achieved by incorporating mineral chemistry data obtained from EMPA data into the QEMSCAN primary mineral list, which contains all the grouped SIP phases of interest, which have been assigned a single density and chemical composition. Data validation was accomplished by comparing QEMSCAN calculated assays against XRF chemical data that measures the actual mineral chemistry (i.e. weighted pixel area). The accuracy of the data was checked by determining if the two data sets shared a 1:1 relationship, by observing how close the points lie along the straight line (Figure 3.3).

Table 3.3: Measurement conditions and information obtained from QEMSCAN.

Measurements	Sample	Size fraction	Pixel spacing	No. of sulphide grains measured
Field Scan (FS)	Sulphide, mixed, and oxide ores	N/A	20 µm	N/A
Bulk Mineralogical Analysis (BMA)	Ore 1 and Ore 2 P80=150 For all Size fractions	+150/ -106 +106/ -75 +75/ -53 +53/-25 +25/-25 -25/-10	5 µm 5 µm 4 µm 3 µm 2 µm 1 µm	N/A
Specific Mineral Search (SMS)	Ore 1 @ P80=150 For all size fractions	+150/ -106 +106/ -75 +75/ -53 +53/-25 +25/-25 -25/-10	5 µm 5 µm 4 µm 3 µm 2 µm 1 µm	782 1072 1235 1462 1802 2196

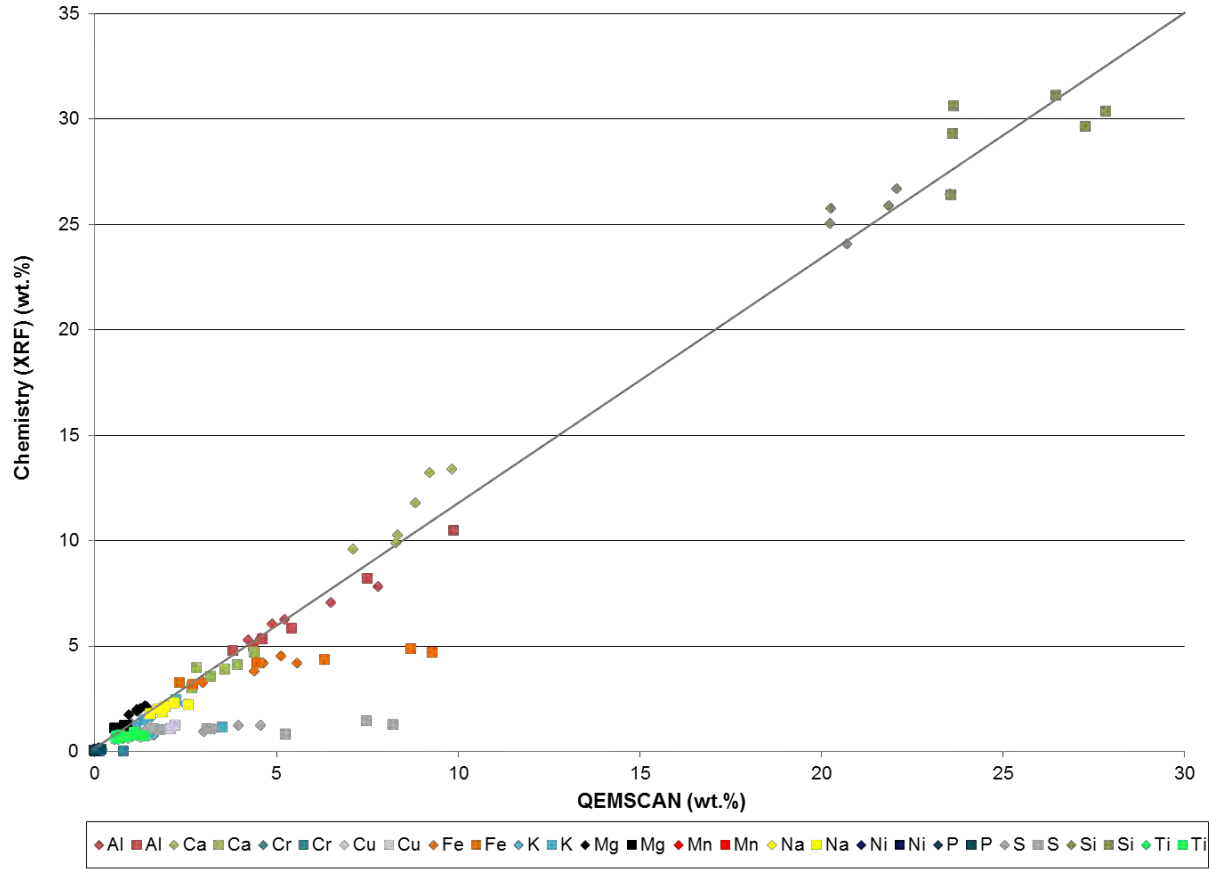

Figure 3.3: Ore 1 (diamond symbol) and Ore 2 (square symbol) data validation graphs accomplished by comparing actual chemistry obtained by XRF against QEMSCAN calculated assay, however the line represents 1:1. However, the sulphur content was determined by Leco.

Silicon, iron and sulphur values show a slight departure, with either the chemical analyses overestimating, or the QEMSCAN underestimating, the values. The poor correction of silicon and iron is likely related to the variable composition of limonite, with iron and silicon values ranging from 11 % to 73 % iron and 72% to 14% silicon depending on lithology, mineral assemblage, and degree of weather and oxidation (Blanchard, 1944).

3.3 FLOTATION EXPERIMENTS

3.3.1 Milling procedure

All milling prior to the flotation experiments was performed using an Eriez Magnetics® MASCLAB belt-driven stainless steel laboratory scale rod mill with an inner chamber diameter of 200 mm and a depth of 297 mm. The mill was charged with twenty rods of three different diameters and total charge weight as shown in Table 3.4.

Table 3.4: Rod diameters and charge weight used for milling.

Diameter (mm)	No. of steel rods	Charge weight (kg)
25	6.00	4.90
20	8.00	3.67
16	6.00	1.53
Total	20.00	10.10

In order to establish a grinding curve for 80% passing 150 µm and 212 µm, three 1 kg samples from Ore 1 and Ore 2 were milled for different lengths of time, shown in Figure 3.4. Calculated milling times obtained for Ore 1 and Ore 2 are shown in Table 3.5.

Table 3.5: Calculated milling times for Ore 1 and Ore 2.

	Ore 1	Ore 2
Grind	Time (minutes)	
P80= 150 µm	3.42	4.30
P80= 212 µm	3.36	3.18

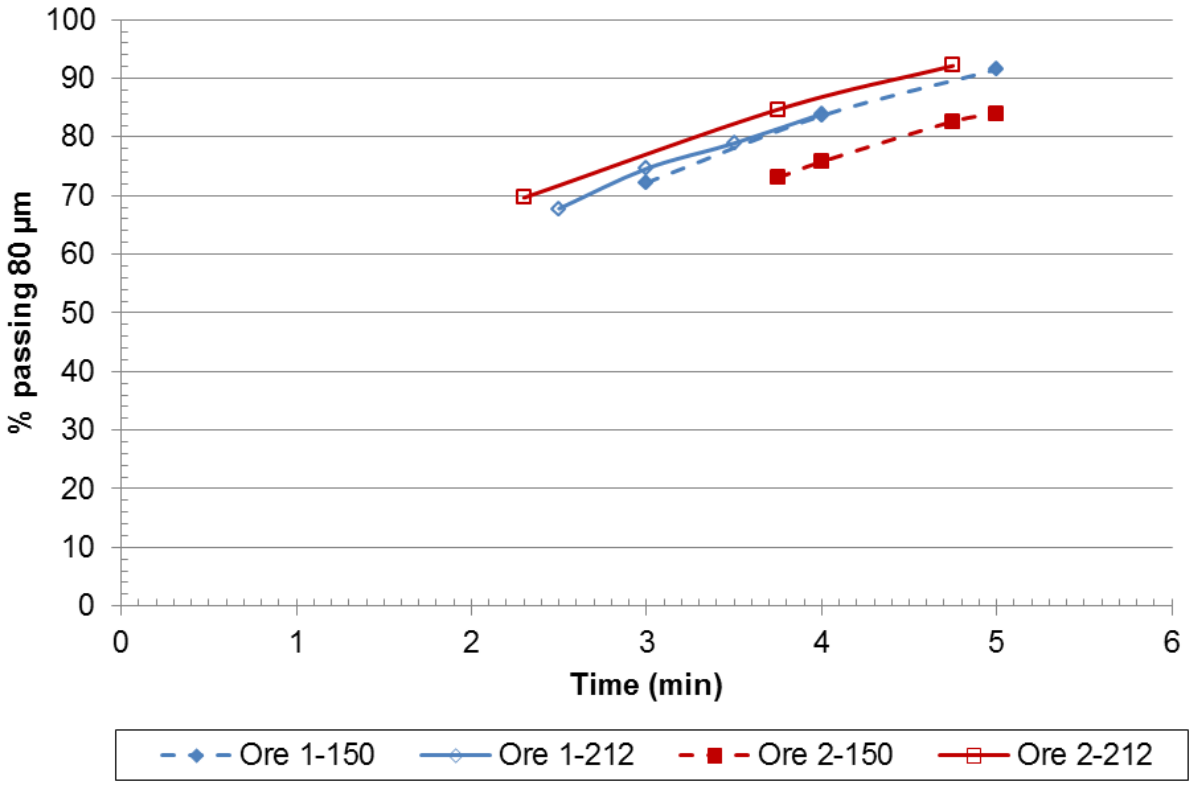

Figure 3.4: Milling curves for Ore 1 and Ore 2 at P80=150 µm and P80= 212 µm.

The particle size distribution curve was established by a combination of wet and dry screening. The 1 kg sample was first wet screened through a 53 µm sieve, all material smaller than 53 µm was then wet screened through a 25 µm sieve and dried.

All material larger than 53 µm was dry screened, by adding the remaining material into a stack of sieves with sizes as follows: 1180, 212, 150, 106, 75, 53 µm.

The stack was placed on a mechanical shaker that ran for 20 minutes. After the shaking was completed the material on each sieve was weighed. The weight of the sample of each sieve was then divided by the total weight to give a percentage retained on each sieve. Thereafter, the particle size distribution (PSD) curves were plotted for the milling times giving 80% passing both grinds (Figure 3.5) in order to validate the times obtained.

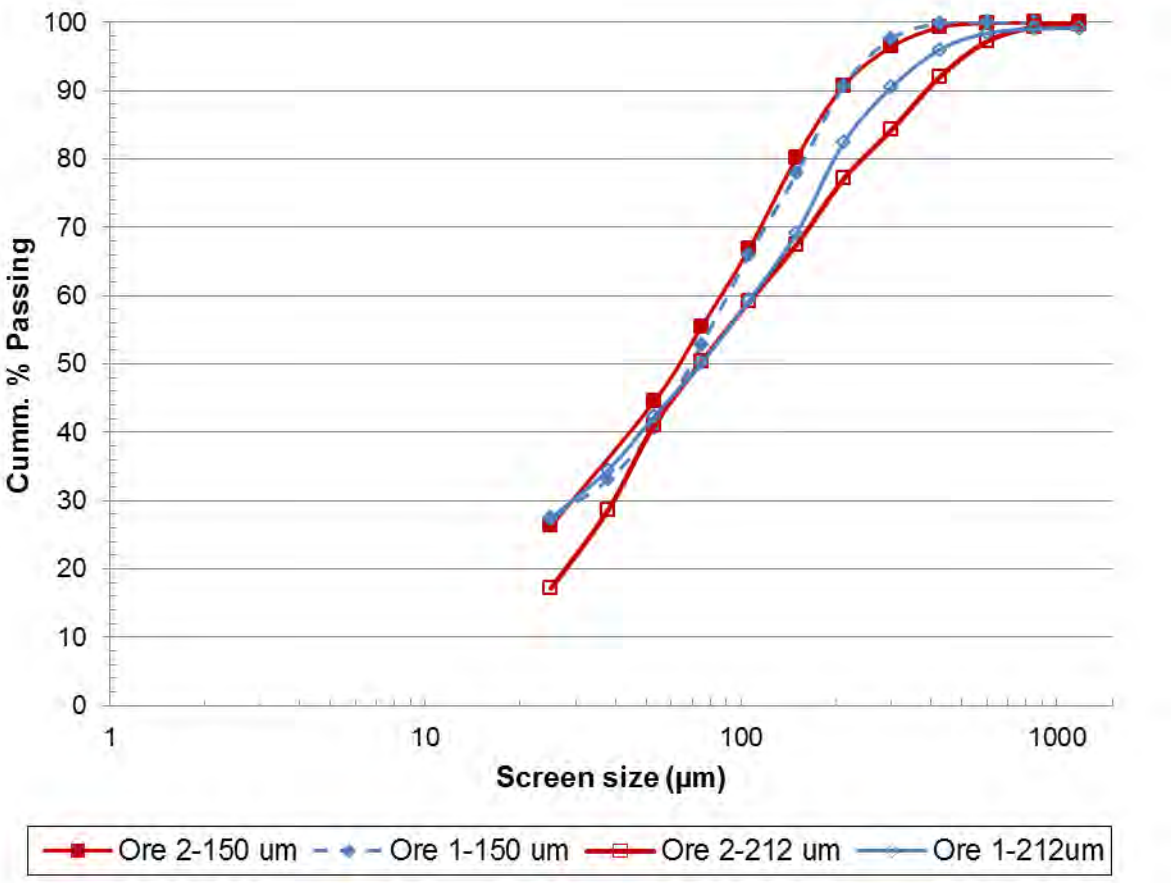

Figure 3.5: PSD obtained at each grind for Ore 1 and Ore 2.

For all flotation experiments, 1 kg of sample and 500 ml of synthetic plant water was added to the mill which was then sealed and rotated at a fixed speed of 253 rpm. The synthetic plant water was made according to the CMR recipe for 40 L batches (Wiese, 2009). The ions present in the plant water are outlined in Table 3.6. No reagents were added to the mill.

Table 3.6: Concentration of ions present within synthetic plant water (Wiese, 2009).

Ions	Ca^{2+}	Mg^{2+}	Na^{+}	Cl^{-}	SO_4^{2-}	NO^{3-}	CO_3^{2-}
Concentration (ppm)	80	70	153	287	240	176	17

3.3.2 Batch flotation procedure

The same reagent suite and dosages were used for all batch flotation tests. Synthetic plant water (Table 3.6) was used for all flotation test work. Subsequent to initial scoping test work the following batch flotation procedure was used, whereby the milled slurry was transferred to a 3 L

modified Leeds batch flotation cell (Figure 3.6). The volume in the cell was made up to produce 35% solids using synthetic plant water.

Figure 3.6: UCT modified Leeds 3L flotation cell used for batch flotation tests.

A feed sample was taken after mixing and suspension using a 60 ml syringe. The speed of the impeller within the flotation cell was maintained at 1250 rpm to ensure the complete mixing and suspension of the pulp. A froth height of 1 cm was maintained throughout the tests. The reagents were added, starting with the collector at 6 g/t which was allowed to condition for 2 minutes, followed by the frother at 16 g/t which was allowed to condition for 1 minute (Table 3.7). The air was then turned on and a flow rate of 6.5 L/min was kept constant for all flotation tests. Four concentrates were collected over 10 minutes, with the froth being scraped into the collecting pan every 15 seconds (Table 3.7).

Two tail samples were collected once the fourth concentrate was obtained, using a 60 ml syringe. At the end of the test the feed, concentrates and tail samples were filtered, dried and weighed before being sent for assaying. All batch flotation experiments were performed in triplicate to ensure reproducibility.

Table 3.7: Summary of batch flotation test procedure.

Action	Time (minute)
Milling	As determined by the milling curve
Collector (MX-5149)	2
Frother (Aerofrother-68)	1
Air turned on	3
Concentrate 1 (C1)	5
Concentrate 2 (C2)	7
Concentrate 3 (C3)	10
Concentrate 4 (C4)	13

3.3.3 Determination of flotation performance

The copper content of the sample had to be determined to establish the copper grade-recovery curves. This information was obtained by sending the feed, concentrates and tails for chemical assay. Total copper (TCu) and iron were analysed with the atomic absorption spectrophotometer (AAS) using a Varian SpectraAA. In preparation for AAS, the samples were digested in aqua regia, consisting of hydrochloric acid (HCL) (32 %), nitric acid (HNO_3) (55 %) and hydrofluoric acid (HF) (~40 %).

Approximately 0.1 g of concentrate material and ~0.5 g of feed and tail material were weighed out into 250 ml wide-mouthed Erlenmeyer flasks. After each sample, the Erlenmeyer flasks were cleaned with distilled water and 6 ml HCL, 2 ml HNO3 and 2 ml HF were added to each sample.

The samples were then placed in a microwave set at 180 ^{0}C for 20 minutes. On completion of digestion, the sample was transferred into a 100 ml volumetric flask and made up to 100 ml by adding distilled water. The sample was then filtered using Whatman No1 into a sample vial. This filtrate was then analysed using the AAS. In order to obtain sulphur data, the finely milled feeds, concentrates and tails were left in powder form before being analysed on the LECO 423 sulphur analyser.

The separation efficiency test (S.E.) proposed by Schulz (1970), equation 1, can be used to assess the metallurgical (not economic) performance of the flotation process whenever the results of two similar test runs are compared. For example, if the grade and recovery are both higher for the test compared to the other the choice of processing is easy. On the other hand, if the result of one test shows a higher grade but a lower recovery then the choice is no longer obvious. Schulz (1970), attempted to combine the recovery and concentrate grade into a single index that could define the metallurgical efficiency of the separation process.

Separation efficiency (S.E.) = Rm – Rg (equation 1)

Where Rm = % recovery of the valuable mineral (i.e. chalcopyrite)

Rg = % recovery of the gangue into the concentrate.

Consequently, this test was used to determine what conditions (i.e. grind) produced the best flotation performance.

3.3.4 Identifying naturally floating gangue minerals

The presence of naturally floating gangue minerals in the concentrate was determined by QXRD. This was accomplished by selecting concentrate one (Conc1) from Ore 1 and Ore 2. The samples were subjected to an additional milling stage using a McCrone micronizing mill, to ensure a particle size of <10 micron, which is required for quantitative X-ray diffraction (Rietveld refinements).

CHAPTER 4: RESULTS

4.1 INTRODUCTION

The primary objective of this research is the detailed process mineralogical characterisation of Kansanshi ore, with a focus on the flotation performance of the sulphide ore. This chapter is divided into two sections: mineralogical characterisation and batch flotation performance. Section one is further subdivided into four subsections based on the mineralisation style (Table 2.1) and geochemical analysis. The lithologies characterized within each subdivision were selected on the basis of their representativeness of the associated mineralisation styles. Section two presents the mineralogical analyses and batch flotation test work carried out on two sulphide ore samples. The mineralogical characteristics presented include; bulk mineralogy, copper deportment, mineral liberation, grain size distribution, mineral associations and locking textures. The full set of the results can be found in Appendix.

4.2 MINERALOGICAL CHARACTERISATION

The following section presents the multi-analytical approach used for the mineralogical characterisation of Kansanshi copper ores. This approach combines traditional (optical microscopy) and modern analytical tools (SEM-based automated systems, for example, QEMSCAN) to acquire qualitative and quantitative mineralogical data, by combining complementary types of information, such as, XRF and QXRD from a given sample. This comprehensive data set is capable of validating and accounting for the limitations associated with each of the individual techniques. The tools used for the identification and characterisation of the ore and gangue minerals associated with each lithology include optical microscopy, QXRD, XRF, EMPA and QEMSCAN.

It is important to consider some of the observed limitations associated with the various techniques, for instance the QXRD and QEMSCAN could not accurately distinguish between minerals that were compositional almost identical, such as malachite and azurite, and chalcocite and digenite.

To account for this shortcoming, optical microscopy was used to identify and distinguish between malachite and azurite. Each sample submitted for QXRD was spiked with an internal standard (periclase) to account of the amorphous character of chrysocolla. EMPA was used to identify and distinguish between chalcocite and digenite by performing spot analyses to obtain the mineral chemical composition of the secondary sulphides. This was used to calculate the exact mineral chemical formulae (Appendix D). The QEMSCAN is also limited in its ability to determine graphite content because graphite is included in the block making process to separate touching particles, making accurate identification of graphite impossible. In this case, QXRD was used for the determination of graphite content. EMPA was unable to provide accurate or reliable chemistry of the copper oxides (for example, chrysocolla and malachite) due to the heterogeneity of samples (i.e. multiple growth bands) and the lack of certified standards for calibration; therefore, the chemistry of these minerals was not obtainable.

The copper ores at Kansanshi have a complex mineralogy mainly composed of ten ore minerals (Table 4.1). The major ore minerals present, include chalcopyrite, chalcocite, covellite, malachite and chrysocolla. The major gangue minerals identified are quartz, albite, biotite and carbonates (calcite and dolomite). Detailed petrographic descriptions of the individual grab samples are provided in the Appendix A.

This sections aims to methodically describe the four different lithological units, namely quartz-carbonate-vein, phyllite, knotted schists and breccia, in the context of the different mineralisation styles presented in Table 2.1. Tables 4.2 to 4.7 summarize the results from the different analytical techniques.

Table 4.1: List of ore minerals present at Kansanshi and their groupings into ideal ore types for the processing circuit.

		Circuits types		
Ore Mineral	**Mineral abbreviations**	**Sulphide**	**Mixed**	**Oxide**
Chalcopyrite	ccp	x	x	
Bornite	bn	x	x	
Chalcocite	cc	x	x	
Djurleite	cdj		x	
Digenite	di		x	
Geerite	ge		x	
Covellite	cv		x	
Malachite	mal		x	x
Azurite	az		x	x
Chrysocolla	ccl		x	x
Cuprite	cup		x	x
Tenorite	ten		x	x
Native copper	cu	x	x	x

Table 4.2: Summary of sample description and type.

Sample	Description	Ore Type
MN -001	Breccia	Mixed
MN-002	Breccia	Oxide
MN-003	Breccia	Mixed
MN-004	Breccia	Oxide
MN-005	Breccia	Oxide
MN-006	Breccia	Oxide
MN-007	Vein hosted in Calcaerous Biotite Schist	Sulphide
MN-008	Vein hosted in Calcaerous Biotite Schist	Sulphide
MN-009	Vein with alteration halo hosted in Knotted Biotite Schist	Sulphide
MN-010	Knotted Schist	Sulphide
MN-011	Veins hosted in Biotite Phyllite	Mixed
MN-012	Carbonaceous Phyllite	Mixed
MN-013	Veins hosted in Biotite Phyllite	Mixed
MN-014	Heavily oxidized Phyllite	Mixed
MN-015	Vein hosted in Schist	Sulphide
MN-016	Vein hosted in Schist	Sulphide
MN-017	Vein hosted in Marble	Sulphide
KANMX-7	Phyllite	Mixed
SX-1-5	Quartz-Carbonate veins	Sulphide

Table 4.3: Whole rock chemistry of hand samples, determined by XRF.

Sample	MN-002 A	MN-002 B	MN-002 C	MN-004 B	MN-006	MN-008	MN-003 A	MN-003 B	MN-001 A	MN-001 B
Locality/ description	Breccia "4800" zone									
Major oxides (wt. %)										
SiO_2	60.54	61.88	70.29	36.64	45.35	42.3	52.55	21.75	16.94	20.99
TiO_2	1.68	0.88	0.19	0.24	1.6	0.95	0.39	-	0.2	0.07
Al_2O_3	19.34	12	2.11	3.79	19.47	10.64	4.18	0.3	6.75	5.99
Fe_2O_3	1.77	1.37	2.86	3.81	4.45	8.47	4.35	-	42.32	-
MnO	0.06	0.06	0.05	0.66	0.04	0.11	0.01	-	0.01	0.01
MgO	0.99	0.32	0.52	0.65	0.5	2.61	0.23	1	0.15	0.88
CaO	0.27	0.34	0.12	1.03	0.49	12.01	0.07	0.01	0.07	0.26
Na_2O	0.69	4.8	0.31	0.56	0.47	3.82	0.27	2.29	0.81	3.8
K_2O	0.57	0.18	0.19	0.05	0.91	0.71	0.2	0.01	0.02	0.26
P_2O_5	0.04	0.37	0.19	0.22	0.07	0.12	0.06	0.06	0.53	0.17
SO_3	0.05	0.02	0.02	0.66	0.32	7.13	0.06			
Cr_2O_3	0.01	-	0.01	0.01	0.01	0.01	0.04	-	0.01	0.12
NiO	0.01	0.01	0.02	0.02	0.02	0.04	0.03	-	0.05	0.03
CuO	5.79	14.28	16.2	43.35	13.49	3.69	26.3			
S								13.31	7.6	19.28
Cu								53.91	3.03	24.63
Fe								3.01	6.62	17.27
LOI	7.84	2.54	6.25	8.4	12.92	7.5	11.03	3.77	14.38	5.93
Total	99.64	99.04	99.34	100.08	100.1	100.1	99.74	99.43	99.47	99.69

Table 4.3: Continued

Sample	MN-008	MN-010	MN-011 A	MN-011 B	MN-012	MN-014 C
Locality/ description	Calcareous Schist-Qtz-carb vein	Knotted Schist	Chalcopyrite-rich Biotite Phyllite		Carbonaceous Phyllite	Oxidized Phyllite
Major oxides (wt. %)						
SiO_2	42.3	61.92	2.27	0.11	59.42	35.95
TiO_2	0.95	1.26	0.01	-	1.33	0.01
Al_2O_3	10.64	13.9	0.77	0.05	17.58	0.25
Fe_2O_3	8.47	11.74	-	-	3.42	9.05
MnO	0.11	0.07	0.01	-	0.03	0.19
MgO	2.61	2.29	0.34	0.07	1.39	0.52
CaO	12.01	0.75	0.15	0.01	1.33	1.56
Na_2O	3.82	2.64	0.63	0.17	0.4	0.13
K_2O	0.71	2.65	0.01	0.01	5.18	0
P_2O_5	0.12	0.19	0.08	0.01	0.06	0.22
SO_3	7.13	0.09			0.77	0.47
Cr_2O_3	0.01	0.01	-	-	0.03	0.01
NiO	0.04	0.01	0.07	-	0.02	0.03
CuO	3.69	0.06			0.18	44.48
S			29.53	28.12		
Cu			31.51	36.16		
Fe			26.98	22.9		
LOI	7.5	2.16	7.07	11.94	8.43	7.01
Total	100.1	99.76	99.43	99.54	99.55	99.88

Table 4.4: Summary of whole rock mineral abundance, determined by QXRD**.** Mica includes: biotite and muscovite.

Sample name	MN-002 A	MN-002 B	MN-002 C	MN-003 A	MN-006	MN-001 A	MN-001 B	MN-003 B	MN-004 B	MN-008
Locality/ description	Breccia									Calcareous Schist-Qtz-carb vein
	A-oxidized					B-partial oxidation				
Pyrite	<lld	<lld	<lld	2	<lld	26	<lld	<lld	1	1
Pyrrhotite	<lld	<lld	<lld	<lld	<lld	<lld	2	<lld	<lld	<lld
Chalcopyrite	<lld	0.7	<lld	<lld	<lld	1	60	30	13	11
Bornite	<lld	<lld	<lld	1	<lld	3	<lld	5	<lld	1
Chalcocite	<lld	1.8	<lld	<lld	<lld	2	<lld	3	<lld	1
Covellite	<lld	<lld	<lld	1	<lld	<lld	<lld	<lld	<lld	11
Malachite/Azurite	2	3	10	21	3	1	<lld	3	14	1
Tenorite	<lld	<lld	<lld	<lld	1	1	<lld	1	1	<lld
Carbonates	<lld	<lld	<lld	1	<lld	<lld	<lld	2	1	13
Quartz	35	20	63	43	17	9	4	33	9	9
Mica	9	7	4	6	24	17	4	3	25	7
Chlorite	7	3	2	3	9	4	<lld	3	5	3
Goethite	2	1	2	2	3	21	<lld	1	3	<lld
Chrysocolla	11	6	7	9	10	<lld	<lld	7	17	<lld
Graphite	5	3	7	5	5	<lld	1	4	1	2
Albite	5	48	<lld	2	9	5	29	<lld	3	34
Cuprite	1	1	<lld	1	1	1	<lld	<lld	1	<lld
Amphibole	<lld	1	<lld	<lld	<lld	4	<lld	5	1	<lld
Kaolinite	23	4	4	5	18	5	<lld	<lld	5	1
Total	100	100	100	100	100	100	100	100	100	100
GOF	13.4	18.9	16.2	14.8	12	16.6	13.7	12.9	8.7	16.9

Table 4.4: Continued

Sample name	MN-009	MN-010	MN-011 A	MN-011 B	MN-012	MN-014 C	SX1
Locality/ description	Knotted Biotite-Schist	Knotted Schist	Chalcopyrite-rich Biotite Phyllite		Carbonaceous Phyllite	Oxidized Phyllite	Qtz-carb vein
Pyrite	<lld	<lld	<lld	<lld	2	2	2
Pyrrhotite	<lld	2	<lld	1	<lld	1	<lld
Chalcopyrite	22	1	90	90	2	9	62
Bornite	1	<lld	<lld	<lld	<lld	<lld	<lld
Chalcocite	<lld	1	<lld	<lld	2	<lld	<lld
Covellite	<lld	12	4	9	<lld	<lld	18
Malachite/Azurite	2	1	<lld	<lld	1	4	<lld
Tenorite	<lld	<lld	<lld	<lld	<lld	<lld	<lld
Carbonates	53	1	<lld	<lld	3	5	14
Quartz	<lld	23	<lld	<lld	30	6	<lld
Mica	3	17	2	<lld	40	19	1
Chlorite	<lld	2	<lld	<lld	3	10	<lld
Goethite	<lld	1	<lld	<lld	1	9	<lld
Chrysocolla	1	<lld	<lld	<lld	1	19	<lld
Graphite	<lld	6	<lld	<lld	6	<lld	<lld
Albite	16	23	3	<lld	1	<lld	2
Cuprite	<lld	<lld	<lld	<lld	1	1	<lld
Amphibole	<lld	1	<lld	<lld	<lld	5	<lld
Kaolinite	<lld	4	<lld	<lld	1	10	<lld
Total	100	100	100	100	100	100	100
GOF	18.7	13.5	3.8	3.9	15.3	11.6	20.8

Table 4.5: Summary of the average weight % and standard deviation for each element analysed for sulphides (chalcopyrite), determined by EMPA, where n = number of analyses.

Mineral Name	**Chalcopyrite**									
Sample	**KANMX7**		**SX1**		**SX2**		**SX3**		**SX4**	
n	7		11		2		18		19	
Locality/ description	Phyllite		ROM		Phyllite		ROM		ROM	
Calc formulae	$CuFeS_2$		$CuFeS_2$		$CuFeS_2$		$CuFeS_2$		$CuFeS_2$	
Metal	Wt. %	St Dev	Wt. %	St Dev	Wt. %	St Dev	Wt. %	St Dev	Wt. %	St Dev
S	35.07	0.29	34.47	0.35	34.85	0.09	34.86	0.28	34.69	0.39
Au	0.03	0.02	0.05	0.03	0.10	-	0.06	0.03	0.04	0.03
Fe	30.68	0.19	30.45	0.25	30.73	0.11	30.28	0.46	30.61	0.31
As	<lld	<lld	0.02	0.01	0.05	-	0.02	0.01	0.03	0.02
Cu	34.81	0.13	34.60	0.30	34.63	0.42	34.75	0.30	34.73	0.28
Co	<lld	<lld	<lld	<lld	0.00	-	0.00	0.00	0.01	0.01
Mn	0.03	0.01	0.03	0.01	0.03	0.01	0.03	0.01	0.03	0.01
Ni	0.01	0.01	0.01	0.01	0.03	-	0.01	0.01	0.01	0.01
Ag	<lld	<lld	<lld	<lld	<lld	<lld	<lld	<lld	<lld	<lld
Mo	<lld	<lld	<lld	<lld	<lld	<lld	<lld	<lld	<lld	<lld
Pb	<lld	<lld	<lld	<lld	<lld	<lld	<lld	<lld	<lld	<lld
Zn	<lld	<lld	<lld	<lld	<lld	<lld	<lld	<lld	<lld	<lld
Ave. Total	100.62		99.59		100.32		99.94		100.11	

Table 4.5: Continued

Mineral Name	**Chalcopyrite**							
Sample	**SX5**		**MN-001 B**		**MN-003 A**		**MN-014 C**	
n	45		14		11		5	
Locality/ description	ROM		Breccia		Breccia		Phyllite	
Calc formulae	$CuFeS_2$		$CuFeS_2$		$CuFeS_2$		$CuFeS_2$	
Metal	Wt. %	St Dev	Wt. %	St Dev	Wt. %	St Dev	Wt. %	St Dev
S	34.51	0.40	34.88	0.58	35.22	0.52	34.98	1.00
Au	0.04	0.04	0.04	0.03	0.07	0.07	0.07	0.08
Fe	30.44	0.34	29.99	0.93	30.11	0.42	29.23	0.97
As	0.04	0.03	0.01	0.01	0.01	0.00	0.01	0.01
Cu	34.77	0.28	34.99	0.92	34.03	0.51	35.47	1.12
Co	0.00	0.00	0.01	0.01	0.00	0.00	0.00	0.00
Mn	0.03	0.01	0.18	0.15	<lld	<lld	0.05	0.06
Ni	0.03	0.05	0.01	0.01	0.01	0.01	0.01	0.01
Ag	<lld	<lld	0.04	0.04	0.01	0.01	0.05	0.04
Mo	<lld	<lld	0.03	0.02	<lld	<lld	0.01	0.01
Pb	<lld	<lld	<lld	<lld	<lld	<lld	<lld	<lld
Zn	<lld	<lld	<lld	<lld	<lld	<lld	<lld	<lld
Ave. Total	99.93		100.17		99.4		99.67	

Table 4.6: Summary of the average weight % and standard deviation for each element analysed for secondary sulphides (chalcocite and covellite) determined by EMPA, where n = number of analyses.

Mineral Name	**Chalcocite**								**Covellite**			
Sample	**KANMX7**		**MN-001 B**		**MN-003 A**		**MN-014 C**		**MN-001 B**		**MN-003 A**	
n	4		4		5		5		2		8	
Locality/ description	ROM		Breccia		Breccia		Phyllite		Breccia		Breccia	
Calc formulae	CuS_2		CuS_2		CuS_2		CuS_2		CuS		CuS	
Metal	Wt. %	St Dev	Wt. %	St Dev	Wt. %	St Dev	Wt. %	St Dev	Wt. %	St Dev	Wt. %	St Dev
S	21.22	1.02	23.71	0.82	24.10	1.14	21.42	2.40	29.91	29.91	29.70	1.23
Au	0.06	0.04	0.05	0.03	0.04	0.03	0.05	0.02	0.06	0.06	0.05	0.04
Fe	2.60	2.21	1.27	0.79	1.13	0.76	1.07	0.31	2.33	2.33	1.14	0.96
As	0.00	-	0.03	0.04	0.02	0.03	0.02	0.02	0.06	0.06	0.04	0.02
Cu	76.77	2.81	75.47	1.21	75.32	1.10	79.24	3.38	67.34	67.34	68.02	1.42
Co	0.01	0.00	0.00	-	0.01	0.01	0.01	0.00	0.01	0.01	0.01	0.00
Mn	0.03	0.01	<lld	<lld	<lld	<lld	<lld	<lld	<lld	<lld	<lld	<lld
Ni	0.01	0.00	0.01	0.01	0.01	0.01	0.02	0.02	0.01	0.01	0.01	0.01
Ag	<lld	<lld	0.01	0.00	0.01	0.00	0.02	0.01	0.01	0.01	0.02	0.02
Mo	<lld	<lld	<lld	<lld	<lld	<lld	<lld	<lld	<lld	<lld	<lld	<lld
Pb	<lld	<lld	<lld	<lld	<lld	<lld	<lld	<lld	<lld	<lld	<lld	<lld
Zn	<lld	<lld	<lld	<lld	<lld	<lld	<lld	<lld	<lld	<lld	<lld	<lld
Avg. Total	100.67		99.78		98.95		100.65		99.11		98.95	

Table 4.7: Summary of the average weight % and standard deviation for the major oxides analysed for the silicates (biotite and chlorite) and feldspar (albite), determined by EMPA, where n = number of analyses.

Mineral Name	**Biotite**		**Chlorite**		**Albite**	
Sample	**MN-010**		**MN-010**		**MN-009**	
n	9		8		12	
Locality/ description	Knotted-Schist		Knotted-Schist		Knotted Biotite Schist	
Calc formula	$K(Mg_{0.93}Fe^{2+}_{1.59})Al_{1.62}\ Si_{2.70}O_{10}(OH)_2$		$Fe_{2.28}Mg_{2.08}Al_{2.9}Si_{2.6}O_{10}\,(OH)_8$		$NaAlSi_3O_8$	
Major oxide	Wt. %	St Dev	Wt. %	St Dev	Wt. %	St Dev
SiO_2	35.40	0.39	24.85	0.25	68.44	0.28
TiO_2	1.39	0.06	0.07	0.03	0.01	0.01
Al_2O_3	18.00	0.29	23.11	0.54	20.23	0.16
FeO	24.89	0.70	30.00	2.47	0.02	0.01
MnO	0.07	0.03	0.09	0.04	0.02	0.02
MgO	8.19	0.43	13.15	1.74	0.01	0.01
CaO	0.01	0.01	0.01	0.01	0.15	0.09
Na_2O	0.10	0.04	0.04	0.02	11.12	0.17
K_2O	9.39	0.09	0.02	0.01	0.08	0.01
CuO	0.47	0.05	0.45	0.45	-	-
Cr_2O_3	0.03	0.02	0.04	0.01	0.02	0.01
Ave. Total	97.57		91.57		100.08	

4.2.1 Sediment-hosted mineralisation

Sediment-hosted mineralisation occurs predominantly within clastic units (i.e. phyllites) in the UMC and MMC and to a lesser extent within the knotted schists. Chalcopyrite is the primary ore mineral and usually occurs as fine grained disseminations and stringers parallel to the bedding plans (Figure 4.1). This mineralisation style makes a minor contribution to the sulphide ore percentage.

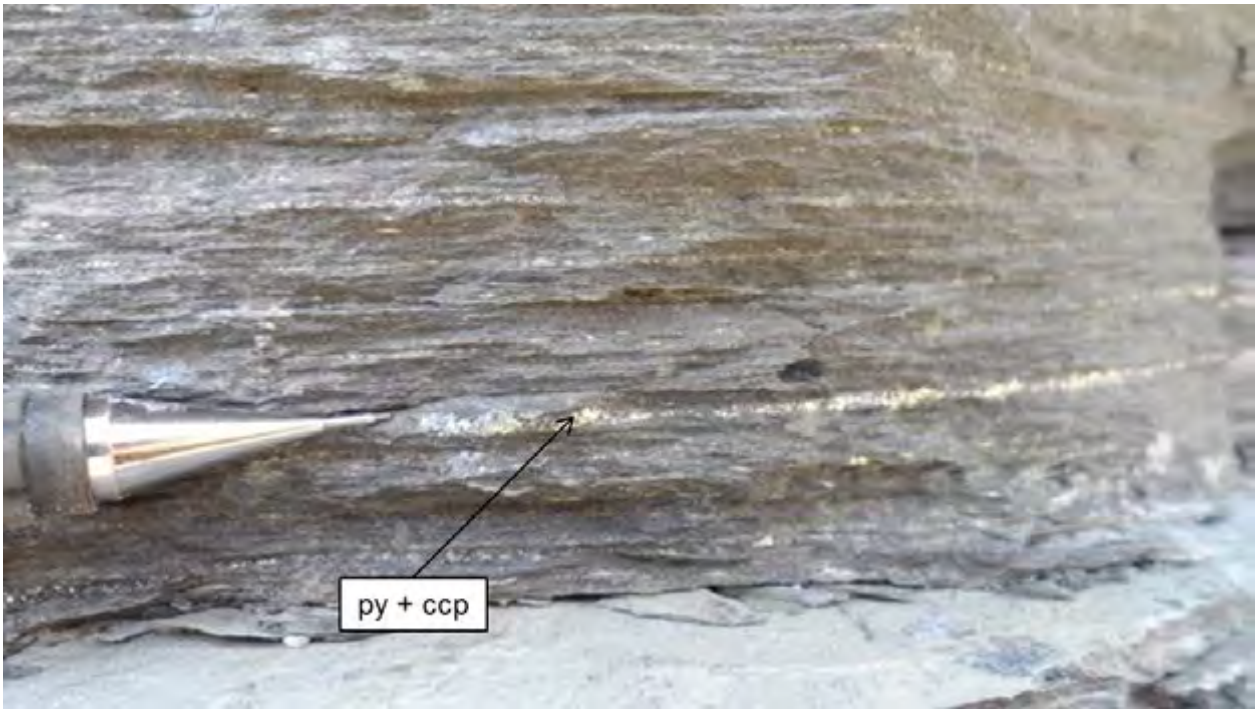

Figure 4.1: Sediment-hosted mineralisation within the Knotted schist of MMC, strike and dip (125/35 ˚), located within the Main pit, characterised by finely disseminated and stringer pyrite and minor chalcopyrite grains oriented parallel to the bedding planes.

Phyllite

The phyllite contains the highest density of sediment-hosted and vein-hosted mineralisation and is found at different stratigraphic levels. Chalcopyrite is the main ore mineral for both mineralisation styles, other ore minerals associated only with vein-hosted mineralisation include covellite with minor amounts of chalcocite, digenite and malachite. The principal gangue minerals irrespective of mineralisation are pyrite, quartz, biotite, chlorite and albite (Figure 4.2).

The carbonaceous phyllites differ with regards to their higher graphite content and low ore mineral content (Figure 4.2). Sample MN-012 is poorly mineralized and consists mostly of SiO_2 (~59 wt. %) with lesser amounts of Al_2O_3 and Fe_2O_3 (Table 4.3). The quartz-carbonate veins that frequently crosscut this lithology are represented by samples MN-011 A and MN-011 B, and are characterized by high Cu, Fe and S quantities. Sample MN-014C has experienced a high degree of weathering and oxidation and differs with respect to its high CuO content (~44 wt. %), which is attributed to the presence of malachite and chrysocolla. It also has high SiO_2, Fe_2O_3 and CaO values, with the excess Fe_2O_3 existing as goethite. Common between all the samples are the high Loss on Ignition (LOI) values (Avg. 8.6 wt. %) that are indicative of the presence of the phyllosilicates (biotite, chlorite and kaolinite), graphite and carbonates.

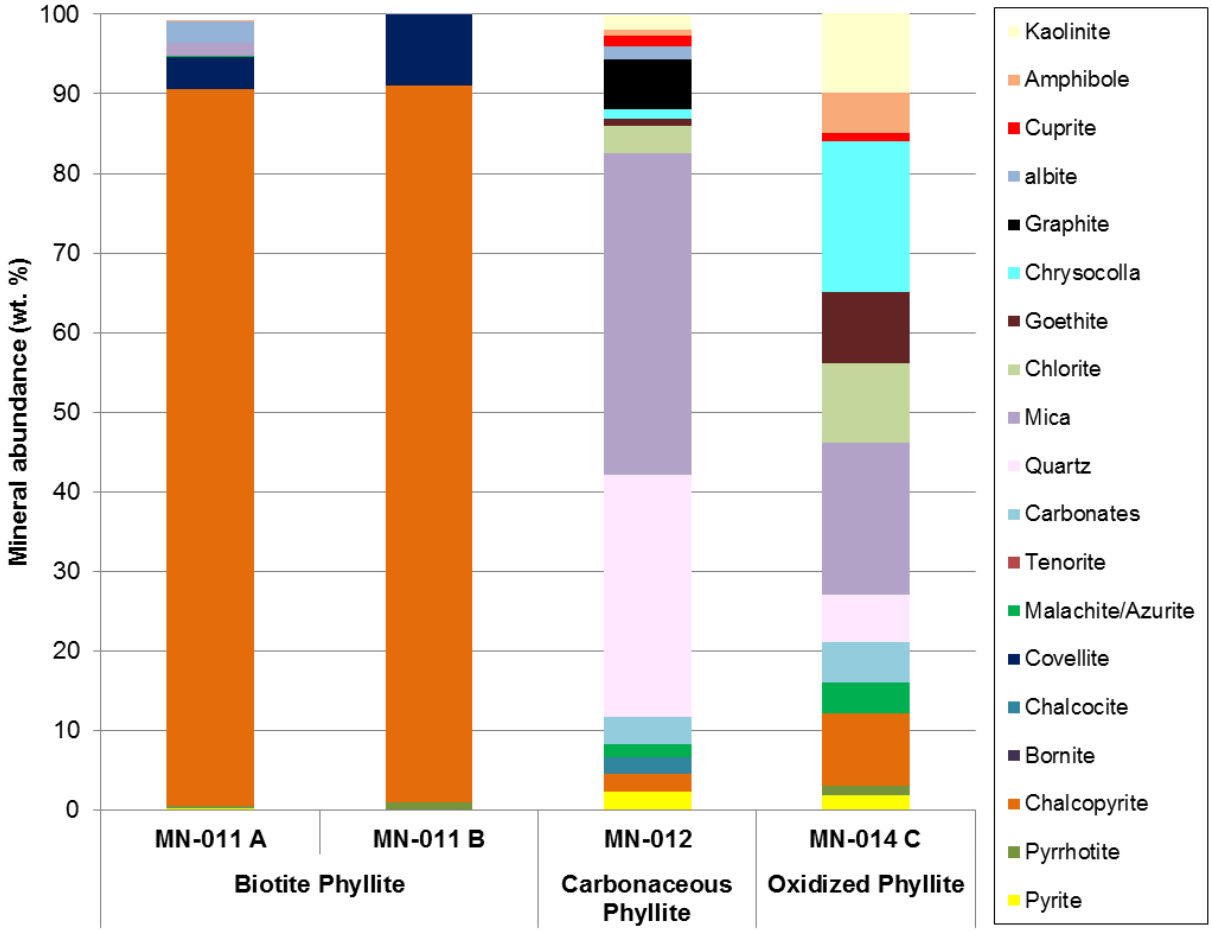

Figure 4.2: Bulk mineralogy of various phyllite samples, as determined by QXRD.

The phyllite units have an overall porphyroblastic texture (Figure 4.3 a), and three characteristic ore textures; coarse-grained, boxwork and disseminated as illustrated in Figure 4.3 a to d. Sulphide mineralisation is primarily coarse-grained (> 0.5 mm), relating to the quartz-carbonate veining that is prevalent within this lithology (Figure 4.3 c). Secondary copper oxide mineralisation is commonly associated with boxwork texture, with replacement being partial or complete depending on the extent of oxidation (Figure 4.3 d). The variety of textures related to the replacement reactions result in grain size variations that cause a decrease in the chalcopyrite grain size and produce secondary copper sulphides that are of equivalent to or of a finer grain size (< 0.2 mm) than that of the primary copper sulphide. Disseminated mineralisation is characterized by fine-grained (≤ 0.1 mm) disseminations of mainly chalcopyrite and pyrite, and pyrrhotite that occur as lenses throughout the matrix and as fine-grained bands that lie parallel to the bedding planes. The mica minerals define the foliation and show a preferred orientation in the direction of minimum stress during deformation (Figure 4.3 c).

The presence of large euhedral pyrite porphyroblasts (0.5 mm to ≥ 50 mm) set in a fine-grained matrix of quartz, sericite, mica and chlorite gives rise to an overall porphyroblastic texture characteristic of the phyllite units (Figure 4.3 d).

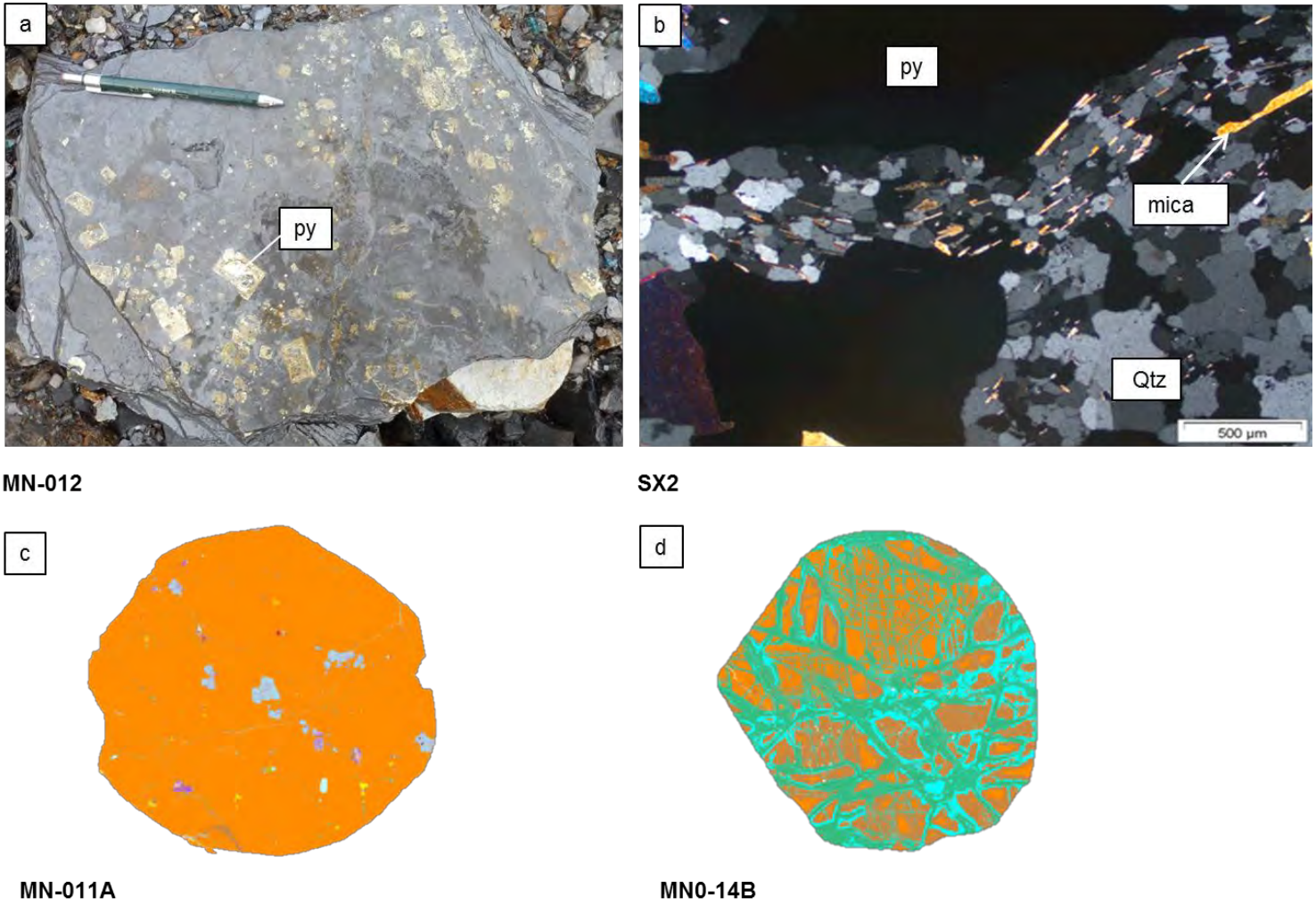

Figure 4.3: Photograph of a) carbonaceous phyllite hand sample from the NW pit with large euhedral pyrite porphyroblasts set in a fine-grained matrix of primarly quartz, sericite, biotite and chlorite. Transmitted light photograph b) sample SX2 was assigned as phyllite because it's fine-grained texture and well developed foliation defined by mica (biotite and chlorite) showing preferred orientation along the plane of minimum stress, representative of sediment-hosted mineralisation. QEMSCAN false coloured images illustrating c) the coarse-grained texture of vein-hosted mineralisation (quartz-carbonate veins) that cross-cut the host lithology d) distinctive box-work texture with chalcopyrite being replaced by iron-hydroxides that form a rim around chalcopyrite, with late stage infilling of fractures with chrysocolla and malachite.

Knotted Schist

The extent of sediment-hosted mineralisation within the schist is dependent upon the degree of albite-carbonate alteration present within the lithological unit. This style of alteration is most prevalent within the MMC with small packets occurring within the UM and much less extensive in the LCS and LM (Chinyuku, 2013). Alteration of this nature occurs within the Biotite Schists and rarely within the Knotted Schists. As a result, the Knotted Schists are not commonly associated with disseminated mineralisation (Chinyuku, 2013). The Quartz-carbonate vein density is also significantly lower within the Schist compared to the Phyllite and as a result, has a lower quantity of Cu-bearing minerals (Chinyuku, 2013). Chalcopyrite and covellite are the main ore minerals, with chalcocite, malachite and chrysocolla also present in minor amounts (Figure 4.4). The gangue mineralogy of mineralized samples consists of carbonates (ferroan dolomite and calcite), albite, quartz, pyrite and minor pyrrhotite, which is to be expected as this mineralisation is associated with albite-carbonate alteration. The occurrence of sericite is rare and is found in association with albite alteration, and generally occurs at the margins of albite bleached zones (Figure 4.5 a). Carbonate alteration is commonly observed within the Biotite Schist, and as a result there is the addition of mostly ferroan dolomite, with minor dolomite, and albite to this lithology. Sericite and carbonate have been shown to occur as replacement products of garnets (Cyprus Amax, 2000).

The chemistry of samples MN-009 and MN-010 obtained by XRF analyses vary significantly, which is to be expected as sample MN-009 represents a quartz-carbonate vein that cross-cuts the knotted biotite schist and MN-010 represents the poorly mineralized knotted schist. Sample MN-009 consists predominantly of CaO (~36 wt. %), with lesser amounts of SiO_2, MgO, Al_2O_3, Fe_2O_3 and CuO, and the highest LOI value (Table 4.2.3). Sample MN-010 differs as it consists largely of SiO_2 (~61 wt. %) with lesser amounts of Al_2O_3, Fe_2O_3, MgO, Na_2O, K_2O, CuO, and the lowest LOI value (Table 4.3). The high LOI value of sample MN-009 and low LOI value of sample MN-010 suggests that MN-009 consists largely of carbonates with lesser phyllosilicates, compared to MN-010, which has lower carbonate content and higher phyllosilicate abundances. The XRF and QXRD data for both samples broadly coincide, with sample MN-009 consisting primarily carbonates with significant amounts of chalcopyrite, compared to sample MN-010 that consists mainly of quartz with minor amounts of chalcopyrite (Figure 4.4). The bulk of the CuO in sample MN-010 is hosted with covellite that formed through the replacement of chalcopyrite.

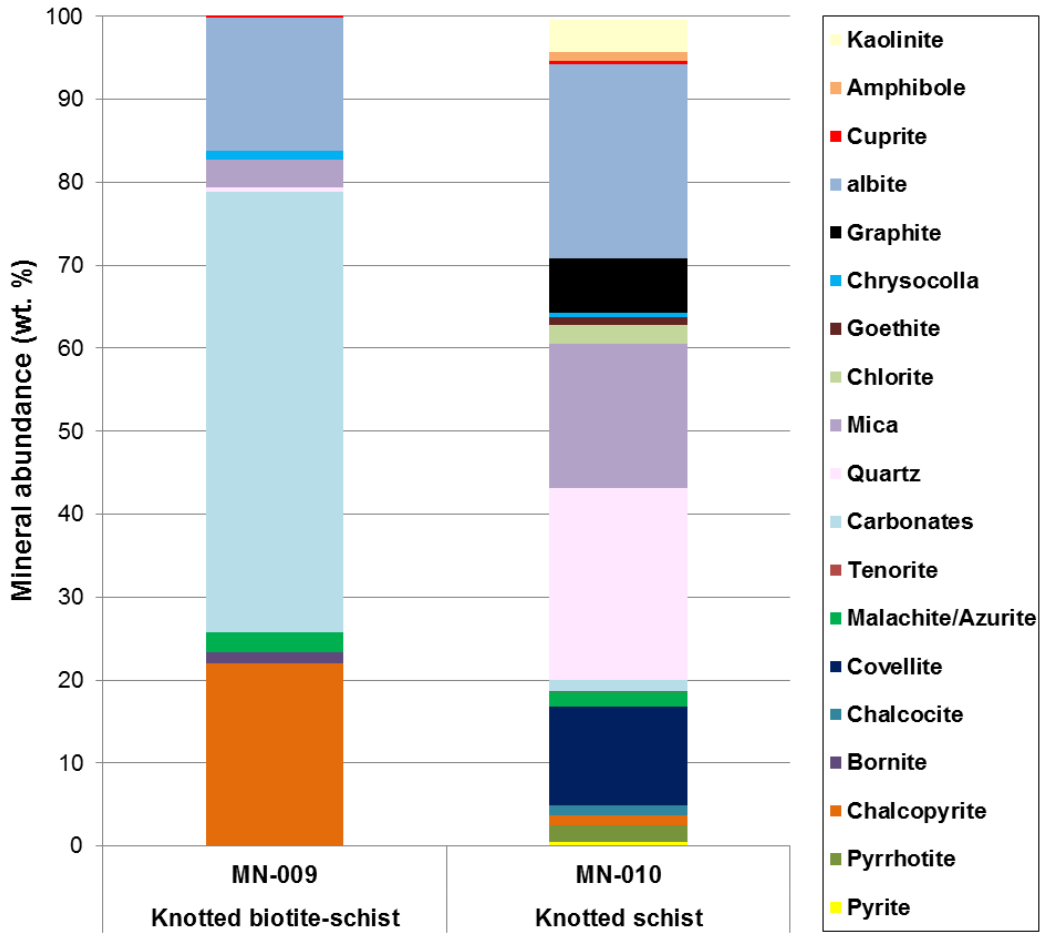

Figure 4.4: Bulk mineralogy of two representative Schist samples, as determined by QXRD.

The knotted and biotite schist are characterized by porphyroblastic textures (Figure 4.5 a-b). The primary sulphides chalcopyrite and pyrite also occur as fine-grained disseminations along bedding/foliations planes and as randomly distributed blebs (≤ 0.2 mm) within the matrix (Figure 4.5 b). The porphyroblasts are defined by large subhedral to euhedral garnet or biotite (≥ 0.5 mm) set in a fine grained matrix composed of quartz, albite, chlorite and occasional carbonates (Figure 4.5 c). Biotite and chlorite define the foliation, showing a distinct preferred orientation parallel to the bedding and direction of minimum stress (Figure 4.5 d). The quartz-carbonate veins that cross-cut this lithology has a massive to coarse-grained texture (Figure 4.5 e).

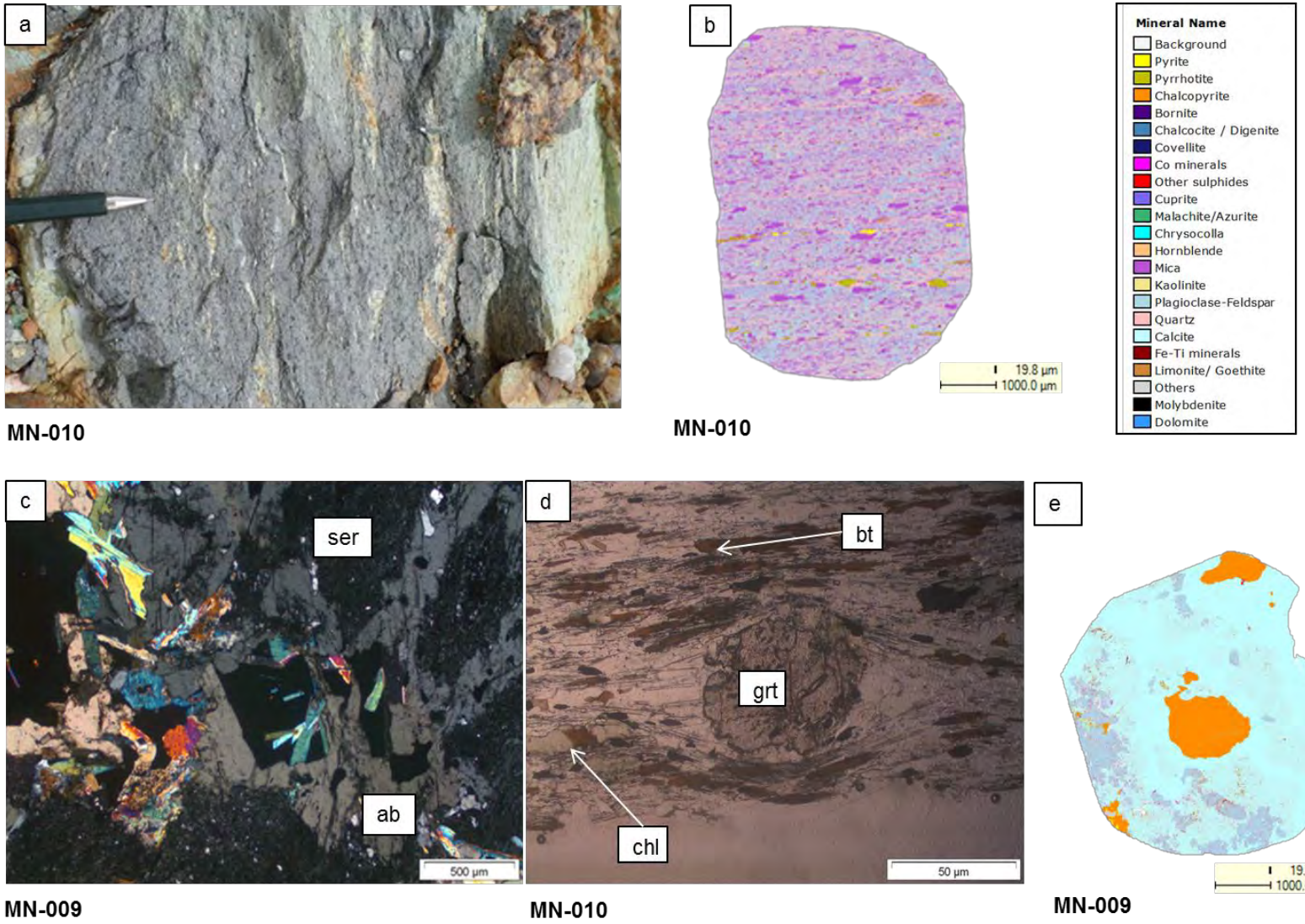

Figure 4.5: Photograph of a) porphyroblastic texture of Knotted Schist. QEMSCAN false coloured images of b) Illustrating the foliated nature of sample, defined by mica and fine-grained pyrite and chalcopyrite disseminations aligned parallel to the foliation. Transmitted light photograph of c) sericite alteration occurring with albite alteration d) barren Knotted Schist sample, with the foliation being defined by mica that wraps around the garnet porphyroblast e) coarse-grained texture of quartz-carbonate veins hosted within mineralized biotite schist samples.

4.2.2 Vein-hosted mineralisation

Quartz-carbonate veins

These mineralized veins are representative of vein-hosted mineralisation and are broadly confined to the Lower Marble (LM) and Middle Mixed Clastic (MMC) units, with veining being most abundant within the MMC of the Kansanshi mine stratigraphy (Figure 4.6). The primary sulphide mineralogy of these veins is characterised by the dominance of chalcopyrite, with lesser amounts of pyrite, chalcocite, covellite and pyrrhotite, and rare bornite, which is more prevalent in the NW Pit (Figure 4.7 and Table 4.4). The abundance of these minerals is highly variable, with chalcopyrite content ranging from 10 to 60 wt. % and the quantity of the secondary sulphides between almost negligible to 18 wt. % as seen in samples MN-008 and SX (Table 4.4), with the quantity of secondary sulphides present within these being heavily dependent upon the extent of oxidation and weathering of the host rock. It should be noted that when these veins are weathered they are classified under the supergene mineralisation type discussed in section 4.2.3.

The associated gangue mineral assemblage is dominated by carbonates (Table 4.3) with variable quartz abundances and minor amounts of biotite and chlorite, with graphite present locally within the carbonaceous lithological units (Figure 4.7 and Table 4.4). Albite alteration commonly occurs in veins that are in contact with either marble units or carbonate alteration bands (Chinyuku, 2013). Major oxides analyses of feldspars by EMPA indicate that the feldspar is albite, which may account for as much as 34 wt. % of the sample (MN-008) (Table 4.4-4.6). XRF and QEMSCAN analyses indicate that the carbonates consist of ferroan calcite and dolomite (Table 4.3).

XRF data of quartz-carbonate-vein samples (i.e. MN-008, MN-009, MN-011 A and B), Table 4.3, illustrate that the samples contain predominantly SiO_2 and CaO, and minor amounts of Al_2O_3, Fe_2O_3, MgO, and CuO. However, samples MN-011 A and MN-011 B consist principally of S and Cu, with Fe present as chalcopyrite. The XRF data indicate that the major elements present coincide broadly with those typical for the minerals identified in the XRD analyses. This indicates that the samples contain mostly quartz and carbonates, with minor amounts of phyllosilicate minerals (biotite and chlorite) as the dominate gangue minerals, and chalcopyrite as the primary sulphide ore mineral present. The high LOI value indicates a high volatile content

and confirms the presence of carbonates and phyllosilicate gangue minerals. The remaining major oxides were present in negligible amounts.

According to Broughton et al., 2002, minor amounts of gold, silver and nickel are a common occurrence with these veins, as well as the rare occurrences of U-Th minerals, molybdenite and uraninite. However, in the samples used for EMPA, gold, silver and nickel were largely below the detection limit (Table 4.5). No U-Th minerals were identified by the various analytical techniques utilized.

Figure 4.6: Vein-hosted mineralisation represented by quartz-carbonate-sulphide veins dolomite units of the Main pit, consisting mainly of calcite, chalcopyrite and pyrite hosted within schist of the MMC. View towards 220^0, strike and dip ($210/80^0$). Field book used for scale.

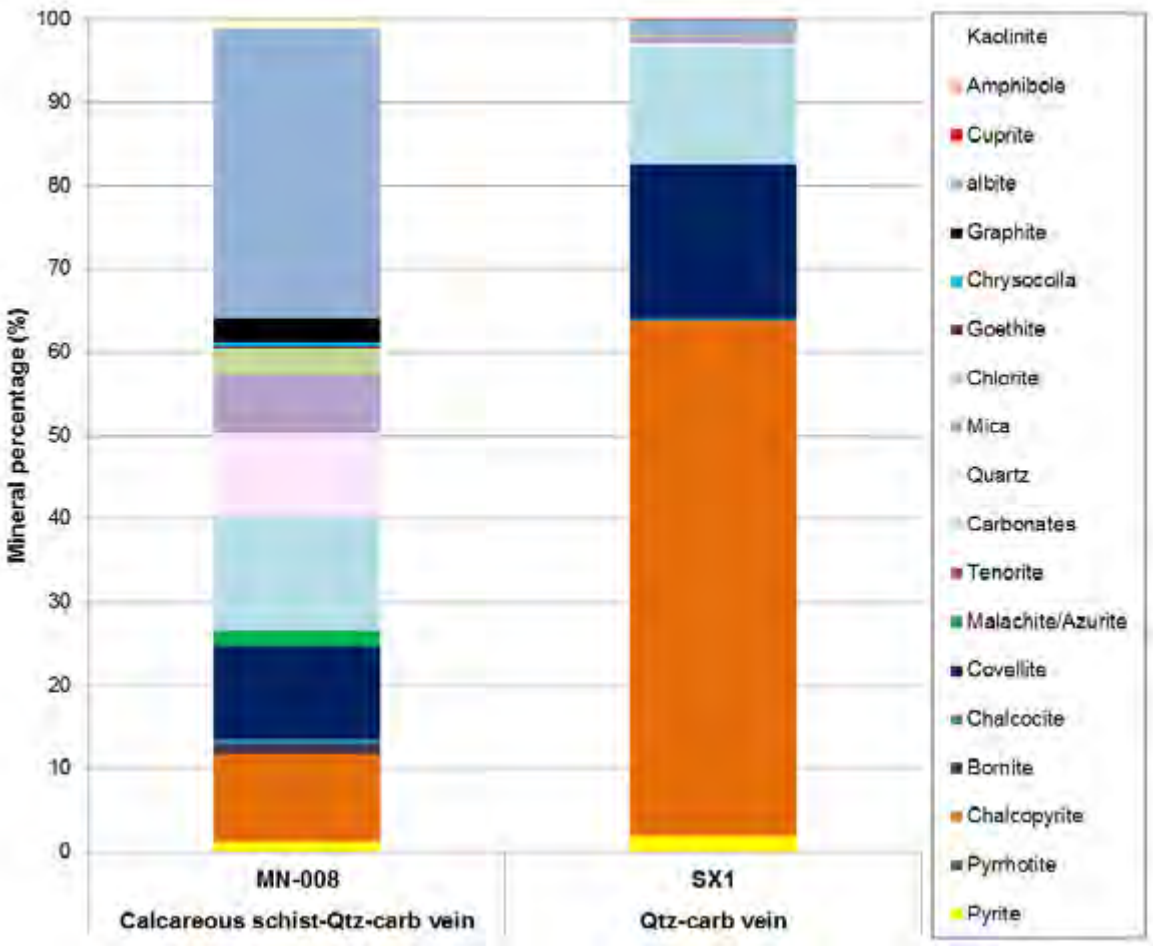

Figure 4.7: Bulk mineralogy of the quartz-carbonate veins samples that cut through differing lithologies, determined by QXRD.

Coarse-grained sulphide mineralisation is characteristic of the quartz-carbonate veins with local disseminated mineralisation and minor stringer mineralisation styles as common occurrences within the Lower Pebble Schist (Figure 4.8 a). The overall textures of these veins vary from massive to brecciated (Figure 4.8 a-c).

Large rounded sulphide (chalcopyrite and pyrite) grains (>0.5 mm), commonly described as having a 'buckshot' texture, are seen frequently within these veins (Figure 4.8 d). Sulphides associated with the disseminated texture occur as isolated grains, as fracture fillings and as fine-grained bands that are aligned parallel to the sedimentary bedding, with the average grain size of chalcopyrite and pyrite being 0.01 mm (Figure 4.8 d-e).

Pyrite occurs as anhedral grains (<0.1 mm) within interstitial sites between clastic sediments (Figure 4.8 e) and as euhedral to subhedral grains (<0.2 mm) enclosed within massive

chalcopyrite grains (>1 mm) (Figure 4.9 a). Mineralized veins are often associated with alteration haloes dominated by albite and to a lesser extent ferroan dolomite and calcite, and green mica (Figure 4.9 b). XRF and XRD analyses suggest this is V-rich muscovite (Appendix B & C).

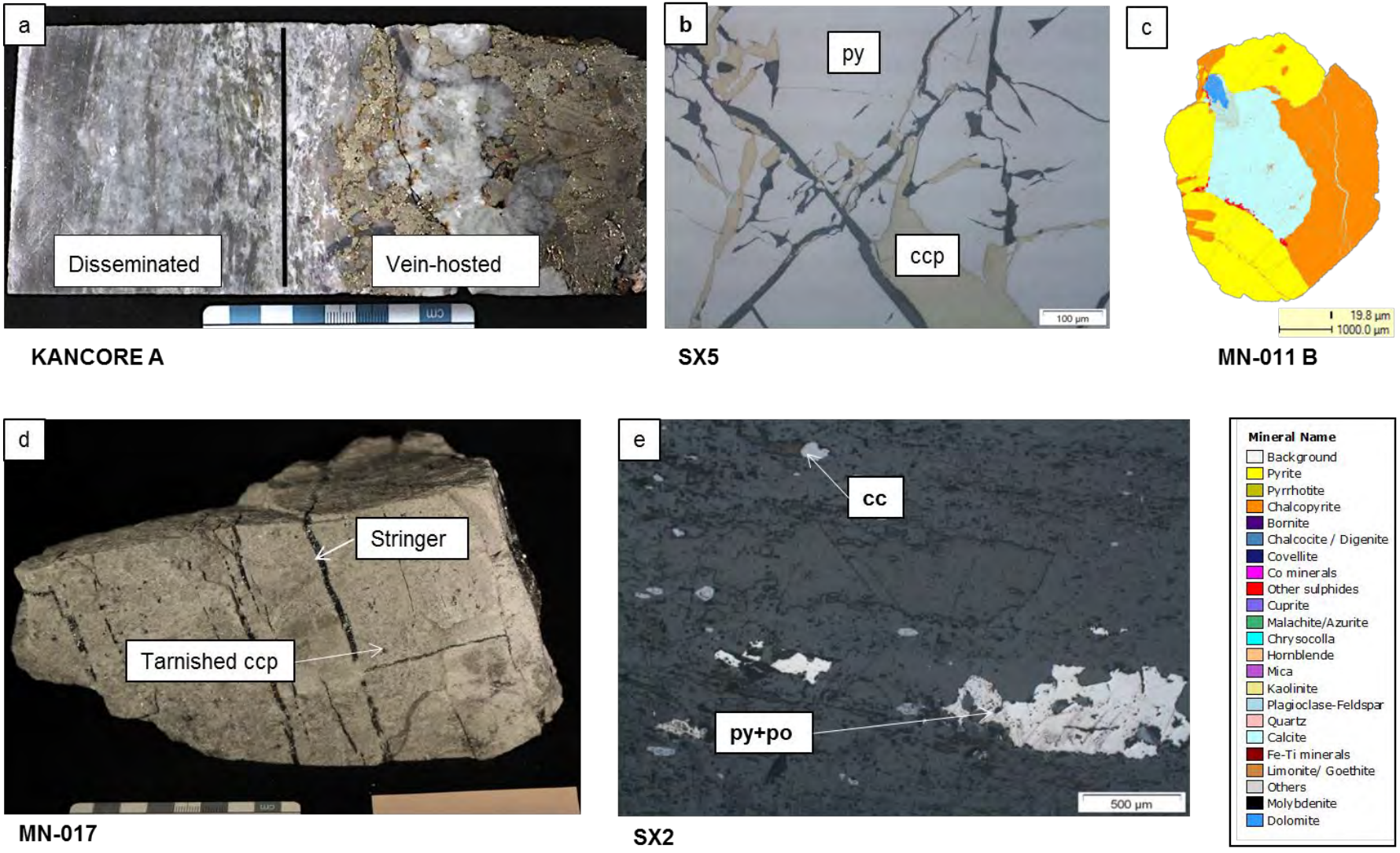

Figure 4.8: The following images are representative of the quartz-carbonate-veins**:** Photograph of sulphide ore core sample representative of the a) massive and laminated textures associated with the quartz-carbonate veins. Reflected light photomicrograph of b) characteristic coarse-grained veins. QEMSCAN false coloured image illustrating c) the coarse grained texture of the sulphides and associated gangue mineralogy. Photograph of d) Stringer type mineralisation that occurs in minor amounts within Lower Pebble Schist and "buckshot" texture (rounded grains of tarnished chalcopyrite of detrital origin) indicated by the arrow. Reflected light photomicrograph of e) disseminated anhedral sulphide grains in a fine-grained meta-sedimentary matrix of quartz, mica, and graphite.

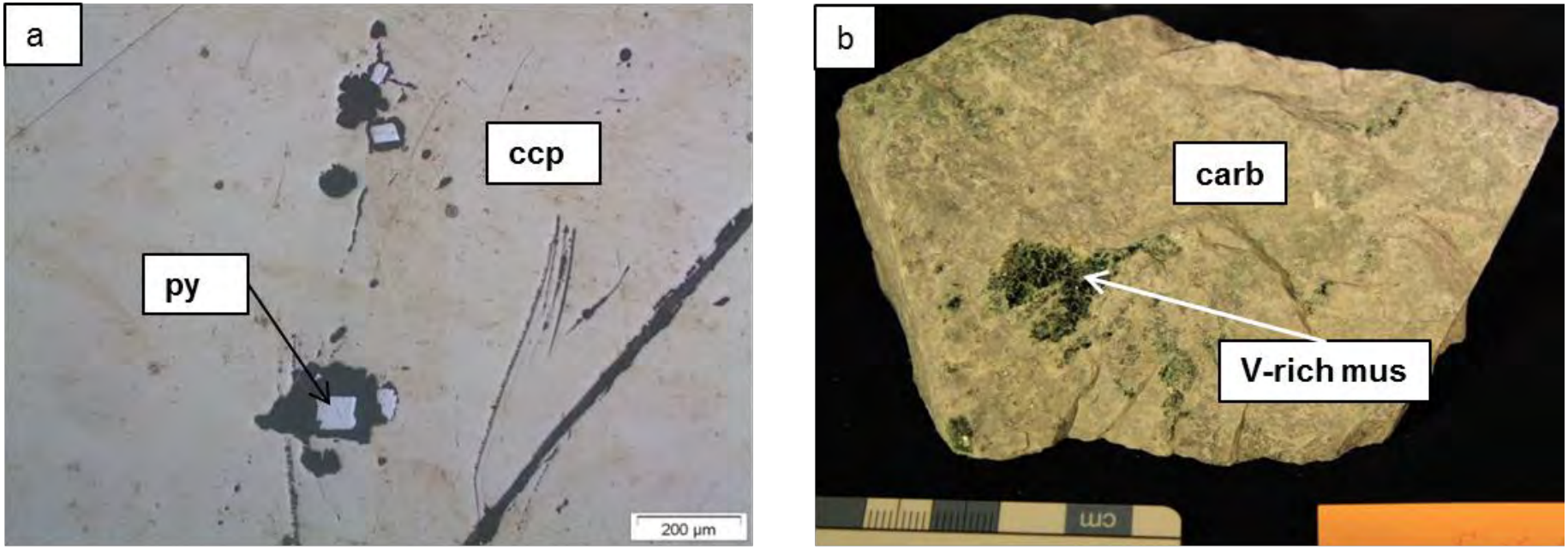

Figure 4.9: The following images are representative of the quartz-carbonate-veins: Reflected light photomicrograph of a) euhedral pyrite grains surrounded by grey pressure shadows within coarse-grained chalcopyrite vein, representative of complex locking texture. Photograph of b) common alteration minerals within mineralized veins including: carbonates (ferroan dolomite and calcite), and "porphyroblasts" of vanadium-rich muscovite, as determined by XRD.

4.2.3 Breccia-hosted and supergene mineralisation

Later supergene related mineralisation overprints all previous mineralisation styles and makes the largest contribution to the overall ore percentage within the deposit, constituting both the mixed and oxide ores. The genesis of the breccia and supergene alteration is poorly understood and is beyond the scope of this study.

Brecciation is structurally controlled and corresponds to zones of greater veining density and occurs as breccia and carbonate breccia (section 2.1.2) (Figure 4.10). There are at least two breccia zones present within the deposit, the 4800 and 5400 zone. These are supported by angular to sub-rounded wall-rock fragments and veins of variable sizes, with wall rock fragments that are often seen to be completely re-oriented. The mineralogy of these mineralized brecciated zones is highly variable, consisting primarily of copper oxide, minor amounts of secondary sulphides and even fewer primary sulphides together with their associated gangue mineral assemblage (Figure 4.11).

Figure 4.10: Photograph of the NW corner of the "4800" zone within the Main Pit, illustrating the extent of supergene enrichment. The breccia zone trends NNE, of the dip, and transgresses the lithologies. This zone is the primary contributor to the oxide ore consisting mainly of chrysocolla and malachite.

Figure 4.11 illustrates that the Breccia “4800” zone is characterised by two distinct mineralogies, namely oxidized (A) samples and partially oxidized (B) samples. The gangue mineralogy of both sample types comprises primarily of fine to medium-grained quartz, often intergrown with lesser albite and carbonates, together with lesser amounts of kaolinite and the chlorite (Table 4.4 and Figure 4.11). The ore minerals associated with the oxidized (A) samples are characterized by the dominance of copper oxides, malachite and chrysocolla, with lesser amounts of tenorite and azurite (Figure 4.11); azurite being identified during petrographic analysis (Figure 4.12). The secondary sulphides, chalcocite, digenite and covellite, are present in minor amounts with primary copper sulphides being generally absent within these oxide samples. The partially (B) oxidized samples are notably differentiated from the oxide samples by the abundance of primary and secondary sulphide ore minerals, such as, chalcopyrite, chalcocite, digenite and covellite. Copper oxide minerals occur in lesser amounts (~11 wt. %) compared to the sulphides (~38 wt. %), but still make a significant contribution to the ore percentage as seen in samples MN-003 B (Table 4.4 and Figure 4.11).

XRF analyses of the oxidized samples (MN-002A-C, MN-006 and MN-003A) illustrate that these samples consist mostly of SiO_2 (Ave. 58 wt. %), with significant amounts Al_2O_3, CuO and minor quantities of Fe_2O_3 (Ave. 2.9 wt. %) (Table 4.3). These samples are characterized by high LOI content (Ave. 8.2 wt. %) and low sulphur abundances (Ave. 0.09 wt. %), which suggest the absence of sulphides and the presences of phyllosilicates (biotite, chlorite and Kaolinite), and carbonate minerals. The partially oxidized samples (MN-004B, MN-003B and MN-001A-B) (Table 4.3) also consist mostly of SiO_2 (Avg. 25 wt. %), Cu, Fe and S, with minor amounts of Al_2O_3 and Fe_2O_3. Sample MN-001 A differs from the norm by its high Fe_2O_3 and LOI content. The high Fe_2O_3 quantity within sample MN-001 A is likely present as Fe-hydroxide (goethite). Sample MN-003 B also differs with respect to its higher Cu and S abundances, with Fe being the limiting element. The excess Cu and S in sample MN-003 B is not associated with chalcopyrite and exists as secondary sulphide (chalcocite) (Table 4.3 and Table 4.4). XRF data broadly coincide with the results obtained from XRD analyses, because the oxidized samples’ mineral assemblages consist mostly of quartz, albite, malachite and chrysocolla, with lesser amounts phyllosilicates (biotite, chlorite and Kaolinite) and carbonates. The partially oxidized samples are dominated by partially oxidized chalcopyrite, quartz and phyllosilicates, with lesser amounts of secondary sulphides and copper oxides, and rare bornite.

The breccia has been the most extensively affected by supergene enrichment (Figure 4.10), because the voids have provided pathways for the movement of fluids, which allowed for the subsequent oxidation of the primary sulphides (Torrealday et al., 2000; Broughton et al., 2002; Gregory et al., 2010; 2012). Consequently, all previous styles of mineralisation have been partially or completely overprinted by supergene processes, which have produced changes in the mineral assemblage and more importantly, in the texture. Minerals within oxidized samples typically occur as colloform and botryoidal aggregates within open spaces (Figure 4.12 a-b), with the most prominent structure being the cellular/boxwork texture, which forms by the dissolution of pyrite (Figure 4.12 c).

Fracturing and partial oxidation results in the formation of a distinctive stockwork associated with the mixed ores and the formation of the characteristic replacement intergrowth type, in which chalcopyrite coated by various secondary copper sulphides (chalcocite and covellite) growing as narrow rims around chalcopyrite (Figure 4.12 d-f). The secondary copper sulphides extend irregularly into the chalcopyrite grains, and in some case penetrate chalcopyrite along its crystallographic planes (Figure 4.12 f).

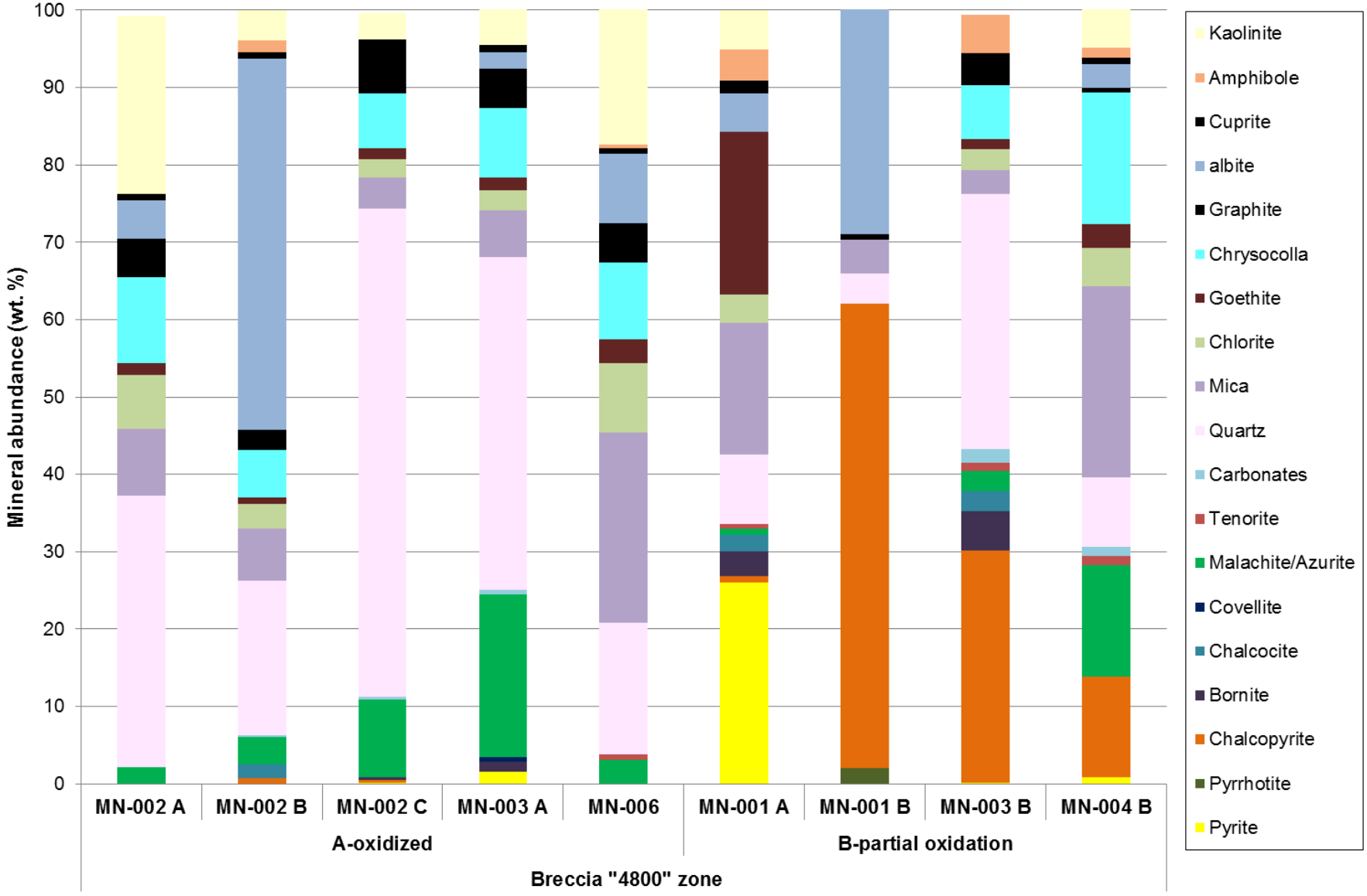

Figure 4.11: Bulk mineralogy of various breccia samples from the "4800" zone, and grouped in order of increasing chalcopyrite content and lithology, as determined by QXRD. The samples have been subdivided into two categories: namely, A-oxidized and B- partial oxidation. These categories are based upon the degree of weathering and oxidation the samples have experienced.

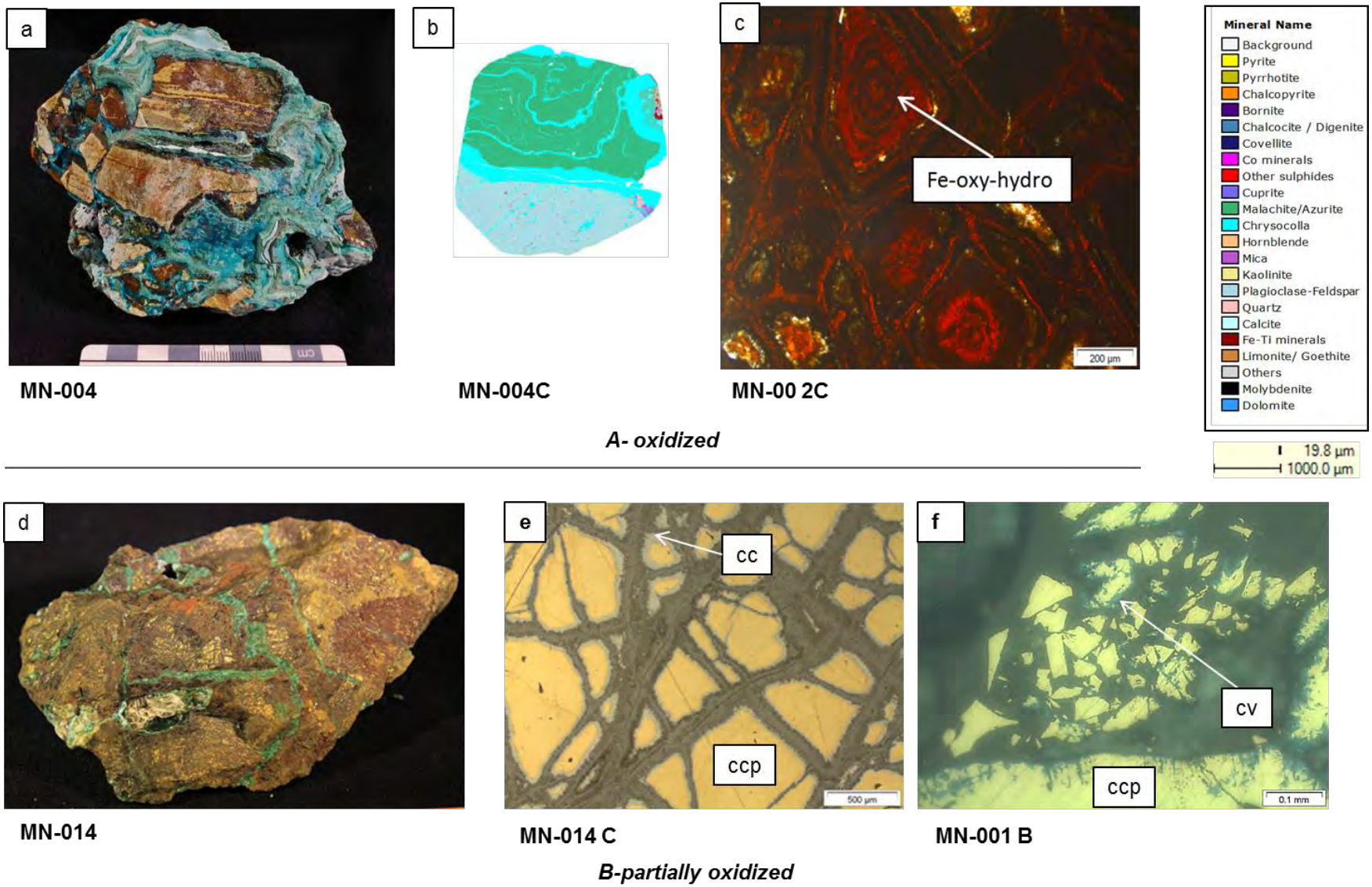

Figure 4.12: Photograph of a) oxidized sample MN004 breccia, representative Oxide ore sample. QEMSCAN false coloured image, b) showing colloform texture of malachite and chrysocolla. Transmitted light photomicrograph of c) celluar/boxwork texture that formed through the dissolution of pyrite during oxidation. Photograph of d) partially oxidized sample MN003, representative Mixed ore sample. Reflected light photomicrographs illustrating e) characteristic stockwork texture of partially oxidized samples and replacement textures characterized by coating of chalcopyrite by secondary copper sulphides (cc) f) replacement of chalcopyrite by covellite along its crystallographic plane.

4.2.4 Sulphide mineral chemistry and textures

Electron microprobe analyses were used to determine the chemistries of the primary and secondary copper sulphide minerals, and to assess if there were any variations in the composition of chalcopyrite between samples. Analyses of the chalcopyrite types (i.e. chalcopyrite grains from five different samples) by EMPA are presented in Table 4.5 &4.8 and Figure 4.13-4.15. The breccia zone is represented by samples MN-003 A and MN-001 B that were collected from locations within the "4800" zone. The bivalent plots contain only chalcopyrite data because the trace element values for the secondary sulphides chalcocite and covellite were below the detection limit.

Compositional analyses of the chalcopyrite types showed no significant variations in the average copper concentration between samples (Figure 4.13). Comparison of the average copper concentrations show ranges from 34.02 ± 0.51 to 35.47 ±1.12 wt. % Cu (Table 4.8). EMPA investigation revealed that there are no distinct chemical differences between the chalcopyrite types from the different samples and different lithologies, particularly with regards to sulphur and iron content (Figure 4.14 a-b).

Conversely, there are slight variations in the concentrations of trace elements in the different chalcopyrite types. The highest gold values are present within the quartz-carbonate vein sample (14.4 c). There is a weak positive correlation between the Cu:Au within the quartz-carbonate vein sample. The gold values greater than 1600 pm as seen in the breccia (MN-003 A) and oxidized phyllite (MN-014 C) are anomalous and statistical outliers, because the average gold grade Kansanshi is much lower than 1.6 g/t Au (Figure 4.14 c). The highest arsenic values are present with the quartz-carbonate vein sample (14.4 d). There is weak positive correlation between Au:As in the quartz-carbonate vein sample (14.4 e). The high concentrations of arsenic within the quartz-carbonate vein sample is of concern because copper production is subjected to extensive environmental regulation related to air and water quality, and materials handling and disposal practices (Matschullat, 2000). The presence of arsenic within copper ores reduces the economic value of the ore because of the penalties imposed on the smelting of ores with high arsenic content. This is because atmospheric arsenic emissions from copper smelting make the largest contribution to the amount of arsenic associated with the mining industry. Consequently, it has become the focus of pollution controls technological advancements (Matschullat, 2000).

There is a negative correlation between Cu:Ag for the breccia (MN-001 B) and oxidized phyllites (MN-014 C) (Figure 4.14 f). Conversely, the breccia (MN-003 A) sample shows a positive correlation between Cu:Ag and has lower silver values (Figure 4.14 f). This difference in Cu:Ag relationship between the breccia samples could be attributed to differing host lithologies. However, the reliability of the Ag data is uncertain, due to the large variability between samples. The highest nickel values are present within quartz-carbonate vein sample (Figure 4.14 g). The quartz-carbonate vein sample shows a weak positive correlation between Cu:Ni (Figure 4.14 g). Cobalt values were all below the detection limit and therefore not present in Figure 4.14.

Overall, trace elements such as Ag, Au and As display wide ranges of concentrations for all the chalcopyrite types, particularly the breccia (MN-003 A) and quartz-carbonate vein samples (Figure 4.14). The trace elements most likely residing in the chalcopyrite lattice at varying concentrations are Au, As, Ag, and Ni, as suggested by their consistent distribution within the different chalcopyrite types (Figure 4.14). According to Hershel (2011), chalcopyrite can contain a variety of trace elements. For example, Ni, Mn and Zn can substitute for Cu and Fe; As can substitute for sulphur. Trace amounts of Ag, Au, Pt, Pd, V, Cr, In, Al and Sb also occur (Baba et al., 2012). Many of these elements are present as minerals finely inter-grown within the chalcopyrite (Hershel, 2011). However, in this study, trace element concentrations of Zn, Pb and Mo were all below the EMPA detection limit, which was unexpected, because these trace elements have been identified in other studies, for example, Broughton et al. (2002).

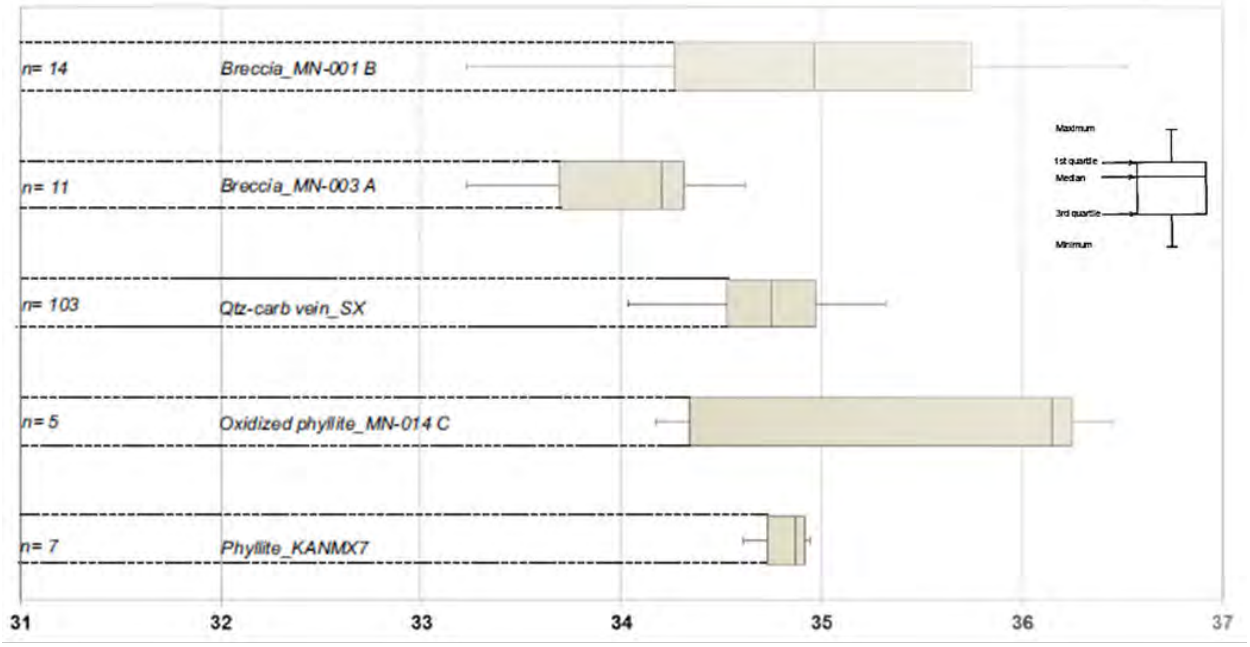

Figure 4.13: Box and whisker plots showing the copper concentration of chalcopyrite from five samples taken from different locations within the Kansanshi mine stratigraphy. The copper weight percent data were obtained by EMPA. The bottom and top of the box give the first and third quartiles, and the band inside the box gives the median. The ends of the whiskers represent the maximum and minimum values.

Table 4.8: Statistical data (maximum, minimum, mean values and number of analyses) of electron probe micro analysis (EPMA) of chalcopyrite. Major oxides are presented as wt. % and trace elements are presented in ppm.

Wt. % + ppm			S	Fe	Cu	Au	Ag	As	Co
Phyllite KANMX-7	n=7	Max	35.42	31	34.94	410	-	<lld	<lld
		Min	34.66	30.43	34.61	64	-	<lld	<lld
		Mean	35.08	30.68	34.87	263.25	-	<lld	<lld
Oxidized Phyllite MN-014 C	n=5	Max	36.6	30.31	36.45	1607	877	287	57
		Min	34.05	28.36	34.17	213	45	38	7
		Mean	34.98	29.23	36.15	685	531	127	32
Qtz-carb vein SX	n=95	Max	35.72	30.94	35.32	1170	-	877	196
		Min	33.97	29.56	34.03	31	-	37	3
		Mean	34.62	30.45	34.745	448	-	306.4	49.53
Breccia (MN-003 A)	n=11	Max	36.6	31.26	34.62	1607	194	151	67
		Min	34.77	29.81	33.23	195	4	38	19
		Mean	35.21	30.11	34.2	739.2	91.28	78.2	44
Breccia (MN-001 B)	n=14	Max	35.91	31.46	36.52	876	1633	171	204
		Min	33.82	27.8	33.23	130	9.19	38	46
		Mean	34.88	29.99	34.965	380.1	383.9	105.7	105.7

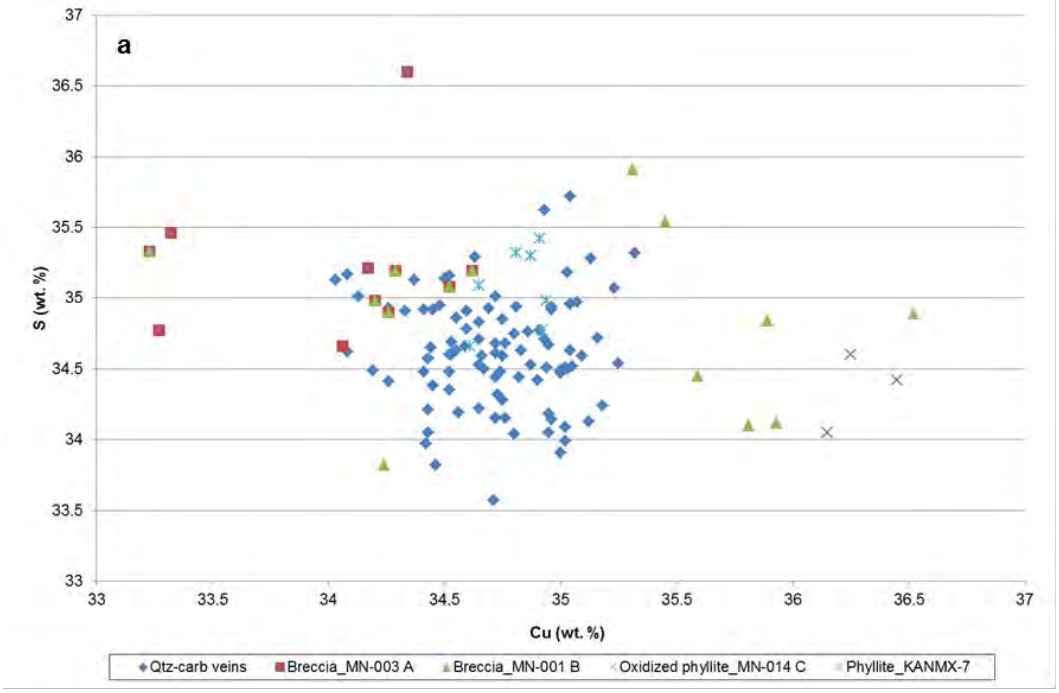

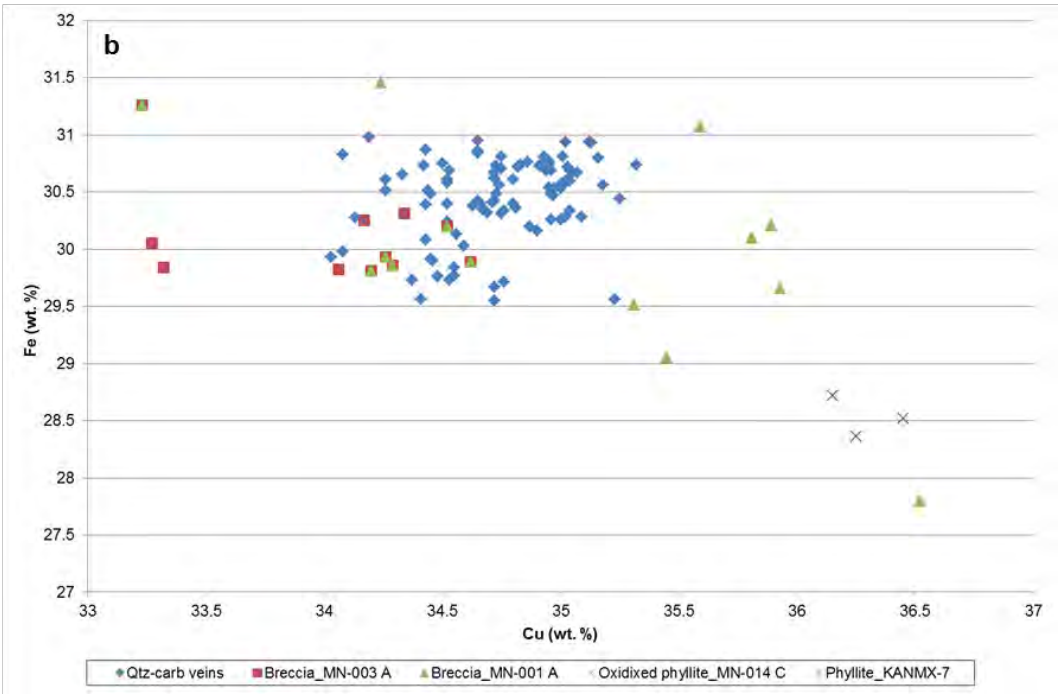

Figure 4.14: Bivariate plots of the trace elements and major oxide concentrations determined by EMPA in chalcopyrite grains from five samples with the following lithologies: breccia, phyllite and quartz-carbonate veins. The plots show the following: a) S vs Cu. b) Fe vs Cu. c) Au vs Cu. d) As vs Cu. e) As vs Au. f) Ag vs Cu. g) Ni vs Cu. Iron, Sulphur and copper presented as weight percent (wt. %). Trace element values are given in part per million (ppm). Ag, Co and As below detection limit for KANMX-7.

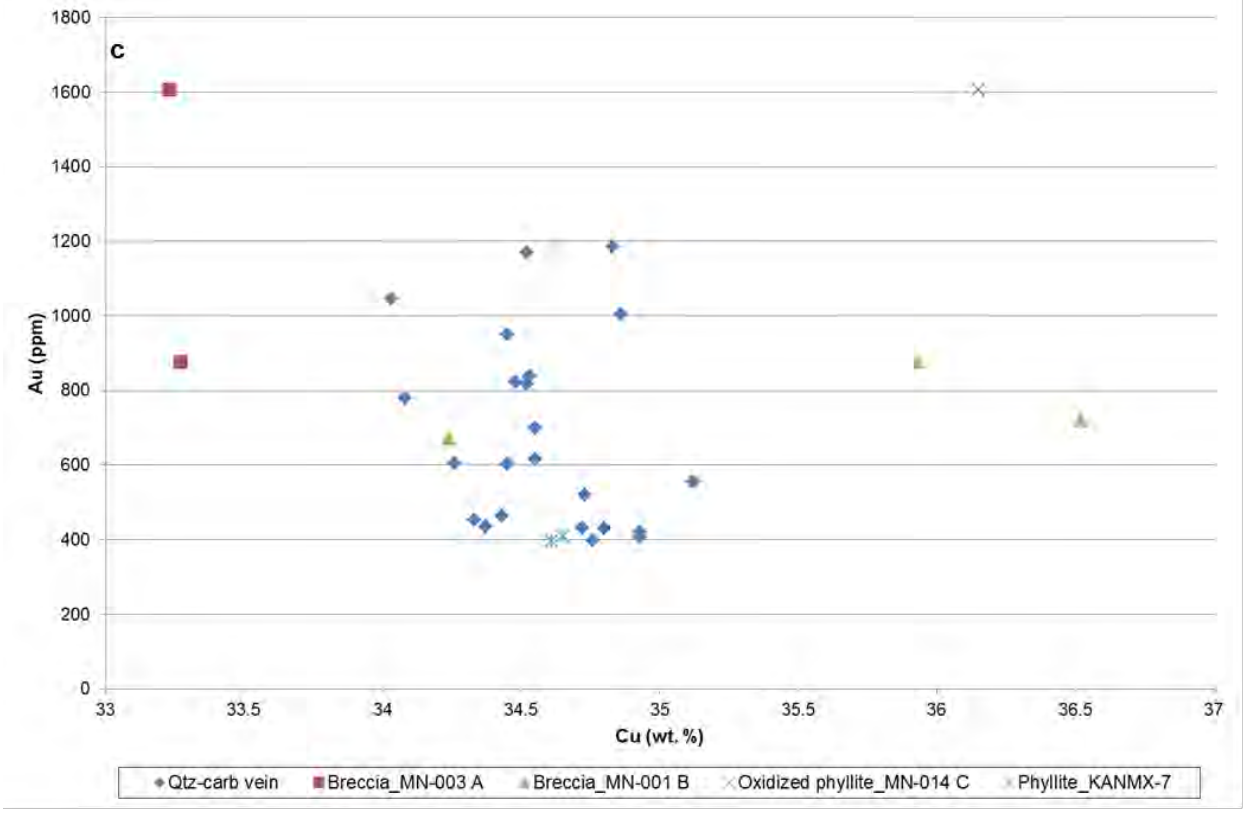

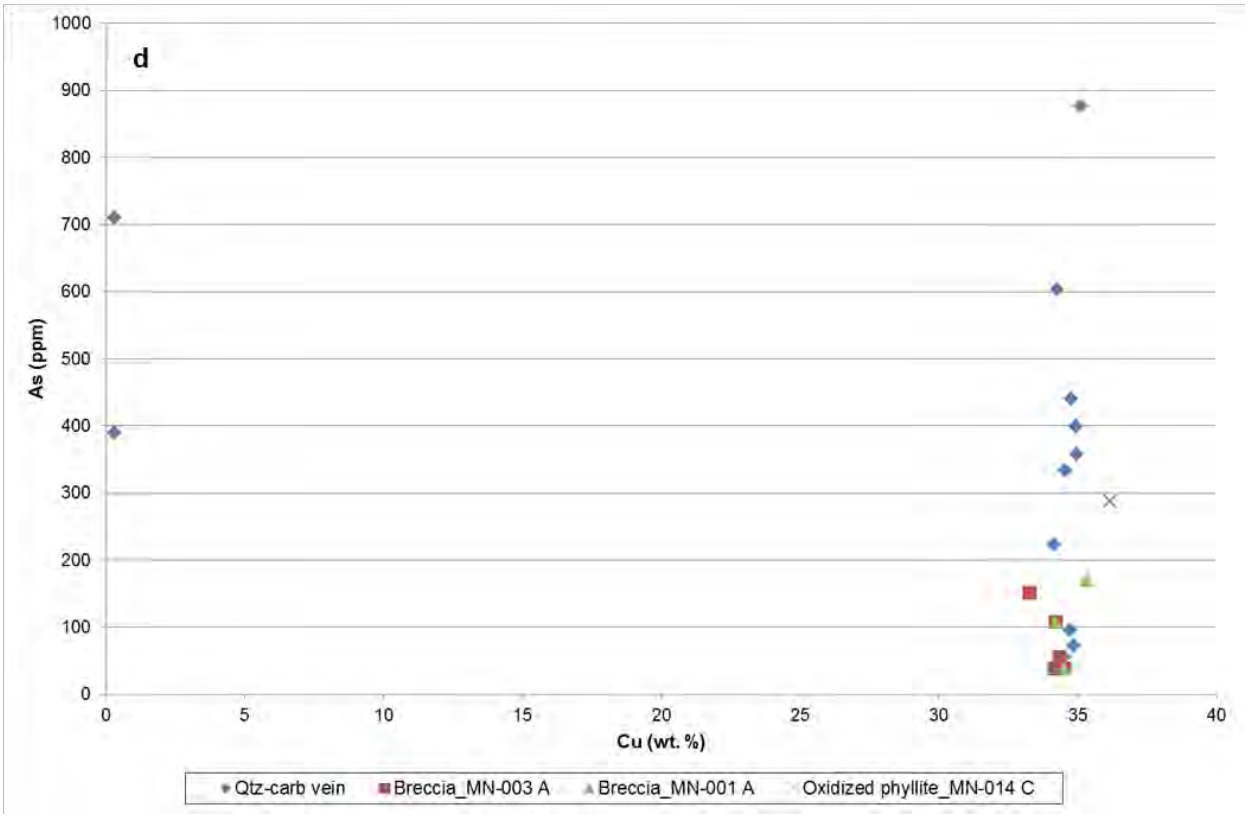

Figure 4.14: Continued

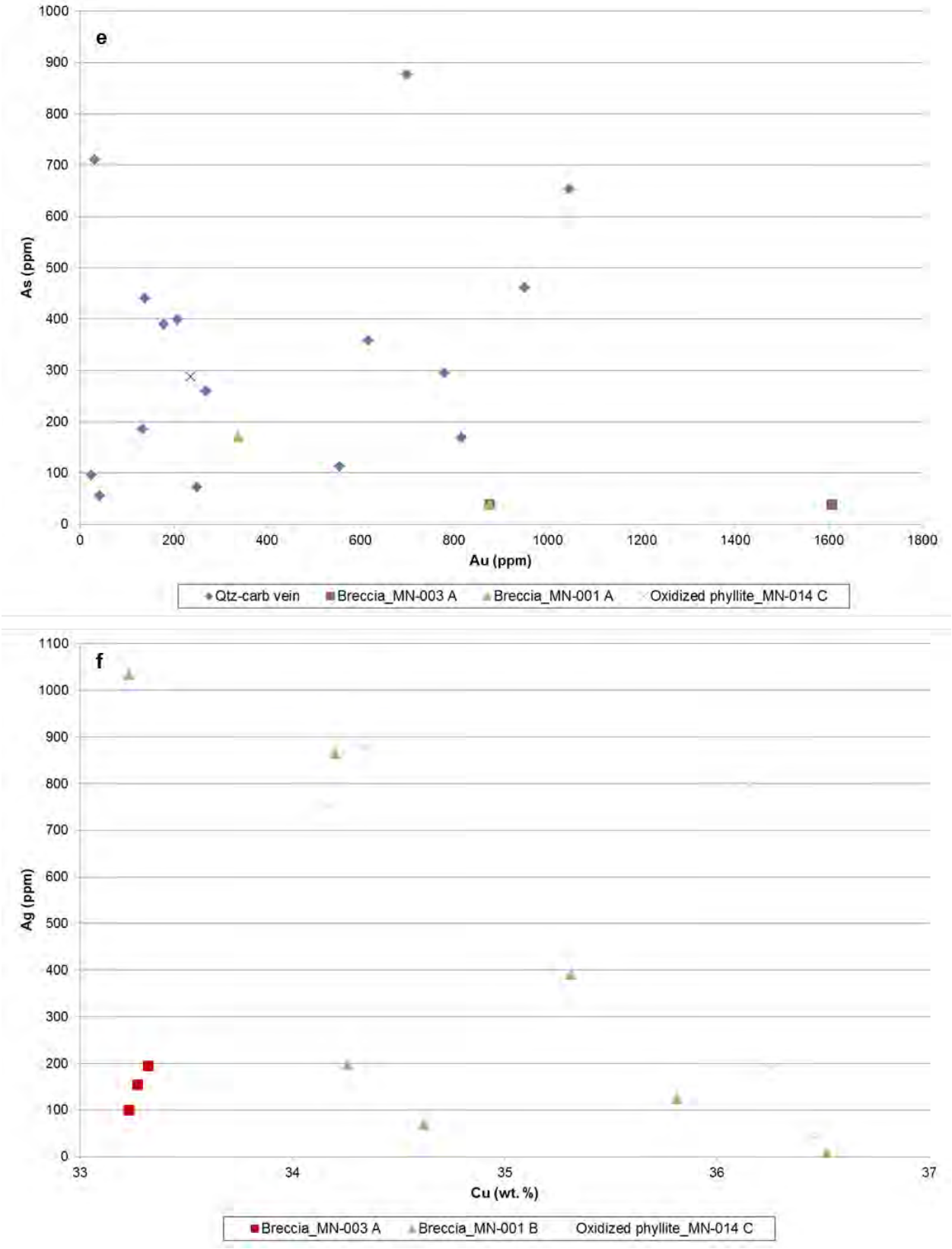

Figure 4.14: Continued

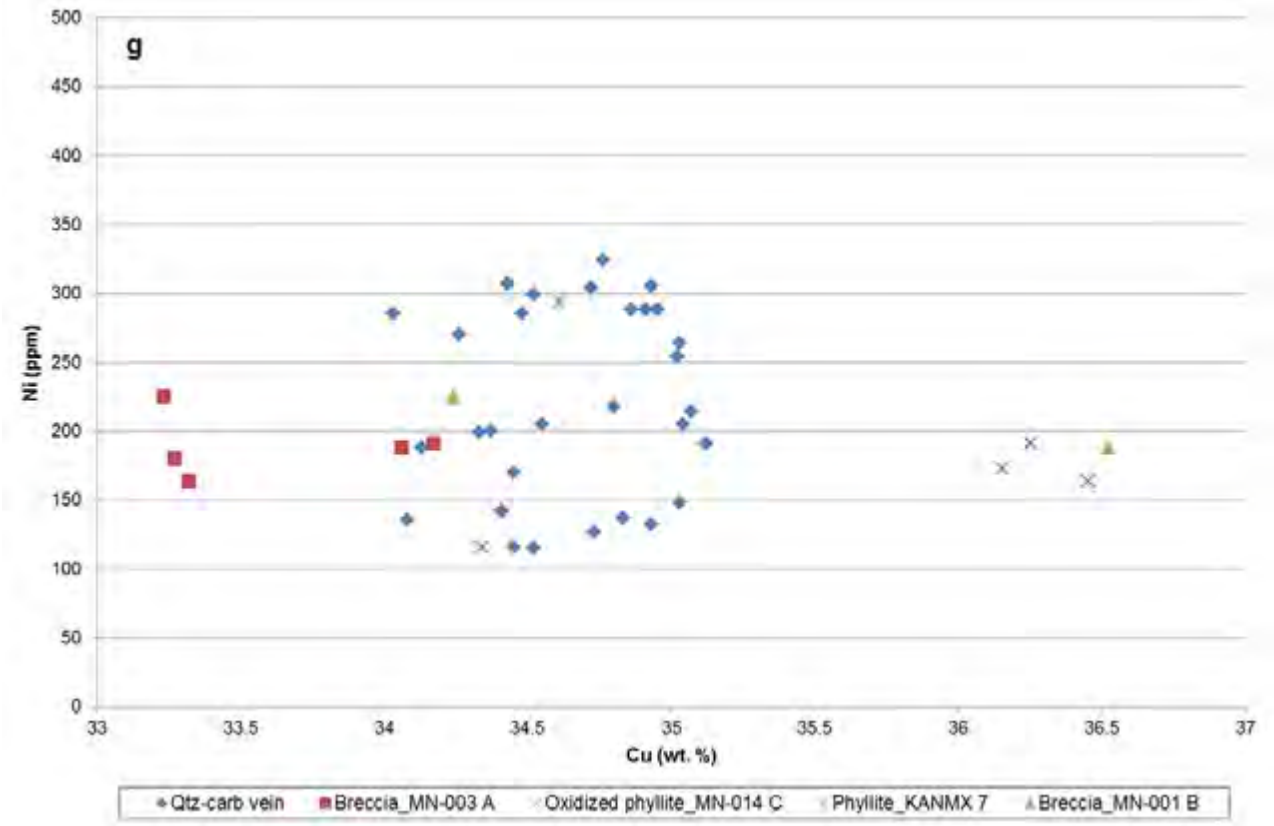

Figure 4.14: Continued

Textures

Petrographic investigations gave evidence of textural complexity in chalcopyrite with frequent intergrowth types between chalcopyrite and secondary copper sulphides. These intergrowth types are associated with samples that have experienced oxidation and subsequent supergene enrichment (Figure 4.15).

Some of the complex intergrowths types that have been recognized are illustrated by the back-scattered electron images obtain by the electron microprobe (Figure 4.16). In some of these mineral particles, chalcopyrite is coated by a rim of secondary sulphides (Figure 4.16 a). In other instances, chalcopyrite is coated and veined by secondary sulphides (Figure 4.16 b). Replacement often occurs at the grain boundaries and progressively moves inward (Figure 4.16 c). Due to the textural complexity of these intergrowths, spot analyses were performed on the secondary copper sulphides to determine their composition. Compositional data obtained from the spot analyses are displayed on a histogram (Figure 4.17).

Each cluster represents an individual mineral phase present. From the histogram, the following mineral phases were identified: chalcocite, covellite, digenite, djurleite, and geerite.

Due to previously stated analytical limitations, QXRD and QEMSCAN data were able to identify only the secondary copper sulphides, chalcocite and covellite. Mineral chemistry calculations were performed on spot analysis data of the secondary copper-sulphides, identifying the additional presence of djurleite, digenite and geerite, which are less common intergrowth minerals associated with chalcocite and covellite.

Djurleite is commonly intergrown with chalcocite and digenite. However, djurleite cannot be distinguished from the associated minerals by traditional optical methods due to structural similarities. Covellite often forms through the replacement of digenite, resulting in the formation of symplectic covellite/digenite intergrowths. These replacement reactions can lead to the development of transition mineral phases (Koski, 2012) as illustrated in Figure 4.17, with mineral compositions that are not diagnostic of any mineral phase. Mineral chemistry calculations also suggest the presence of geerite (Cu_8S_5). The occurrence of djurleite and geerite is not expected, because no previous literature on Kansanshi mentions these minerals, nor are they visible through optical petrography. EMPA analysis confirms the presence of chalcocite and covellite, with the addition of digenite, djurleite, and geerite as common intergrowth minerals that replace chalcopyrite during supergene enrichment

Compositional analyses of biotite and chlorite indicate that these minerals contained low amounts of refractory copper, accounting for 0.47 ± 0.05 wt. % CuO of biotite and 0.23 ± 0.17 of chlorite (Table 4.7), (EMPA data is reported as most common major element oxides). The chemistry obtained from EMPA analysis coincides with the XRF data and supports the bulk mineralogy determined by XRD and QEMSCAN.

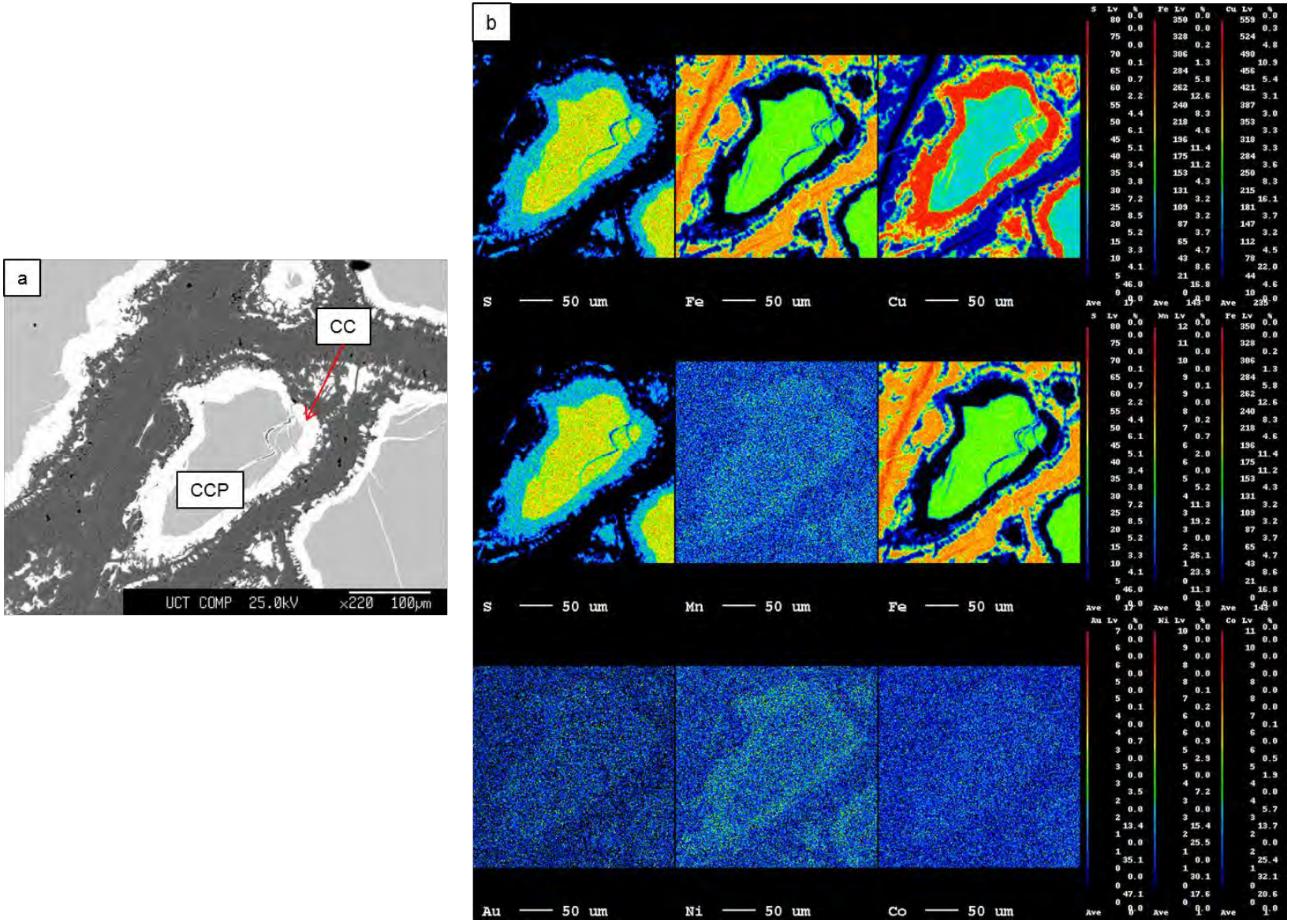

Figure 4.15: BSE image of a) rimming texture displayed by chalcopyrite and chalcocite, as determined by EMPA. This replacement texture is also seen with chalcopyrite and covellite, and pyrite and limonitic minerals (For example, goethite). Elemental maps of sample KANMX7 b) showing the element distribution represented as concentrations, as determined by EMPA.

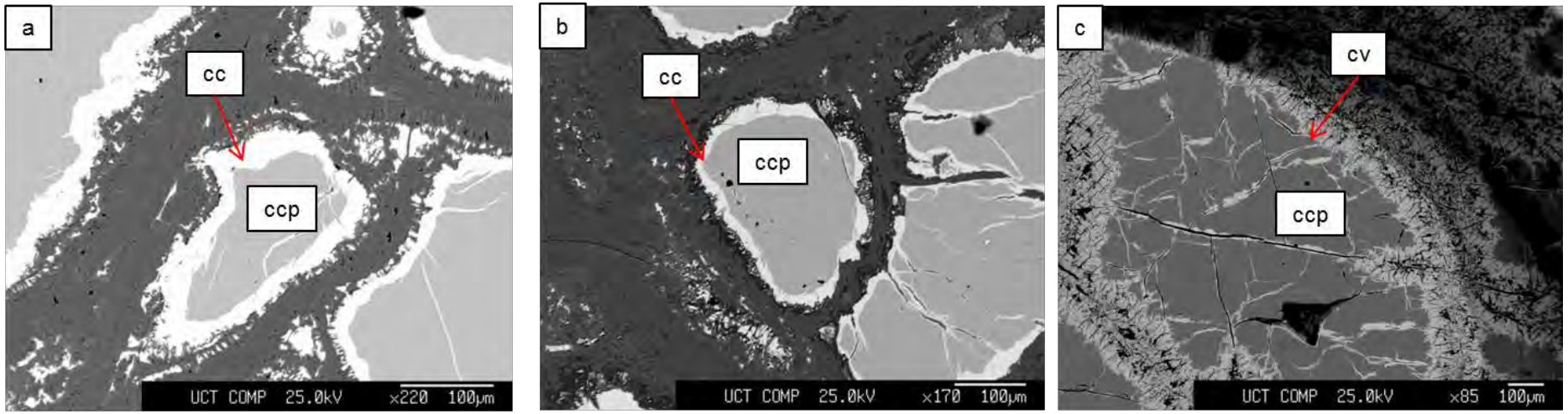

Figure 4.16: BSE images of frequent intergrowth between chalcopyrite (light grey phase) and secondary copper sulphides (light phase) common to the mixed ores at Kansanshi, as determined by EMPA.

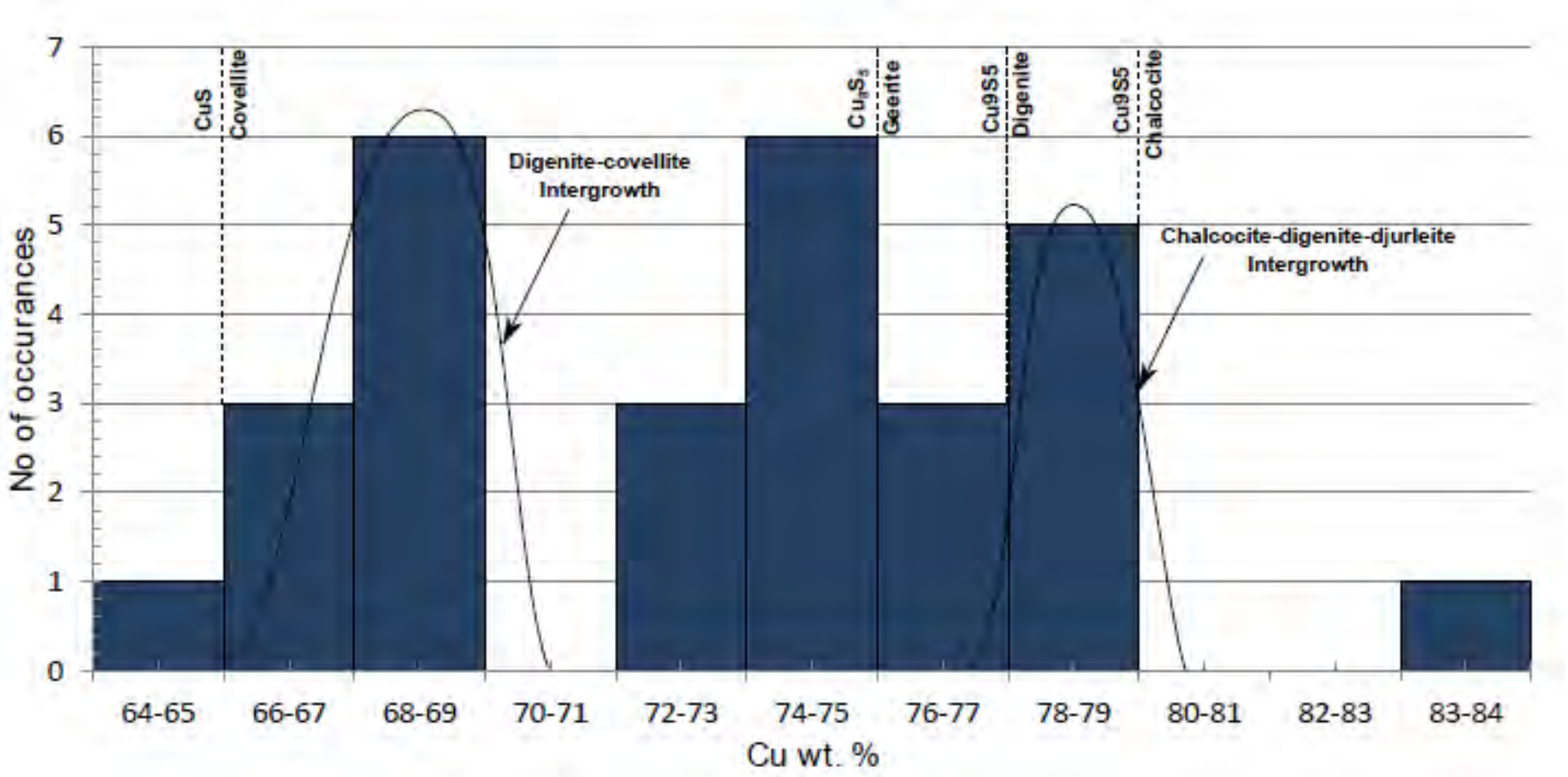

Figure 4.17: Frequency distribution of Cu wt. % of secondary copper sulphide grains from samples throughout the Kansanshi stratigraphy. Ideal compositions are quoted.

4.3 MINERALOGY AND BATCH FLOTATION RESULTS

This section describes the mineralogical and batch flotation results of Ore 1 and Ore 2. These tests were conducted to investigate the effect of mineralogy and a coarsening in grind size from 80% passing 150 µm (P80 = 150 µm) to 80% passing 212 µm (P80 = 212 µm) on the flotation performance of the two sulphide ore samples. The mineralogical features presented in this study are bulk mineralogy, copper deportment, mineral liberation and mineral associations of both ores at each grind. Flotation performance was evaluated using copper grade versus recovery curves, the amount of solids versus water recovered, the amount of gangue minerals recovered in the concentrate, and separation efficiency. The mineralogy data will be presented first, followed by batch flotation results. The complete set of mineralogy and batch flotation results are given in the Appendix G and H.

4.3.1 Bulk mineralogy of flotation feeds of two ROM samples

Both ores have the same mineralogy in terms of the individual minerals present but with varying abundances as illustrated in table 4.9. The principal copper-bearing mineral for both ore types is chalcopyrite, accounting for 3.4 wt. % of Ore1 and 3.6 wt. % of Ore 2 with the major gangue minerals being albite, quartz, mica (biotite) and the carbonates (Table 4.9). The secondary sulphides chalcocite, digenite and covellite are noticeably absent from these samples (Table 4.9). Ore 1 has lower concentrations of albite, quartz, mica and iron sulphides (i.e. pyrrhotite and pyrite), but significantly higher carbonate content (~24 wt. %) compared to Ore 2 (~9 wt. %) (Table 4.9). Ore 1 and Ore 2 have similar amounts of graphite (~5 wt. %) and negligible amounts of kaolinite within the feed (Table 4.9). The mineralogy of the feed samples for Ore 1 and Ore 2 is comparable to that of the quartz-carbonate veins, that have undergone carbonate alteration (refer to section 4.2.1), with both sharing common mineralogy that is characterized by the abundance of chalcopyrite, quartz, carbonate and albite. This result is expected as the quartz-carbonate veins that cross-cut the Kansanshi stratigraphy are the principal sulphide ore component within the deposit.

Table 4.9: Summary of normalized mineral abundances of the primary ore and gangue minerals present within the feed samples of Ore 1 and Ore 2, as determined by QEMSCAN. Graphite abundance was determined by QXRD to account for the limitation of the QEMSCAN.

Minerals	Ore 1 (wt. %)	Ore 2 (wt. %)
Chalcopyrite	3.2	3.4
Pyrite	3.2	4.5
Pyrrhotite	0.7	1.4
Bornite	<0.01	<0.01
Chalcocite	<0.01	<0.01
Covellite	<0.01	<0.01
Other sulphides	<0.01	0.1
Cuprite	<0.01	<0.01
Malachite/Azurite	<0.01	<0.01
Chrysocolla	0.1	0.1
Amphibole	2.5	0.9
Mica	17.8	21.6
Kaolinite	0.2	0.2
Albite	24.1	26.2
Quartz	19.3	27.7
Calcite	23.3	9.1
Fe-Ti minerals	1.5	2.0
Limonite	1.4	1.9
Graphite	5.3	5.7
Others	1.91	2.31

4.3.2 Characterisation of sulphide minerals in flotation feeds

Copper deportment

Kansanshi is a supergene type deposit with complex mineralogy. Therefore, it is important to review the copper deportment before looking at its processing behaviour, because supergene processes can produce multiple primary and secondary copper minerals, each with their own grain size distributions. Within the sulphide samples Ore 1 and Ore 2, copper deportment occurs almost exclusively within chalcopyrite, accounting for more than 99 % of the copper present in the samples (Figure 4.18). The remaining copper is hosted within chrysocolla contributing to less than 1% of the copper present within the samples. Given that the majority of copper within these two ores is hosted almost exclusively by chalcopyrite, the following investigation of mineral properties will focus only on chalcopyrite.

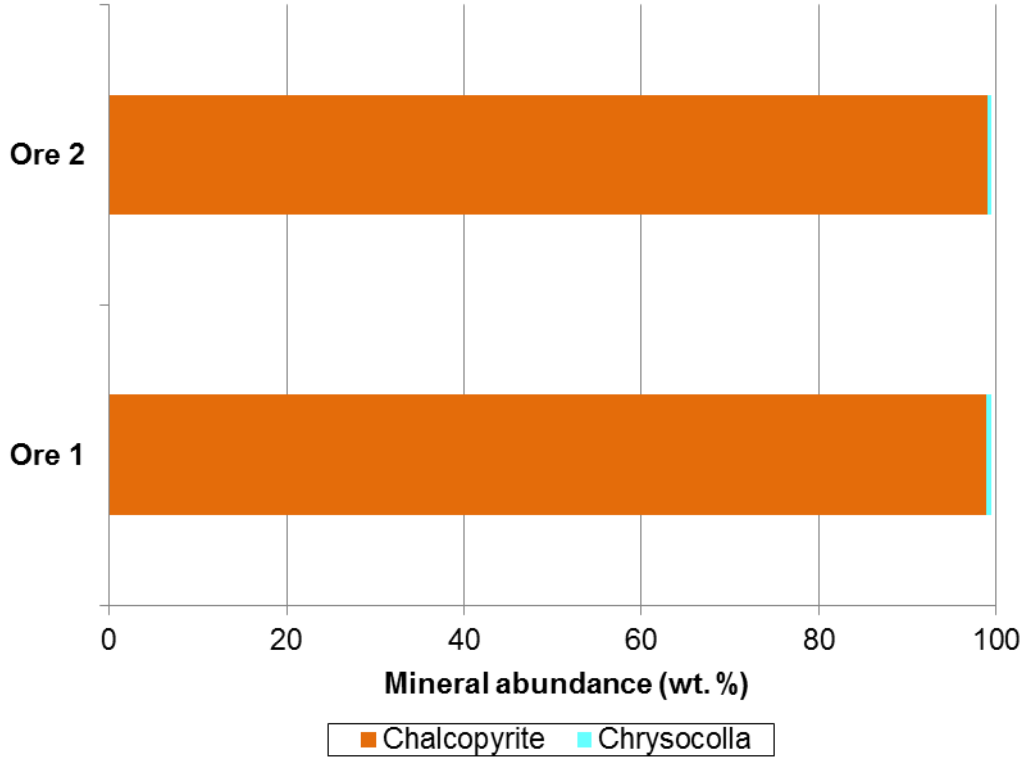

Figure 4.18: Copper deportment in Ore 1 and Ore 2, as determined by QEMSCAN.

Liberation

Figure 4.19 illustrates chalcopyrite liberation that has been normalized to feed grade. The liberation characteristics for the feed samples according to the locking-liberation characteristics criteria are shown in Table 4.10. The results indicate that both ores have similar degrees of chalcopyrite liberation for P_{80}= 150 µm, with 94% of chalcopyrite in Ore 1 and 97% in Ore 2 being fully liberated. The high degree of liberation can be attributed to the

characteristic massive and coarse-grained texture of the sulphide ore (Figure 4.8). The massive textures produce coarse chalcopyrite grains (> 0.5 mm), inter-grown with coarse-grained pyrite and carbonate (calcite and dolomite) (Figure 4.8). This coarse grain size of chalcopyrite, results in only minimal grinding being required for liberation.

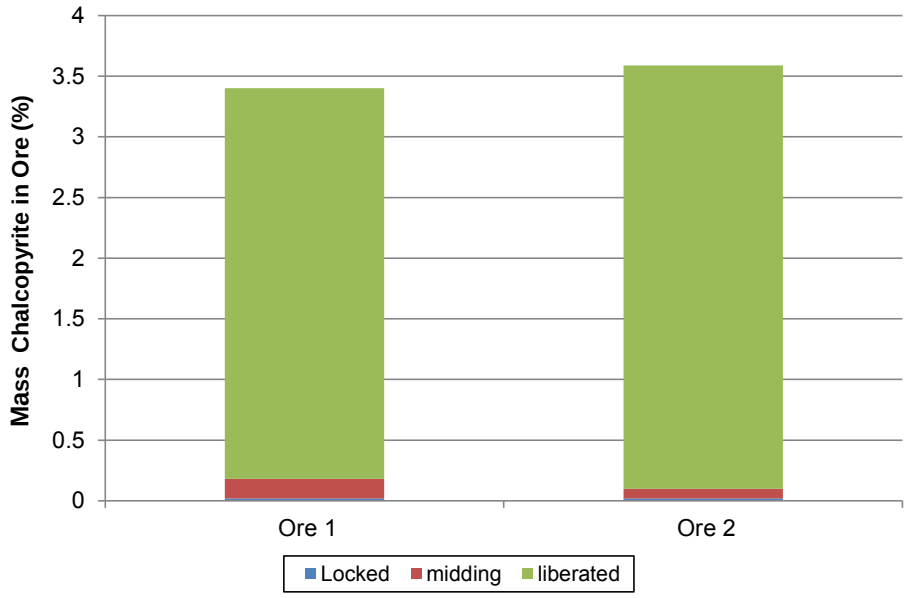

Figure 4.19: Chalcopyrite liberation for Ore 1 and Ore 2 at P80= 150 µm, as determined by QEMSCAN.

Table 4.10: Detailed locking-liberation characteristics criteria, including the percentage of chalcopyrite in the ores across locking-liberation criteria in feed.

Class	Classification	Ore 1	Ore 2
Liberated	Area percent ≥ 90 %	94	97
Middlings	Area percent ≤ 60 %, ≥ 30%	5	2
Locked	Area percent ≤ 30 %	1	1

Grain size distribution

Understanding the grain size distribution is essential because it determines the grinding targets for the liberation of these minerals. Consequently, it plays a significant role throughout mining operations, from blending and processing, to setting expectations of the theoretical grade-recovery curve, among others.

The curves in Figure 4.20 indicate that after milling, the two ores have broadly similar grain size distributions, differing subtly in the amounts of grains within the size below 30 µm. Ore 1 has a slightly higher percentage of mineral grains that are less than 30 µm in size, with ~45 % of Ore 1 and ~36 % of Ore 2 chalcopyrite grains reporting to <30 µm size fractions. Within the sulphide ore samples both coarse-grained and disseminated textures have been identified, as seen in Figure 4.8. Ore 1 might be slightly more disseminated in nature than Ore 2, and therefore have a higher percentage of chalcopyrite grains that fall into the ≤ 30 µm size fractions.

The two ores have the same cumulative chalcopyrite mass in the grain size fraction <180 µm. After this point of intersection, Ore 2 shows a higher percentage of coarse chalcopyrite grains with ~3.5 % of the grain sizes >500 µm. The shape of the curves can be attributed to the varying textures associated with the sulphide ores (Figure 4.8).

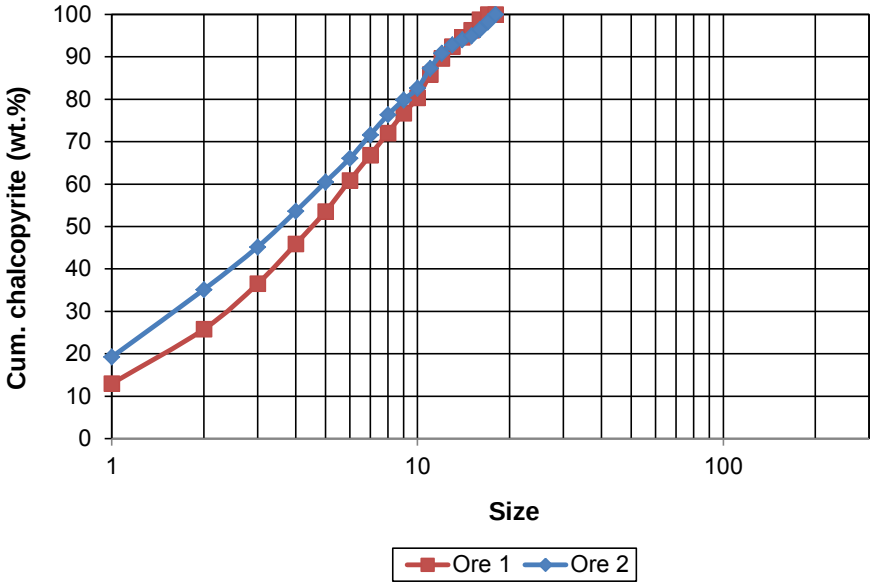

Figure 4.20: Cumulative chalcopyrite grain size distribution curve of Ore 1 and Ore 2, as determined by grind size.

Butcher (2010) described two broad classes of texture; equigranular – grains of similar size – or inequigranular grains with different size distributions. This description can be used to describe the size distribution of chalcopyrite grains, which have grains that could be of similar or differing sizes, depending on the texture. The massive texture illustrated in Figure 4.8.a would produce grains of a similar size (>1 mm), whereas the stockwork (≥0.5 mm) and disseminated textures (<0.2 mm) could lead to an increase in production of middlings

and fines (i.e. particles that are smaller than 75 μm in size) (Gay, 2004; Butcher, 2010; Barnuevo et al., 2013). However, intergrowth types such as stockwork and coated are not common within the sulphide ores, and are more prevalent within the mixed ores (Figure 4.12). The characteristic massive texture of the sulphide ore is the cause of the high degree of liberation and as result minimal chalcopyrite mineral associations (Figure 4.19 & Figure 4.21).

Mineral associations

As previously mentioned chalcopyrite liberation at P80= 150 μm for both ores is excellent and mineral associations are minimal, contributing only 5.3 wt. % of Ore 1 and 2.8 wt. % of Ore 2. For the two ores, chalcopyrite is mainly associated with chrysocolla and pyrite, and minor amounts of other gangue minerals, which include carbonate, quartz, mica and albite at P80= 150 μm (Figure 4.21). These results are in agreement with the coarse-grained textures seen figure 4.8.

Pyrite liberation and association data is also provided here, since the recovery of pyrite is undesirable at Kansanshi. Pyrite mineral association data shows that pyrite is highly liberated and mostly associated with pyrrhotite (Figure 4.22). Due to the minimal association between pyrite and chalcopyrite, any flotation recovery of pyrite is more likely to be related to reagent chemistry than mineralogy.

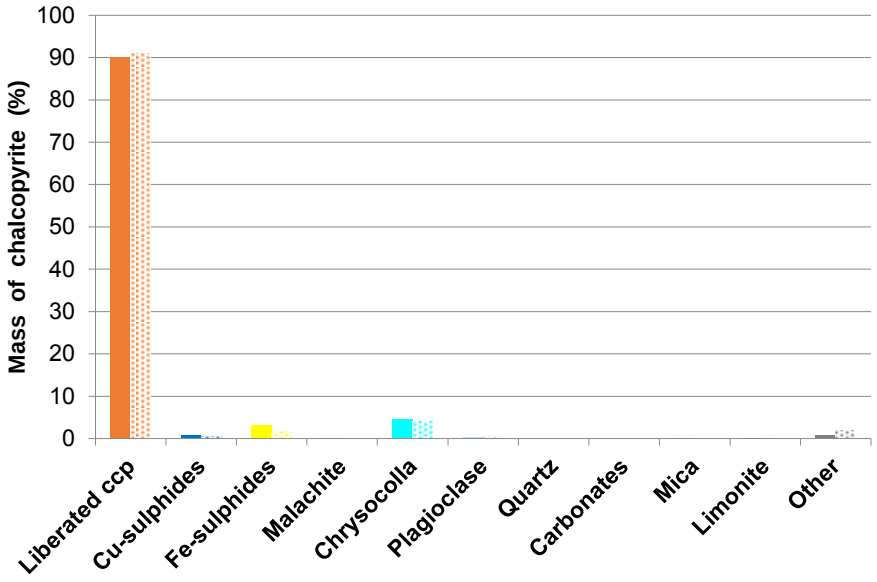

Figure 4.21: Associations between chalcopyrite and other minerals in Ore 1 and Ore 2 at P80 =150, as determined by QEMSCAN. Ore 1 is represented by solid fill and Ore 2 is represented by pattern fill.

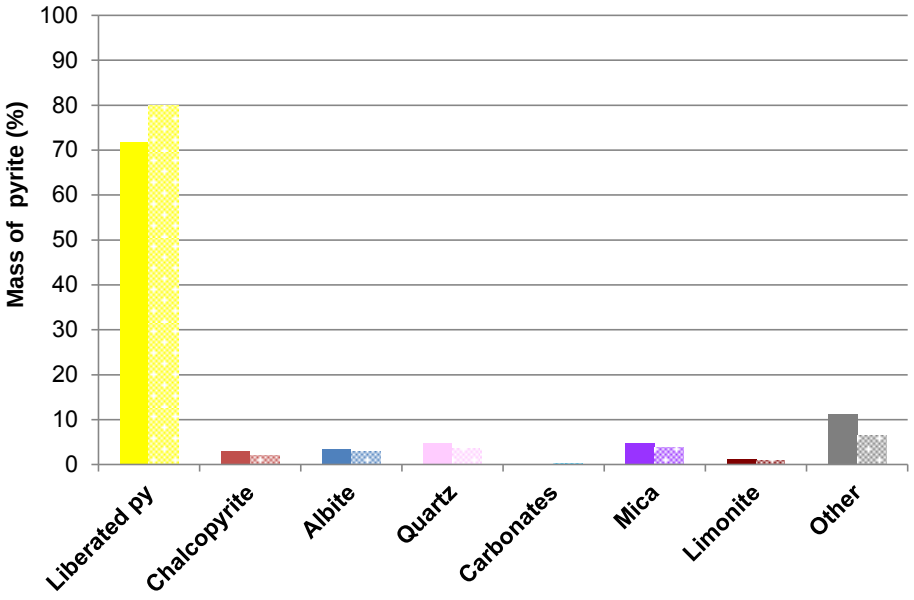

Figure 4.22: Associations between pyrite and other minerals in Ore 1 and Ore 2 at P80 =150, as determined by QEMSCAN. Ore 1 is represented by solid fill and Ore 2 is represented by pattern fill.

Locking textures of composite particles

Even though mineral associations are minimal, Figure 4.23 illustrates that some composite particles of chalcopyrite and gangue minerals do exist in simple and complex locking textures. According to Wang (2010), a simple locking texture is defined as a particle having only one interface between the phases while complex locking occurs when the particle has more than one interface between the phases (Fosu et al., 2015). Chalcopyrite is locked in composites with five major gangue minerals, namely albite, quartz, carbonate, mica and pyrite. These particles with locked textures are seen primarily within the size fraction ≥ 53 µm. The presence of these composite particles may cause a trade-off between recovery and grade to increase. This is because the increase in the recovery of composites carries more gangue to the concentrate, reducing the overall grade (Sutherland, 1989).

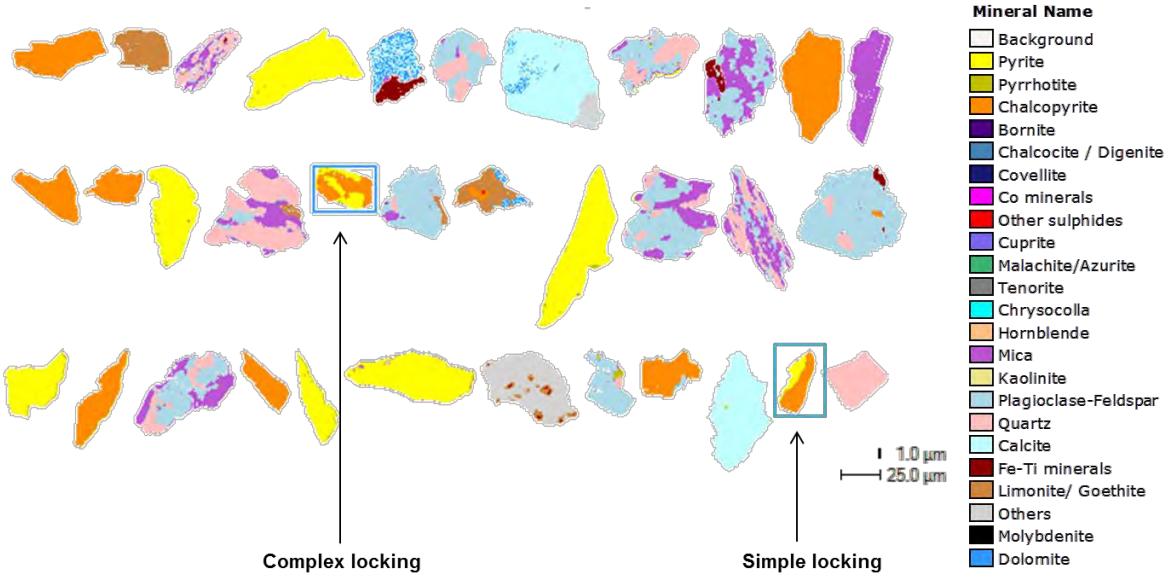

Figure 4.23: QEMSCAN image of chalcopyrite particles within the +53/-25 µm size fraction of the feed sample. The Arrows highlight an example of a simple and complex locking texture.

4.3.3 BATCH FLOTATION RESULTS

Mineralogical characterisation of the two feed ores indicate that chalcopyrite is the primary copper host for Ore 1 and Ore 2 (Table 4.9) making up 99% of the ore percentage of the sulphide sample. The copper assay can therefore be used to infer the chalcopyrite behaviour since there is no secondary copper (i.e. acid soluble copper).

4.3.4 Solids versus water recovery

Figure 4.24 shows the final cumulative values for solids and water recovery, together with their statistical variation, represented by the error bars. From Figure 4.24 it is evident that a coarsening of grind from P80 = 150 to P80= 212 µm has resulted in a reduction in the solids and water recovery. This is attributed to the increase in the proportion of fine particles at the P80= 150 µm, stabilizing the froth and thereby promoting entrainment (Subrahmanyam & Forssberg, 1988).

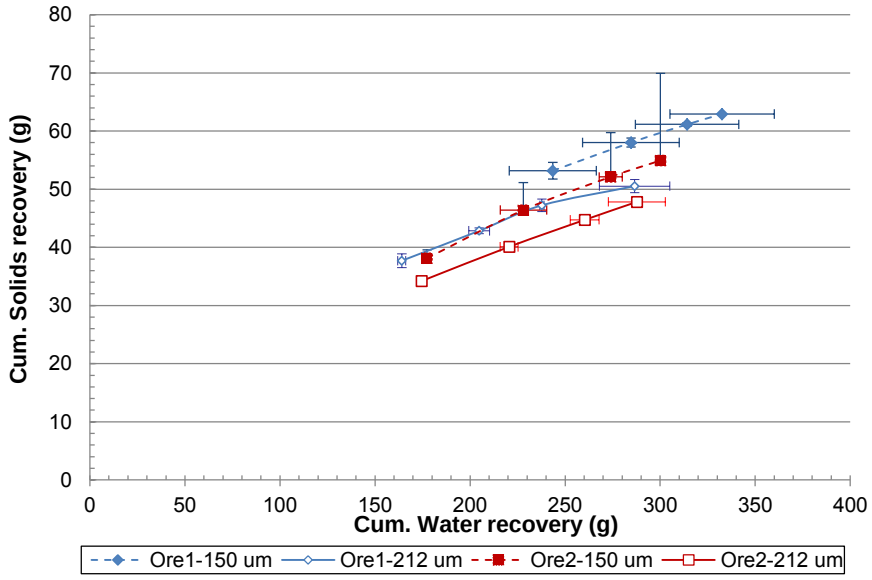

Figure 4.24: Cumulative concentrate solids recovered as a function of cumulative water recovered for Ore 1 and Ore 2 with increasing grind from P80= 150 µm to P80= 212 µm. Error bars represent the standard error between triplicate tests.

4.3.5 Copper grade and recovery

Figure 4.25 illustrates the copper grade versus recovery curves obtained for Ore 1 and Ore 2 at grind of 150 µm and 212 µm respectively. The recoveries obtained for each ore sample at both grinds 150 µm and 212 µm were the same within error (Table 4.11 and Figure 4.25).

Table 4.11: Summary of the grade and recovery results obtained for Ores 1 and 2 with a coarsening in grind size from (P80 = 150 µm) to (P80 = 212 µm) at two different grind sizes. Error bars represent the standard error calculated from triplicate tests.

	Cu recovery (%)		Cu grade (%)	
	Ore 1	Ore2	Ore 1	Ore2
P80= 150µm	89.1 ± 0.93	89.7 ± 1.00	9.3 ± 0.20	10.6 ± 0.20
P80= 212µm	86.9 ± 1.78	87.9 ± 0.95	12.5 ± 0.01	11.9 ± 0.53

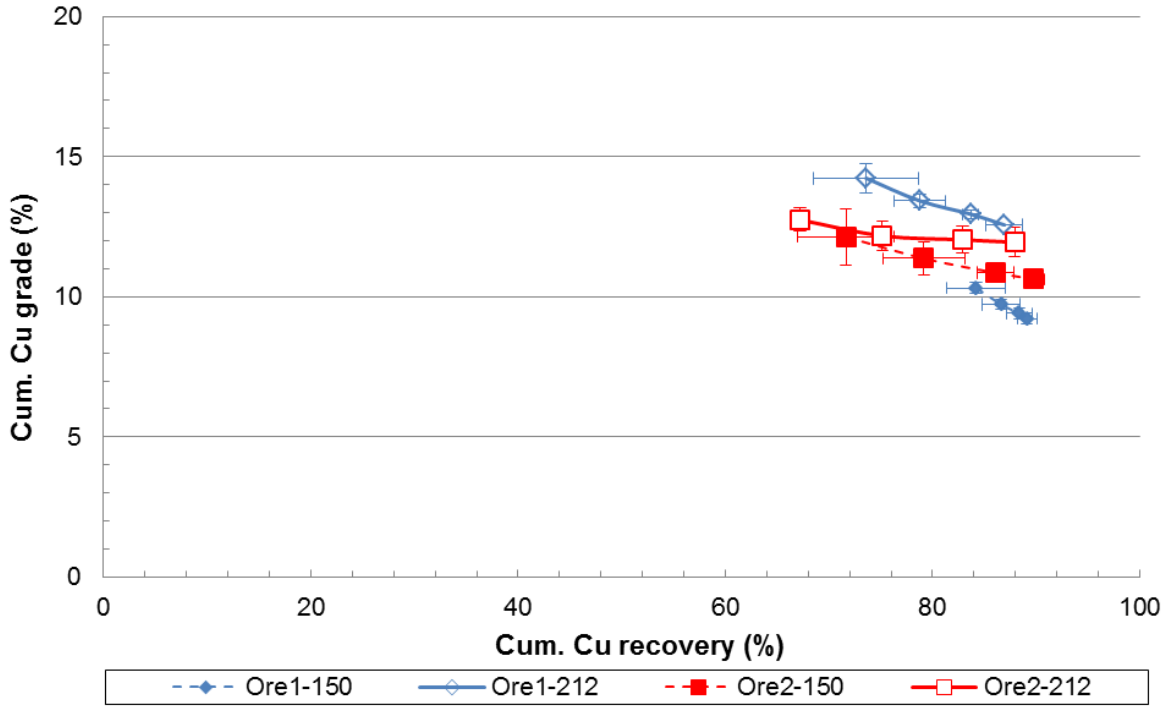

Figure 4.25: Cumulative concentrate copper grade as a function of cumulative copper recovery for Ore 1 and Ore 2 for a coarsening in grind size from (P80 = 150 µm) to (P80 = 212 µm). Error bars represent standard error between triplicate tests.

In order to determine whether any of these differences were statistically significant (especially small differences in concentrate grades between the two ores), the separation efficiency was calculated (see section 3.3.3). The best separation efficiency was achieved for Ore 2 at P80= 212µm (Table 4.12).

Table 4.12: Separation efficiency of Ore 1 and Ore 2 at P80= 150 µm and P80= 212 µm.

	P80= 150 µm		**P80= 212 µm**	
Parameters	Ore 1	Ore 2	Ore 1	Ore 2
Rm	13.40	16.51	17.88	20.01
Cc	9.15	10.70	12.22	11.07
Ff	0.68	0.65	0.68	0.55
Rg	75.05	70.43	66.03	69.13
M	34.63	34.63	34.63	34.63
max rec	100	100	100	100
SE	12.65	15.81	17.22	19.32

4.3.6 Gangue recovery

It is essential to understand the nature and abundances of gangue minerals recovered, because these factors influence the choices of metallurgical treatment and flow sheet design. For example, the presences of various phyllosillicate minerals, such as kaolinite and smectite, in the ore, as a result of supergene enrichment, can be detrimental to processing, due to slime effects or rheological effects (Patra et al., 2010; Ndlovu et al., 2011). The presence of other minerals, such as graphite which are naturally hydrophobic can dilute the grade. Consequently, any processing improvements rely heavily on understanding the gangue mineralogy of the concentrate.

QXRD was used to determine the mineralogy of the first concentrate collected for Ore 1 and Ore 2. Concentrate one was selected based on performance, with the highest cumulative recovery occurring in the first four minutes of flotation. The results are reported as major (>10 wt. %), minor (2-10 wt. %), and trace (< 2 wt. %) minerals rather than absolute mineral abundances given some of the relative differences in datasets between QEMSCAN and QXRD (Table 4.13). Gangue minerals recovered in the concentrate from the batch flotation tests under all conditions are pyrite, albite, quartz, mica and carbonate.

Table 4.13: Mineralogy of the feed and concentrate one at P80= 150 µm given in weight %, as determined by QXRD.

	Ore1		Ore 2	
	Feed	**Conc**	**Feed**	**Conc**
Chalcopyrite	Minor	Major	Minor	Major
Pyrite	Minor	Minor	Minor	Minor
Carbonate	Major	Minor	Major	Minor
Albite	Major	Major	Major	Minor
Quartz	Major	Minor	Major	Minor
Biotite	Major	Major	Major	Major
Graphite	Minor	Trace	Minor	Trace

Mineralogical and liberation analysis of the feed shows that there are minimal composite particles of chalcopyrite locked within different gangue minerals although in instances where particles are present – it is these same gangue minerals that are associated with chalcopyrite (Figure 4.23). The prevalence of pyrite in the concentrate was not expected, because the collector (MX-5149) also acts as a pyrite depressant and chalcopyrite mineral association with pyrite was minimal (Figure 4.22). Graphite is also present in the concentrate although only in trace to minor abundances (Table 4.13). Significant amounts of biotite was recovered into the concentrate, due it association with both chalcopyrite (Figure 4.21) and pyrite (Figure 4.22). This is consistent with the mineralogy of the feed, which indicates that the contribution of more carbonaceous lithologies is low. It is important to note that no cleaning was done in the laboratory rougher floats. Further cleaning may well remove some of these gangue phases whose presence in the concentrate cannot simply be attributed to mineralogical factors (Figure 2.12).

4.3.7 Summary

From the mineralogical investigations and batch flotation tests the following key features were noted:

1. Phyllite units commonly contain the highest degree of vein-hosted and sediment-hosted mineralisation because these units have the highest density of veining and have also experienced extensive albite-carbonate alteration. Chalcopyrite is the primary ore mineral with lesser amounts covellite, malachite and chrysocolla being

present as a result of supergene enrichment. The gangue mineral assemblage consists mostly of pyrite, quartz and albite, with a significant increase in the clay mineral content within weathered/oxidized samples. The carbonaceous phyllites are unique with regards to their high graphite content. The overall texture of the phyllites is porphyroblastic – that is, defined by large euhedral pyrite grains (> 0.5 mm) forming the most prominent feature of this lithology.

2. In general schists have a lower degree of mineralisation compared to the phyllites, with the degree of mineralisation depending on the extent of carbonate alteration affecting the unit. The main ore minerals are chalcopyrite and covellite with a gangue mineralogy dominated by quartz, albite and phyllosilicates (biotite and chlorite). Units that have been affected by carbonate alteration, ferroan dolomite and calcite are typically present with rare occurrences of sericite. The main texture is porphyroblastic, defined by large euhedral garnet or biotite porphyroblasts (≤ 0.5 mm) depending on the unit. The schists are often foliated with biotite and chlorite defining the foliation.
3. The mineralogy of the quartz-carbonate veins are dominated by chalcopyrite, quartz and carbonates (ferroan calcite and dolomite). Albite and vanadium-rich muscovite commonly occur where albite-carbonate alteration has overprinted the host lithology. Coarse-grained primary sulphide mineralisation is characteristic of the Quart-carbonate veins with local stringer and disseminated mineralisation styles as common occurrences within the Lower Pebble Schist (Figure 4.2 a). The overall textures of these veins vary from massive to breccia to stockwork, with an average grain size that is ≥0.5 mm.
4. Mineralisation associated with breccia and supergene related mineralisation over-printes all previous mineralisation styles is categorized by two distinct mineralogies, namely oxidized samples and partially oxidized samples. The main copper oxide and secondary sulphide minerals are malachite, chrysocolla, covellite and chalcocite. The gangue mineralogy consists predominantly of quartz, albite and phyllosilicates (biotite and kaolinite). Textures associated with the oxidized samples are colloform and botryoidal, with the partially oxidized samples being dominated by the distinctive boxwork texture. The grain sizes are variable (≤0.2 mm to 0.5 mm), depending largely on the extent of replacement.
5. Geochemical analyses of chalcopyrite grains illustrated that there are no significant variations between chalcopyrite types from different samples. However, there are slight variations in trace element concentrations within the different chalcopyrite types. Secondary sulphide minerals identified through EMPA are chalcocite,

covellite, digenite, djurleite and geerite, which occur as complex intergrowth. An insignificant amount of refractory copper is present.

6. The mineralogical characterisation of the flotation feeds illustrated that both ores have the same bulk mineralogy with varying mineral abundances. The principal copper-bearing mineral is chalcopyrite, the major gangue minerals are pyrite, quartz, albite and carbonates. Copper deportment occurs almost entirely within chalcopyrite. Both ores show high degrees of liberation at P80=150 μm with chalcopyrite being 94 % in Ore 1 and 97 % in Ore 2 fully liberated. The high degree of liberation can be attributed to the characteristic massive texture of the sulphide ore.
7. Overall the copper flotation recovery of both ores at both grinds was good (~88% recovery) with little significant difference in recovery between ores and grinds. Copper grade was slightly lower at p80=150 μm due to the slightly finer grind resulting in greater solids recovery.

CHAPTER 5: DISCUSSION

5.1 INTRODUCTION

Mineralogical characteristics of ore show significant variations over the scale of millimetres to meters in complex orebodies (Powell, 2013). These variations include differences in mineral composition, relative abundances and physical characteristics, such as grain size, liberation and mineral associations. Consequently, ore treatment processes must be flexible in order to accommodate the changes in ore being processed (Powell, 2013; Olubambi et al., 2008). Process mineralogical investigations are important in benchmarking production, problem-solving and plant optimization. Kansanshi is an example of a complex deposit, which has experienced a protracted geological history with multiple ore forming processes, including both hypogene and later, supergene mineralisation.

The specific objectives of this process mineralogy study are to determine the mineralogy and texture of four lithologies, representative of the different mineralisation types common to the Kansanshi deposit and then to determine the effects of these ore characteristics on the performance of mineral processing. Experimental work was limited to the flotation of sulphide ore only (Section 4.4); however, based on the appropriate literature, some discussion and interpretation for the other ores is possible. Ultimately, this study aims to provide detailed process mineralogical information suitable for populating the geometallurgical models in use at Kansanshi. Due to confidentiality requirements, Kansanshi was unable to share further details of their models for discussion in this study.

Figure 5.1 illustrates a simple process mineralogy matrix formulated for Kansanshi that describes the continuum of mineralogy and textures due to supergene enrichment, and their effects on mineral processing. The description of this matrix forms the basis of the discussion for this thesis.

	Continuum in mineralogy and texture		
	Hypogene 	**Mixed** 	**Supergene** 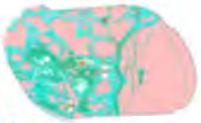
	Progessive replacement of primary sulphides during supergene enrichment →		
Mineralogy			
Valuable minerals	ccp & minor bn	ccp, cc, cv & minor mal, az, ccl	mal, az, ten, ccl & minor cc, cv, ccp
Gangue minerals	qtz, carb, alb & py	qtz, carb, alb, py & minor Fe-oxides	qtz, carb, alb, py, Fe-oxides & clays *Clays (e.g. Kaolinite)
Particle textures			
Liberation and associations	Easily liberated	(Dependent on intergrowth pattern type) →	Hard to liberated
Hardness	Hard	(Dependent on gangue mineral assemblage) →	Soft
Throughput	Standard *Potential to increase	High *Production of middlings	Low *Potential rheological effects
Flotation			
Liberated valueable mineral	ccp & bn *Fast floating with good recovery	ccp, cc, cv, mal, az *Controlled Potential Sulphidisation (CPS)	ccp, cc, cv, mal, az (Sulphidisation) *ccl doesnt respond to sulphidisation
Composites	Few *Simple locking texture	Abundant *Simple & complex locking texture	Abundant (simple & Locking textures) *Secondary porosity (box-work texture)
Naturally floating gangue	Graphite *Froth stabilizing properties	Graphite &Fe-oxides *Froth stabilizing properties	Clays and Fe-oxides *Froth stabilizing
Entrainment	Low *Coarse-grained	(Dependent on particle size) →	High *Fine-grained
Other	Inadvertent activation of py	Inadvertent activation of py & tarnished particles	Inadvertent activation of py
Other			
Leaching	Not applicable	Not applicable	High acid consumption *Soluble gangue (Carbonates)

Figure 5.1: Process mineralogy matrix for Kansanshi, showing the effects of a continuum in mineralogy and texture on the behaviour of the ore during mineral processing and the associated challenges. Interpretation based on observed and literature data.

5.2 INFLUENCE OF SUPERGENE ENRICHMENT ON MINERALOGY

The primary copper sulphide mineral assemblage, represented by the hypogene ore in Figure 5.2, and representative of the sediment-hosted and vein-hosted mineralisation styles in Table 2.1, is dominated by chalcopyrite, with minor bornite occurring predominately in the NW pit (Figure 5.1). The associated gangue mineral assemblage consists mainly of pyrite, pyrrhotite, quartz, biotite, chlorite, albite and carbonates (i.e. calcite and dolomite) and minor sericite (Figure 5.1 & 5.2).

This early hypogene mineral assemblage was later overprinted by supergene processes, leading to the formation of a vertically stratified weathering profile, consisting of primary, unaltered hypogene ore, an enriched zone, an oxide zone and a leached capping, known as a gossan (Figure 2.5). This process resulted in the replacement of the primary sulphide mineral assemblage with secondary mineral assemblages. These secondary assemblages consist either mainly of secondary copper sulphides, copper oxides and iron-oxy-hydroxides, or of a combination of these minerals, depending on the extent of weathering, and on the location of the assemblage within the weathering profile. The ore has been classified into three ore types: sulphide, oxide and mixed. Each of these has unique mineralogical characteristics and so has different processing requirements. The study of Kalichini (2015) on the flotation characteristics of the mixed ore at Kansanshi provides a useful quantitative comparison illustrating the influence of supergene enrichment on mineralogy.

Mixed ores form under reducing conditions below the water table and are usually located within the enriched zone of the weathering profile (Figure 2.5). They are characterized by an increased content of secondary copper sulphides (Figure 5.1 & 5.2), and a greater number of overgrowth and replacement textures. Examples of secondary copper sulphides include, in order of formation: covellite, digenite, geerite, djurleite and chalcocite. However, only chalcocite and covellite are of economic importance at Kansanshi. The differences in mineralogy between the mixed and sulphide ores are illustrated in Figure 5.2. It is evident from Figure 5.2 that mixed ores are transitional and show the progressive effects of supergene enrichment, because they consist of primary sulphides, copper oxides, clays and iron-oxy-hydroxides.

Oxide ores form the extreme in the continuum of supergene enrichment and are characterized by the replacement of primary copper sulphide minerals with copper oxides (for example, malachite), copper silicates (for example, chrysocolla), carbonate minerals (for example, tenorite), clays and iron oxy-hydroxides (for example, goethite). This replacement occurs during formation.

It is important to note that the replacement processes can be partial or complete. In the case of partial replacement, there remnants of other minerals besides the newly formed oxide minerals present in the oxide ore, such as secondary copper sulphides, clays, iron oxy-hydroxides and remnant unaltered chalcopyrite. The primary and secondary copper sulphides are usually present in trace or minor amounts, while the clays and iron oxy-hydroxides are usually present in larger amounts (Petruk, 2000). The presence of remnant primary and secondary copper within the oxide zone is due to the boundaries between the primary sulphide, oxide and mixed zones being gradational. They are gradational because the replacement reactions are generally selective in the minerals they affect and are commonly localized within a deposit (Craig and Vaughan, 1994). The presence of these secondary minerals complicates the new oxide mineral assemblage and makes processing more difficult, because these secondary sulphide minerals need to be accounted for during processing, and may necessitate different or additional processing methods.

The formation of a leached cap zone, also known as a gossan, occurs during the final stage of supergene process and is characterized by the presence of abundant goethite, limonite, hematite and clay minerals (for example, kaolinite). This increase in clay and iron-oxy-hydroxide mineral abundances has a significant effect on both the hardness of the ore, which affects comminution and on the rheology of the slurry during flotation. These effects will be discussed further in section 5.2 and 5.3

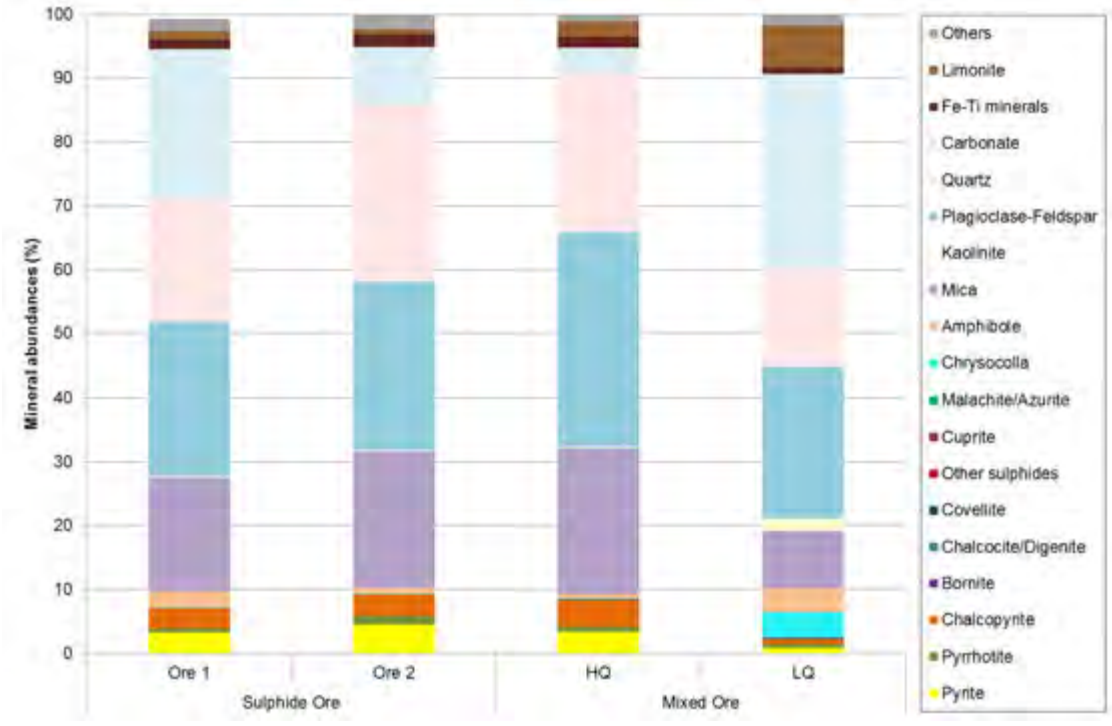

Figure 5.2: Comparison of the bulk mineralogy of the Sulphide ore and Mixed ore. The mixed ore data, presented as high quality (HQ) and low quality (LQ) ore is sourced from Kalichini, 2015.

5.3 INFLUNECE OF SUPERGENE ENRICHMENT ON PARTICLE TEXTURE

It is well established that texture plays a significant role in the behavior of ores during comminution and mineral processing, making it critically important. Ore texture is a fundamental parameter in mineral processing, defining the target grind size, the degree of liberation, the proportion of fine particles and the number of composite particles and their mineral associations (Figure 5.1) (Petruk, 2000; Butcher, 2010; Evans, 2010). In particular, previous work on the textural characterisation of supergene copper ores by Pérez-Barnuevo (2013) emphasized the importance of grain size and intergrowth type on particle textures and breakage. The majority of the chalcopyrite particles are well-liberated; however there are four intergrowth types that are present in lesser amounts as illustrated in Figure 5.3. This figure shows various chalcopyrite-bearing particles in which chalcopyrite may behave differently during comminution and flotation.

The coarse-grained (> 0.5 mm) chalcopyrite intergrown with iron-sulphides and gangue minerals is representative of a composite particle with a simple locking texture in the hypogene ores (Figure 5.3 a). The presence of this intergrowth type will result in good chalcopyrite liberation (Figure 5.3 e), because the mineral grains will most likely break at their boundaries, freely liberating the valuable minerals and making them easily recoverable through flotation (Figure 4. 18 & Figure 5.3 e). This is important, because coarse composite particles can cause a significant loss of valuable minerals to the tails (Pérez-Barnuevo, 2013).

Composite particles containing locked, fine-grained (< 0.2 mm) euhedral pyrite within coarse-grained chalcopyrite, representing complex locking textures, are also present in the hypogene ore, but to a minor extent (Figure 5.3.b). This texture has a large impact on mineral processing because it is difficult to separate the chalcopyrite from pyrite. Further and sometimes costly fine grinding would be needed to liberate the chalcopyrite to avoid dilution of copper concentrate grade (Figure 5.2.b) (Bilgili and Scarlett, 2005; Olubambi et al., 2007).

A commonly-occurring intergrowth pattern in Kansanshi supergene ores is stockwork, in which chalcopyrite forms the stockwork, and gangue minerals form the matrix (Figure 5.2 c & 5.2 e). This intergrowth type is associated with overgrinding and an increased production of middlings during comminution, due to the differences in the mechanical properties (such as hardness) of the minerals forming the matrix and those forming the stockwork (Pérez-Barnuevo, et al., 2013).

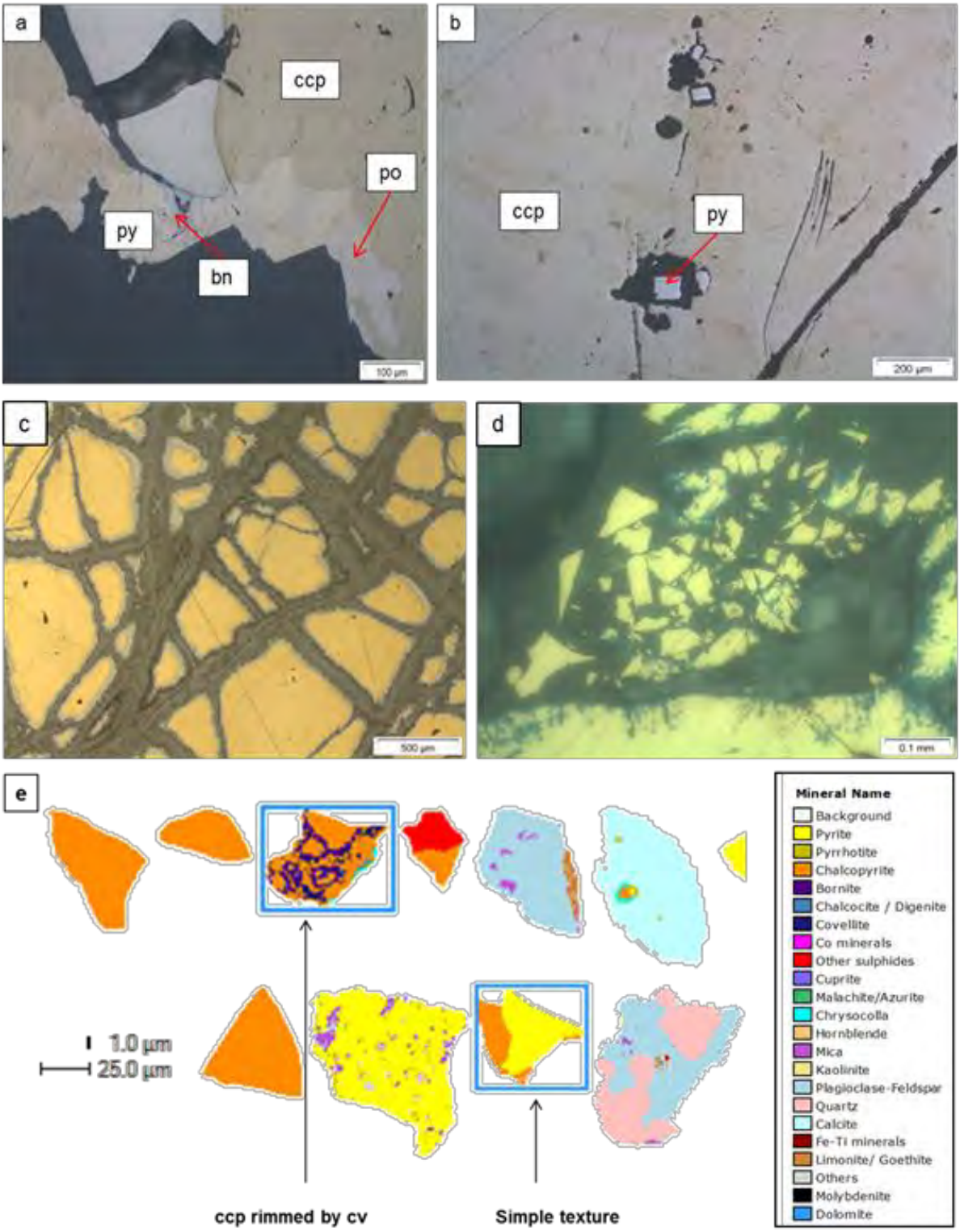

Figure 5.3: Reflected light and QEMSCAN particle images illustrating common textures and intergrowth types most relevant in comminution and flotation. The following textures are representative of hypogene mineralisation, a) simple locking, coarse-grained texture, b) complex locking, euhedral pyrite locked within chalcopyrite. These intergrowth types are representative of supergene mineralisation c) stockwork, chalcopyrite forming the stockwork and gangue the matrix, ccp is also rimmed by cc, d) coated, chalcopyrite rimmed by secondary copper sulphide (cv). e) Feed particles of Ore 1 illustrating the simple and complex intergrowth types associated with hypogene and supergene mineralisation, obtained by QEMSCAN at P80=150 µm.

Another frequent intergrowth pattern is the coating of chalcopyrite by various secondary copper sulphides in the supergene ores; for example, the coating of chalcopyrite by covellite (Figure 5.3 d). This is an important texture to identify in mineral processing because it can lead to dilution and/or copper losses to the tails. Dilution or copper losses are dependent on whether the mineral of interest is forming the coat or being coated itself. The possible loss of copper is a consequence of the added difficulties in floating secondary copper sulphides requiring special treatment; refer to section 5.3 for details.

The development of secondary porosity, through the formation of porous and spongy textures, particularly the cellular boxwork texture resulting from the dissolution of pyrite is another major textural change occurs with (Figure 4.12 c). Iron oxy-hydroxides and secondary copper minerals, such as malachite, chrysocolla, azurite and tenorite, typically appear as colloform and botryoidal infillings within void spaces, or as microcrystalline coating on gangue minerals, such as quartz and carbonates (Figure 4.12 a-b). The formation of these new textures results in grain sizes that are equal to or finer than those of the primary sulphide minerals.

Understanding the ore mineralogy and texture can provide valuable information on how the ore will behave during comminution (Tungpalan et al., 2015). For instance, these characteristics help to identify the appropriate grind size to achieve liberation and minimizing overgrinding (Tungpalan et al., 2015). The bulk mineralogy of the ore provides information of the hardness and mineral associations between value mineral and gaugue minerals, these factors influence how much grinding is required in order to achieve optimal liberation. The change in minerals assemblages and grain sizes, as a result of replacement and secondary porosity, both correspond to a reduction in grind size, due to the production of middling and fines. Have a significant effect on the grinding targets with the ore requiring longer milling times to achieve liberated fine composite particles. The change in bulk mineralogy due to gossan development results in an increase in the amount of iron hydroxides and clay mineral; this causes the ores to become slightly softer and with an opportunity for greater milling throughput. This is seen when comparing the milling times (at P80= 150 μm) of the sulphide Ore 1 from this study against the milling times of low quality mixed ore (which has higher clay mineral content), from Kalichini (2015) (Table 5.1). The similarity in milling time between HQ ore (Kalichini 2015) and Ore 1 is to be expected, due to the similarity between HQ ore and sulphide ore. These observations have been integrated into the process mineralogy matrix (Figure 5.1).

Table 5.14: Comparison between sulphide and mixed ore milling times. Mixed ore data sourced from Kalichini (2015).

	Sulphide ore		Mixed ore	
	Ore 1	**Ore 2**	**High Quality**	**Low Quality**
Milling time	3min. 42 sec	4min. 6sec	3min.42 sec	3min. 18sec

The relative milling times of Ore 1 versus Ore 2 suggest that Ore 2 is slightly harder than Ore 1.The grain size and degree of liberation for both ores are similar, and their mineralogies are the same. However, their mineral abundances differ. Ore 2 has 10 % more quartz than Ore 1 (Figure 5.2) with the higher quartz making the ore harder and as a result increasing the milling time of Ore 2The major implication of this result is that Ore 1 is expected to have a slightly higher throughput time compared to Ore 2.

The overall texture of the sulphide ore (representative only of vein-hosted mineralisation investigated) in this study is coarse (> 0.5 mm), so the amount of grinding required to achieve liberation was minimal. Dilution of the copper concentrate and copper losses to the tails is to be expected, due to the presence of composite particles in the coarse and middling size fractions (Figure 4.23). However, this effect is minimal, because there are few coarse composite particles, and those that there are, have a simple locking texture (Figure 4.23 & Figure 5.3 a). These ore characteristics suggest that these ores are more forgiving when higher throughput is needed. This does not hold true when processing particles with complex locking textures, such as fine grained euhedral pyrite locked within chalcopyrite (Figure 5.3 b). These mineralogical factors highlight the importance of upfront ore characterisation, using textures to informing mineral processing.

5.4 INFLUENCE OF SUPERGENE ENRICHMENT ON FLOTATION

Once the ore has been milled and the various particle types have been produced, the ores are upgraded using flotation. The sulphide ore in this study is representative of vein-hosted mineralisation (i.e. quartz-carbonate veins), which has an overall coarse-grained texture, and so responds well to flotation. Results of this laboratory study show good copper recoveries (~89%) during rougher flotation, because chalcopyrite liberation was over 90%. The effect of increasing the grind caused an insignificant loss of copper recovery. This good performance during flotation can be attributed to a number of mineralogical characteristics, including minimal fine composite particles, the natural hydrophobicity of chalcopyrite and the high

degree of liberation of chalcopyrite associated with the overall coarse texture of the sulphide ore. The results of this study also show relatively low copper grades were produced using only rougher floats, indicating that the grades have the potential to be further improved using cleaner floats.

There are two ways in which copper grade can be impacted. Firstly, the copper ion activation of pyrite results in more pyrite being recovered. Consequence of this pyrite recovery is reduced copper grades because the concentrate has become more dilute (Owusu et al., 2011). Secondly, pyrite can be advantageous in a smelter because it produces sulphuric acid, which can be sold. Conversely, at times when the smelter is operating at full capacity the excess pyrite is undesirable since it restricts the capacity (tonnage) for smelting copper concentrate.

Sulphide ore associated with other lithologies, such as carbonaceous phyllites and schist, have the potential to behave differently during processing to quartz-carbonate veins, because of their differences in mineralogy and texture. For example, carbonaceous phyllites, which are host to vein-hosted and sediment-hosted mineralisation, have higher graphite content than other phyllites samples (Figure 4.3). This difference in mineralogy has a direct effect on the flotation performance of the ore, resulting in an overall decrease in the grade of the ore, due to the froth stabilizing effects of graphite (Wakamatsu & Numata, 1991; Kaya & Canbazoglu, 2007). Phyllite units, and to a lesser extent knotted schists, are associated with disseminated mineralisation (Chinyuku, 2013). This mineralisation style produces fine chalcopyrite grains < 0.2 mm (Figure 4.8). This reduction in grain size may result in a decreased in copper recovery, if the mechanical parameters of the flotation cells are not configured for the recovery of fine particles. In this case, adjusting the parameters of the flotation cells to recover fine chalcopyrite particles is a potential area for optimization.

Copper deportment results from Kalichini (2015) illustrate the differences in the amount of secondary copper sulphides recovered both before and after controlled potential sulphidisation (CPS) indicate that the recovery of these minerals is possible with an additional sulphidisation step after flotation with SIBX (Figure 5.4). A mineralogical analysis of the flotation tails showed that chrysocolla was the dominant copper mineral not recovered during flotation, with other copper minerals such as cuprite and malachite responding well to the CPS.

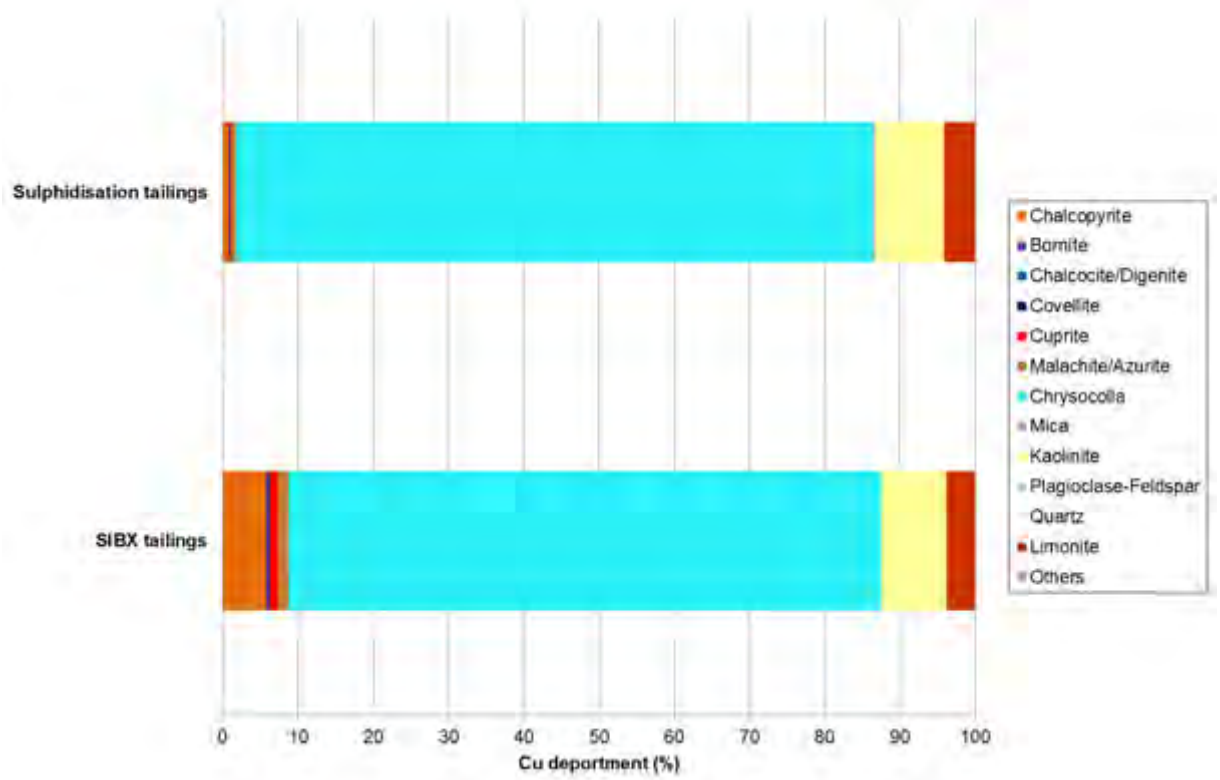

Figure 5.4: Comparison of copper deportment of LQ tailings before and after Controlled Potential Sulphidisation. Data sourced from Kalichini (2015).

The association of iron oxy-hydroxides with ore minerals is another important mineralogical factor, as demonstrated in a study by Paquot and Ngulube (2015), which shows that variability in flotation performance of the mixed ore, can be attributed to complexities in mineralogy and texture. In the study by Paquot and Ngulube (2015), the final copper losses were attributed mainly to liberated chalcopyrite and malachite that should have been recoverable but was rendered unrecoverable due to unliberated malachite associated with chalcopyrite and iron oxides. This is a consequence of iron oxy-hydroxides, such as goethite and limonite, being particularly problematic during flotation. If the surface of the copper-bearing mineral is coated by an iron oxy-hydroxide, the copper-bearing mineral cannot be recovered. This is because iron oxy-hydroxides do not respond to xanthate collectors, consequently effective flotation is hindered (Woods, 2003; Paquot & Ngulube, 2015).

The presence of various clay minerals (for example, kaolinite and smectite) in the oxide ore can be detrimental to processing, due to slime or rheological effects. It is well known that clay minerals tend to cause increased viscosities, especially when fine or ultrafine grinding is required. This is because an increase in fines particles results in more complex rheology that affecting pumping, flotation and tailings treatment (Patra et al., 2010; Ndlovu et al., 2011;

Burdukova et al., 2008). In the context of flotation, viscous slurries can also cause poor gas dispersion to the detriment of flotation recovery (Shabalala et al., 2011).

5.5 INFLUNECE OF SUPERGENE ENRICHEMNT ON LEACHING

Those copper minerals that are not separated during flotation are instead targeted for recovery by acid leaching: malachite, azurite and chrysocolla. Characterisation of the oxide ores (Figure 4.11 & 4.12) shows that the main ore minerals are malachite and azurite (copper carbonates), which are expected to leach easily, and chrysocolla (hydrous copper silicate), which is difficult to leach (Mena & Olson, 1985). These oxide ore minerals are commonly associated with quartz, albite, mica, clays and iron-oxy-hydroxides, such as limonite and goethite, and to a lesser extent, carbonate (Figure 4.6). The presence of carbonate (calcite and dolomite) can be linked to the quartz-carbonate veins that cross-cut the stratigraphy and carbonate alteration that is commonly associated with the marble units and biotite-rich schist (Chinyuku, 2013).

The quartz-carbonate-chalcopyrite veins show significant changes in mineralogy with depth, showing a downward increase in carbonate content: from quartz-carbonate in the upper part of the MMC, to carbonate-rich in the lower units of the LCS and LM (Broughton et al., 2002). This is important because oxide ores that are high in acid-consuming gangue minerals, such as carbonates, are not ideal for acid leaching, due to the high volume of acid needed for dissolution, resulting in an overall increase in reagent costs. Chrysocolla is effectively a refractory mineral because it does not respond well to flotation and requires a special leaching process in order to extract the copper. Chrysocolla can be leached using various agents, including cyanide solutions and sulphuric acid; however, the high amounts of carbonates can cause a tremendous increase in acid consumption, so a more selective reagent, such as ammonia, may be required. Ammonia has become known as an effective leaching agent in hydrometallurgical procedures and is gaining popularity as an alternative to sulphuric acid because it does not react with carbonates, resulting in reduced reagent costs (Wei et al., 2010; Radmehr et al., 2013; Baba et al., 2014).

Results from this study, and other literature (e.g. Sikazwe et al, 2008), have shown that some refractory copper is carried within clays and micas, such as chlorite and biotite, which contained 0.47 and 0.45 wt. % CuO, respectively. These values are lower when compared to the copper oxide (CuO) content within biotite (0.54 wt. %) from Refractory copper ores at Nchanga (Sikazwe et al., 2008).

Copper in clays and micas are difficult and costly to process and will remain in stockpiles until such time as new and innovative technologies have been developed to make their extraction profitable (Sikazwe et al., 2008).

5.6 INTERGRATING MINERALOGY INTO THE OPERATING MINE SITE

There have been many useful writings in the literature on what the focus areas should be for mine site integration of mineralogy; for example, Petruk, 2000; Goodall, 2005; 2008; Baum, 2004; Lotter et al., 2011 etc. Seven key questions posed by Goodall (2015), are considered in the context of this work characterizing the Kansanshi copper ore.

Table 5.15: Key questions for consideration for the mine site integration of process mineralogy at Kansanshi. Key questions are quoted from Goodall (2015).

Question	**Suggested focus areas for Kansanshi copper ore**
"What is the core goal of the process mineralogy program?"	Routine mineralogical investigations in order to monitor changes in grades and recovery on a long-term basis for the purpose of identifying key problem areas and opportunities for optimization.
"What are the key minerals and material characteristics that should be tracked routinely?"	Copper mineral deportment – which cannot necessarily be adequately determined using assays (acid soluble Cu, vs acid insoluble Cu; Kalichini, 2015).
"At what interval should routine analysis be undertaken?"	Regular sampling is important to quantitatively capture ore variability which can be 'averaged' out if composites are taken. However the practicality of achieving this may be challenging, hence weekly sampling is recommended (depending on the take up and the value which is defined, then more regular sampling can be motivated).

“Where and how should samples be collected?”	Representative samples in priority order of feed, final tails and concentrate for each of the three circuits.
“Who will be taking samples and running the process mineralogy program?”	Site personnel who know the operation well and who have a clear understanding of the purpose of the measurement and sampling theory. This person should have adequate knowledge of the ore body mineralogy, how the results should be reported and interpreted. The most important part of running a successful mineralogical program is to ensure on going comminution between the geologist and metallurgist so that the value of the information is improved.
“How will the data be reported and what are the key metrics?”	The data should be presented in timeous, concise, short reports (1-2 pages) that make the information accessible. It is important to avoid lengthy and tedious reports with irrelevant data. Key metrics are copper deportment, liberation, associations and bulk mineralogy. These mineralogical characteristics should be measured on a size by size basis.
“How will the results be integrated with operations and continuous improvement programs?”	The mineralogy reports should be easily available across departments (store in a central virtual location), within a framework that encourages and facilitates discussion. The mineralogy results should be linked to other key plant performance indicators (ASCu, AiSCu, recovery, grade, throughput etc). The long term objective is to fully integrate this formation into the geometallurgical block model, which will serve as a linkage between all aspects of the operation.

CHAPTER 6: CONCLUSIONS AND RECOMMENDATIONS

Kansanshi mine is a mineralogically and texturally complex deposit due to supergene enrichment resulting in the presence of a variety of primary and secondary copper minerals. This necessitates the processing of ore through three separate circuits. The primary objective of this research is the detailed process mineralogical characterisation of the Kansanshi ore using modern mineralogical tools, with a focus on the flotation performance of the sulphide ore. The ultimate goal of this research is to provide process mineralogical information that can be fed into the geometallurgical framework currently being developed by Kansanshi mining. The chapter summarizes the conclusions of this study, and provides recommendations for further study.

6.1 Conclusions

The following conclusions can be drawn with a focus on meeting the objectives and answering the initial key questions outlined in Chapters 1:

There are four main types of mineralisation present at Kansanshi. Mineralized zones within the deposits are characterized by vein-hosted mineralisation and to a lesser extent sediment-hosted mineralisation. Subsequent, breccia-hosted and supergene related mineralisation has overprinted these previous mineralisation styles. These four mineralisation styles are hosted within different lithologies within the Kansanshi stratigraphy, namely: phyllite, schists, breccia and quartz-carbonate veins.

Sediment-hosted mineralisation primarily occurs within clastic units, such as, phyllite and to a lesser extent within the knotted schist. Chalcopyrite is the main ore mineral and usually occurs as fine grained disseminations and stringers parallel to the bedding plans. This mineralisation style makes a minor contribution to the sulphide ore percentage. The gangue mineral assemblage consists mostly of pyrite, quartz, albite, biotite and chlorite. The phyllites and knotted schist may contain samples with high graphite content. The overall texture of the host lithologies is porphyroblastic – that is, defined by euhedral pyrite grains that range in size range between <0.2 mm to >0.5 mm, forming the most prominent feature of the phyllite

units. The secondary sulphides are associated with a boxwork texture that forms through replacement reactions and result in grain size variations that cause a decrease in the chalcopyrite grain size and produce secondary copper sulphides that are of equivalent to or of a finer grain size (< 0.2 mm) than that of the primary copper sulphides. Potential processing challenges are associated with the presence of graphite which is froth stabilising leading to excess solids recovery in flotation and a reduction of copper concentrate grade. Other potential challenges are associated chalcopyrite locked in composite with fine-grained euhedral pyrite, resulting in the dilution the copper grade. Separating the chalcopyrite from pyrite would require fine-grinding.

Vein-hosted mineralisation, represented by the quartz-carbonate veins is dominated by chalcopyrite, quartz and carbonates (ferroan calcite and dolomite). Albite and vanadium-rich muscovite are common occurrences where albite-carbonate alteration has overprinted the host lithology. The abundance of quartz associated with this mineralisation style increases the overall ore hardness. Coarse-grained primary sulphide mineralisation is characteristic of the quartz-carbonate veins with local stringer and disseminated mineralisation styles as common occurrences within the Lower Pebble Schist (Figure 4.2 a). The overall textures of these veins vary from massive to breccia to stockwork, with an average grain size that is ≥0.5 mm. The coarse-grained texture of the veins is likely to result in very good liberation with minimal fine composites.

Mineralisation associated with breccia and supergene related mineralisation over-prints all previous mineralisation styles and consists of partially oxidized and fully oxidised samples. The main copper oxide and secondary sulphide minerals are malachite, chrysocolla, covellite and chalcocite. The gangue mineralogy consists predominantly of quartz, albite, biotite, kaolinite (clay) and iron-hydroxides. This mineralisation style is associated with an increase in clay and iron-hydroxide mineral content, due to gossan formation. The increase in clay mineral content results in an overall decrease in ore hardness. Textures associated with the partially oxidized samples are distinctive stockwork and boxwork textures, which formed as a result of partial replacement reactions. Textures associated with fully oxidized samples, include colloform and botryoidal, which formed as a consequence of dissolution reactions. The grain sizes of the copper minerals are variable (≤0.2 mm to 0.5 mm), depending largely on the extent of replacement. Potential processing challenges associated with this mineralisation is related to the copper deportment that occurs across multiple mineral phases, such as secondary copper sulphides and copper oxides. These minerals require tailored processing steps for recovery such as controlled potential sulphidisation during flotation, and appropriate leaching of chrysocolla which is generally considered refractory.

Mineral chemical analyses of chalcopyrite grains indicated that there are no significant variations in major element composition, whereas there are slight variations in trace element composition from different samples, across the different lithologies. Secondary sulphide minerals identified through EMPA were chalcocite, covellite, digenite, djurleite and geerite, which occur as complex intergrowths. A minor amount of refractory copper is present in mica and chlorite.

The mineralogical characterisation of two sulphide flotation feed samples was relatively similar. The principal copper-bearing mineral is chalcopyrite, the major gangue minerals are pyrite, quartz, albite and carbonates. The bulk mineralogy suggests the samples are dominantly representative of the quartz-carbonate veins with coarse grained sulphide mineralisation. Copper deportment occurs almost entirely within chalcopyrite. Both ores showed high degrees of liberation at a grind of 80% passing 150 μm (94 and 97% liberated respectively). The high degree of liberation can be attributed to the characteristic massive texture of the sulphide ore. Overall the copper rougher flotation recovery of both ores at two grinds (80% passing 150μm, 80% passing 212 μm) was good (~88% recovery) with little significant difference in recovery between ores and grinds indicating that this particular ore is likely to be more forgiving in times when higher throughput is needed. Copper grade was slightly lower at the finer grind.

A process mineralogy matrix was proposed for Kansanshi on the basis of the material characterised in this study, as well by making use of other descriptions of the Kansanshi ore in the literature. The process mineralogy matrix allows for predictions to be made on the possible changes in mineral assemblage and texture with progressive weathering and how these changes may effect mineral processing. This information together with other key plant performance indicators, such as ASCu, AiSCu, recovery, grade, and throughput can be used to populate the geometallurgical models in use at Kansanshi, which will serve as a linkage between all aspects of the operation.

6.2 Recommendations

In light of the research carried out within this study the following recommendations can be made for further work:

i. The extension of mineral chemistry investigations, through further EMPA and XRF analysis of samples containing the oxide ore minerals, chrysocolla, malachite and

azurite once suitable calibration standards for analysis have been acquired. The ability to accurately report the chemical compositions of these minerals at Kansanshi is key to fully accounting for the copper deportment of the deposit.

ii. Detailed characterisation of other lithological units containing sulphide ore minerals (for example, phyllite units), focusing on their similarities and differences, as well as comparing their differences in flotation performance.

iii. A complimentary study to fully determine the characteristics of gold at Kansanshi focusing on its mineralogy, composition, liberation and association, grain size distribution and deportment through the various lithologies and the mineral processing circuit.

iv. Due to the heterogeneous nature of the ore deposit, it is recommended that further characterisation studies should be done on a regular basis for bench marking. This should include size-by-size analysis of feed, concentrate and tailings samples from processing. These investigations are important to quantitatively capture ore variability which can be 'averaged' out if composites are taken. This information should be linked back to the geometallurgical model with the purpose of identifying key problem areas and opportunities for optimization.

v. Further mineral chemistry analyses for both major and trace elements (including analysing samples from lithological units lower in the stratigraphy such as the Lower Pebble Schist). This information can be used to facilitate interpretations on how the mineral deposit was formed. Understanding ore deposit formation is a key tool for further exploration of the Kansanshi deposit, and other similar deposits globally.

REFERENCES

Ackerman, P.K., Harris, G.H., Klimpel, R.R. & Aplan, F.F. 1987. Evaluation of flotation collectors for copper sulphides and pyrites, III. Effect of xanthate chain length and branching. International Journal of Minerals Processing. 21 (1–2): 141–156.

Allen, D, Baber, B, Eady, S and Baum, W, 2007. Ore characterisation, alteration coding and plant feed control in copper operations as directed by routine semi-automated mineralogical analysis, in Proceedings Cu 2007 MetSoc: The John E Dutrizac International Symposium on Copper Hydrometallurgy, IV (book 2), (Canadian Institute of Mining, Metallurgy and Petroleum: Toronto).

Armstrong, R.A., Master S., Robb L.J., 2005. Geochronology of the Nchanga Granite, and constraints on the maximum age of the Katanga Supergroup, Zambian Copperbelt. Journal of African Earth Sciences. 42: 32-40.

Armstrong, R.A., Robb, L.J., Master, S., Kruger, F.J., Mumba, P.A.C.C. 1999. New U–Pb age constraints on the Katanga sequence, Central African Copperbelt. Journal of African Earth Sciences. 28 (4A): 6–7.

Awatey, B., Thanasekaran, H., Kohmuench, J., Skinner, W., Zanin, M. 2013. “Optimization of operating parameters for coarse sphalerite flotation in the HydroFloat® fluidised-bed separator”, Minerals Engineering. 50(51): 99-105.

Ayling, B., Rose, P., Petty, S., Zemach, E., Drakos, P. 2012. QEMSCAN® (quantitative evaluation of minerals by scanning electron microscopy): capability and application to fracture characterisation in geothermal systems. PROCEEDINGS, Thirty-Seventh Work. Geotherm. Reserv. Eng. Stanford Univ. Stanford, California, January 30 - Febr. 1, 2012 SGP-TR-194.

Ayres, R. 2007. On the practical limits to substitution. Ecology Economy. 61: 115–128. Available at: http://www.sciencedirect.com/science/article/pii/S0921800906000838 [accessed August 16, 2013].

Ayres, R.U., Ayres, L.W., Rade, I. 2002. The Life Cycle of Copper, its Co-Products and By-Products. Mining, Minerals and Sustainable Development.

Baba, A. A., Ayinla, K. I., Adekola, F. A., Ghosh, M., Ayanda, O., Bale, R., Sheik, A., Pradhan, S. 2012. A review on novel techniques for chalcopyrite ore processing. International Journal of Mining Engineering and Minerals Processing. 1(1): 1-16.

Baba, A.A., Ghosh, M.K., Pradhan, S.R., Rao, D.S., Baral, A., Adekola, F.A. 2014. Characterisation and kinetic study on ammonia leaching of complex copper ore. Transactions of Nonferrous Metals Society of China. 24: 1587-1595.

Ballantyne, G.R. & Powell, M.S. 2014. Benchmarking comminution energy consumption for the processing of copper and gold ores. Minerals Engineering. 65: 109-114.

Barron, J.W. 2003. The stratigraphy, metamorphism and tectonic history of the Solwezi Area, Northwest Province, Zambia: Integrating geological field observations and airborne geophysics in the interpretation of regional geology. PhD thesis (unpublished), Colorado.

Baum, W., 1999. The use of a mineralogical database for production forecasting and troubleshooting in copper leach operations. Copper ’99 International Conference IV, 393 – 408.

Baum, W., 2014. Ore characterisation, process mineralogy and lab automation a roadmap for future mining. Minerals Engineering. 60, 69-73.

Baum, W., Lotter, N.O. & Whittaker, P.J. 2004. Process Mineralogy a new generation for ore characterisation and plant optimization. SME Annual Meeting Feb 23-25, Denver, Colorado. Preprint 04-12.

Becker, M., Harris, P., Wiese, J. & Bradshaw, D. 2006: The use of quantitative mineralogical data to interpret the behavior of gangue minerals in the flotation of Merensky Reef ores. Paper presented at Automated Mineralogy, Brisbane.

Becker, M., Wiese, J., Ramonosti., M. 2014. Investigation into the mineralogy and flotation performance of oxidized PGM ore. Minerals Engineering. 65: 24-32.

Belogub, E.V., Novoselov, K.A., Yakovleva, V.A. & Spiro, B. 2008. Supergene sulphides and related minerals in the supergene profiles of VHMS deposits from the South Urals: Ore Geology Review. 33: 239-254.

Beniscelli, J. 2011. Geometallurgy-Fifteen Years of Development in Codelco: Pedro Carrasco. The First AusIMM International Geometallurgy Conference. Brisbane, Australia.

Berger, B.R., Ayuso, R.A., Wynn, J.C., & Seal, R.R., 2008, Preliminary model of porphyry copper deposits: U.S.Geological Survey Open-File Report 2008–1321, 55 p.

Benzer, H. 2005. Modeling and simulation of a fully air swept ball mill in a raw material grinding circuit. Power Technology. 153, 59-71.

Bilgili, E., Scarlett, B. 2005. Population balance modelling of non-linear effects in milling processes. Power Technology. 153: 59-71.

Blanchard, R. 1944. Chemical and mineralogical composition of twenty typical "limonites." American Mineralogist. 29: 111-114.

Bosecker, K. 1997. Bioleaching: metal solubilisation by microorganisms, FEMS Microbiology Reviews. 20 (3-4): 591-604.

Bradshaw, D.J., Triffett, B. & Kashuba, D. 2011. The role of Process Mineralogy in identifying the cause of low recovery of chalcopyrite at KUCC. Presented at the 10th International Congress for Applied Mineralogy, 1-5 August 2011, ICAM, Trondheim, Norway, pp. 73–80.

Brough, C. 2008. An investigation into process mineralogy of the Merensky Reef at Northen Platinum Limited. MSc thesis, University of Cape Town.

Broughton, D.W., Hitzman, M.W. & Alan, J.S. 2002. Exploration History and geology of the Kansanshi Cu (-Au) deposit. Society of Economic Geologists, Special Publication. 9: 141–153.

Bulled, D. & McInnes, C., “Flotation plant design and production planning through Geometallurgical modelling”; Centenary of flotation conference, Brisbane, 2006.

Bulatovic, S.M. 2007. Handbook of Flotation Reagents: Chemistry, Theory and Practice: Volume 1: Flotation of Sulfide Ores. Technology & Engineering, 458 pages.

Cailteux J., Binda P.L., Katekesha W.M., Kampunzu A.B., Intiomale M.M., Kapenda D., Kaunda C., Ngongo K., Tshiauka T., Wendorff M. 1994. Lithostratigraphical correlation of the Neoproterozoic Roan Supergroup from Shaba (Zaire) and Zambia, in the central African copper-cobalt metallogenic province. Journal of African Earth Sciences. 19(4): 265-278.

Cailteux, J.L.H., Kampunza, A.B., Lerouge, C., Kaputo, A.K., milesi, J.P. 2005. Genesis of sediment-host stratiform copper-cobalt deposits, central African Copperbelt. Journal of African Earth Sciences. 42: 134-158.

Cailteux, J.L.H., Kampunzu, A.B. & Lerouge, C. 2007. The Neoproterozoic MwashyaKansuki sedimentary rock succession in the central African Copperbelt, its Cu–Co mineralisation, and regional correlations. Gondwana Research. 11: 414–431.

Chadwick, J. 2011. Copper bottomed. International Mining, August, 98–114.

Chadwick, J. 2012. Better processing. International Mining, September, 125–138.

Chandra, A.P. & Gerson, A.R. 2009. A review of the fundamental studies of the copper activation mechanism for selective flotation of sulphide minerals, sphalerite and pyrite. Advances in Colloid and Interface Science. 14: 97-110.

Chávez, J.R. 2000. Supergene oxidation of copper deposits: Zoning and Distribution of Copper Oxide Minerals. Society of Economic Geologist. 41: 10-21.

Chinyuku, D.T. 2013. The Kansanshi Cu-Au deposit, Domes Region, Zambia: Geology, Mineralisation and Alteration characteristics in the Main pit. MSc.Thesis. Rhodes University.

Cilek, E.C., Umucu, Y. 2001. A statistical model for gangue entrainment into froths in flotation of sulphide ores. Minerals Enginnering. 14(9):1055-1066.

Coelho, A., 2007. TOPAS, version 4.2, Copyright _ 1999–2009 Bruker AXS. Technical

Reference.

Coetzee, L.L., Theron, S.J., Martin, G.J., Van Der Merwe, J.D. and Stanek, T. 2011. Modern gold deportments and its application to industry. Minerals Engineering. 24: 565–575.

Cooke, D.R. & Hollings, P. 2005. Gaint porphyry Deposits: Characteristics, Distribution, and Technoic Controls. Economic Geology. 100(5): 801-818.

Connolly, R. 2010. Introduction Quantitative X-Ray Diffraction Methods. https://lists.man.lodz.pl/pipermail/odlew-pl/2011/04/att-0005/09-Quant-intro_1_.pdf. [Accessed 05-01-2015].

Corriveau, L. 2011. Iron Oxide Copper-Gold (±AG±NB±P±REE±U) Deposits. Natural Resources Canada, Geological Survey of Canada, 490

Cox, D.P., Lindsey, D.A., Singer, D.A., and Diggles, M.F., 2003, Sediment-hosted copper deposits of the world: Deposit models and database: U.S. Geological Survey Open-File Report 03-107(url: http://geopubs.wr.usgs.gov/open-file/of03-107/).

Craig, J. R. and Vaughan, D. J. (1994). *Ore Microscopy and Ore.* Petrography (2nd edition). Wiley Interscience, New York.

Cropp, A.F., Goodall, W.R. & Bradshaw, D.J. 2013. The influence of textural variation and gangue mineralogy on recovery of copper by flotation from porphyry ore- A Review. Foreward, in: The second AusIMM International Geometallurgy Conference. Brisbane, Australia.

Cullity, B.D. 1956. Elements of X-Ray Diffraction. Addison-Wesley Publishing Company, Inc. Osmania University.

Deng, J., Wen, J.L., Wu, D. & Feng, Q. 2014. Adsorption and activation of copper ions on chalcopyrite surfaces: A new viewpoint of self-activation. Transactions of Nonferrous Metals society of China. 24: 3955-3963.

Dey, S. & Pathak, P.N. 2005. Comparative studies of amenability to processing of graphite from different sources. Transactions of Indian Institute of Metallurgy. 58 (5): 905–910.

Dobby,G, Kosick, G. & Amuluxen, A. 2002. A focus on variability within the orebody for improved design of flotation plants, in Proceedings 34th Annual Meeting (Canadian Mineral Processors: Ottowa).

Dominy, S. 2011. Foreward, in: The First AusIMM International Geometallurgy Conference. Brisbane, Australia.

Du Plessis, J.J.L., Marx, W.M., Nell, C. 2014. Efficient use of energy in ventilation and cooling of mines. The Journal of The Southern African Institute of Mining and Metallurgy. 114: 1033-1037

Ehrig. K. 2011. Quantitative mineral mapping-A Building Block for Geometallurgy Initiatives. The First AusIMM International Geometallurgy Conference. Brisbane, Australia.

Engelbrecht, C. 2011. XRF analysis of Base Metals prepared by fused bead method. Witwatersrand.

Enzweiler, J. & Webb, P.C. 1996. Determination of Trace Elements in Silicate Rocks by X-ray Fluorescence Spectrometry on 1:5 Glass beads Discs: Comparison of Accuracy and Precision with Pressed Powder Pellet Analysis. Chemical Geology. 130: 195–202.

Evans, A.M. 1993. Ore Geology and Industrial Minerals: An Introduction. London: Blackwell.

Evans, C.L., Wightman, E.M., Manlapig, E.V., Coulter, B.L. 2011. Application of Process Mineralogy as a tool in sustainable processing. Minerals Engineering. 24: 1242-1248.

Fandrich, R., Gu, Y., Burrows, D., Moeller, K. 2007. Modern SEM-based mineral liberation analysis. International Journal of Minerals Processing. 84: 310–320.

Farrokhpays, S., Ametor, I. & Grano, S. 2011. Improving the recovery of low grade coarse composite particles in porphyry copper ores. Advanced Powder Technology. 22: 464-470.

Finkelstein, N.P. & Goold, L.A. 1972. The reaction of sulphide minerals with thiol compounds. Mintek Report No. 1439.

Fourie P.H., Mulendwa, C., Shaw, E., Kaemba R. 2012. Current understanding of the Fous, S., Pring, A., Skinner, W., Zanin, M. 2015. Characterisation of coarse composite sphalerite particles with respect to flotation. Minerals Engineering. 71: 105-112.

Fragomeni, D., Boyd, L.J., Charland, A., Kormos, L.J., Lotter, N.O., Potts, G. 2005. The use of end-members for grind-recovery modelling, tonnage prediction and flowsheet development at Raglan. In: Proc. Canadian Mineral Processors. 6: 75–98.

François A. 1995. Problèmes relatifs au Katanguien duShaba. In: M. Wendorff and L. Tack (eds.), Late Proterozoic Belts in Central and Southwest Africa. Annales Sciences Géologiques Musée Royal de l'Afrique Centrale, Tervuren, Belgique, 101, 1-20.

Feng, D. & Aldrich, C. 1999. Effect of particle size on flotation performance of complex sulphide ores. Minerals Engineering. 12(7): 721-731.

Frew, J.A. & Davey, K.J. 1993. Effect of liberation on the flotation performance of a complex ore. In: Proc. XVIII International Mineral Processing Congress, AusIMM, Parkville, Victoria, 905–912.

Fuerstenau, M. C., Miller, J. D., and Kuhn, M. C. 1985. Chemistry of Flotation, Society of

Mining Engineers, AIME, New York, 170 pages.

Gaudin A.M. 1939. Principles of Mineral Dressing. McGraw-Hill Book Company: New York.

Gaudin, A.M., Groh, J.O., Henderson, H.B. 1931. Effect of particle size on flotation. American Institute of Mining and Metallurgical Engineering. 3-23.

Gibson, H. L., Allen, R. L., Riverin, G. & Lane, T. E. 2007. The VMS Model: Advances and Application to Exploration Targeting. Ore Deposits and Exploration Technology. 49: 713-730.

Goodall, W.R. 2008. Characterisation of mineralogy and gold deportment for complex tailings deposits using QEMSCAN. Minerals Engineering. 21: 518-523.

Goodall, W.R., Scales, P.J., Butcher, A.R., 2005a. The use of QEMSCAN and diagnostic leaching in the characterisation of visiable gold in complex ores. Minerals Engineering. 18: 877-886.

Godel, B. 2013. High-Resolution X-Ray Computed Tomography and Its applications to Ore Deposits: From Data Acquisition to Quantitative Three-Dimensional Measurements with Case Studies from Ni-Cu-PGE Deposits . Society of Economic Geology. 108: 2005-2019.

Gontijo, C. de F., Fornasiero, D., Ralston, J. 2007. The limits of fine and coarse particle flotation. Canadian Journal of Chemical Engineering.85: 739–747.

Gottlieb, P. 2008. The revolutionary impact of automated mineralogy on mining and mineral processing. In: 24th International Mineral Processing Congress. 165-174. (Science Press: Beijing).

Govender, D., Lelinski, D. &Traczyk, F. 2012. Hybrid energy flotation- on the optimization of fine and coarse particle kinetics in single row. The Southern African Institute of Mining and Metallurgy.

Gregory, J., Journet, N., Cameron, A., Titley, M. 2012: Technical Report for the Update of Mineral Resources and Reserves of the Kansanshi Mine, http://www.sedar.com, 224 pp.

Greyling L.N., Robb L.J., Master S., Boiron M.C., Yao, Y. 2005. The nature of early basinal fluids in the Zambian Copperbelt: A case study from the Chambishi deposit. Journal of African Earth Sciences. 42: 159-172.

Grewal, I. (n.d.). Introduction to mineral processing. Retrieved January 16, 2015, from

http://met-solvelabs.com/library/articles/mineral-processing-introduction.

Gunning, H.C. 1961, in Mendelsohn F (ed), Geology of the Northern Rhodesian Copperbelt, McDonald, London, pp 3-10.

Guilbert, J.M. & Parks, C.F. 1986. The Geology of Ore Deposits. New York, Waveland Press.

Habashi, F.1999. Solvent extraction in hydrometallurgy. A historical perspective. Bulletin of the Canadian Institute of Mining and Metallurgy. 92 (1033):103–106.

Habashi, F. 2005. A short history of Hydrometallurgy. Hydrometallurgy. 79: 15-22.

Hadler, K., Smith, C.D. & Cilliers, J.J. 2010. Flotation performance improvement by air recovery optimisation of roughers and scavengers. In: Proceedings of XXV IMPC, Brisbane, Australia.

Haest, M. & Muchez, P. 2011. Stratiform and vein-type deposits in the Pan-African Orogen in Central and Southern Africa: evidence for multiphase mineralisation. Geologica Belgica, 14(1-2): 23-44.

Harris, M.C., Runge, K.C., Whiten, W.J. & Morrison, R.D. 2002. JKSimFloat as a practical tool for flotation process designand optimisation. Proceedings of the SME Mineral Processing Plant Design, Practice and Control Conference, SME, Vancouver, 461-478.

Haynes, W. M. 2009. CRC handbook of chemistry and physics: A ready-reference book of chemical and physical data. Boca Raton: CRC Press.

Henley K.J. 1983. Ore-dressing mineralogy - a review of techniques, applications and recent developments. In: JPR De Villiers and PA Cawthorn (eds.) Proceedings of the International Congress of Applied Mineralogy 1981, 175-200. (GSSA: Johannesburg).

Herrera-Urbina, H., Hanson, J.S., Harris, G.H., Fuerstenau, D.W. 1990. Sulphide deposits their origin and processing, principles and practices of sulphide mineral flotation. 87-10.

Hitzman, M., Selley, D. & Bull, S. 2010. Formation of Sedimentary Rock-Hosted Stratiform Copper Deposits through Earth History. Journal of Economic Geology. 105: 627–639.

Hitzman, M.W, Broughton, D, Selley, D, Woodhead J, Wood D and Bull, S. 2012 - The Central African Copperbelt: Diverse Stratigraphic, Structural, and Temporal Settings in the World's Largest Sedimentary Copper District: *in* Hedenquist J W, Harris M and Camus F, 2012 Geology and Genesis of Major Copper Deposits and Districts of the World – A tribute to Richard H Sillitoe *Society of Economic Geologists* Special Publication 16: 487–514

Hoal K.O. 2008. Getting the Geo into Geomet. SEG Newsletter. 73: 11-15.

Hoal, K.O., Woodhead, J. & Smith, K.S. 2013. The importance of mineralogical input into Geometallurgical program. The Second AusIMM International Geometallurgy Conference. Brisbane, Australia.

Hunt, J.P. 1977. Porphyry copper deposits. Geological Society, London, Special Publications, 7:98.

Hunt, J., Berry, R. & Bradshaw, D. 2011. Characterising chalcopyrite liberation and flotation potential: Examples from an IOCG deposit. Minerals Engineering. 24: 1271–1276.

Irving J.D. 1906. University training of engineers in economic geology: Discussion. Economic Geology1: 77-82.

Jameson, G.J. 2010. New direction in flotation machine design. Minerals Engineering. 23(11-13): 835-841.

Jameson, G.J. 2010. The effect of surface liberation and particle size on flotation rate constants. Minerals Engineering. 36-38:132-137.

Jameson, G.J. 2012. The effect of surface liberation and particle size on flotation rate constants. Minerals Engineering. 36(38): 132-137.

Johnson, N.W. 2006. Liberated 0-10 µm particles from sulphide ores, their production and separation-Recent developments amd future needs. Minerals Engineering. 19: 666-674.

Kalichini, K. 2015. Flotation of copper oxide ores. MSc thesis, University of Cape Town.

Kampunzu, A. B. & Cailteux, J.L.H. 1999. Tectonic evolution of the Lufilian Arc during the Pan-African orogenesis. Gondwana Research, 2(3): 401-421.

Kampunzu, A.B., Cailteux, J.L.H., Kamona, A.F., Intiomale, M.M., Melcher, F. 2009. Sediment-hosted Zn–Pb–Cu deposits in the Central African Copperbelt. Ore Geology Reviews. 35: 263-297.

Kansanshi Antiform geology, Unpublished FQM Technical Meeting presentation, Solwezi,

Kaya, O. & Canbazoglu, M.E. 2007. A study on the floatability of graphite ore from Yozgat Akdagmadeni (Turkey). Journal of Ore Dressing. 9 (17):40–44.

Kelebek, S., Wells, P.F. & Fekete, S. O. 1996. Differential Flotation of Chalcopyrite, Pentlandite and Pyrrhotite in Ni–Cu Sulphide Ores. Canadian Metallurgical Quarterly. 35(4): 329-336.

Kelly, E.G. & Spottiswood, D.J. 1982. Introduction to mineral processing. New York: Wiley.

Key, R. M., Liyungu, A. K., Njamu, F. M., Somwe, V., Banda, J., Mosley, P. N., Armstrong, R. A. 2001. The Western arm of the Lufilian Arc, NW Zambia and its potential for copper mineralisation. Journal of African Earth Sciences. 33 (3-4): 503-528.

Klimpel, R. D. 1984. Froth Flotation: The kinetic approach. Proceedings of Mintek 5,

Johannesburg, South Africa.

Klimpel, R. R. 1995. "The Influence of Frother Structure on Industrial Coal Flotation", High-

Efficiency Coal Preparation (Kawatra, ed.), Society for Mining, Metallurgy, and

Exploration, Littleton, CO,141-151.

King, R.P. 1982. Flotation of fine particles. In: King RP, editor. Principles of Flotation. Johannesburg: South African Institute of Mining and Metallurgy.

King, R.P. 1994. Comminution and Liberation of Minerals. Minerals Engineering. 7(2 & 3): 129-140.

King, R.B. Ed. 2006. Encyclopedia of Inorganic Chemistry. 2nd ed. New York: Wiley. Kiraz, E. 2014. The recovery of copper from oxide copper ores by flotation and leaching. MSc thesis, Middle East Technical University.

Klassen, V. I. & Mokrousov, V. A. 1963. "An Introduction to the Theory of Flotation" (translated by J. Leja and G. W. Poling), Butterworths, London.

Klimpel, R. D. 1984. Froth Flotation: The kinetic approach. Proceedings of Mintek 5,

Johannesburg, South Africa.

Koski, R, A**.** 2010. Supergene Ore and Gangue Characteristics of Volcanogenic Massive Sulphide Occurrence Model. Scientific Investigations Report, viewed October 2014, from http://www. pubs.usgs.gov/sir/2010/5070/c/Chapter12SIR10-5070-C-3.pdf. [Accessed 05-01-2015]

Kribek, B., Kneesl, I, Pasava, J., Maly, K., Caruthers, H., Sykorova, I., Jehlicka, J. 2005. Hydrothermal alteration of the graphitized organic matter at the Kansanshi Cu (Au-,U-) deposit, Zambia: in Mao J and Bierlein P (Eds.), 2005 Mineral Deposit Research: Meeting the Global Challenge Proceedings of the Eighth Biennial SGA Meeting Beijing, China, 18-21 August 2005, 277-280.

Kyle, J.R., Mote A.S and Ketcham, R.., Kyle, J.R., Mote, A.S., Ketcham, R. a. 2008. High resolution X-ray computed tomography studies of Grasberg porphyry Cu-Au ores, Papua, Indonesia. Mineral Deposits. 43: 519-523.

Lestage, R., Pomerleau, A., Hodouin, D. 2002. Constrained real-time optimization of a grinding circuit using steady-state linear programming supervisory control. Power Technology. 124(3):254-263.

Li, H., Feng, Q., Yang, S., Ou, L. & Lu, Y. 2014. The entrainment behaviour of sericite in microcrystalline graphite flotation. International Journal of Mineral Processing. 127: 1-9.

Lodder, A.J., Padilla, R., Shaw, R., Garzon, T., Palacio, E., Jahoda, R., 2010. Discovery History of the La Colosa Gold Porphyry Deposit, Cajamarca, Columbia, special publication 15: 19-28 (Society of Economic Geologists: Littleton).

Lorenzen, L. & Barnard, M.J. 2011. Why is Mineralogical Data Essential for Designing a Metallurgical Test Work Program for Process Selection and Design?. The First AusIMM International Geometallurgy Conference. Brisbane, Australia.

Lotter N., Whittaker P.J., Kormos L., Stickling J.S., Wilkie G.J. 2002. The development of process mineralogy at Falconbridge Limited, and the application to the Raglan Mill. Paper presented at the 34th Annual Meeting of the Canadian Mineral Processors, Ottawa.

Lotter, N.O., Kormos, L.J., Oliveira, J., Fragomeni, D., Whiteman, E. 2011. Modern Process Mineralogy: Two case studies. Minerals Engineering. 24: 638–650.

Lotter, N.O. (2010). Modern Process Mineralogy: An integrated multi-disciplined approach to flowsheeting. Minerals Engineering. 24: 1229–1237.

Lotter, N.O., Kowal, D.L., Tuzun, M.A., Whittaker, P.J., Kormos, L.J. 2003. Sampling and flotation testing of Sudbury Basin drill core for Process Mineralogy modelling. Minerals Engineering. 16: 857–864

Lowell, J.D & Guilbert, J.M. 1968. Geology of the Kalamazoo ore body, San Manuel district, Arizona, Economic Geology. 63:645-654.

Lund, C., Lamberg, P. & Lindberg, T. 2015. Development of a geometallurgical framework to quantify mineral textures for process prediction. Minerals Engineering. 82:61-77

Lynch, A.J., Johnson, N.W., McKee, D.J., Thorne, G.C. 1974. The behaviour of minerals in sulphide flotation processes, with reference o simulation and control. Journal of the South African Institute of Mining and Metallurgy. 349-362.

Matschullat, J. Arsenic in the Geosphere- A Review. The Science of Total Enviroment, 2000 [cited 249; 16]. Available from: http://jbouzan.com/files/class/chem360/arsenicInTheGeosphere-AReview.pdf.

Mathur, R., Ruiz, J., Titley, S., Liermann, L., Buss, H., Brantley, S. 2005. Cu isotopic fractionation in the supergene environment with and without bacteria. Geochimica et Cosmochimica Acta. 69(22): 5233-5246.

McCusker, L.B., Von Dreele, R. B., Cox, D.E., Lou r, D., Scardie, P. 1999. Rietveld refinement guidelines. Journal of Applied Crystallography. 32: 36-50.

McGowan, R.R., Roberts, S., Foster, R.P., Boyce, A.D. & Coller, D. 2003. Origin of the copper-cobalt deposits of the Zambian Copperbelt: An epigenetic view from Nchanga. The Geological Society of America. 31: 497-500.

McGowan, R., Roberts, S., & Boyce, A. 2006, Origin of the Nchanga copper–cobalt deposits of the Zambian Copperbelt: Mineralium Deposita. 40(6): 617-638.

McGoldrick, P.J. & Large, R.R. 1998. Introduction to Geology and Mineralisation in the Proterozoic Carpentaria Zinc Belt' of northern Australia. Australian Journal of Earth Sciences.45; 33-49.

Mjettinen, T., Ralston, J., Fornasiero, D. 2010. The limits of fine particle flotation. Minerals Engineering. 23(5): 420-437.

Moore-Roth, M.N. 2012. Supergene enrichment profile at copper basin Battle Mountain, Nevada. MSc Thesis. New Mexico Institute of Mining and Technology.

Mielli, F & Bongiovanni, M. 2013. Production energy and optimization in mining. World Mining Congress.

Misra, K.C. 1999.Understanding Mineral Deposits. Kluwer Academic Publishers Group, Dordrecht, Netherlands.

Ndlovu, B.N., Becker, M., Forbes, E.., deglon, D.A. & Franzidis, J.P. 2011. The influence of phyllosilicate mineralogy on the rheology of mineral slurries. Minerals engineering. 24(12): 1314-1322.

Neethling, S.J. & Cilliers, J.J. 2002. The entrainment of gangue into flotation froth. Internation Journal of Mineral Processing. 64: 123-134.

Norgate, T.E., Jahanshahi, S. & Rankin, W.J. 2006. Accessing the environmental impacts of metal production processes. Journal of Cleaner Production. Accessed: 03 March 2016. Available from : https://www.researchgate.net/publication/222402610

Norgate, T.E & Jahanshahi, S., 2007. Opportunities for reducing energy consumption and greenhouse gas emissions in mineral processing and metal production. In: Proceedings Chemeca 2007 Conference, Melbourne, September 2007.

Norgate, T.E & Jahanshahi, S. 2010. Low grade ores- Smelting, leaching or concentrate?. Minerals Engineering. 23: 65-73.

O'Meara, A.E. 1961. Contributions to the Study of the Mount Isa Copper Orebodies (The Australasian Institute of Mining and Metallurgy Proceedings, No. 197, 1961).

Olubambi, P.A., Ndlovu, S., Potieter, J.H., Borode, J.O. 2007. Effect of ore mineralogy on the microbial leaching of low grade complex sulphide ores. 86: 96-104.

Owusu, C., Zanin, M., Fornasiero, D., Addai-Mensah, J. 2011. Influence of pyrite content on the flotation of chalcopyrite after regrinding with isamill. Ian Wark Research Institute, University of South Australia, Mawson Lakes, SA 5095, Australia.

Oyarzún, M. & Arévalo, A. 2011. Rock texture and BWi relationships, El Teniente ore deposit, Chile, in Proceedings First AusIMM International Geometallurgy Conference (GeoMet), 181-186 (The Australian Institute of Mining and Metallurgy: Melbourne).

Parekh, B.K.., Miller, J.D. 1999, Advances in Flotation Technology, SME Publishers, New York.

Paquot, F.X and Ngulube, C. 2015. Development and optimization of mixed sulphide/oxide copper ore treatment at Kansanshi. The Journal of the Southern African Institute of Mining and Metallurgy. 115: 1253-1258.

Patra, P., Bhambhani, T., Nagaraj, D.R. & Somasundaran, P. 2010, Effect of morphology of altered silicate minerals on metallurgical performance: Transport of Mg silicates to the froth phase. In: Rheology in Mineral Processing in Proc. 49th Conference of Metallurgists of CIM, pp. 31–42.

Pease, J.D., Curry, D.C., Young, M.F. 2006. Designing flotation circuits for high fines recovery. Minerals Engineering. 19: 831-840.

Perez-Barnuevo, L., Pirard, E. & Castroviejo, R. 2013. Automated characterisation of intergrowth textures in mineral particles . A case study. Minerals Engineering. 52: 136-142.

Petruk W., Wilson J.M.D., Lastra R., Healy R.E. 1991. An image analysis and materials balancing procedure for evaluating ores and mill products to obtain optimum recoveries. In: Proceedings of 23rd Annual Meeting of the Canadian Mineral Processors, 1–16 (Section 19).

Petruk, W. & Hughson, M.R. 1977. Image analysis evaluation of the effect of grinding media on selective flotation of two zinc–lead–copper ores. CIM Bull. 787: 128–135.

Petruk,W. 2000. Applied Mineralogy in the Mining Industry (Elsevier Science BV).

Porada, H. & Berhorst, V. 2000. Towards a new understanding of the Neoproterozoic-Early Palaeozoic Lufilian and northern Zambezi Belts in Zambia and the Democratic Republic of Congo. Journal of African Earth Sciences. 30(3): 727-771.

Powell, M.S. 2013. Utilising Orebody Knowledge to Improve Comminution Circuit Design and Energy Utilisation. The Second AusIMM International Geometallurgy Conference. Brisbane, Australia.

Pownceby, M.I., Aral, H. & Hackl, R. 2011. Geometallurgy and processing of Australia'suranium deposits. Proceedings ALTA 2011 Uranium, Perth, WA, Australia, 26–27 May 2011. ALTA Metallurgical Services (18 pp.).

Radmehr, V., Mohammad, S., Reza, M. 2013. Ammonia Leaching: A new approach of copper industry to hydrometallurgical processes. Journal of the Institute of Engineering. 94(2): 95-104.

Rahman, R.M., Graeme, S.A. & Jameson, J. 2012. The effect of flotation variables on the recovery of different particle size fractions in the froth and the pulp. International Journal of Mineral Processing. 106(109):70–77.

Rainaud C., Master S. & Robb L.J. 1999. A fertile Palaeoproterozoic magmatic arc beneath the Central African Copperbelt. In: C.J. Stanley et al. (eds), Mineral Deposits: Processes to Processing. Proceedings of the Fifth Biennial SGA Meeting and the Tenth Quadrennial IAGOD symposium, London, 22-25 August 1999, 1427-1430.

Rainaud, C., Master S., Armstrong R.A., Robb L.J. 2005a. Geochronology and nature of the Palaeoproterozoic basement in the Central African Copperbelt (Zambia and the Democratic Republic of Congo), with regional implications. Journal of African Earth Sciences. 42: 1-31.

Rainaud, C.L., Armstrong, R.A., Master, S., Robb, L.J., Mumba, P.A.C.C., 2002. Contributions to the geology and mineralisation of the central African Copperbelt. I. Nature and geochronology of the pre-Katangan basement. In: G.S.o. Namibia (Ed.), Proceedings of the 11th IAGOD Quadrennial Symposium and Geocongress. Geological Survey of Namibia,Windhoek, Namibia,p. 5.

Rao, D.S., Kumar, T.V., Raju, G.B., Prabhakar, S. 2011. The effect of particle size on flotation performance of siliceous limestone sample. Journal of Mining and Metallurgy. 47 A(1): 37-49.

Reich, M., Palacios, C., Vargas, G., Luo, S., Cameron, E.M., Leybourne., M.L., Parada, M.A., Zúñiga, A. You, C. 2009. Supergene enrichment of copper deposits since the onset of modern hyperaridity in the Atacama Desert, Chile. Mineralium Deposita. 44:497-504.

Robb L.J., Master S., Armstrong R., Rainaud C., Greyling L., 2003. Timing of Cu-Co and Pb-Zn mineralisation in the Central African Copperbelt: alink to Neoproterozoic glaciations? Transactions of the Institute of Mining and Metallurgy, 112, 2, 164-166.

Robb, L. 2005. Introduction to Ore-forming Processes. Blackwell Publishing, Oxford, p.373.

Robb, L.J., Master, S., Greyling, L., Yao, Y., Rainaud, C., 2002.Contributions to the geology and mineralisation of the Central African Copperbelt: V. Speculations regarding the ‘‘Snowball Earth’’ and redox controls on stratabound Cu–Co and Pb–Zn mineralisation. In: Proceedings of Geocongress 2002, Windhoek, Namibia, pp. 6.

Robertson, M. 2013. Kitumba- a new kind of copper deposits in a Zambian context. The Southern African Institute of Mining and Metallurgy. Base Metal Conference.

Schouwstra, R., de Vaux, D., Hey, P., Malysiak, V., Shackleton, N., Bramdeo, S., 2010. Understanding Gamsberg - A geometallurgical study of a large stratiform zinc deposit. Minerals Engineering. 23, 960–967.

Selley D., Broughton D., Scott R., Hitzman M., Bull S., Large R., McGoldrick P., Croaker M., Pollington N., Barra F., 2005. A new look at the geology of the Zambian Copperbelt. In: J.W. Hedenquist, J.F.H., Thompson, R.J., Goldfarb, J.P. Richards (eds.), Economic Geology 100th Anniversary Volume, 100, 965-1000.

Shabalala, N.Z.P., Harris, M., Leal Filho, L.S. & Deglon, D.A. 2011. Effect of slurry rheology on gas dispersion in a pilot-scale mechanical flotation cell. Minerals Engineering. 24(13): 1448-1453.

Shean, B.J. & Cilliers, J.J. 2011. A review of froth flotation control. International Journal of Mineral Processing. 100(3-4): 57-71.

Sherman, M. & Engelhardt, D. 1993. Gold-copper ore treatment at the Telfer mine, Telfer, WA, in Australasian Mining and Metallurgy: The Sir Maurice Mawby Memorial Volume(ed: J T Woodcock and J K Hamilton) (The Australasian Institute of Mining and Metallurgy: Melbourne).

Sikazwe, O., Hagni, A.M., Hagni, R.R., 2008. Applied Mineralogy of Refractory Copper Pres From Nchanga Mine in the Copperbelt of Northern Zambia. Ninth International Congress For Applied Mineralogy. Brisbane.

Sillitoe, R., Perello, J., Garcia, A., 2010. Sulphide-bearing veinlets throughout the stratiform mineralisation of the Central African Copperbelt: Temporal and Genetic implications. Journal of Economic Geology, 105 (8), 1361–1368.

Sinclair, W.D., 2007. Porphyry deposits, in Mineral Deposits of Canada: A Synthesis of Major Deposit-Types, District Metallogeny, the Evolution of Geological Provinces, and Exploration Methods, special publication 5, 223-243 (Geological Association of Canada, Mineral Deposits Division: St John's).

Smith, P.G. & Warren, L. J. 1989. Entrainment of particles into flotation froths. Minerals processing and Extractive Metallurgy Review. 8: 289-327.

Smith, A.J.B., Viljoen, K.S., Schouwstra, R., Roberts, J., Schalkwyk, C., Gutzmer, J. 2013. Geological variations in the Merensky Reef at Bafokeng Rasimone Platinum Mine and its influence on Flotation performance. Minerals Engineering. 52: 155-168.

Speiser, A., Hein, U.F., Porada, H. 1995. The Kansanshi copper mine (Solwezi area, northwestern Zambia): Geology, wall-rock alteration and fluid inclusions. In: Pasava, J., Kribek, B., Zak, K. (Eds.), Mineral Deposits: From their Origin to their Environmental Impacts. A.A. Balkema, Rotterdam, pp. 389–392.

Subrahmanyam, T.V. & Forssberg, E.1988. Froth Stability, Particle Entrainment and Drainage in Flotation- A Review. International Journal of Mineral Processing. 23:33-53
Sutherland, D.N. 1989. Batch flotation behaviour of composite particles. Minerals Engineering. 3: 351-367.

Swaby, A. 2013. Copper country. First Quantum Minerals: Kansanshi Mining Plc. Available: http://www.bus-ex.com/article/first-quantum-minerals-kansanshi-mining-plc [2016, February 02]

Sweet, C., van Hoogstraten, J., Harris, M., Laskowski, J.S. 1997. The effect of frotherson bubble size and frothability of aqueous solutions. In: Finch, J.A., Rao, S.R., Holubec, I. (Eds.), Processing of Complex Ores, 2nd UBC-McGill Symposium Series on Fundamental in Mineral Processing. The Metallurgical Society of CIM, pp. 235–246.

Sweeney, M.A. and Binda, P.L., and Vaughan, D.J., 1991, Genesis of ores of the Zambian Copperbelt: Ore Geology Reviews. 6: n51-7.

Sweeney, M.A. and Binda, P.L., 1989, The role of diagenesis in the formation of the Konkola Cu-Co orebody of the Zambian Copperbelt *in* Boyle, R.W., Brown, A.C., Jefferson, C.W., Jowett, E.C., and Kirkham, R.V. eds., Sediment-hosted Stratiform Copper Deposits: Geological Association of Canada Special Paper 36. p. 499-518.

Theron, S.J. 2013. The origin of the Central African Copperbelt: in a nutshell. The Southern African Institute of Mining and Metallurgy Base Metals Conference. Available: http://www.saimm.co.za/Conferences/BM2013/021-Theron.pdf [2015, October 14]

Torrealday, H. I., Hitzman, M. W., Stein, H. J., Markley, R. J., Armstrong, R., Broughton, D. 2000. Re-Os and U-Pb dating of the vein-hosted mineralisation at the Kansanshi copper deposit, Northern Zambia. Journal of Economic Geology. 95(5):1165-1170.

Trahar, W.J. 1981. A rational interpretation of the role of particle size in flotation. International Journal of Mineral Processing. 8: 289-327.

U.S. Congress, Office of Technology Assessment, Copper: Technology and Competitiveness, OTA-E-367 (Washington, DC: U.S. Government Printing Office, September 1988).

Valero, A. & Valero, A. 2012. Energy of comminution and the Thanatia earth's model. Energy. 44: 1085–1093.

Vasumathi, N., Vijaya Kumar, T.V., Ratchambigai, S., Subba Rao, S., Bhaskar Raju, G. 2015. Flotation studies on low grade graphite ore from eastern India. International Journal of Mining Science and Technology. 25(3):415-420.

Velasco, F., Herrero, J.M., Suárez, S., Yusta, I., Alvaro, A., Tornos, T. 2013. Supergene features and evolution of gossans capping massive sulphide deposits in the Iberian Belt. Ore Geology. 53: 181–203.

Veras, M., Bosco de Araújo Paulo, M., Pereira Leite, J., Magalhães Baltar, J. & Adolpho, C. 2014. Comparative study of the main flotation frothers using a new HYDROMESS adapted technique Rem: Revista Escola de Minas [online] 2014, 67 (Enero-Marzo): Date accessed 02-08-2016. Available in:<http://www.redalyc.org/articulo.oa?id=56430643013> ISSN 0370-4467

Wakamatsu, T. & Numata,Y. 1991. Flotation of graphite. Minerals. Engeering., 4(7): 975-982.

Wang, W. 2010. The flotation of coarse composite particles. Ph.D Thesis, University of South Australia, Adelaide.

Warren, L.J. 1985. Determination of the contributions of true flotation and entrainment in batch flotation tests. International Journal of Mineral Processing. 14: 33– 44.

Wei, L., Mo-tang, T., Chao-bo, T., Jing, H., Sheng-hai, Y., Jian-guang, Y. 2010. Dissolution kinetics of low grade complex copper ore in ammonia-ammonium chloride solution. Transactions of Nonferrous Metals Society of China. 20: 910-917.

Wen, Q. G., Valenta, M. 1996. A QEM*SCAN study of the flotation of composite particles. International Journal of Mineral Processing. 34(1-2): 71-82.

Wendorff M. 2005. Evolution of Neoproterozoic-LowerPalaeozoic Lufulian arch, Central Africa: a new model based on syntectonic conglomerates. Journal of the Geological Society, London: 162: 5-8.

Wiese, J.G. 2009.Investigating depressant behaviour in the flotation of selected Merensky ores. MSc thesis, University of Cape Town.

Wills, B.A. 1997. Mineral Processing Technology, An introduction to the practical aspects of ore treatment and mineral recovery, sixth edition. *Buttenvorth-Heinmann, Reed Educational and Professional Publishing Ltd.*

Willams, S.R. 2013. A Historical Perspective of the Application and Success of Geometallurgical Methodologies. The Second AusIMM International Geometallurgy Conference. Brisbane, Australia.

Wills, B. A. 1990. Comminution in the minerals industry – an overview. Minerals Engineering. 3: 3–5.

Wills, B.A., Napier-Munn, T.J. 2008. Wills Minerals Processing Techonology. Elsevier, Oxford.

Woodcock, J.T., Sparrow, G.J. & Bruckard, W.J., 2007. Flotation of Precious Metals and Their Minerals. In: Fuerstenau, M.C., Jameson, G., Yoon, R.-H. (Eds.), Froth Flotation, a Century of Innovation. SME, pp. 575–609.

Wright, P.J. 1993. Nickel ore concentration at Leinster Nickel Operations, Western Mining Corporation Limited, Leinster, WA, in Australasian Mining and Metallurgy: The Sir Maurice Mawby Memorial Volume (eds: J T Woodcock and J K Hamilton) (The Australasian Institute of Mining and Metallurgy: Melbourne.

Xu, D., Ametov, I. & Grano, S.R. 2012. Quantifying rheological and fine particle attachment contributions to coarse particle recovery in flotation. Minerals. Engineering. 39: 89-98.

Xu, D., Wang, W., Ametov, I., Fornasiero, D. & Grano, S. 2010. The detachment of coarse, composite particles from bubbles. In: XXV International Mineral Processing Congress (IMPC) Proceedings. 2601–2610.

Xu, M, Finch, J.A., Rao, S.R. & Lin, D. 1995. Reverse flotation of pyrite from a zinc-concentrate using nitrogen. Minerals Emgineering. 8(10): 1159-1173.

Ying, G., Schouwstra, R.P. & Rule, C. 2014. The value of automated mineralogy. Minerals Engineering. 58:100-103.

Yoon, R.H. & Basilio, C.I. 1993. Adsorption of thiol collectors on sulphide mineral and precious metals — a new perspective. XVIII International Mineral Processing Congress, Sydney.

Zengqian, H., Liquan, W., Zaw, K., Xuanxue, M., Mingjie, W., Dingmou, L. & Guitang, P. 2003. Post-collisional crustal extension setting and VHMS mineralisation in the Jinshajiang orogenic belt, southwestern China. Ore Geology Reviews. 22: 177-199.

http://blogs.wsj.com/moneybeat/2014/03/14/china-copper-premiums-point-to-weak-demand/

www.aqmcopper.com

www.businessinsider.com

www.icsg.org

www.mining-technology.com

www.mining-technology.com

www.oraclemining.com/copper

www.copper.co.za

APPENDIX A- PETROGRAPHIC DISCRIPTION

TS= Thin Sections

PTS= Polished Thin Sections

A1: Petrographic descriptions.

Sample summary		Mineralogy	Sample Description
Sample name	MN-001	Chalcopyrite Chalcocite Pyrite Malachite Quartz Feldspar Chlorite Kaolinite	Partially oxidized quartz-carbonate vein with cavities filled with primary and secondary sulphide minerals. The sulphide grains are anhedral to subhedral in shape. The over-texture is coarse- grained. Minor amounts of malachite and kaolinite.
Ore type	Oxide		
Lithology	Breccia		
Sample type	PTS		

Sample summary		Mineralogy	Sample Description
Sample name	MN-002	Chalcopyrite Pyrrhotite Malachite Azurite Quartz Feldspar Mica Chlorite Kaolinite	Oxidized quartz-carbonate vein. Malachite and azurite display a colloform and boytriodal texture. Sulphides are subhedral to euhedral in shape. Sulphides show disseminated texture.
Ore type	Oxide		
Lithology	Breccia		
Sample type	PTS		

Sample summary		Mineralogy	Sample Description
Sample name	MN-003	Chalcopyrite Covellite Chalcocite Malachite Chrysocolla Tenorite Quartz Feldspar Mica	Partially oxidized quartz-carbonate vein with cavities filled with primary and secondary sulphide minerals. The sulphide grains are anhedral to subhedral in shape. Dominated by celluar boxwork texture.
Ore type	Oxide		
Lithology	Breccia		
Sample type	PTS		

Sample summary		Mineralogy	Sample Description
Sample name	MN-004 & MN005	Chrysocolla Malachite Azurite Tenorite Quartz Mica Kaolinite	Oxidized quartz-carbonate vein. Malachite, chrysocolla and azurite display complex intergrown textures, including a colloform and boytriodal textures.
Ore type	Oxide		
Lithology	Breccia		
Sample type	PTS		

Sample summary		Mineralogy	Sample Description
Sample name	MN-004 & MN005	Chrysocolla Malachite Azurite Tenorite Quartz Mica Kaolinite	Oxidized quartz-carbonate vein. Malachite, chrysocolla and azurite display complex intergrown textures, including a colloform and boytriodal textures.
Ore type	Oxide		
Lithology	Breccia		
Sample type	PTS		

Sample summary		Mineralogy	Sample Description
Sample name	MN-006	Chrysocolla Malachite Azurite Tenorite Quartz Goethite Graphite Kaolinite	Matrix contains various lithology including hale and sandstones. That has been cut by high-angled veins composed of malachite, chrysocolla, azurite and goethite display complex intergrown textures, including a colloform and boytriodal textures.
Ore type	Oxide		
Lithology	Breccia		
Sample type	PTS		

Sample summary		Mineralogy	Sample Description
Sample name	MN-007	Chalcopyrite Pyrite Quartz Carbonate Mica	Veinlet with fine-grained disseminated ccp and py, running along bedding and foliation planes. Sulphide grains are subhedral to euhedral.
Ore type	Sulphide		
Lithology	calcareous-biotite -schist		
Sample type	PTS		

Sample summary		Mineralogy	Sample Description
Sample name	MN-008	Chalcopyrite Chalcocite Pyrite Quartz Carbonate Mica Feldspar	Veinlet with fine-grained disseminated ccp and py, running along bedding and foliation planes. Sulphide grains are subhedral to euhedral.
Ore type	Sulphide		
Lithology	calcareous-biotite -schist		
Sample type	PTS		

Sample summary		Mineralogy	Sample Description
Sample name	MN-009	Chalcopyrite Chalcocite Pyrite Quartz Carbonate Mica feldspar	Coarse-grained sulphides located within quartz-carbonate veins. These veins are surrounded by alteration halos composed of feldspar and quartz with disseminated sulphide mineralisation.
Ore type	Sulphide		
Lithology	Knotted-biotite-schist		
Sample type	PTS		

Sample summary		Mineralogy	Sample Description
Sample name	MN-010	Chalcopyrite Chalcocite Pyrite Quartz Carbonate Mica feldspar	Knotted Schist, with mica displaying preferred orientation. Minor amounts of disseminated sulphide mineralisation.
Ore type	Sulphide		
Lithology	knotted-schist		
Sample type	PTS		

Sample summary		Mineralogy	Sample Description
Sample name	MN-011	Chalcopyrite Chalcocite Pyrite Quartz Carbonate Mica feldspar	Quartz-carbonate veins containing coarse-grained sulphides hosted with Biotite Phyliite. Coarse-grained to massive texture.
Ore type	Mixed		
Lithology	biotite phyllite		
Sample type	PTS		

Sample summary		Mineralogy	Sample Description
Sample name	MN-012	Chalcopyrite Chalcocite Pyrite Quartz Carbonate Mica feldspar	Euhedral pyrite grains hosted within carbonaceous phyllites.
Ore type	Mixed		
Lithology	carbonaceous phyllite		
Sample type	PTS		

Sample summary		Mineralogy	Sample Description
Sample name	MN-013	Chalcopyrite Pyrite Quartz Mica feldspar	Heavily tarnished coarse-grained-sulphide within quartz-carbonate veins hosted with Biotite Phyllite. Sample represents initial stages of primary sulphide mineral replacement.
Ore type	Mixed		
Lithology	biotite phyllite		
Sample type	PTS		

Sample summary		Mineralogy	Sample Description
Sample name	MN-014	Chalcopyrite Chalcocite Pyrite Pyrrhotite Malachite Chrysocolla Quartz Mica Goethite	Variably oxidized sample, which displays a distinctive boxwork texture. Minerals show complex intergrown textures.
Ore type	Mixed		
Lithology	Heavily oxidized-phyllite		
Sample type	PTS		

Sample summary		Mineralogy	Sample Description
Sample name	MN-015 to MN-016	Chalcopyrite Pyrite Pyrrhotite Quartz Carbonate Mica	Coarse-grained sulphides in quartz-carbonate veins. Contains distinctive green mica that may be vanadium rich. Overall massive texture.
Ore type	Sulphide		
Lithology	Schist		
Sample type	PTS		

A1- Kansanshi sample details

Ore Characterization										
Sample	Location	GPS co-ordinates	Discription	Ore Type	Thin section	Polished section	QXRD	XRF	EMPA	QEMSCAN
MN 001	Main pit, Fault breccia "4800" zone	78°2'3.27"N, 6°18'58.5"E	Fault breccia	Mixed			X	X	X	X
MN 002	Main pit, Fault breccia "4800" zone	78°2'3.30"N, 6°18'58.56"E	Fault breccia	Oxide	X		X	X		X
MN 003	NE corner of Main pit, Fault breccia "4800" zon	78°1'56.20"N, 6°17'41.05"E	Fault breccia	Mixed			X	X	X	X
MN 004	NE corner of Main pit, Fault breccia "4800" zon	78°1'56.20"N, 6°17'41.05"E	Fault breccia	Oxide	X		X	X	X	X
MN 005	NE corner of Main pit, Fault breccia "4800" zon	78°1'55.23"N, 6°19'2.53"E	Fault breccia	Oxide						
MN 006	NE corner of Main pit, Fault breccia "4800" zon	78°2'3.30"N, 6°18'58.57"E	Fault breccia	Oxide			X	X		
MN 007	Main pit, Calcaerous biotite schist (LCS)	78°1'19.97"N, 6°19'17.78"E	Vein hosted in calcaerous biotite schist	Sulphide						
MN 008	Main pit, Calcaerous biotite schist (LCS)	78°1'19.99"N, 6°19'17.78"E	Vein hosted in calcaerous biotite schist	Sulphide	X		X	X	X	X
MN 009	Main pit, knotted biotite schist (LCS)	78°1'36.12"N, 6°18'54.15"E	Vein + alteration halo hosted in knotted biotite Sc	Sulphide	X		X	X	X	X
MN 010	NW pit, Knotted schist (MMC)	78°1'32.45"N, 6°19'3.52"E	Knotted Schist	Sulphide			X	X	X	
MN 011	NW pit, Biotite phyllite (MMC)	78°3'3.36"N, 6°16'5.92"E	Veins hosted in Biotite phyllite	Mixed		X	X	X		X
MN 012	NW pit, Carbonaceous phyllite (MMC)	78°2'53.37"N, 6°16'8.17"E	carbonaceous phyllite	Mixed			X	X		
MN 013	NW pit, Biotite phyllite (MMC)	78°3'3.36"N, 6°16'5.92"E	Veins hosted in Biotite phyllite	Mixed						
MN 014	NW pit in mixed middle clastics	78°2'53.59"N, 6°16'8.12"E	Heavily oxidised phyllite	Mixed			X	X	X	X
MN 015	NW pit in mixed middle clastics	78°2'48.92"N, 6°14'58.40"E	Vein hosted in Schist	Sulphide						
MN 016	NW pit in mixed middle clastics	78°2'48.92"N, 6°14'58.40"E	Vein hosted in Schist	Sulphide	X					
MN 017	Main pit, Lower Calcaerous Sequence	Grab sample	Vein hosted in marble	Sulphide						X
KANCORE3a-c	Grab sample	Grab sample	Vein hosted	Sulphide	X					
KANOXA-C_Coarse	Grab sample	Grab sample	Fault breccia	Oxide	X					
KANMX_CoarseA-C	Grab sample	Grab sample	Phyllite/ schist	Mixed						X
KANMX_CoarseD	Grab sample	Grab sample	Phyllite/ schist	Mixed						
KANMX1-6	Grab sample	Grab sample	Heavily oxidised phyllite	Mixed	X					
KANMX7	Grab sample	Grab sample	Heavily oxidised phyllite	Mixed	X				X	X
KANMX2_CoarseA-C	Grab sample	Grab sample	Vein hosted	Mixed						
KANSX3A_CORE	Grab sample	Grab sample	Vein hosted + alteration halo	Sulphide	X					
KANSX3B-G_CORE	Grab sample	Grab sample	Vein hosted + alteration halo	Sulphide	X					
KC2a-c	Grab sample	Grab sample	Mineralized phyllite	Sulphide	X					
SX1	Grab sample	Grab sample	Vein hosted	Sulphide			X	X	X	X
SX2	Grab sample	Grab sample	Phyllite	Sulphide			X	X		X
SX3-1	Grab sample	Grab sample	Vein hosted	Sulphide			X	X	X	X
SX3-2	Grab sample	Grab sample	Vein hosted	Sulphide			X			X
SX4-1 to SX4-3	Grab sample	Grab sample	Phyllite/ schist	Sulphide			X		X	X
SX5-1 to SX5-4	Grab sample	Grab sample	Vein hosted	Sulphide			X		X	X
Flotation Performance										
Ore Type	Lithology		Copper wt %	No. of batch float tests			QXRD	XRF	EMPA	QEMSCAN
Ore 1	Quartz-carbonate vein		0.68 ± 0.23	21			X	X		X
Ore 2	Stockpile blend of several lithologies		0.83 ± 0.22	21			X	X		X

A2- Location of samples in relation to Kansanshi stratigraphy

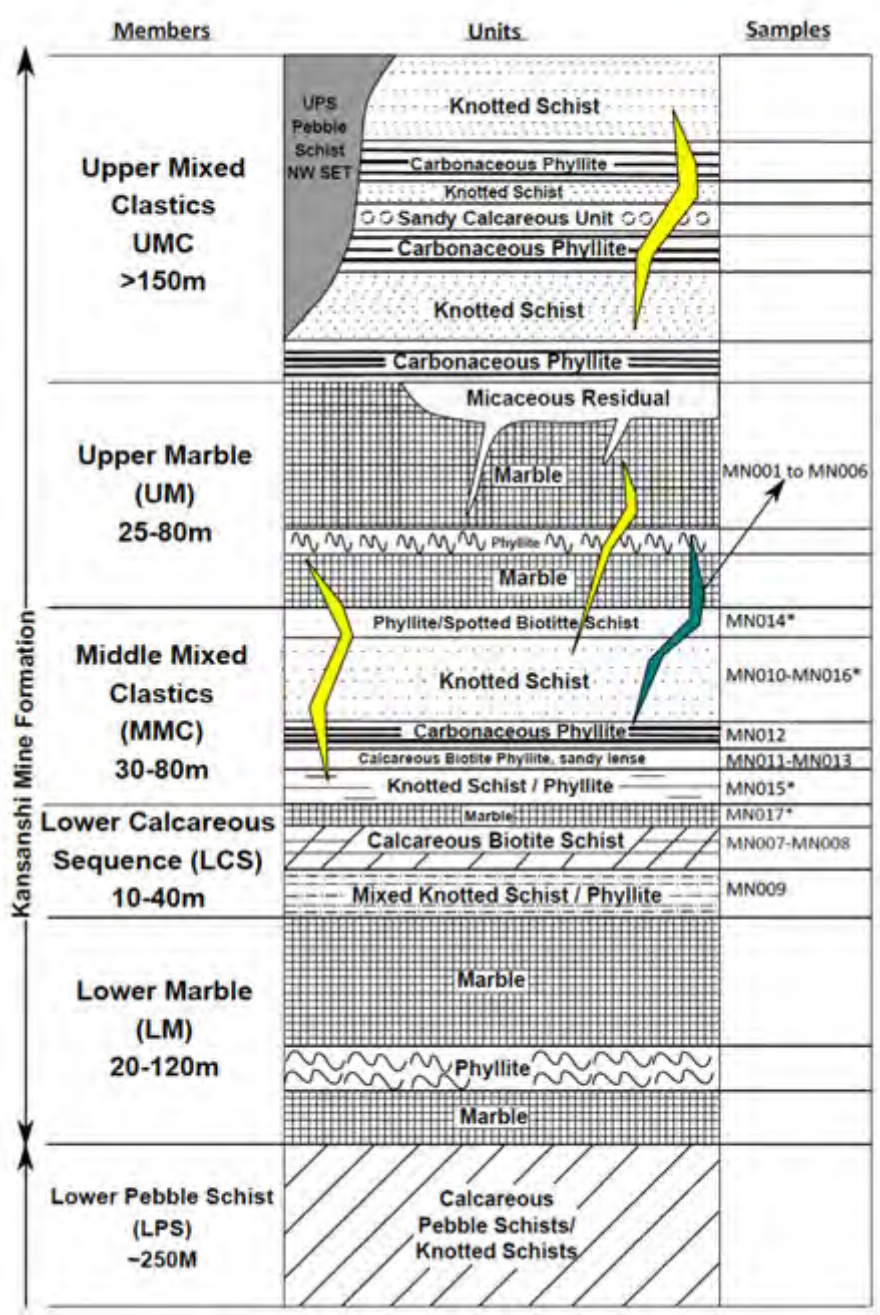

APPENDIX B- X-RAY DIFFRACTION DATA

B1-XRD scan of Vanadium muscovite (Green mica), code from the Philips X-pert software at UCT geology.

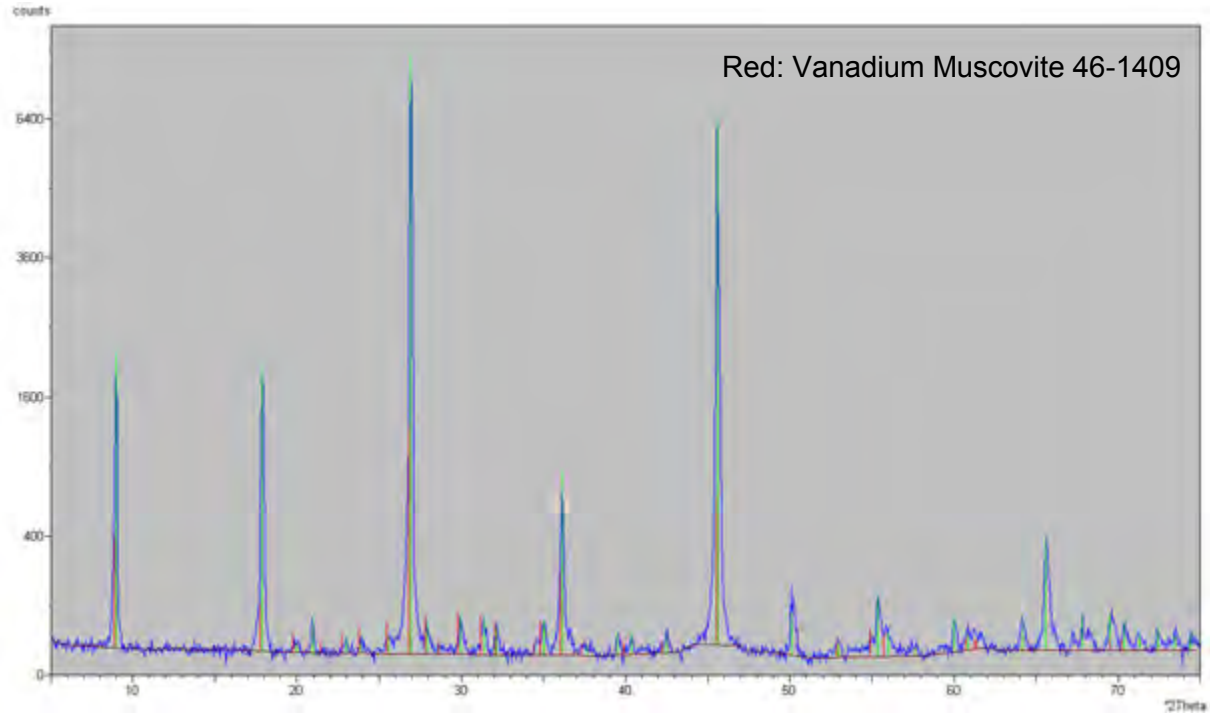

APPENDIX C- X-RAY FLOURESCENCE DATA

C1-Original XRF data for Ore 1 size fractions

Sample	HEAD	+150	+106	+75	+53	+25	-25
SiO_2	47.78	45.44	47.57	49.09	51.93	51.43	53.56
TiO_2	0.92	0.79	0.80	0.91	0.99	1.08	0.85
$Al2O_3$	11.73	10.38	8.78	8.94	10.30	12.07	14.29
Fe_2O_3	5.09	5.65	5.26	5.22	4.91	4.30	4.46
MnO	0.06	0.07	0.07	0.07	0.06	0.06	0.07
MgO	2.92	2.71	2.92	3.14	3.16	2.93	2.75
CaO	14.01	16.30	16.61	14.58	12.51	12.14	13.92
Na_2O	2.42	2.12	2.38	2.55	2.83	2.72	2.46
K_2O	1.89	1.54	1.05	1.20	1.42	1.73	2.58
P_2O_5	0.14	0.10	0.10	0.13	0.21	0.25	0.16
SO_3	2.12	2.60	2.64	2.28	2.00	1.68	1.44
Cr_2O_3	0.04	0.02	0.02	0.04	0.04	0.06	0.08
NiO	0.01	0.01	0.01	0.01	0.01	0.01	0.02
CuO	0.72	0.71	0.79	0.73	0.69	0.62	0.68
Total							
	0.17	0.18	0.31	0.22	0.15	0.30	0.29
H_2O^-	9.83	10.61	9.82	10.09	8.59	8.31	2.28
LOI							

C2-Original XRF data for Ore 2 size fractions.

Sample	+150	+106	+75	+53	+38	-25
SiO_2	60.19	60.03	63.93	62.51	60.51	52.99
TiO_2	1.06	1.09	1.22	1.43	1.20	1.11
$Al2O_3$	9.66	8.27	9.06	10.62	14.82	18.58
Fe_2O_3	6.69	6.13	5.95	5.76	4.31	4.39
MnO	0.05	0.05	0.05	0.05	0.04	0.05
MgO	1.58	1.61	1.96	1.94	1.63	1.72
CaO	6.31	5.27	5.20	4.79	3.98	5.20
Na_2O	2.56	2.30	2.49	2.67	2.99	2.90
K_2O	1.30	1.11	1.32	1.69	2.82	3.86
P_2O_5	0.09	0.07	0.09	0.17	0.19	0.16
SO_3	5.10	4.50	3.74	3.67	2.26	2.05
Cr_2O_3	0.01	0.02	0.02	0.03	0.06	0.08
NiO	0.01	0.01	0.01	0.02	0.02	0.03
CuO	1.45	1.21	1.01	0.96	0.69	0.73
Total	96.13	91.68	96.06	96.31	95.53	93.86
H_2O^-	0.13	0.31	0.15	0.16	0.24	0.33
LOI	3.72	7.02	3.67	3.29	3.75	5.53

C3- Vanadium-rich muscovite (Green mica) data

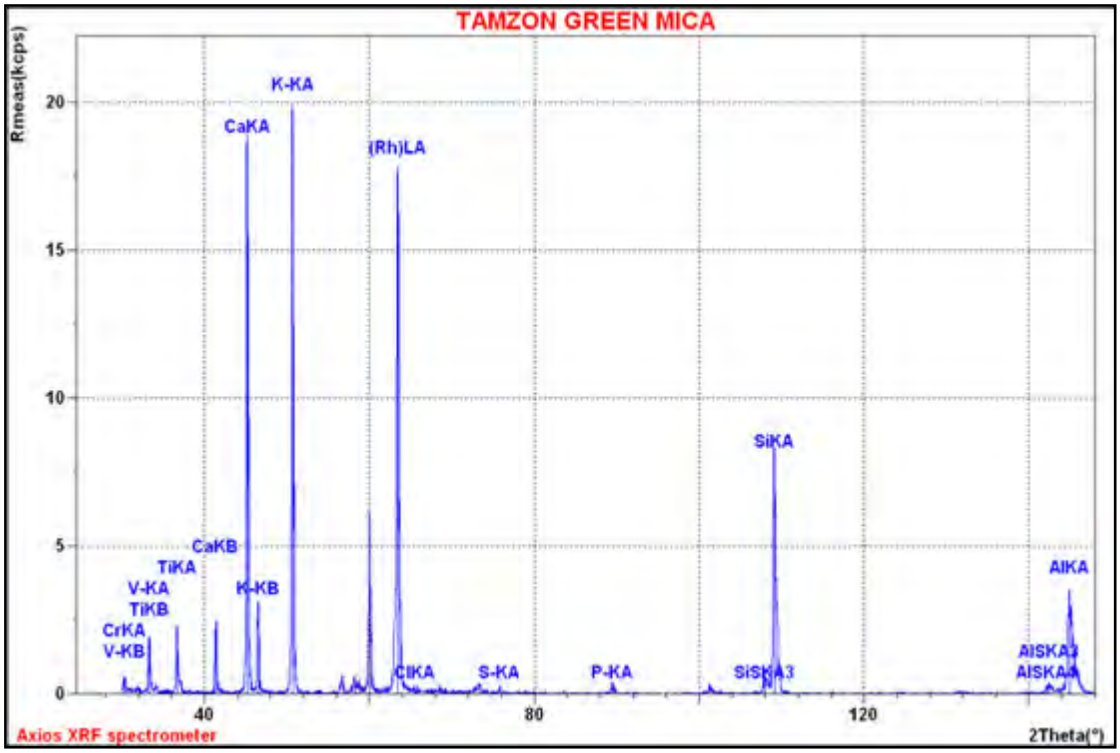

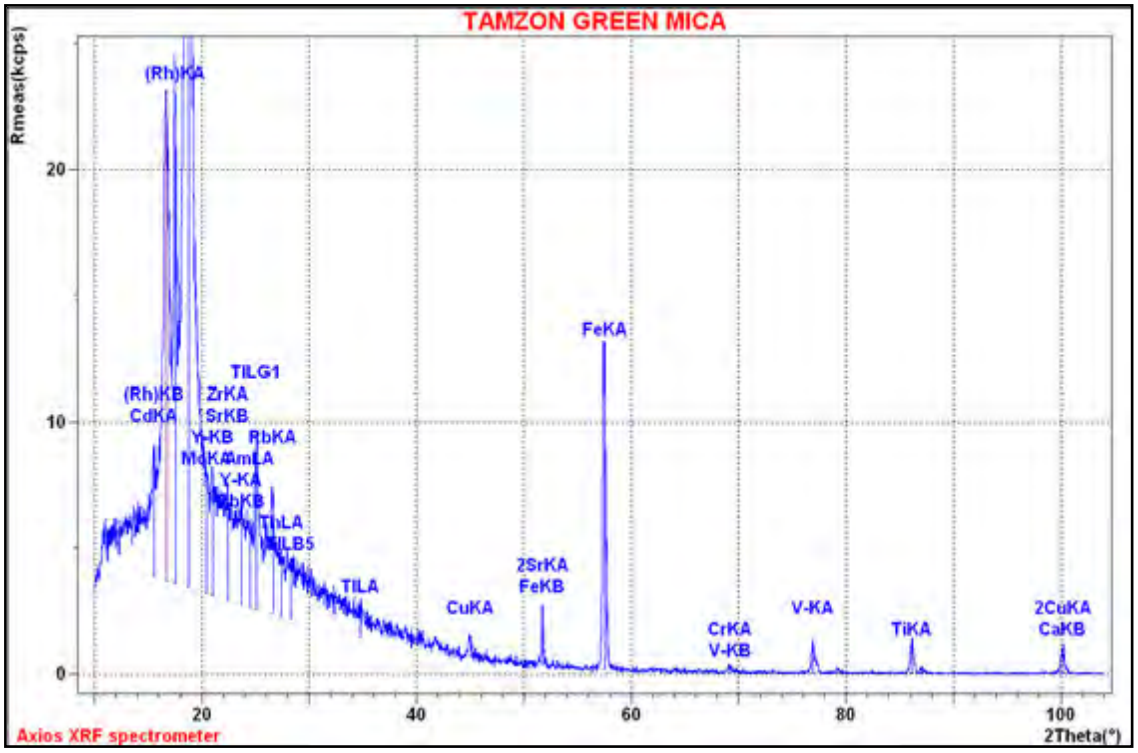

APPENDIX D- ELECTRON MICROPROBE ANALYSER (EMPA)

D1- BIOTITE PROBE DATA

Spot 1									
Oxide	wt % of oxides	mol. prop of ox	mole units	Oxygen factor	Oxygen units	Norm.Ox units	Atom units	Cations	Oxygen units
SiO_2	60.09	34.75	0.58	2.00	1.16	4.29	2.15	Si	1.16
TiO_2	79.90	1.39	0.02	2.00	0.03	0.13	0.06	Ti	0.03
Al_2O_3	101.96	17.75	0.17	3.00	0.52	1.94	1.29	Al	0.52
FeO	71.85	24.83	0.35	1.00	0.35	1.28	1.28	Fe^{2+}	0.35
MnO	70.94	0.10	0.00	1.00	0.00	0.01	0.01	Mn	0.00
MgO	40.31	8.40	0.21	1.00	0.21	0.77	0.77	Mg	0.21
CaO	56.08					0.00		Ca	
Na_2O	61.98	0.05	0.00	1.00	0.00	0.00	0.01	Na	0.00
K_2O	94.20	9.46	0.10	1.00	0.10	0.37	0.75	K	0.10
CuO	79.55	0.51	0.01	1.00	0.01	0.02	0.02	Cu	0.01
H_20	18.02	2.42						O	14.87
Total		97.23	1.43	0.00	2.38	8.82	6.34		
Spot 2									
Oxide	wt % of oxides	mol. prop of ox	mole units	Oxygen factor	Oxygen units	Norm.Ox units	Atom units	Cations	Oxygen units
SiO_2	60.09	35.05	0.58	2.00	1.17	53349.16	26674.6	Si	1.17
TiO_2	79.90	1.37	0.02	2.00	0.03	1566.54	783.3	Ti	0.03
Al_2O_3	101.96	18.36	0.18	3.00	0.54	24702.19	16468.1	Al	0.54
FeO	71.85	25.22	0.35	1.00	0.35	16051.59	16051.6	Fe^{2+}	0.35
MnO	70.94	0.09	0.00	1.00	0.00	56.21	56.2	Mn	0.00
MgO	40.31	8.19	0.20	1.00	0.20	9290.43	9290.4	Mg	0.20
CaO	56.08			1.00		0.00		Ca	
Na_2O	61.98	0.10	0.00	1.00	0.00	74.66	149.3	Na	0.00
K_2O	94.20	9.51	0.10	1.00	0.10	4616.27	9232.5	K	0.10
CuO	79.55			1.00				Cu	0.00
H_20	18.02	2.45						O	14.73
Total		100.33		0.00	2.40	109707.05	78706.1		
Spot 3									
Oxide	wt % of oxides	mol. prop of ox	mole units	Oxygen factor	Oxygen units	Norm.Ox units	Atom units	Cations	Oxygen units
SiO_2	60.09	35.18	0.59	2.00	1.17	409.93	204.97	Si	1.17
TiO_2	79.90	1.25	0.02	2.00	0.03	10.92	5.46	Ti	0.03
Al_2O_3	101.96	18.23	0.18	3.00	0.54	187.77	125.18	Al	0.54
FeO	71.85	24.09	0.34	1.00	0.34	117.38	117.38	Fe^{2+}	0.34
MnO	70.94	0.03	0.00	1.00	0.00	0.15	0.15	Mn	0.00
MgO	40.31	8.26	0.20	1.00	0.20	71.73	71.73	Mg	0.20
CaO	56.08			1.00		0.00		Ca	
Na_2O	61.98	0.07	0.00	1.00	0.00	0.37	0.75	Na	0.00
K_2O	94.20	9.27	0.10	1.00	0.10	34.45	68.90	K	0.10
CuO	79.55			1.00				Cu	
H_20	18.02	3.90		1.00				O	9.25
Total			1.42	0.00	2.38	832.71	594.51		
Spot 4									
Oxide	wt % of oxides	mol. prop of ox	mole units	Oxygen factor	Oxygen units	Norm.Ox units	Atom units	Cations	Oxygen units
SiO_2	60.09	35.29	0.59	2.00	1.17	38865.90	19432.95	Si	1.17
TiO_2	79.90	1.40	0.02	2.00	0.03	1156.27	578.13	Ti	0.03
Al_2O_3	101.96	18.27	0.18	3.00	0.54	17786.02	11857.35	Al	0.54
FeO	71.85	23.64	0.33	1.00	0.33	10886.74	10886.74	Fe^{2+}	0.33
MnO	70.94	0.10	0.00	1.00	0.00	45.76	45.76	Mn	0.00
MgO	40.31	9.15	0.23	1.00	0.23	7510.19	7510.19	Mg	0.23
CaO	56.08			1.00		0.00		Ca	
Na_2O	61.98	0.18	0.00	1.00	0.00	94.54	189.09	Na	0.00
K_2O	94.20	9.42	0.10	1.00	0.10	3308.56	6617.12	K	0.10
CuO	79.55	0.43	0.01	1.00	0.01	180.73	180.73	Cu	0.01
H_20	18.02	3.95		1.00				O	9.12
Total		101.83	1.45	0.00	2.41	79834.71	57298.06		

Spot 5									
SiO_2	wt % of oxides	mol. prop of ox	mole units	Oxygen factor	Oxygen units	Norm.Ox units	Atom units	Cations	Oxygen units
TiO_2	60.09	35.40	0.59	2.00	1.18	416.44	208.22	Si	1.18
Al_2O_3	79.90	1.39	0.02	2.00	0.03	12.32	6.16	Ti	0.03
FeO	101.96	17.97	0.18	3.00	0.53	186.86	124.57	Al	0.53
MnO	71.85	25.15	0.35	1.00	0.35	123.71	123.71	Fe^{2+}	0.35
MgO	70.94	0.09	0.00	1.00	0.00	0.45	0.45	Mn	0.00
CaO	40.31	7.97	0.20	1.00	0.20	69.87	69.87	Mg	0.20
Na_2O	56.08			1.00		0.00		Ca	
K_2O	61.98	0.10	0.00	1.00	0.00	0.56	1.12	Na	0.00
CuO	94.20	9.52	0.10	1.00	0.10	35.72	71.43	K	0.10
H_20	79.55			1.00				Cu	
Total	18.02	3.92		1.00				O	9.19
Total		101.51	1.43	0.00	2.39	845.93	605.54		
Spot 6									
Oxide	wt % of oxides	mol. prop of ox	mole units	Oxygen factor	Oxygen units	Norm.Ox units	Atom units	Cations	Oxygen units
SiO_2	60.09	35.34	0.59	2.00	1.18	411.36	205.68	Si	1.18
TiO_2	79.90	1.36	0.02	2.00	0.03	11.89	5.94	Ti	0.03
Al_2O_3	101.96	17.45	0.17	3.00	0.51	179.55	119.70	Al	0.51
FeO	71.85	26.11	0.36	1.00	0.36	127.09	127.09	Fe^{2+}	0.36
MnO	70.94	0.02	0.00	1.00	0.00	0.12	0.12	Mn	0.00
MgO	40.31	7.72	0.19	1.00	0.19	66.97	66.97	Mg	0.19
CaO	56.08			1.00		0.00		Ca	
Na_2O	61.98	0.06	0.00	1.00	0.00	0.32	0.63	Na	0.00
K_2O	94.20	9.28	0.10	1.00	0.10	34.45	68.90	K	0.10
CuO	79.55			1.00				Cu	
H_20	18.02	3.90		1.00				O	9.25
Total		101.23	1.43	0.00	2.38	831.74	595.03		
Spot 7									
Oxide	wt % of oxides	mol. prop of ox	mole units	Oxygen factor	Oxygen units	Norm.Ox units	Atom units	Cations	Oxygen units
SiO_2	60.09	35.91	0.60	2.00	1.20	428.81	214.40	Si	1.20
TiO_2	79.90	1.47	0.02	2.00	0.04	13.22	6.61	Ti	0.04
Al_2O_3	101.96	17.91	0.18	3.00	0.53	189.05	126.03	Al	0.53
FeO	71.85	24.98	0.35	1.00	0.35	124.73	124.73	Fe^{2+}	0.35
MnO	70.94	0.07	0.00	1.00	0.00	0.33	0.33	Mn	0.00
MgO	40.31	7.94	0.20	1.00	0.20	70.66	70.66	Mg	0.20
CaO	56.08	0.01	0.00	1.00	0.00	0.09	0.09	Ca	0.00
Na_2O	61.98	0.13	0.00	1.00	0.00	0.76	1.53	Na	0.00
K_2O	94.20	9.38	0.10	1.00	0.10	35.72	71.44	K	0.10
CuO	79.55			1.00				Cu	
H_20	18.02	3.94		1.00				O	9.14
Total		101.75	1.44	0.00	2.41	863.38	615.83		
Spot 8									
Oxide	wt % of oxides	mol. prop of ox	mole units	Oxygen factor	Oxygen units	Norm.Ox units	Atom units	Cations	Oxygen units
SiO_2	60.09	35.90	0.60	2.00	1.19	424.12	212.06	Si	1.19
TiO_2	79.90	1.41	0.02	2.00	0.04	12.57	6.29	Ti	0.04
Al_2O_3	101.96	18.22	0.18	3.00	0.54	190.27	126.84	Al	0.54
FeO	71.85	24.96	0.35	1.00	0.35	123.30	123.30	Fe^{2+}	0.35
MnO	70.94	0.05	0.00	1.00	0.00	0.24	0.24	Mn	0.00
MgO	40.31	7.77	0.19	1.00	0.19	68.41	68.41	Mg	0.19
CaO	56.08	0.01	0.00	1.00	0.00	0.05	0.05	Ca	0.00
Na_2O	61.98	0.14	0.00	1.00	0.00	0.83	1.65	Na	0.00
K_2O	94.20	9.37	0.10	1.00	0.10	35.30	70.60	K	0.10
CuO	79.55			1.00				Cu	
H_20	18.02	3.95		1.00				O	9.13
Total		101.78	1.44	0.00	2.41	855.08	609.44		

D 2 – CHLORITE PROBE DATA

Spot 1									
Oxide	**wt % of oxides**	**mol. prop of ox**	**mole units**	**Oxygen factor**	**Oxygen units**	**Norm.Ox units**	**Atom units**	**Cations**	**Oxygen units**
SiO_2	60.09	24.88	0.41	2.00	0.83	10.35	5.17	Si	0.83
TiO_2	79.90	0.10	0.00	2.00	0.00	0.03	0.02	Ti	0.00
Al_2O_3	101.96	22.86	0.22	3.00	0.67	8.40	5.60	Al	0.67
FeO	71.85	32.12	0.45	1.00	0.45	5.59	5.59	Fe2+	0.45
MnO	70.94	0.15	0.00	1.00	0.00	0.03	0.03	Mn	0.00
MgO	40.31	11.54	0.29	1.00	0.29	3.58	3.58	Mg	0.29
CaO	56.08	0.02	0.00	1.00	0.00	0.01	0.01	Ca	0.00
Na_2O	61.98	0.05	0.00	1.00	0.00	0.01	0.02	Na	0.00
K_2O	94.20	0.02	0.00	1.00	0.00	0.00	0.01	K	0.00
CuO	79.55	0.04	0.00	1.00	0.00	0.01	0.01	Cu	0.00
H_20	18.02	11.53		1.00				O	12.50
Total			1.38	0.00	2.24	28.00	20.02		
Spot 2									
Oxide	**wt % of oxides**	**mol. prop of ox**	**mole units**	**Oxygen factor**	**Oxygen units**	**Norm.Ox units**	**Atom units**	**Cations**	**Oxygen units**
SiO_2	60.09	24.53	0.41	2.00	0.82	10.40	5.20	Si	0.82
TiO_2	79.90	0.04	0.00	2.00	0.00	0.01	0.01	Ti	0.00
Al_2O_3	101.96	22.12	0.22	3.00	0.65	8.29	5.53	Al	0.65
FeO	71.85	31.33	0.44	1.00	0.44	5.55	5.55	Fe^{2+}	0.44
MnO	70.94	0.07	0.00	1.00	0.00	0.01	0.01	Mn	0.00
MgO	40.31	11.57	0.29	1.00	0.29	3.66	3.66	Mg	0.29
CaO	56.08	0.00	0.00	1.00	0.00	0.00	0.00	Ca	0.00
Na_2O	61.98	0.05	0.00	1.00	0.00	0.01	0.02	Na	0.00
K_2O	94.20			1.00		0.00		K	0.00
CuO	79.55	0.38	0.00	1.00	0.00	0.06	0.06	Cu	0.00
H_20	18.02	11.53		1.00				O	12.74
Total			1.36	0.00	2.20	28.00	20.04		
Spot 3									
Oxide	**wt % of oxides**	**mol. prop of ox**	**mole units**	**Oxygen factor**	**Oxygen units**	**Norm.Ox units**	**Atom units**	**Cations**	**Oxygen units**
SiO_2	60.09	24.95	0.42	2.00	0.83	10.32	5.16	Si	0.83
TiO_2	79.90	0.07	0.00	2.00	0.00	0.02	0.01	Ti	0.00
Al_2O_3	101.96	23.10	0.23	3.00	0.68	8.45	5.63	Al	0.68
FeO	71.85	31.38	0.44	1.00	0.44	5.43	5.43	Fe^{2+}	0.44
MnO	70.94	0.07	0.00	1.00	0.00	0.01	0.01	Mn	0.00
MgO	40.31	12.16	0.30	1.00	0.30	3.75	3.75	Mg	0.30
CaO	56.08	0.01	0.00	1.00	0.00	0.00	0.00	Ca	0.00
Na_2O	61.98	0.07	0.00	1.00	0.00	0.01	0.03	Na	0.00
K_2O	94.20	0.03	0.00	1.00	0.00	0.00	0.01	K	0.00
CuO	79.55			1.00				Cu	0.00
H_20	18.02	11.60		1.00				O	12.43
Total			1.38	0.00	2.25	28.00	20.03		
Spot 4									
Oxide	**wt % of oxides**	**mol. prop of ox**	**mole units**	**Oxygen factor**	**Oxygen units**	**Norm.Ox units**	**Atom units**	**Cations**	**Oxygen units**
SiO_2	60.09	24.96	0.42	2.00	0.83	10.20	5.10	Si	0.83
TiO_2	79.90	0.06	0.00	2.00	0.00	0.02	0.01	Ti	0.00
Al_2O_3	101.96	23.51	0.23	3.00	0.69	8.50	5.66	Al	0.69
FeO	71.85	27.87	0.39	1.00	0.39	4.76	4.76	Fe^{2+}	0.39
MnO	70.94	0.03	0.00	1.00	0.00	0.01	0.01	Mn	0.00
MgO	40.31	14.77	0.37	1.00	0.37	4.50	4.50	Mg	0.37
CaO	56.08			1.00		0.00		Ca	
Na_2O	61.98	0.04	0.00	1.00	0.00	0.01	0.02	Na	0.00
K_2O	94.20	0.02	0.00	1.00	0.00	0.00	0.01	K	0.00
CuO	79.55			1.00				Cu	0.00
H_20	18.02	11.73		1.00				O	12.28
Total			1.40	0.00	2.28	28.00	20.07		

Spot 5									
Oxide	**wt % of oxides**	**mol. prop of ox**	**mole units**	**Oxygen factor**	**Oxygen units**	**Norm.Ox units**	**Atom units**	**Cations**	**Oxygen units**
SiO_2	60.085	25.24	0.420071565	2	0.840143131	10.23461902	5.117309509	Si	0.830823001
TiO_2	79.899	0.1223	0.001530682	2	0.003061365	0.037293531	0.018646766	Ti	0.001602023
Al_2O_3	101.961	23.66	0.232049509	3	0.696148527	8.480477551	5.6536517	Al	0.691735075
FeO	71.846	27.47	0.382345572	1	0.382345572	4.657731671	4.657731671	Fe^{2+}	0.387913036
MnO	70.937	0.0992	0.001398424	1	0.001398424	0.017035593	0.017035593	Mn	0.000489166
MgO	40.311	15.11	0.374835653	1	0.374835653	4.566245871	4.566245871	Mg	0.36640123
CaO	56.079	0.0162	0.000288878	1	0.000288878	0.003519113	0.003519113	Ca	
Na_2O	61.979	0.0075	0.000121009	1	0.000121009	0.001474128	0.002948255	Na	0.000656674
K_2O	94.203	0.0124	0.000131631	1	0.000131631	0.001603524	0.003207047	K	0.000246277
CuO	79.545			1				Cu	0
H_20	18.015	11.83057501		1				O	12.18199453
Total			1.412772924	0	2.29847419	28	20.04029553		
Spot 6									
Oxide	**wt % of oxides**	**mol. prop of ox**	**mole units**	**Oxygen factor**	**Oxygen units**	**Norm.Ox units**	**Atom units**	**Cations**	**Oxygen units**
SiO_2	60.085	25.03	0.416576517	2	0.833153033	11.71567289	5.857836443	Si	0.833153033
TiO_2	79.899	0.0571	0.000714652	2	0.001429304	0.020098665	0.010049333	Ti	0.001429304
Al_2O_3	101.961	26.01	0.255097537	3	0.765292612	10.76142983	7.174286552	Al	0.765292612
FeO	71.846	0.0222	0.000308994	1	0.000308994	0.004345031	0.004345031	Fe^{2+}	0.000308994
MnO	70.937	0.0401	0.00056529	1	0.00056529	0.007949028	0.007949028	Mn	0.00056529
MgO	40.311	15.71	0.389719928	1	0.389719928	5.480183119	5.480183119	Mg	0.389719928
CaO	56.079	0.0127	0.000226466	1	0.000226466	0.003184534	0.003184534	Ca	0.000226466
Na_2O	61.979	0.0168	0.00027106	1	0.00027106	0.003811599	0.007623197	Na	0.00027106
K_2O	94.203	0.0115	0.000122077	1	0.000122077	0.001716626	0.003433251	K	0.000122077
CuO	79.545	0.0091	0.000114401	1	0.000114401	0.001608685	0.001608685	Cu	0.000114401
H_20	18.015	10.24900715		1				O	14.06184989
Total			1.063716922	0	1.991203165	28	18.55049917		
Spot 7									
Oxide	**wt % of oxides**	**mol. prop of ox**	**mole units**	**Oxygen factor**	**Oxygen units**	**Norm.Ox units**	**Atom units**	**Cations**	**Oxygen units**
SiO_2	60.085	24.57	0.408920696	2	0.817841391	10.19189863	5.095949316	Si	0.828160107
TiO_2	79.899	0.0376	0.000470594	2	0.000941188	0.011729041	0.005864521	Ti	0.001775813
Al_2O_3	101.961	23.14	0.22694952	3	0.68084856	8.484700797	5.656467198	Al	0.691020516
FeO	71.846	31.36	0.436489157	1	0.436489157	5.439506111	5.439506111	Fe^{2+}	0.360994747
MnO	70.937	0.0791	0.001115074	1	0.001115074	0.013895996	0.013895996	Mn	0.001098359
MgO	40.311	12.32	0.305623775	1	0.305623775	3.808668244	3.808668244	Mg	0.330218267
CaO	56.079	0.022	0.000392304	1	0.000392304	0.004888869	0.004888869	Ca	0.000231561
Na_2O	61.979			1		0		Na	0.000543041
K_2O	94.203			1		0		K	0.000145886
CuO	79.545	0.2854	0.003587906	1	0.003587906	0.044712308	0.044712308	Cu	0.001284089
H_20	18.015	11.56480314		1				O	12.46195013
Total			1.383549026	0	2.246839356	28	20.06995256		

D 3 – FELDSPAR PROBE DATA

Spot 1							
Oxide	**wt % of oxides**	**mol. prop of ox**	**mole units**	**Oxygen factor**	**Oxygen units**	**Norm.Ox units**	**Atom units**
SiO_2	60.09	68.44	1.14	2.00	2.28	5.96	2.98
TiO_2	79.90	0.02	0.00	2.00	0.00	0.00	0.00
Al_2O_3	101.96	20.24	0.20	3.00	0.60	1.56	1.04
FeO	71.85	0.02	0.00	1.00	0.00	0.00	0.00
MnO	70.94	0.02	0.00	1.00	0.00	0.00	0.00
MgO	40.31	0.00	0.00	1.00	0.00	0.00	0.00
CaO	56.08	0.15	0.00	1.00	0.00	0.01	0.01
Na_2O	61.98	11.12	0.18	1.00	0.18	0.47	0.94
K_2O	94.20	0.08	0.00	1.00	0.00	0.00	0.00
Total		99.82	1.52	0.00	3.06	8.00	4.97
Spot 2							
Oxide	**wt % of oxides**	**mol. prop of ox**	**mole units**	**Oxygen factor**	**Oxygen units**	**Norm.Ox units**	**Atom units**
SiO_2	60.09	68.40	1.14	2.00	2.28	5.96	2.98
TiO_2	79.90	0.08	0.00	2.00	0.00	0.01	0.00
Al_2O_3	101.96	20.06	0.20	3.00	0.59	1.54	1.03
FeO	71.85	0.00	0.00	1.00	0.00	0.00	0.00
MnO	70.94	0.02	0.00	1.00	0.00	0.00	0.00
MgO	40.31	0.00	0.00	1.00	0.00	0.00	0.00
CaO	56.08	0.11	0.00	1.00	0.00	0.01	0.01
Na_2O	61.98	11.20	0.18	1.00	0.18	0.47	0.95
K_2O	94.20	0.08	0.00	1.00	0.00	0.00	0.00
Total		99.95	1.52	0.00	3.05	7.99	4.97
Spot 3							
Oxide	**wt % of oxides**	**mol. prop of ox**	**mole units**	**Oxygen factor**	**Oxygen units**	**Norm.Ox units**	**Atom units**
SiO_2	60.09	68.56	1.14	2.00	2.28	5.97	2.99
TiO_2	79.90	0.02	0.00	2.00	0.00	0.00	0.00
Al_2O_3	101.96	20.25	0.20	3.00	0.60	1.56	1.04
FeO	71.85	0.03	0.00	1.00	0.00	0.00	0.00
MnO	70.94	0.04	0.00	1.00	0.00	0.00	0.00
MgO	40.31	0.00	0.00	1.00	0.00	0.00	0.00
CaO	56.08	0.25	0.00	1.00	0.00	0.01	0.01
Na_2O	61.98	10.81	0.17	1.00	0.17	0.46	0.91
K_2O	94.20	0.09	0.00	1.00	0.00	0.00	0.00
Total		100.06	1.52	0.00	3.06	8.00	4.96
Spot 4							
Oxide	**wt % of oxides**	**mol. prop of ox**	**mole units**	**Oxygen factor**	**Oxygen units**	**Norm.Ox units**	**Atom units**
SiO_2	60.09	68.56	1.14	2.00	2.28	5.97	2.99
TiO_2	79.90	0.02	0.00	2.00	0.00	0.00	0.00
Al_2O_3	101.96	20.25	0.20	3.00	0.60	1.56	1.04
FeO	71.85	0.03	0.00	1.00	0.00	0.00	0.00
MnO	70.94	0.04	0.00	1.00	0.00	0.00	0.00
MgO	40.31	0.00	0.00	1.00	0.00	0.00	0.00
CaO	56.08	0.25	0.00	1.00	0.00	0.01	0.01
Na_2O	61.98	10.81	0.17	1.00	0.17	0.46	0.91
K_2O	94.20	0.09	0.00	1.00	0.00	0.00	0.00
Total		100.06	1.52	0.00	3.06	8.00	4.96

Spot 5							
Oxide	wt % of oxides	mol. prop of ox	mole units	Oxygen factor	Oxygen units	Norm.Ox units	Atom units
SiO_2	60.09	68.46	1.14	2.00	2.28	5.96	2.98
TiO_2	79.90	0.00	0.00	2.00	0.00	0.00	0.00
Al_2O_3	101.96	20.21	0.20	3.00	0.59	1.56	1.04
FeO	71.85	0.01	0.00	1.00	0.00	0.00	0.00
MnO	70.94	0.01	0.00	1.00	0.00	0.00	0.00
MgO	40.31	0.00	0.00	1.00	0.00	0.00	0.00
CaO	56.08	0.06	0.00	1.00	0.00	0.00	0.00
Na_2O	61.98	11.08	0.18	1.00	0.18	0.47	0.94
K_2O	94.20	0.06	0.00	1.00	0.00	0.00	0.00
Total		99.90	1.52	0.00	3.05	7.99	4.96
Spot 6							
Oxide	wt % of oxides	mol. prop of ox	mole units	Oxygen factor	Oxygen units	Norm.Ox units	Atom units
SiO_2	60.09	68.18	1.13	2.00	2.27	5.94	2.97
TiO_2	79.90	0.00	0.00	2.00	0.00	0.00	0.00
Al_2O_3	101.96	20.10	0.20	3.00	0.59	1.55	1.03
FeO	71.85	0.00	0.00	1.00	0.00	0.00	0.00
MnO	70.94	0.01	0.00	1.00	0.00	0.00	0.00
MgO	40.31	0.00	0.00	1.00	0.00	0.00	0.00
CaO	56.08	0.08	0.00	1.00	0.00	0.00	0.00
Na_2O	61.98	11.16	0.18	1.00	0.18	0.47	0.94
K_2O	94.20	0.08	0.00	1.00	0.00	0.00	0.00
Total		99.61	1.51	0.00	3.04	7.96	4.95
Spot 7							
Oxide	wt % of oxides	mol. prop of ox	mole units	Oxygen factor	Oxygen units	Norm.Ox units	Atom units
SiO_2	60.09	68.24	1.14	2.00	2.27	5.94	2.97
TiO_2	79.90	0.01	0.00	2.00	0.00	0.00	0.00
Al_2O_3	101.96	20.34	0.20	3.00	0.60	1.57	1.04
FeO	71.85	0.02	0.00	1.00	0.00	0.00	0.00
MnO	70.94	0.01	0.00	1.00	0.00	0.00	0.00
MgO	40.31	0.00	0.00	1.00	0.00	0.00	0.00
CaO	56.08	0.31	0.01	1.00	0.01	0.01	0.01
Na_2O	61.98	11.22	0.18	1.00	0.18	0.47	0.95
K_2O	94.20	0.09	0.00	1.00	0.00	0.00	0.00
Total		100.24	1.52	0.00	3.06	8.00	4.98
Spot 8							
Oxide	wt % of oxides	mol. prop of ox	mole units	Oxygen factor	Oxygen units	Norm.Ox units	Atom units
SiO_2	60.09	68.95	1.15	2.00	2.30	6.00	3.00
TiO_2	79.90	0.02	0.00	2.00	0.00	0.00	0.00
Al_2O_3	101.96	20.21	0.20	3.00	0.59	1.56	1.04
FeO	71.85	0.00	0.00	1.00	0.00	0.00	0.00
MnO	70.94	0.02	0.00	1.00	0.00	0.00	0.00
MgO	40.31	0.00	0.00	1.00	0.00	0.00	0.00
CaO	56.08	0.04	0.00	1.00	0.00	0.00	0.00
Na_2O	61.98	11.26	0.18	1.00	0.18	0.48	0.95
K_2O	94.20	0.08	0.00	1.00	0.00	0.00	0.00
Total		100.59	1.53	0.00	3.07	8.04	5.00

Spot 9							
Oxide	wt % of oxides	mol. prop of ox	mole units	Oxygen factor	Oxygen units	Norm.Ox units	Atom units
SiO_2	60.09	68.83	1.15	2.00	2.29	5.99	3.00
TiO_2	79.90	0.00	0.00	2.00	0.00	0.00	0.00
Al_2O_3	101.96	20.45	0.20	3.00	0.60	1.57	1.05
FeO	71.85	0.00	0.00	1.00	0.00	0.00	0.00
MnO	70.94	0.02	0.00	1.00	0.00	0.00	0.00
MgO	40.31	0.00	0.00	1.00	0.00	0.00	0.00
CaO	56.08	0.07	0.00	1.00	0.00	0.00	0.00
Na_2O	61.98	11.38	0.18	1.00	0.18	0.48	0.96
K_2O	94.20	0.07	0.00	1.00	0.00	0.00	0.00
Total		100.83	1.53	0.00	3.08	8.06	5.02
Spot 10							
Oxide	wt % of oxides	mol. prop of ox	mole units	Oxygen factor	Oxygen units	Norm.Ox units	Atom units
SiO_2	60.09	68.09	1.13	2.00	2.27	5.93	2.96
TiO_2	79.90	0.00	0.00	2.00	0.00	0.00	0.00
Al_2O_3	101.96	19.99	0.20	3.00	0.59	1.54	1.03
FeO	71.85	0.05	0.00	1.00	0.00	0.00	0.00
MnO	70.94	0.00	0.00	1.00	0.00	0.00	0.00
MgO	40.31	0.00	0.00	1.00	0.00	0.00	0.00
CaO	56.08	0.12	0.00	1.00	0.00	0.01	0.01
Na_2O	61.98	11.16	0.18	1.00	0.18	0.47	0.94
K_2O	94.20	0.08	0.00	1.00	0.00	0.00	0.00
Total		99.49	1.51	0.00	3.04	7.95	4.94
Spot 11							
Oxide	wt % of oxides	mol. prop of ox	mole units	Oxygen factor	Oxygen units	Norm.Ox units	Atom units
SiO_2	60.09	68.11	1.13	2.00	2.27	5.93	2.97
TiO_2	79.90	0.01	0.00	2.00	0.00	0.00	0.00
Al_2O_3	101.96	20.33	0.20	3.00	0.60	1.57	1.04
FeO	71.85	0.02	0.00	1.00	0.00	0.00	0.00
MnO	70.94	0.04	0.00	1.00	0.00	0.00	0.00
MgO	40.31	0.03	0.00	1.00	0.00	0.00	0.00
CaO	56.08	0.19	0.00	1.00	0.00	0.01	0.01
Na_2O	61.98	10.79	0.17	1.00	0.17	0.46	0.91
K_2O	94.20	0.09	0.00	1.00	0.00	0.00	0.00
Total		99.61	1.51	0.00	3.05	7.97	4.94
Spot 12							
Oxide	wt % of oxides	mol. prop of ox	mole units	Oxygen factor	Oxygen units	Norm.Ox units	Atom units
SiO_2	60.09	68.72	1.14	2.00	2.29	5.98	2.99
TiO_2	79.90	0.00	0.00	2.00	0.00	0.00	0.00
Al_2O_3	101.96	20.51	0.20	3.00	0.60	1.58	1.05
FeO	71.85	0.03	0.00	1.00	0.00	0.00	0.00
MnO	70.94	0.03	0.00	1.00	0.00	0.00	0.00
MgO	40.31	0.01	0.00	1.00	0.00	0.00	0.00
CaO	56.08	0.27	0.00	1.00	0.00	0.01	0.01
Na_2O	61.98	11.07	0.18	1.00	0.18	0.47	0.93
K_2O	94.20	0.07	0.00	1.00	0.00	0.00	0.00
Total		100.71	1.53	0.00	3.08	8.05	5.00

D4- Secondary sulphides

KANMX7							
No.	**element**	**atomic weights**	**weights %**	**atomic prop**	**subscript**	**Formulae**	**Mineral**
216	Cu	63.54	79.18	1.25	30.72	Cu31S16	Djurleite
	S	32.06	20.81	0.65	15.98		
229	Cu	63.54	78.27	1.23	9.24	Cu9S5	Digenite
	S	32.06	21.36	0.67	5.05		
233	Cu	63.54	76.82	1.21	1.92		unknown
	S	32.06	20.15	0.63	1.04		
232	Cu	63.54	72.82	1.15	8.15	Cu8S5	geerite
	S	32.06	22.55	0.70	5.02		
MN-003 A							
No.	element	atomic weights	weights %	atomic prop	subscript		
7	Cu	63.54	65.94	1.04	1.10	CuS	Covellite
	S	32.06	30.29	0.94	1.01		
4	Cu	63.54	66.02	1.04	1.11	CuS	Covellite
	S	32.06	29.93	0.93	1.00		
10	Cu	63.54	67.61	1.06	9.15	Cu9S8	Yarrowite
	S	32.06	29.81	0.93	8.00		
3	Cu	63.54	68.27	1.07	1.11	CuS	Covellite
	S	32.06	31.08	0.97	1.00		
5	Cu	63.54	68.5	1.08	1.13	Cu9S8	Yarrowite
	S	32.06	30.6	0.95	1.00		
34	Cu	63.54	68.66	1.08	1.16		unknown
	S	32.06	29.88	0.93	1.00		
9	Cu	63.54	69.36	1.09	1.21		unknown
	S	32.06	28.93	0.90	0.99		
6	Cu	63.54	69.79	1.10	1.30		unknown
	S	32.06	27.08	0.84	1.01		
25	Cu	63.54	73.85	1.16	1.49		unknown
	S	32.06	24.93	0.78	1.00		
26	Cu	63.54	74.74	1.18	1.47		unknown
	S	32.06	25.69	0.80	1.00		
28	Cu	63.54	75.45	1.19	8.17	Cu8S5	geerite*
	S	32.06	23.31	0.73	4.98		
35	Cu	63.54	75.8	1.19	8.19	Cu8S5	geerite
	S	32.06	23.36	0.73	4.99		
32	Cu	63.54	76.77	1.21	8.34	Cu8S5	geerite*
	S	32.06	23.22	0.72	5.03		
MN-001 B							
No.	element	atomic weights	weights %	atomic prop	subscript		
4	Cu	63.54	66.02	1.04	1.11	CuS	Covellite
	S	32.06	29.93	0.93	1.00		
25	Cu	63.54	73.85	1.16	1.49		unknown
	S	32.06	24.93	0.78	1.00		
34	Cu	63.54	68.66	1.08	1.16		unknown
	S	32.06	29.88	0.93	1.00		
32	Cu	63.54	76.77	1.21	8.34	Cu8S5	geerite*
	S	32.06	23.22	0.72	5.03		
35	Cu	63.54	75.8	1.19	8.19	Cu8S5	geerite*
	S	32.06	23.36	0.73	4.99		
28	Cu	63.54	75.45	1.19	8.17	Cu8S5	geerite*
	S	32.06	23.31	0.73	4.98		
MN-014 C							
No.	element	atomic weights	weights %	atomic prop	subscript		
26	Cu	63.54	74.74	1.18	1.47		unknown
	S	32.06	25.69	0.80	1.00		
72	Cu	63.54	78.83	1.24	31.49	Cu31S16	djurleite
	S	32.06	20.21	0.63	16.01		
69	Cu	63.54	78.79	1.24	31.26	Cu31S16	djurleite
	S	32.06	20.35	0.63	16.12		
66	Cu	63.54	79.61	1.25	2.00	Cu2S	chalcocite
	S	32.06	20.05	0.63	1.01		
63	Cu	63.54	84.23	1.33	2.04	Cu2S	chalcocite
	S	32.06	20.82	0.65	1.00		

D5- Chalcopyrite data

No.	S	Au	Fe	As	Cu	Co	Mn	Ni	Total	Sample name	Lithology
214	34.66	-	30.43	-	34.61	-	0.05	-	99.75	KANMX7	Unknown
219	35.09	0.04	30.73	-	34.65	-	0.03	0.01	100.55	KANMX7	Unknown
227	35.32	0.02	30.68	-	34.81	-	0.03	-	100.86	KANMX7	Unknown
224	35.3	-	30.8	-	34.87	-	0.02	0.01	101.00	KANMX7	Unknown
217	35.42	0.01	30.51	-	34.91	-	-	0.03	100.88	KANMX7	Unknown
236	34.77	-	30.64	-	34.92	-	0.03	-	100.36	KANMX7	Cross-cutting veins
231	34.98	0.04	31	-	34.94	-	0.03	-	100.99	KANMX7	Unknown
8	35.17	-	29.98	-	34.08	-	0.01	0.00	99.24	SX1	Cross-cutting veins
17	34.41	-	30.51	-	34.26	-	0.03	-	99.21	SX1	Cross-cutting veins
4	34.21	0.08	30.39	0.0295	34.43	-	0.04	-	99.17	SX1	Cross-cutting veins
5	34.38	0.06	30.48	-	34.45	-	0.03	0.01	99.41	SX1	Cross-cutting veins
14	34.48	-	30.4	0.0297	34.52	-	0.05	-	99.48	SX1	Cross-cutting veins
11	34.35	0.05	30.24	-	34.52	-	0.04	0.00	99.20	SX1	Cross-cutting veins
10	35.01	-	30.42	0.0148	34.72	-	0.02	0.03	100.21	SX1	Cross-cutting veins
18	34.32	-	30.48	-	34.73	-	0.04	-	99.57	SX1	Cross-cutting veins
3	34.04	-	30.4	-	34.80	-	0.03	-	99.27	SX1	Cross-cutting veins
2	34.71	-	30.76	-	34.93	-	0.04	0.00	100.44	SX1	Cross-cutting veins
1	34.13	0.01	30.94	-	35.12	-	0.04	0.00	100.24	SX1	Cross-cutting veins

No.	S	Au	Fe	As	Cu	Co	Mn	Ni	Ag	Total	Sample name	Lithology
64	34.05	0.02	28.72	0.03	36.15	0.01	0.10	0.02	0.08	99.24	MN014C_Area	Phyllite
55	34.60	0.02	28.36	-	36.25	-		0.00	0.02	99.39	MN014C_area	Phyllite
68	34.42	-	28.52	-	36.45	0.00	0.01	0.00	0.00	100.12	MN014C_area	Phyllite
19	36.60	-	30.31	0.01	34.34	-		0.02	0.09	99.81	test 4	Phyllite
22	35.21	0.16	30.25	0.00	34.17	-		0.02	0.08	99.81	test 4	Phyllite

No.	S	Au	Fe	As	Cu	Co	Mn	Ni	Ag	Total	Sample name	Lithology
59	34.91	0.08	29.93	0.02	34.03	-	0.03	0.01		99.01	SX3	Cross-cutting veins
2	35.62	-	29.73	-	34.37	-	-	-		99.72	SX3	Cross-cutting veins
66	35.13	-	29.91	0.03	34.45	-	0.03	0.00		99.55	SX3	Cross-cutting veins
65	35.13	0.12	29.76	-	34.48	-	0.01	-		99.50	SX3	Cross-cutting veins
62	34.92	-	29.73	-	34.53	-	0.03	0.01		99.22	SX3	Cross-cutting veins
5	34.95	-	29.77	0.02	34.55	-	-	-		99.29	SX3	Cross-cutting veins
63	34.69	-	29.84	0.03	34.55	-	0.02	-		99.13	SX3	Cross-cutting veins
67	34.86	-	29.71	-	34.76	-	0.03	-		99.36	SX3	Cross-cutting veins
48	34.63	-	30.74	-	34.83	0.00	0.03	0.00		100.24	SX3	Cross-cutting veins
50	34.68	-	30.76	-	34.86	-	0.03	-		100.33	SX3	Cross-cutting veins
57	34.63	0.04	30.73	-	34.91	-	0.02	0.00		100.33	SX3	Cross-cutting veins
49	34.76	0.05	30.74	-	34.95	-	0.03	-		100.53	SX3	Cross-cutting veins
46	34.77	0.03	30.69	0.03	34.96	-	0.05	-		100.52	SX3	Cross-cutting veins
47	34.67	-	30.28	-	35.02	-	0.03	0.00		100.00	SX3	Cross-cutting veins
56	34.94	-	30.72	-	35.03	-	0.03	-		100.72	SX3	Cross-cutting veins
54	34.51	0.04	30.6	-	35.03	-	0.03	-		100.21	SX3	Cross-cutting veins
55	34.5	0.04	30.69	-	35.04	0.00	0.04	0.03		100.34	SX3	Cross-cutting veins
44	35.18	-	30.67	0.00	35.07	0.00	0.02	-		100.95	SX3	Cross-cutting veins

No.	S	Au	Fe	As	Cu	Co	Ni	Ag	Total	Sample name	Lithology
2	35.33	-	31.26	-	33.23	-	0.02	0.01	99.85	MN003A_Area	Breccia
20	34.77	-	30.05	0.02	33.27	-	0.01	-	98.11	test 2	Breccia
14	35.46	-	29.84	-	33.32	-	0.02	0.02	98.65	MN003A_Area	Breccia
31	34.66	-	29.82	-	34.06	0.00	0.00	0.01	98.55	MN003A_Area	Breccia
22	35.21	0.16	30.25	0.00	34.17	-	0.02	0.00	99.81	test 4	Breccia
30	34.98	-	29.81	0.01	34.20	-	0.02	-	99.02	MN003A_Area	Breccia
33	34.90	-	29.93	-	34.26	-	0.00	0.02	99.12	MN003A_Area	Breccia
27	35.19	0.02	29.86	-	34.29	0.00	-	-	99.36	MN003A_Area	Breccia
19	36.60	-	30.31	0.01	34.34	-	0.02	-	101.27	test	Breccia
23	35.08	0.09	30.20	0.00	34.52	-	-	0.01	99.91	MN003A_Area	Breccia
29	35.19	0.03	29.89	-	34.62	0.01	0.00	0.00	99.73	MN003A_Area	Breccia

No.	S	Au	Fe	As	Cu	Co	Mn	Ni	Ag	Total	Sample name	Lithology
71	35.72	-	29.56	0.06	34.13	-	0.04	0.03		99.53	SX4-2	Cross-cutting veins
115	34.97	0.02	30.87	0.04	34.41	-	0.05	0.01		100.36	SX4-2	Cross-cutting veins
107	35.01	0.01	30.75	0.02	34.41	0.01	0.03	0.00		100.23	SX4-2	Cross-cutting veins
108	34.48	0.06	30.69	0.01	34.43	0.00	0.04	0.01		99.71	SX4-2	Cross-cutting veins
120	34.92	0.05	30.84	-	34.5	0.02	0.02	0.01		100.36	SX4-2	Cross-cutting veins
109	34.57	-	30.71	-	34.53	0.01	0.02	-		99.84	SX4-2	Cross-cutting veins
119	35.14	-	30.81	0.01	34.65	-	0.02	0.02		100.65	SX4-2	Cross-cutting veins
117	34.6	-	30.72	0.02	34.75	-	0.05	0.01		100.16	SX4-2	Cross-cutting veins
111	34.83	0.04	30.34	-	34.75	-	0.04	0.02		100.02	SX4-2	Cross-cutting veins
110	34.59	0.10	30.86	0.07	34.82	-	0.02	-		100.46	SX4-2	Cross-cutting veins
121	34.85	-	30.56	0.04	35.04	0.00	0.04	-		100.54	SX4-2	Cross-cutting veins
71	34.44	-	30.31	0.00	34.65	-	0.04	0.00		99.44	SX4-3	Cross-cutting veins
83	34.63	-	30.69	-	34.74	-	0.02	0.01		100.09	SX4-3	Cross-cutting veins
81	34.22	-	30.94	-	34.75	0.01	0.03	0.02		99.97	SX4-3	Cross-cutting veins
86	34.48	-	30.6	0.01	34.94	-	0.01	0.03		100.07	SX4-3	Cross-cutting veins
82	34.28	0.04	30.67	-	35.02	0.01	0.02	0.01		100.05	SX4-3	Cross-cutting veins
85	34.51	-	30.56	0.01	35.04	-	0.03	0.00		100.15	SX4-3	Cross-cutting veins
80	33.99	0.03	30.73	-	35.05	-	0.03	-		99.83	SX4-3	Cross-cutting veins
72	34.96	-	30.38	-	35.18	-	0.03	-		100.55	SX4-3	Cross-cutting veins

No.	S	Au	Fe	As	Cu	Co	Mn	Ni	Ag	Total	Sample name	Lithology
133	34.52	0.04	30.03	-	34.26	-	0.03	0.13		99.01	SX5-1	Cross-cutting veins
130	34.24	-	30.35	0.06	34.52	0.01	0.04	0.01		99.22	SX5-1	Cross-cutting veins
135	34.93	0.06	30.32	-	34.59	-	0.03	0.03		99.95	SX5-1	Cross-cutting veins
128	34.6	-	30.34	-	34.67	-	0.04	0.02		99.67	SX5-1	Cross-cutting veins
140	34.66	-	30.6	-	34.69	-	0.02	0.02		99.99	SX5-1	Cross-cutting veins
127	34.5	0.08	30.28	-	34.76	-	0.02	0.03		99.67	SX5-1	Cross-cutting veins
144	34.93	0.00	30.44	0.01	35.02	-	0.04	-		100.44	SX5-1	Cross-cutting veins
142	34.15	-	30.51	-	35.09	-	0.03	-		99.78	SX5-1	Cross-cutting veins
131	34.09	0.08	30.58	-	35.25	-	0.03	0.02		100.06	SX5-1	Cross-cutting veins
173	34.59	0.02	30.38	0.04	34.44	-	0.02	0.03		99.52	SX5-2	Cross-cutting veins
196	34.54	0.07	30.42	0.09	34.52	-	-	0.01		99.65	SX5-2	Cross-cutting veins
189	34.65	0.00	30.62	0.07	34.63	-	0.04	0.01		100.02	SX5-2	Cross-cutting veins
87	35.16	-	29.55	0.04	34.65	-	0.04	-		99.44	SX5-2	Cross-cutting veins
88	35.29	-	29.67	-	34.72	0.00	0.00	0.00		99.69	SX5-2	Cross-cutting veins
185	34.53	-	30.62	-	34.72	-	0.04	0.03		99.94	SX5-2	Cross-cutting veins
174	34.44	-	30.36	-	34.72	-	0.03	0.22		99.77	SX5-2	Cross-cutting veins
195	34.15	-	30.48	-	34.72	-	0.01	0.01		99.37	SX5-2	Cross-cutting veins
194	34.68	0.01	30.57	-	34.81	-	0.00	-		100.07	SX5-2	Cross-cutting veins
181	34.15	-	30.81	-	34.96	-	0.03	-		99.95	SX5-2	Cross-cutting veins
182	34.94	0.00	30.8	0.01	35	-	0.03	-		100.78	SX5-2	Cross-cutting veins
89	34.92	-	29.56	-	35.01	-	0.04	-		99.53	SX5-2	Cross-cutting veins
183	34.47	-	30.98	0.03	35.16	-	0.03	-		100.68	SX5-2	Cross-cutting veins
177	34.49	0.01	30.73	0.04	35.23	-	0.03	0.01		100.55	SX5-2	Cross-cutting veins

No.	S	Au	Fe	As	Cu	Co	Mn	Ni	Ag	Total	Sample name	Lithology
162	34.72	0.03	30.08	0.01	34.19	-	0.03	-		99.05	SX5-3	Cross-cutting veins
170	35.07	0.04	29.9	-	34.42	-	0.04	0.03		99.49	SX5-3	Cross-cutting veins
163	34.49	-	30.13	-	34.43	-	0.04	0.00		99.09	SX5-3	Cross-cutting veins
161	33.97	0.06	30.4	0.04	34.46	-	0.05	0.03		99.00	SX5-3	Cross-cutting veins
147	34.05	-	30.41	-	34.56	-	0.03	0.03		99.08	SX5-3	Cross-cutting veins
153	33.82	0.03	30.67	-	34.66	-	0.03	0.01		99.21	SX5-3	Cross-cutting veins
164	34.19	-	30.2	-	34.71	-	0.04	0.02		99.16	SX5-3	Cross-cutting veins
154	34.59	-	30.16	-	34.72	-	0.04	-		99.51	SX5-3	Cross-cutting veins
145	33.57	0.02	30.54	-	34.87	-	0.03	0.01		99.04	SX5-3	Cross-cutting veins
157	34.61	-	30.77	-	34.9	-	0.01	-		100.29	SX5-3	Cross-cutting veins
166	34.53	-	30.26	0.02	34.95	-	0.02	-		99.78	SX5-3	Cross-cutting veins
167	34.42	-	30.26	-	34.95	-	0.04	-		99.67	SX5-3	Cross-cutting veins
148	34.18	0.04	30.53	-	34.96	-	0.05	-		99.76	SX5-3	Cross-cutting veins
155	34.05	0.12	30.93	-	35	0.00	0.02	0.00		100.12	SX5-3	Cross-cutting veins
151	34.14	0.00	30.74	-	35	-	0.03	0.02		99.93	SX5-3	Cross-cutting veins
158	33.91	-	30.83	-	35.13	-	0.01	0.00		99.89	SX5-3	Cross-cutting veins
152	34.49	0.10	30.95	-	35.32	-	0.02	-		100.88	SX5-3	Cross-cutting veins
210	35.28	-	30.61	-	34.08	-	0.02	0.01		100.00	SX5-4	Cross-cutting veins
208	35.32	0.00	30.53	-	34.65	-	0.01	-		100.52	SX5-4	Cross-cutting veins
198	34.62	-	30.47	-	34.8	0.00	0.03	-		99.92	SX5-4	Cross-cutting veins
211	34.71	0.01	30.79	-	34.97	0.00	0.03	0.02		100.53	SX5-4	Cross-cutting veins
205	34.75	-	30.64	-	34.97	-	0.03	0.01		100.40	SX5-4	Cross-cutting veins

No.	S	Au	Fe	As	Cu	Co	Mn	Ni	Ag	Total	Sample name	Lithology
44	34.89	0.01	27.80	-	36.52			0.00	0.00	99.55	MN001B	Breccia
36	33.82	0.03	31.46	-	34.24			-		99.73	MN001B	Breccia
50	34.12	0.02	29.66	-	35.93			-		100.05	MN001B	Breccia
41	34.10	0.02	30.10	-	35.81			0.00	0.01	100.13	MN001B	Breccia
37	35.54	0.07	29.05	-	35.45	0.02	0.35	-		100.79	MN001B	Breccia
39	35.91	0.03	29.51	0.02	35.31	-		0.01	0.04	100.97	MN001B	Breccia
38	34.84	0.03	30.21	-	35.89	-		-		101.20	MN001B	Breccia
47	34.45	0.07	31.07	-	35.59	-		-		101.91	MN001B	Breccia
30	34.98	-	29.81	0.01	34.20	-		0.02	0.09	99.10	MN001B	Breccia
33	34.90	-	29.93	-	34.26	0.00	0.08	0.00	0.02	99.36	MN001B	Breccia
27	35.19	0.02	29.86	-	34.29	-		-		99.73	MN001B	Breccia
29	35.19	0.03	29.89	-	34.62	-		0.00	0.01	99.74	MN001B	Breccia
2	35.33	-	31.26	-	33.23	-		0.02	0.10	99.88	MN001B	Breccia
23	35.08	0.09	30.20	0.00	34.52	0.01	0.11	-		100.26	MN001B	Breccia

APPENDIX E- QEMSCAN

E1-Copper deportment of Ore 1 and Ore 2 at P_{80}=150 µm, as determined by QEMSCAN.

	Ore Type	
Mineral	**Ore 1**	**Ore 2**
Chalcopyrite	99.44	99.49
Bornite	0.09	0.02
Chalcocite / Digenite	0.04	0.20
Covellite	0.11	0.08
Cuprite	0.04	0.01
Malachite/Azurite	0.04	0.02
Chrysocolla	0.14	0.07
Mica	<0.01	<0.01
Kaolinite	<0.01	<0.01
Plagioclase-Feldspar	<0.01	<0.01
Quartz	0.07	0.10
Limonite	0.01	0.01
Others	0.01	<0.01

E2- Chalcopyrite liberation and mineral associations data for Ore 1 and Ore 2 at P_{80}=150 µm, as determined by QEMSCAN.

Ore Type	Mineral	Associations					
		Liberated	Chrysocolla	Malachite	Cu-sulphides	Fe-sulphides	Others
Ore 1	Chalcopyrite	94.63	3.51	0.09	0.10	0.79	0.88
Ore 2	Chalcopyrite	97.20	1.68	0.00	0.03	0.53	0.56

E3- Pyrite liberation and mineral associations data for Ore 1 and Ore 2 at P_{80}=150 µm, as determined by QEMSCAN.

Ore Type	Mineral	Associations									
		Liberated	Chalcopyrite	Albite	Quartz	Carbonates	Mica	Limonite	Kaolinite	Pyrrhotite	Others
Ore 1	Pyrite	76.86	2.34	3.18	3.78	0.00	3.14	1.03	0.00	9.61	0.07
Ore 2	Pyrite	84.83	1.22	2.30	2.57	0.00	2.40	0.90	0.00	5.74	0.05

E4-Normalized chalcopyrite liberation for Ore 1 and Ore 2 at P80=150 µm, as determined by QEMSCAN.

Ore Type	Classes	Locked	Middlings	Liberated
Ore 1	% of chalcopyrite	0.73	4.64	94.63
Ore 2	% of chalcopyrite	0.5	2.31	97.2

E5-Grain size distribution of chalcopyrite for Ore 1 and Ore 2 at P_{80}=150 µm, as determined by QEMSCAN.

Size Fraction	Ore 1	Ore 2
<10	6.32	2.01
<20	5.29	3.04
<30	3.40	4.75
<40	2.89	4.73
<50	2.36	3.03
<60	1.94	2.31
<70	1.84	1.37
<80	1.40	1.01
<90	1.22	0.90
<100	0.92	0.62
<120	1.43	1.07
<140	1.18	0.80
<160	0.75	0.67
<180	0.54	0.58
<200	0.43	0.48
<250	0.56	0.68
<500	0.59	0.35
<1000	0.42	0.00

E6- QEMSCAN false colour images

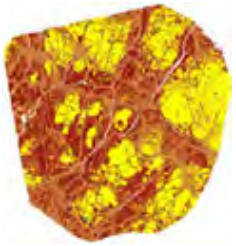

MN001

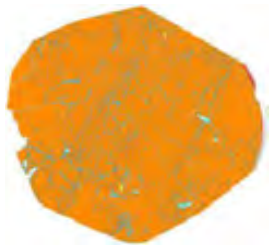

MN001B

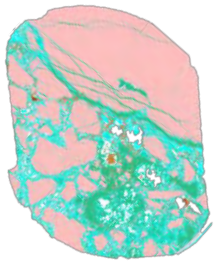

MN00 2C

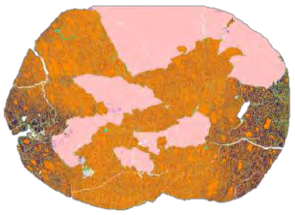

MN003

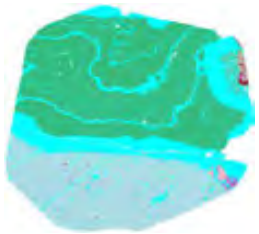

MN004

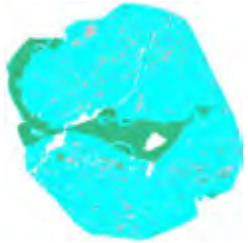

MN004

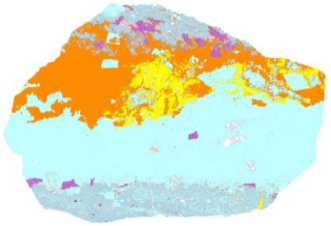

MN00

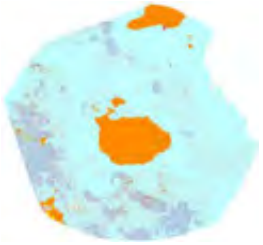

MN00

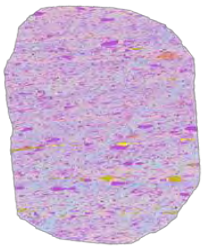

MN01

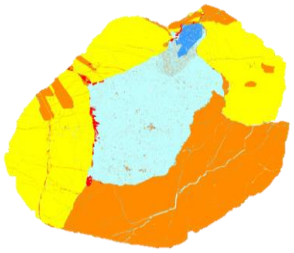

MN011

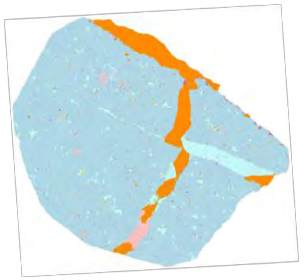

MN01

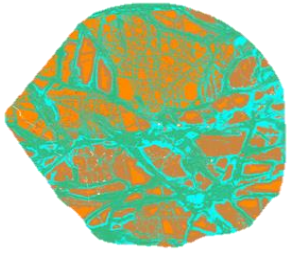

MN014

Appendix F- MILLING CURVE.

F1-Particle size distribution data for Ore 1 and Ore 2, at P80=150 μm

Ore Type	Screen size	Mass Retained	Normalized Mass %
Ore 1	+150	25.70	22.13
	+106/-75	13.85	11.93
	+75/-53	15.23	13.11
	+53/-25	14.23	12.25
	+25	15.34	13.21
	-25	31.79	27.37
	Total	116.14	100.00
Ore 2	+150	41.49	19.72
	+106/-75	13.85	6.58
	+75/-53	15.23	7.24
	+53/-25	14.23	6.76
	+25	93.76	44.57
	-25	31.79	15.11
	Total	210.35	100.00

F2-Particle size distribution of Ore 1 and Ore 2, at P80=212 μm

Ore Type	Screen size	Mass Retained	Normalized Mass %
Ore 1	+150/-106	302.88	30.82
	+106/-75	97.19	9.89
	+75/-53	89.32	9.09
	+53/-38	77.56	7.89
	+38/-25	76.44	7.78
	+25	69.95	7.12
	-25	269.50	27.42
	Total	982.84	100.00
Ore 2	+150/-106	345.29	32.52
	+106/-75	88.91	8.37
	+75/-53	92.98	8.76
	+53/-38	99.24	9.35
	+38/-25	130.89	12.33
	+25	122.14	11.50
	-25	182.39	17.18
	Total	1061.84	100.00

F3-Grind curves for Ore 1 and Ore 2 at P80= 150 and 212 µm.

	150 µm			212 µm		
	Time (min)	mass (g)	% passing	Time (min)	mass (g)	% passing
Ore 1	3	154.1	72.2	2.5	687.9	67.79
	4	399.1	83.6	3	745.5	74.62
	5	384.9	91.5	3.5	802.6	78.95
				4	846.1	83.95
Ore 2	3.75	777.1	73.0	4.8	999.4	92.2
	4	796.6	75.8	3.8	887.8	84.7
	4.75	884.3	82.7	2.3	715.1	69.7
	5	865.3	84.0			

F1- Bulk Mineralogy data of both ore samples

	Ore Code	
	Mass per cent	
Minerals	**Ore 1**	**Ore 2**
Pyrite	3.21	17.61
Pyrrhotite	0.64	5.46
Chalcopyrite	3.36	15.47
Bornite	0.00	0.00
Chalcocite / Digenite	0.00	0.01
Covellite	0.00	0.01
Other sulphides	0.03	0.17
Cuprite	0.00	0.00
Malachite/Azurite	0.00	0.00
Chrysocolla	0.03	0.02
Amphibole (Hornblende)	2.46	0.65
Mica	18.34	13.90
Kaolinite	0.17	0.11
Albite	24.23	15.70
Quartz	19.14	16.77
Calcite	23.10	5.61
Fe-Ti minerals	1.53	2.44
Limonite	1.39	1.14
Others	2.36	4.91

APPENDIX G- EXPERIMENTAL PROCEDURE

G1 - Synthetic plant water

Recipe for a 40-litre batch

Chemical salt	Mass in grams
$MgSO_4.7H_2O$	24.6
$Mg(NO_3).6H_2O$	4.28
$Ca(NO_3)2.4H_2O$	9.44
$CaCl_2$	4.44
NaCl	14.24
Na_2CO_3	1.2

Chemicals salts were added to 4 litres of distilled water in the order as listed in the above table. After each salt was added the solution was thoroughly mixed to ensure complete dissolution.

Note: All salts are chemically pure (CP) grade.

APPENDIX H - ANALYTICAL METHODS

H1 - Acid Absorption Spectroscopy (AAS)

In preparation for AAS, the samples were digested in aqua regia, consisting of hydrochloric acid (HCL) (32 %), nitric acid (HNO_3) (55 %) and hydrofluoric acid (HF) (~40 %). ~0.1 g of concentrate material and ~0.5 g of feed and tail material were weighed out into 250 ml wide-mouthed Erlenmeyer flasks. After each sample, the Erlenmeyer flasks were cleaned with distilled water. 6 ml HCL, 2 ml HNO3 and 2 ml HF were added to each sample. The samples were then placed in the microwave set at 180^0C for 20 min.

Once digestion was complete, the sample was transferred into a 100 ml volumetric flask and made up to 100 ml by adding distilled water. The sample was then filtered using Whatman No1 into a sample vial. This filtrate was then analysed using the AAS. In order to obtain sulphur data, the finely milled feeds, concentrates and tails were left in powder form before being analysed on the LECO 423 sulphur analyser.

H2 – LECO sulphur analyser

Sulphur analyses were performed on all feed, concentrate and tails samples using the LECO 423 sulphur analyser with automatic loader, housed within the Department of Chemical Engineering at the University of Cape Town. For standard operating conditions the sample is first weighed out (between 0.1g and 0.5g) before being placed into a furnace and burned in the presence of excess medical oxygen. The flowrate for the medical oxygen was 3.25 l/min and the temperature was 1350 ^{o}C. Analysis is by infrared detection. Linear calibration was performed using four standards with different sulphide concentrations (0.56%, 5.05%, 14.0%, and 29.87%). Each standard was analysed using its own method setting integration times using either low or high infrared cells.

APPENDIX I- BATCH FLOTATION DATA.

I 1-Batch flotation data for Ore 1 at P80= 150 µm.

Flotation conditions	Sample I.D	Time mins	Mass g	Cum mass g	Cum water g	Cum Cu grade %	Cum Cu recovery %	Cum Fe grade %	Cum Fe recovery %	Cum S grade %	Cum S recovery %
Ore 1 P80=150 µm Test 1	C1	2	54.62	54.62	266.36	10.5	87.07	15.52	30.52	18.9	72.67
	C2	4	4.17	58.79	310.09	9.91	88.49	14.94	31.61	18.11	74.96
	C3	7	2.66	61.45	341.39	9.6	89.57	14.53	32.14	17.57	75.99
	C4	10	1.46	62.91	360.06	9.43	90.05	14.3	32.38	17.24	76.36
	Feed		999.6								
	Tails		936.7								
Ore 1 P80=150 µm Test 2	C1	2	51.73	51.73	220.66	10.13	81.36	17.24	29.31	19.1	66.88
	C2	4	5.54	57.27	259.17	9.54	84.79	16.68	31.38	18.13	70.27
	C3	7	3.58	60.85	287.02	9.22	87.15	16.18	32.36	17.48	71.99
	C4	10	2.09	62.94	305.12	9.02	88.18	15.83	32.75	17.03	72.57
	Feed		1014								
	Tails		951.9								
Ore 1 P80=150 µm Test 3	C1	2	55.95	55.95	197.29	8.77	68.68	20.21	37.16	22.3	84.45
	C2	4	8.48	64.43	270.38	8.1	73.09	18.96	40.14	20.71	90.3
	C3	7	4.11	68.54	309.62	7.8	74.87	18.33	41.29	19.95	92.54
	C4	10	1.65	70.19	324.9	7.68	75.46	18.07	41.67	19.62	93.22
	Feed		992.9								
	Tails		922.9								

I 2-Batch flotation data for Ore 2 at P80= 150 µm.

Flotation Conditions	Sample I.D	Time mins	Mass g	Cum mass g	Cum water g	Cum Cu grade %	Cum Cu recovery %	Cum Fe grade %	Cum Fe recovery %	Cum S grade %	Cum S recovery %
Ore 2 P80=150 µm Test 1	C1	2	36.54	36.54	178.82	11.13	67.01	16.28	20.59	23.5	57.3
	C2	4	5.84	42.38	240.23	10.77	75.21	15.32	22.48	23.07	65.25
	C3	7	5.93	48.31	280.03	10.59	84.31	15.46	25.86	22.61	72.89
	C4	10	3.35	51.66	297.64	10.43	88.76	15.44	27.61	22.33	76.98
	Feed		960.79								
	Tails		909.13								
Ore 2 P80=150 µm Test 2	C1	2	37.14	37.14	175.95	13.15	76.25	16.69	19.32	22.2	49.97
	C2	4	7.35	44.49	215.82	11.97	83.14	16.7	23.15	21.95	59.19
	C3	7	6.02	50.51	267.92	11.13	87.8	16.4	25.82	21.84	66.86
	C4	10	3.14	53.65	302.64	10.84	90.77	16.31	27.27	21.66	70.41
	Feed		963.52								
	Tails		909.87								
Ore 2 P80=150 µm Test 3	C1	2	39.12	39.12	172.89	14.49	71.97	17.09	21.52	18.1	44.75
	C2	4	9.22	48.34	228.75	13.46	82.6	16.27	25.32	17.81	54.43
	C3	7	5.39	53.73	282.03	13.1	89.33	15.97	27.61	17.49	59.4
	C4	10	2.48	56.21	333.79	12.96	92.48	15.82	28.62	17.24	61.23
	Feed		966.95								
	Tails		910.74								

I 3-Batch flotation data for Ore 1 at P80= 212 µm.

Flotation Conditions	Sample I.D	Time (min)	Mass (g)	Cum mass (g)	Cum water (g)	Cum Cu grade %	Cum Cu recovery %	Cum Fe grade %	Cum Fe recovery %	Cum S grade %	Cum S recovery %
Ore 1 P80=212 µm Test 1	C1	2	36.54	36.54	162	13.71	68.45	18.9	24.43	28.9	67.82
	C2	4	5.84	42.38	199.36	13.18	76.32	18.56	27.82	27.96	76.11
	C3	7	5.93	48.31	236.74	12.8	84.47	18.33	31.31	27	83.77
	C4	10	3.35	51.66	268.04	12.57	88.71	18.12	33.11	26.58	88.18
	Feed		969.66								
	Tails		918								
Ore 1 P80=212 µm Test 2	C1	2	38.87	38.87	166.19	14.76	78.71	15.9	21.27	20.3	62.78
	C2	4	4.45	43.32	210.26	13.67	81.24	15.25	22.74	19.25	66.36
	C3	7	2.83	46.15	238.8	13.1	82.95	14.8	23.51	18.57	68.2
	C4	10	3.25	49.4	264.27	12.56	85.15	14.32	24.35	17.79	69.93
	Feed		990.7								
	Tails		941.3								
Ore 1 P80=212 µm Test 3	C1	2	36.86	36.86	162.65	13.17	63.55	17.2	22.22	22.2	58.31
	C2	4	5.79	42.65	202.65	12.68	70.79	16.95	25.34	21.72	66.03
	C3	7	4.88	47.53	233.57	12.52	77.88	16.8	27.97	21.54	72.95
	C4	10	2.66	50.19	258.23	12.48	81.98	16.73	29.43	21.3	76.17
	Feed		967.63								
	Tails		917.44								

I 4-Batch flotation data for Ore 2 at P80= 212 µm.

Flotation Conditions	Sample I.D	Time mins	Mass g	Cum mass g	Cum water g	Cum Cu grade %	Cum Cu recovery %	Cum Fe grade %	Cum Fe recovery %	Cum S grade %	Cum S recovery %
Ore 2 P80=212 µm Test 1	C1	2	35.61	35.61	169.06	13.24	77.12	17.34	23.3	24.1	61.08
	C2	4	6.22	41.83	226.07	12.03	82.28	16.76	26.46	23.06	68.65
	C3	7	3.89	45.72	250.69	11.64	87.09	16.87	29.11	22.76	74.05
	C4	10	2.16	47.88	262.29	11.52	90.21	16.98	30.68	22.76	77.55
	Feed		968.74								
	Tails		920.86								
Ore 2 P80=212 µm Test 2	C1	2	34.15	34.15	173.11	12.33	66.25	16.69	20.51	22.8	53.45
	C2	4	6.73	40.88	225.25	11.65	74.92	16.38	24.11	22.6	63.43
	C3	7	4.41	45.29	252.66	11.55	82.27	16.43	26.78	22.41	69.67
	C4	10	3.16	48.45	272.69	11.41	86.99	16.38	28.56	22.41	74.55
	Feed		967.38								
	Tails		918.93								
Ore 2 P80=212 µm Test 3	C1	2	34.28	34.28	165.08	13.17	68.15	16.74	19.69	22.3	56.2
	C2	4	5.03	39.31	203.94	12.71	75.4	16.41	22.14	22.07	63.78
	C3	7	4.86	44.17	236.66	12.53	83.54	16.36	24.8	22.05	71.6
	C4	10	3.01	47.18	254.99	12.48	88.89	16.35	26.46	22.03	76.4
	Feed		966.99								
	Tails		919.81								